New Organic π-Conjugated System Using Dithiafulvenes and Tetrathiafulvalenes as Building Blocks

by

© Eyad Ahmad Younes

A Thesis Submitted to the

School of Graduate Studies

in Partial Fulfillment of the Requirements

for the degree of

Doctor of Philosophy

Department of Chemistry

Memorial University of Newfoundland

August 2017

St. John's Newfoundland

Abstract

This thesis describes a systematic study of new functional π-conjugated organic materials. The detailed investigations can be summarized in two research themes. The first theme deals with the design and synthesis of redox-active conjugated co-polymers using tetrathiafulvalene vinylogue (TTFV) and pyrene as repeat units. TTFV has been known to be an excellent π-electron donor and shows intriguing conformational switching properties associated with its redox reactions. Pyrene is a widely used organic chromophore with rich photophysical and supramolecular properties. The newly designed TTFV-pyrene co-polymers have been found to show redox-activity and stimuli-responsive aggregation behaviour in organic solvents. Their electronic and supramolecular properties have been elucidated by various spectroscopic and microscopic analyses (e.g., CV, UV-Vis, GPC, and DLS). In addition, the conformational properties of the co-polymers were modeled by molecular mechanics (*MM*) simulations to provide theoretical explanations for the obtained experimental data.

In the second research theme, efforts have been dedicated to the development of new π-extended analogues based on pentacene-5,7,12,14-tetraone. By introducing redox-active 1,3-dithiole groups *via* Wittig-type olefination, a highly π-extended TTF analogue was created, and its structural, electronic, and redox properties were investigated by NMR, UV-Vis absorption and electrochemical analyses in conjunction with density functional theory (DFT) calculations. Pentacene-5,7,12,14-tetraone was also subjected to selective olefination and cross-coupling reactions to yield a new class of pentacene-based π-conjugated systems functionalized with geminal enediyne and 1,3-dithiole groups. The electron-donating and accepting effects exerted by the enediyne and dithiole units deliver intriguing structural and electronic properties, as well

as redox activities which were systematically investigated by experimental and theoretical analyses. The bis(enediyne) substituents also provided synthetic access to novel carbon-rich cross-linked polymers and polycyclic aromatic hydrocarbons (PAHs) through transition metal-catalyzed cross-coupling and cyclization reactions.

Acknowledgements

First of all, I would like to thank my advisor, Prof. Yuming Zhao, for giving me the opportunity to join in his group, and also for his genuine guidance and support during my graduate program at Memorial University. Dr. Zhao has broad knowledge in chemistry. I have learnt from him a lot during my program. My thanks go also to my supervisory committee members, Dr. Francesca Kerton and Dr. Christopher Flinn, for their encouragement and helpful suggestions during my PhD program. I would like to thank all of the organic chemistry professors at Memorial, including Prof. Paris Georghiou, Prof. Graham Bodwell, and Prof. Sunil Pansare, for their advice and well-considered suggestions during my study.

I am warmly thankful to Prof. Bodwell and his students, Kerry-Lynn Williams and Joshua Walsh, who carried out excellent collaborations on the TTFV–pyrene-based copolymer project. I would also like to thank all of the current and former members of the Zhao Group for their help and support during my study, especially to Mr. Mohammadreza Khadem for his assistance and kind help.

I would like to acknowledge Prof. Alex Adronov of McMaster University, for assistance in the GPC analysis of copolymer **55**. I am so grateful to Prof. Qiying Chen of Memorial University for his help in the surface optical profiling analysis of copolymer **55**. I would like to extend my gratitude to my friend Dr. Ahmad Alrawashdeh of Memorial University for his assistance and kind help.

Furthermore, I would like to thank Dr. Celine Schneider, Ms. Linda Winsor, Mr. Adam Beaton, and other C-CART staff for their kind assistance in all the instrumental analyses described in this dissertation.

I would also like to acknowledge the Department of Chemistry and the School of Graduate Studies at Memorial University. I also wish to thank NSERC for financial support, and Compute Canada and ACEnet for providing me the computational resources. My deep gratefulness goes to Prof. Ahmad Hussein and Prof. Raed Al-Qawasmeh of the University of Jordan for their help and support. I am especially grateful to Dr. Osama Ali for everything he did for me.

Finally, I would like to thank my wonderful family, my parents, my wife, my brothers, sisters, and my children for their unconditional love and support throughout the course of my PhD program.

Contents

List of Figures

List of Schemes

List of Tables

List of Abbreviations and Symbols

A	acceptor
ca	circa
calcd	calculated
CV	cyclic voltammetry
DMF	dimethylformamide
D	donor
d	doublet
D-A	donor-acceptor
dd	doublet of doublets
DFT	density functional theory
DLS	dynamic light scattering measurements
eq	equivalent(s)
FMO	frontier molecular orbital
FTIR	Fourier transform Infrared
GPC	gel permeation chromatography
g	gram(s)
h	hour(s)
HOMO	highest occupied molecular orbital
IR	infrared
LC-MS	liquid chromatography mass spectrometry
LUMO	lowest unoccupied molecular orbital

m	multiplet
mA	milliampere
MALDI-ToF	matrix-assisted laser desorption ionization-time of flight
mol	mole
MHz	megahertz
min	minute(s)
mg	milligram(s)
mmol	millimole
mp	melting point
MS	mass spectrometry
m/z	mass to charge ratio
NMR	nuclear magnetic resonance spectroscopy
rt	room temperature
t	triplet
TD-DFT	time-dependent density functional theory
tlc	thin layer chromatography
TFA	trifluoroacetic acid
THF	tetrahydrofuran
TMS	trimethylsilyl
TMSA	trimethylsilylacetylene
TTF	tetrathiafulvalene
TTFAQ	anthraquinone-type π-extended tetrathiafulvalene

TTFV	tetrathiafulvalene vinylogue
s	singlet
UV-Vis	ultraviolet-visible
VT-NMR	variable temperature nuclear magnetic resonance
δ	chemical shift (NMR)
λ_{max}	maximum absorption wavelength

Chapter 1

Introduction

1.1 Tetrathiafulvalenes and π-Extended Analogues: Chemistry and Applications

1.1.1 A Brief Introduction to Tetrathiafulvalenes and π-Extended Tetrathiafulvalenes

Tetrathiafulvalene (TTF) as an organic semiconductor was first reported by Wudl and co-workers in the early 1970s.[1] Since then, TTF has become one of the most widely studied organic heterocyclic systems. TTF is an electron-rich molecule that can readily and sequentially donate up to two electrons to form thermodynamically stable radical cation $TTF^{\bullet+}$ and dication TTF^{2+} at relatively low oxidation potentials. The electron-donating nature of TTF is due to the gained aromaticity (stability) of its cation and dication in which the dithiole ring(s) of TTF upon oxidation becomes a 6-π electron Hückle aromatic system (Scheme 1.1).[2-6]

In addition to their unique π-electron donating properties, TTF and its derivatives show conformational switching properties. For example, neutral TTF has a boat-like conformation, while the radical cation of TTF takes a nearly planar shape. For the dication, however, the two dithiolium groups prefer to have a perpendicular geometry so as to minimize the disfavored charge repulsion.[3]

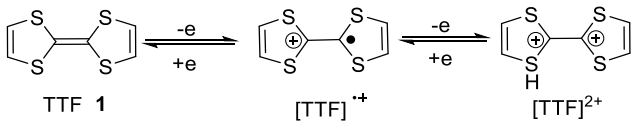

Scheme 1.1: The sequential and reversible oxidations of neutral TTF.

The design of new π-extended analogues of TTF by attachment of π-conjugated moieties to the two dithiole rings can significantly enhance their electronic and crystallographic properties. Most of the new TTF derivatives show significantly lowered oxidation potentials as a result of their oxidized forms (*e.g.*, radical cations and dications) being better stabilized by extended π-delocalization and reduced charge repulsion. On the other hand, the extended π-structures lead to enhanced intramolecular π–π interactions, which in turn improve and/or modify microscopic ordering in the solid state. Many TTF derivatives show unique properties that are particularly beneficial to the development of new organic electronic materials and optoelectronic devices.[7-10]

The design of π-extended TTF derivatives (exTTFs) can be made by either having the two 1,3-dithiole units annulated with π-conjugated arenes (*e.g.*, dibenzo-TTF **2** shown in Figure 1.1) or having a π-spacer inserted in between the two dithiole heterocycles, such as the anthraquinoidal and vinylogous exTTFs **3** and **4** shown in Figure 1.1.

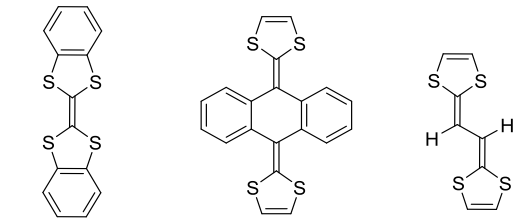

Fig 1.1: Representatives of exTTFs.

1.1.2 Synthetic Methods for TTF and Functionalized TTF Derivatives

As shown in Scheme 1.2, the synthesis of TTFs can be achieved by different synthetic methods. The most popular and straightforward methods for making symmetrical TTF derivatives are the base or phosphate-promoted coupling of dithiolium salt or 1,3-dithiole-2-thione (Scheme 1.3

Methods A and B respectively) [11]. Unsymmetrically substituted TTFs can be easily synthesised by a Wittig-Horner reaction.[12] The synthetic methods for the most important TTF precursors 1,3-dithiol-2-thione and 1,3-dithiolium salt are shown in Scheme 1.3.

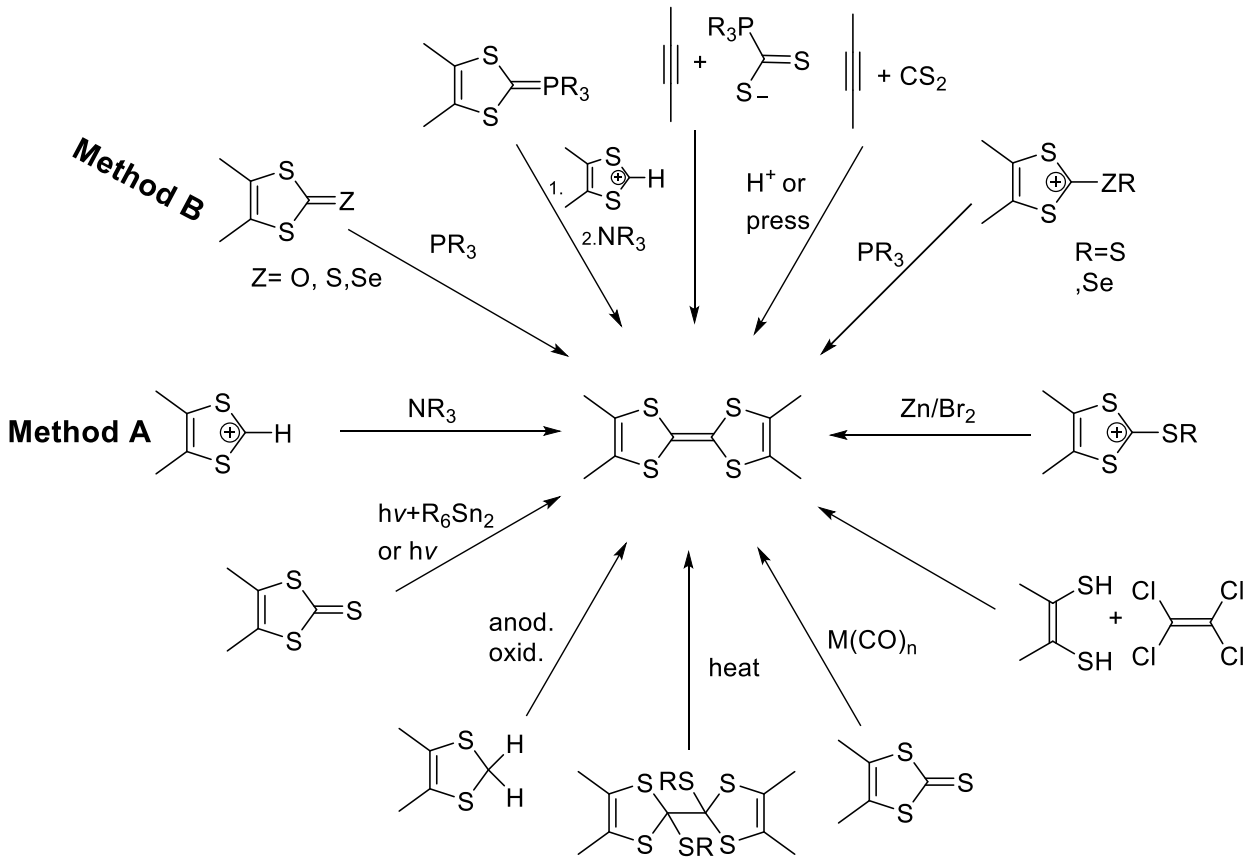

Scheme 1.2: Synthetic methods for preparation of TTF skeleton (adapted from reference 11).

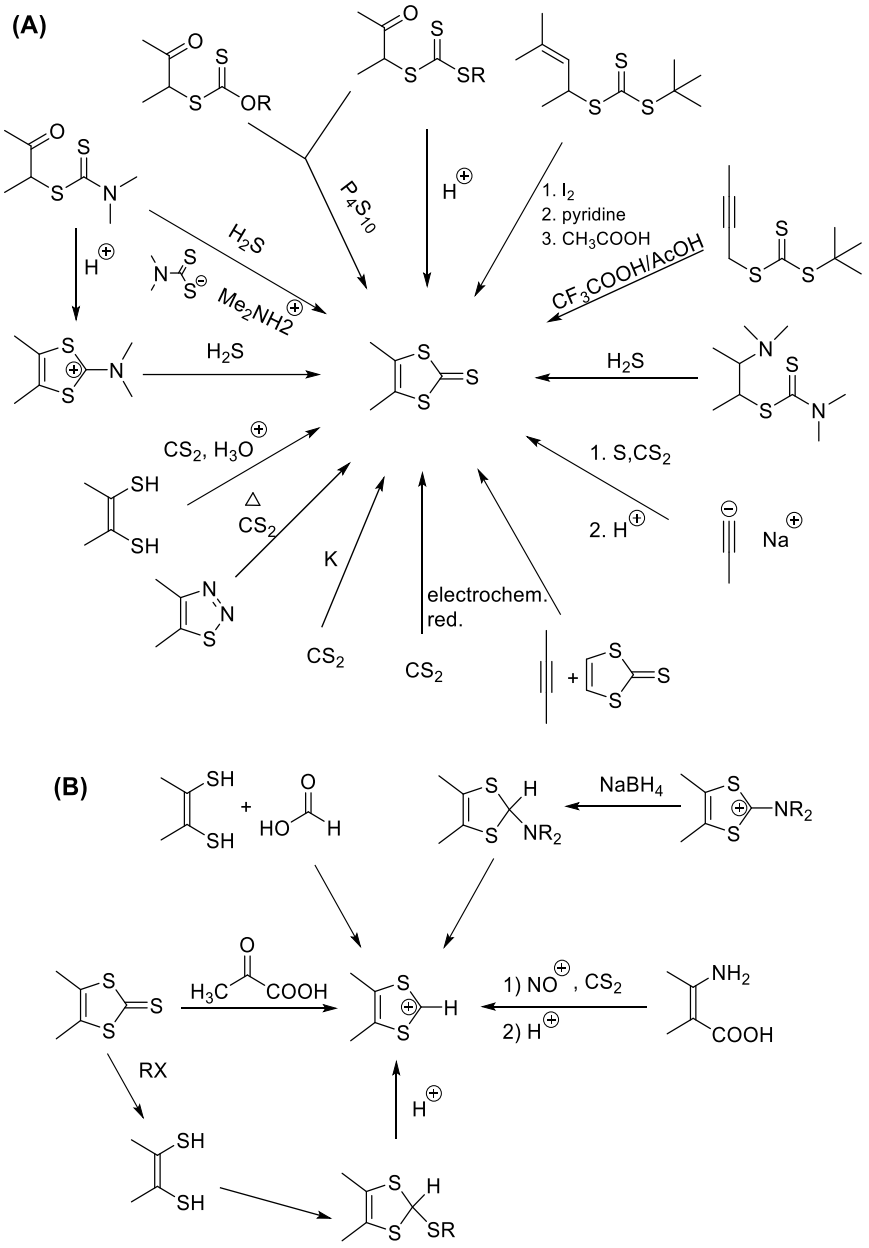

Scheme 1.3: Synthetic methods for A:1,3-dithiole-2-thione and B:1,3-dithiolium salt (adapted from reference 11).

1.1.3 Tetrathiafulvalene Vinylogues

Tetrathiafulvalene vinylogues (TTFVs) are an important family of exTTFs which have various vinyl bridges between the two dithiole rings. TTFVs are known to be excellent electron donors and can undergo reversible electron transfers under mild redox conditions.[4-5,13] Moreover, TTFVs can switch their conformation in their different oxidation states.[14-16] For example, the conformation of TTFV **2** (Scheme 1.4) can be transformed from a pseudo *cis* to a complete *trans* conformation upon oxidation. In the neutral state, the favoured conformation of TTFV is the *cis*-like structure as a result of minimal steric interactions between the phenyl and dithiole moieties. In the dicationic state, the molecular shape of TTFV is changed to a *trans* conformation because the charge repulsion between the two dithiolium rings outplays the steric effect.[17]

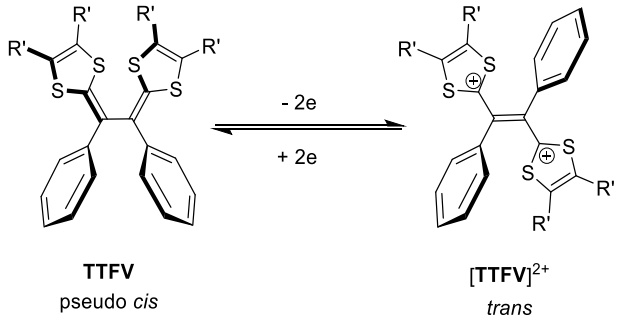

Scheme 1.4: Redox-induced conformational switching of diphenyl TTFV.

1.1.4 Synthetic Methods for Tetrathiafulvalene Vinylogues

The most efficient synthetic method for TTFVs is the oxidative dimerization of 1,4-dithiafulvene (DTF) precursors. For example, DTF **5** (Scheme 1.5) when treated with an oxidizing reagent such as $AgBF_4$, Br_2, and I_2, can undergo a radical dimerization reaction, yielding TTFV **6** after reductive

workup. The DTF can be prepared by a phosphite-promoted olefination reaction between an aldehyde precursor **4** and a thione counterpart **3** as illustrated in Scheme 1.4.[18-19]

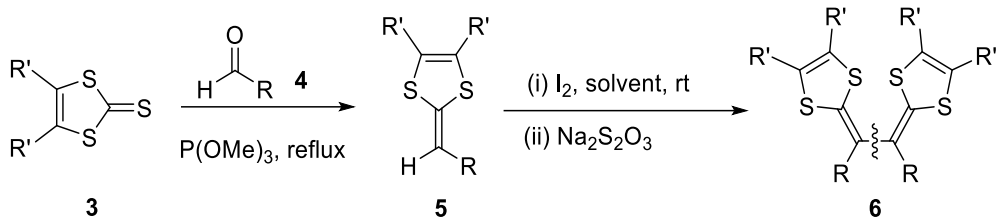

Scheme 1.5: General DTF synthetic methodology for TTFVs.

The mechanism of the DTF oxidative dimerization reaction is described in Scheme 1.6. The first step is a single electron transfer from DTF to the oxidant, which generates a radical cation intermediate. Dimerization of the DTF radical cation then occurs to form a new carbon-carbon bond. After elimination of the acidic protons in the resulting dimer intermediate, neutral TTFV is formed and is then immediately oxidized to the TTFV dication due to the lower oxidation potential of TTFV relative to DTF. In the last step, a reducing agent such as sodium thiosulfate ($Na_2S_2O_3$) is added to quench the excess oxidant and to reduce the TTFV dication back to the neutral state.

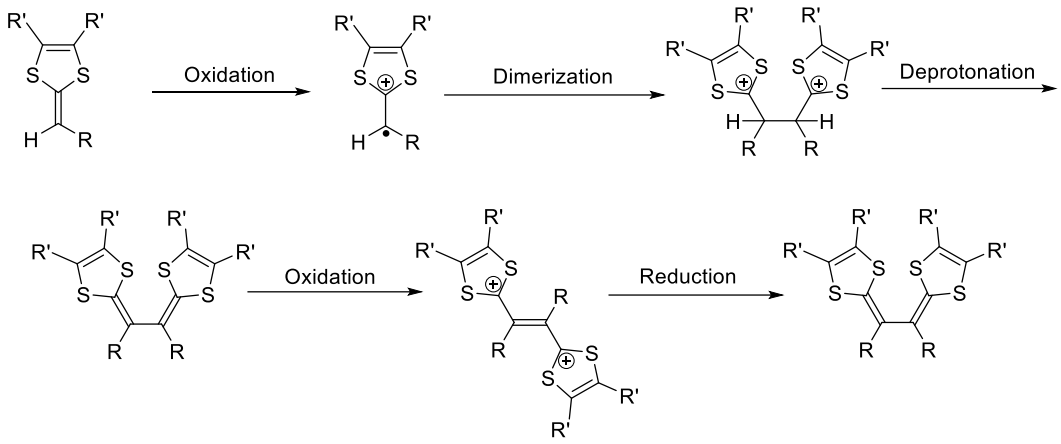

Scheme 1.6: Mechanism of the DTF oxidative dimerization reaction.

The thione precursor **3** with different R groups can be readily made from the reaction of zinc complex **7** with an electrophile (*e.g.*, an alkyl halide). The zinc complex itself can be obtained from the reaction between carbon disulfide (CS_2) and an alkali metal such as sodium (Scheme 1.7).[20]

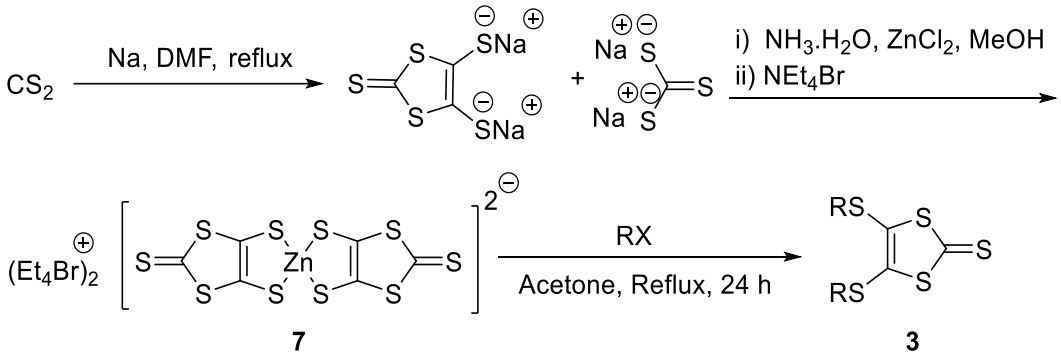

Scheme 1.7: Synthesis of thione **3**.

The detailed mechanism of the 1,3-dithiole-2-thione preparation is shown in Scheme 1.8.[21] In the beginning, sodium metal reduces carbon disulfide (CS_2) to form a reactive radical species, which can dimerize quickly. The dimeric intermediate continues to react with another two

molecules of CS_2 followed by a series of rearrangement to form a five-member ring dithiolate anion which then coordinates with Zn(II) ion to generate a red-coloured stable solid complex.

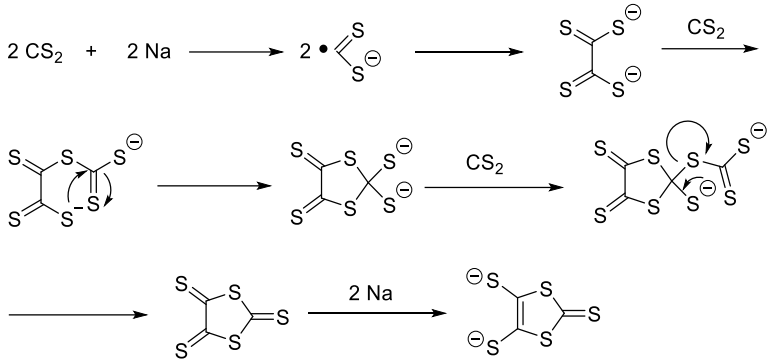

Scheme 1.8: Mechanism of the reduction of CS_2 into dithiolate.

TTFV-based π-conjugated materials have been the subject of growing interest over the past years. In this section, a brief review of the most recent studies on the synthesis and applications of TTFV-based functional materials is presented. The applications of these materials are mainly dependent on the redox activity and controllable conformational switching behaviour of TTFVs.

The integration of highly π-conjugated aromatic units in a TTFV polymer backbone gives rise to appealing properties and applications. In 2014, a TTFV-fluorene co-polymer **10** was synthesized through Sonogashira cross-coupling polymerization between a phenylacetylene-substituted TTFV **8** and 2,7-diiodofluorene **9** (Scheme 1.9).[22] The polymer **10** was found to show excellent efficiency and selectivity in dispersing small-diameter single-walled carbon nanotubes (SWNTs). This polymer can wrap around SWNTs via strong π-π interactions forming stable polymer/SWNT suspension in toluene (Figure 1.2). Addition of trifluroacetic acid (TFA) to the co-polymer/SWNT dispersion triggers the release of SWNTs from the polymer/SWNT assemblies, since TFA protonates the TTFV units to cause conformational changes of the polymer backbone which in turn leads to dissociation of the polymer from the SWNT surface.

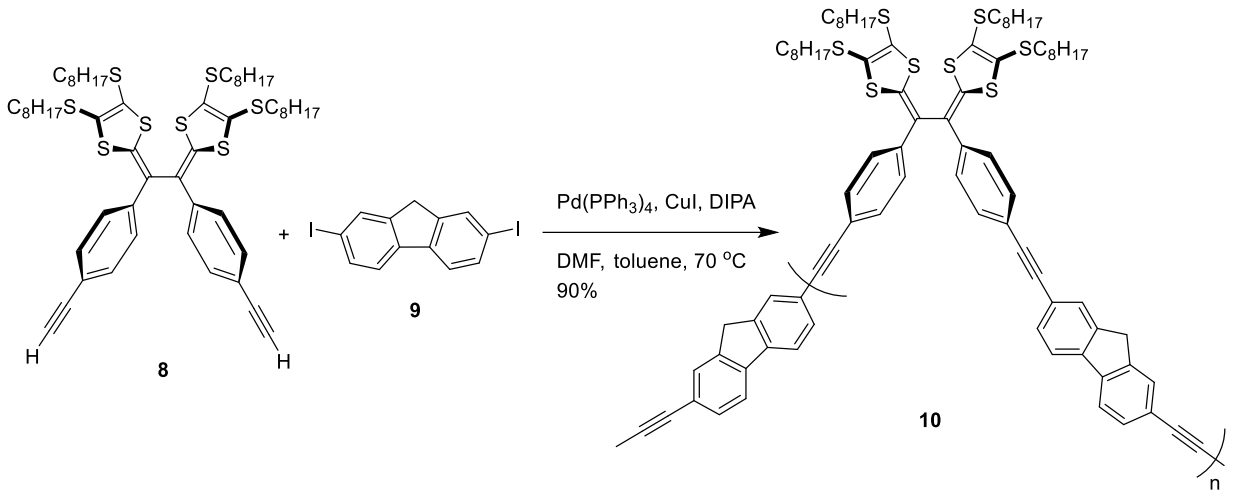

Scheme 1.9: Synthesis of TTFV-fluorene co-oligomer **10**.

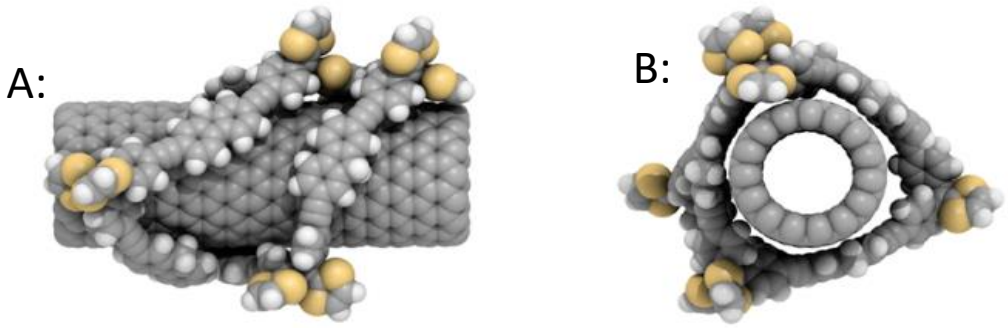

Figure 1.2: Two projections of the conformation of a model hexamer wrapping around a (10,0) SWNT were investigated by molecular mechanics calculations using the SYBYL force field implemented with the Spartan'10 software package: (A) side view and (B) front view. Reprinted with permission from {Liang, S.; Zhao, Y.; Adronov, A. *J. Am. Chem. Soc*. **2014**, *136*, 970-977}. Copyright {2014} American Chemical Society.

Recently, Khadem and Zhaoreported another type of TTFV−fluorene co-oligomers. The TTFV−fluorene co-oligomers were synthesized through one-pot iodine-promoted oxidative polymerization in the solution phase at the room temperature (Scheme 1.10A). The same oxidative coupling procedure was applied to a bis(DTF) dimer **11**, but only cyclic oligomer products were formed as a result of favoured intramolecular DTF coupling (Scheme 1.10B). The TTFV−fluorene co-oligomers have been found to show strong supramolecular interactions with SWNTs in different organic solvents. [23]

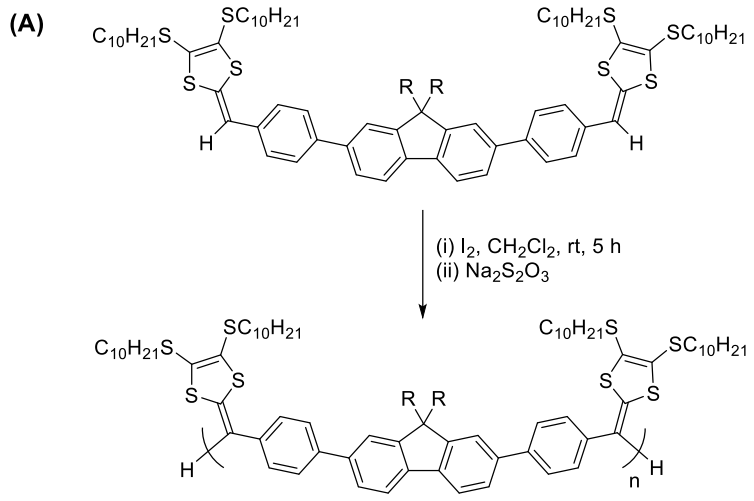

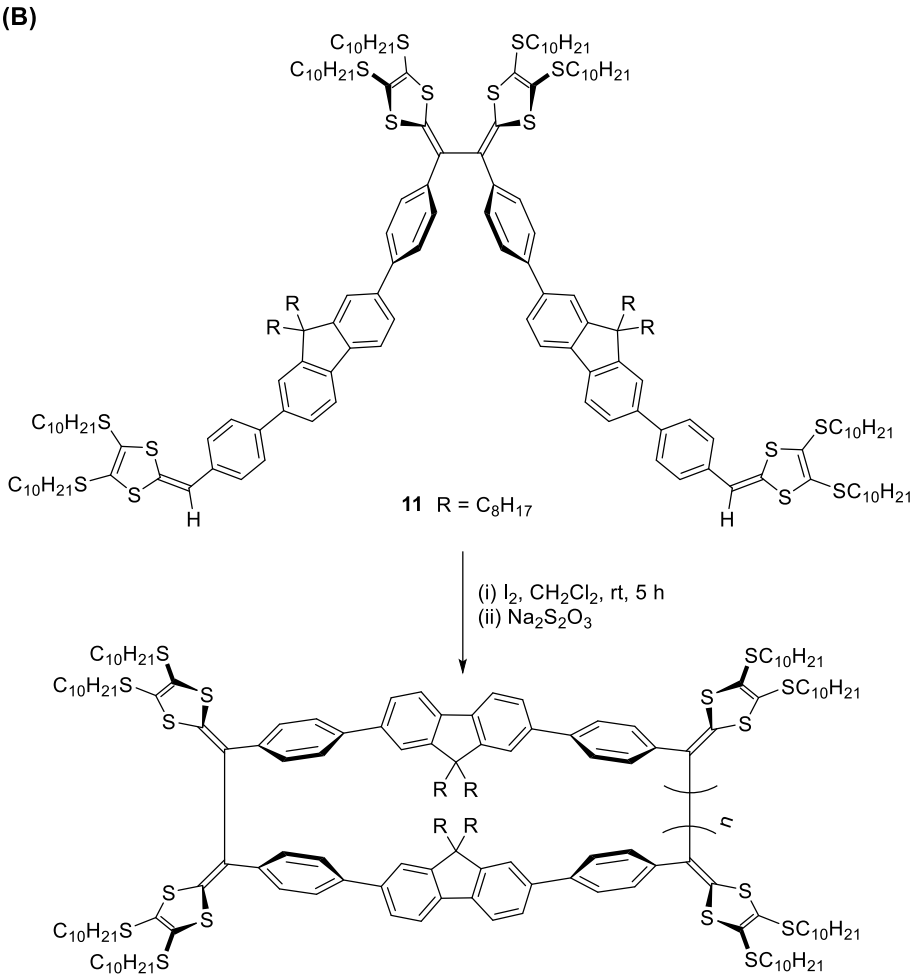

Scheme 1.10: Synthesis of (A) acyclic TTFV−fluorene oligomers, and (B) cyclic TTFV−fluorene oligomers.[23]

The combination of different π-building units with TTFV system can provide new materials with different functions and properties. In 2013, the Zhao group[24] designed and synthesized TTFV-arene hybrid molecules with a tweezer-like molecular shape. These molecular tweezers were found to be good synthetic receptors for fullerenes (C_{60} and C_{70}). The synthesis of these compounds was undertaken through a Cu-catalyzed alkyne-azide [3+2] cycloaddition reaction as shown in Scheme 1.11. Interestingly, the TTFV-anthracene hybrid **13b** can selectively

bind to C_{70} fullerene in the presence of a large excess of C_{60}, and such an excellent selectivity arises from the shape of the cavity created by the TTFV moiety of the tweezer which fits very well for ellipsoidal C_{70} fullerene (see the modeling results shown in Figure 1.3).

In the same paper, TTFV **12** was reported to couple with different diazidoarene *via* the CuAAC reaction. The click reactions led to a one-pot cyclization process and formation of [2 + 2] cycloadducts **14** in very good yields (Scheme 1.12). The Cu(I) catalyst is believed to participate in a templating effect, aside from its catalytic function, to produce the macrocycles in high yields. The triazole group resulting from the click reaction is known to coordinate to transition metal ions such as (Cu^+) to form stable complexes. This coordination can pre-organize the reactive intermediates to favour macrocyclization over other possible oligomerization reactions.

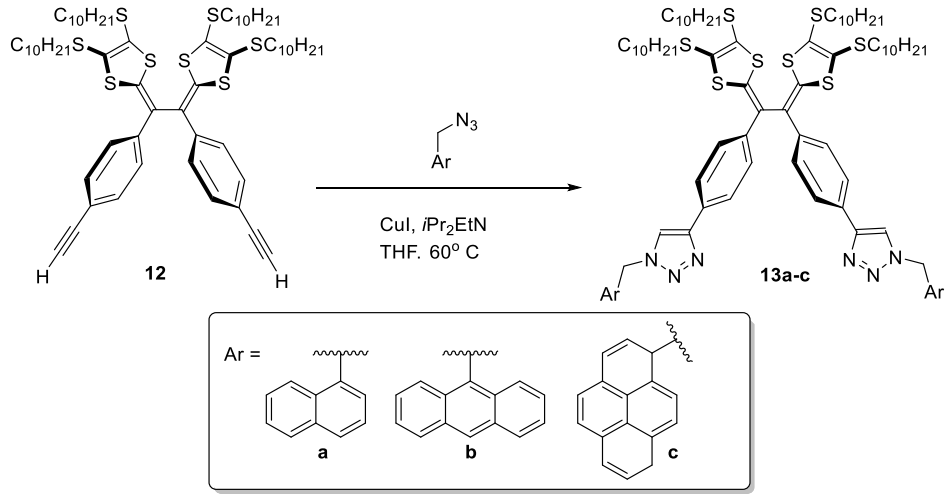

Scheme 1.11: Synthesis of TTFV-arene tweezers by click reactions.[24]

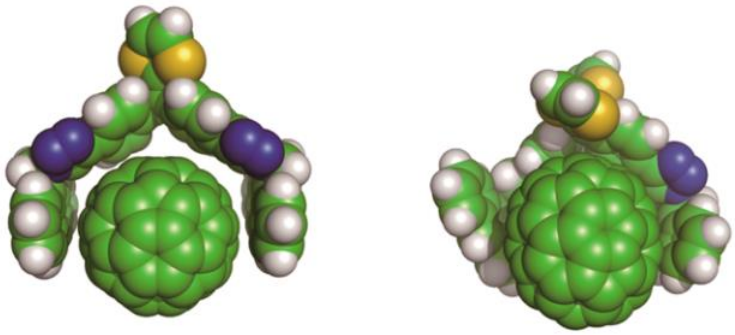

Figure 1.3: Optimized molecular structures for the 1:1 complexes of **13b** with C_{60} (left), and **13b** with C_{70} (right). Reprinted with permission from {Mulla, K.; Shaik, H.; Thompson, D. W.; Zhao, Y. *Org. Lett*. **2013**, *15*, 4532-4535}. Copyright {2013} American Chemical Society.

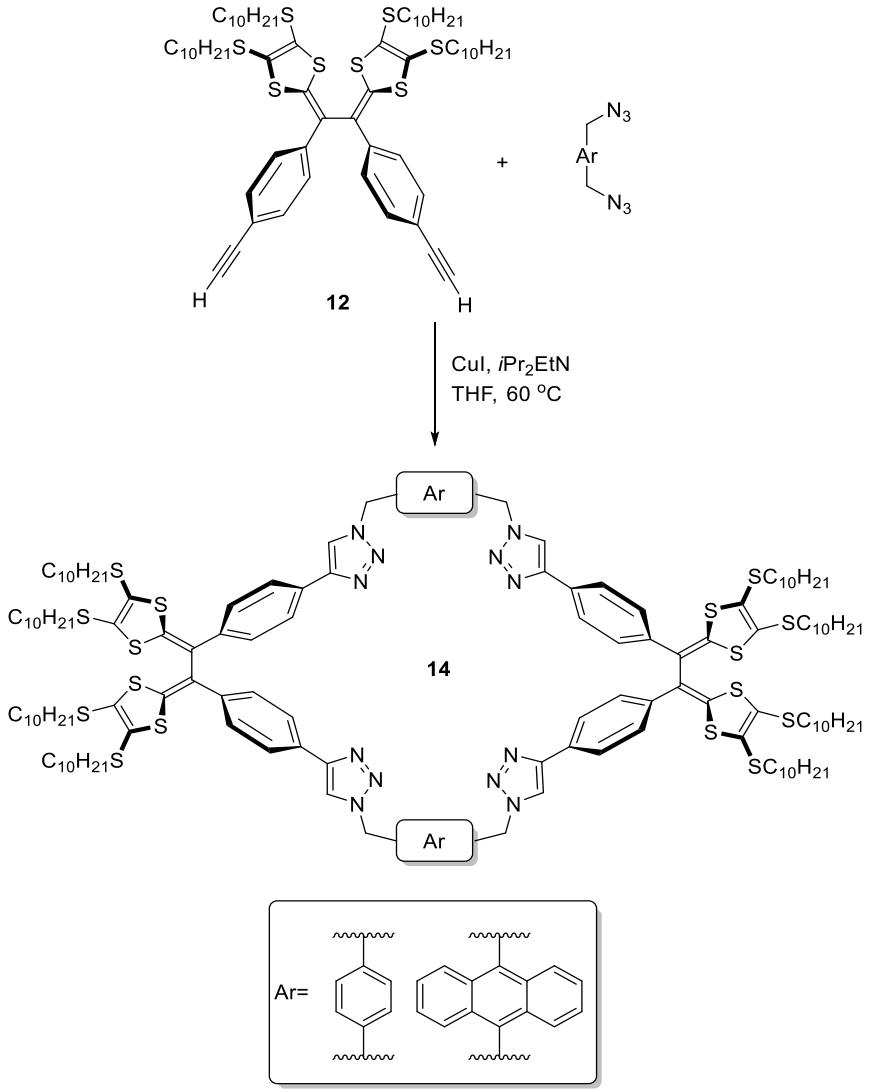

Scheme 1.12: Synthesis of TTFV-based macrocycles **14** via click reactions.[24]

In a very recent study on the application of TTFVs in molecular machines,[25] Chen and Zhao reported a redox-regulated TTFV molecular rotary device (Scheme 1.13). Dynamic NMR studies showed that oxidation of the TTFV moiety in this redox-active gearset caused its two triptycyl units to rotate at a faster rate than in the neutral state as a result of the dramatic conformational changes after oxidation on the TTFV moiety.

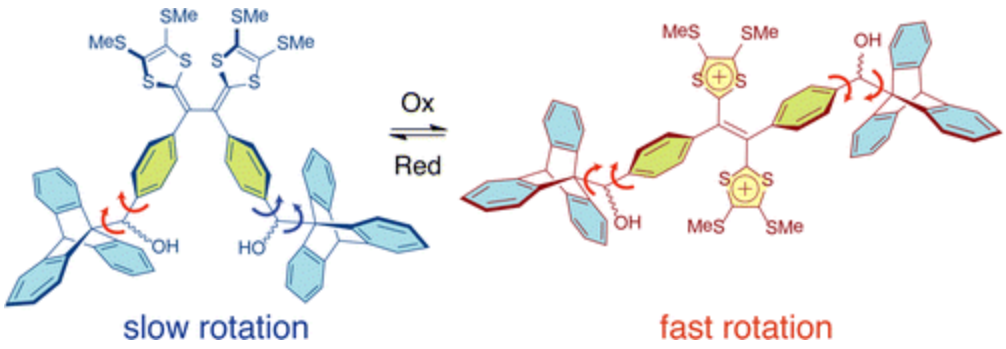

Scheme 1.13: Redox-regulated rotary motion of bis(9-triptycyl)-TTFV system. Reprinted with permission from {Chen, G.; Zhao, Y. *Org. Lett*. **2014**, *16*, 668-671}. Copyright {2014}American Chemical Society.

TTFV compounds that have carboxyl groups are expected to be intriguing candidates for redox-active organic ligands. For example, the carboxyl-substituted TTFV compound **15** (Scheme 1.14) was synthesized and used as a ligand to coordinate with Zn(II) ions in order to form a stable Zn-TTFV coordination polymer.[26] Interestingly, the polymer retains the redox activity and electrochemical reactivity of its TTFV ligand in the solid state. Moreover, the polymer was found to possess microporosity and a large surface area, with a BET surface of 148.2 m^2 g^{-1} and an average pore diameter of 10.2 nm.[26]

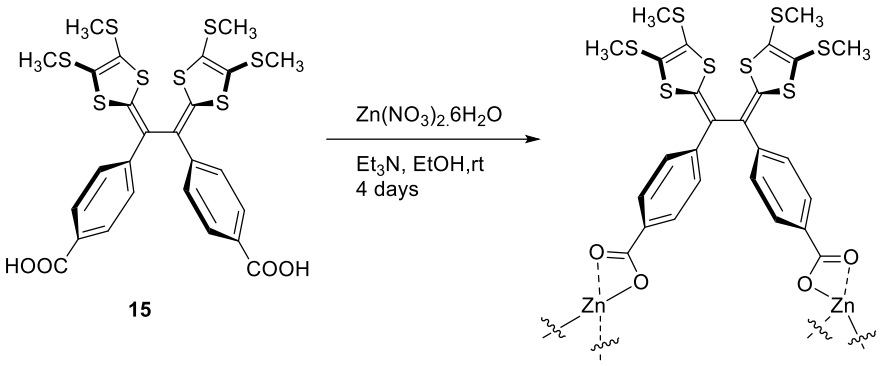

Scheme 1.14: Complexation of compounds **15** with Zn(II) ions.

1.1.5 Anthraquinoid-type exTTFs

TTFAQs are an important class of π-extended TTFs, containing anthraquinoid-type conjugated π-linkage located between the two dithiole rings. In 1978, Akiba and co-workers reported the synthesis of the first TTFAQ **17** through a Horner–Wadsworth-Emmons (HWE) reaction between anthraquinone and a phosphonate-stabilized carbanion generated *in situ* from deprotonation of compound **16** under relatively mild conditions (Scheme 1.15).[27] Because some compounds are not stable in basic media and the preparation of the phosphonate is usually time-consuming and costly, the HWE synthetic strategy may not always be the best for making TTFAQs. On the other hand, TTFAQs can be prepared by the direct coupling of the anthraquinone with a 1,3-dithiole-2-thione precursor in the presence of a large excess of trialkyl phosphite (e.g., $P(OCH_3)_3$) at relatively high temperatures.

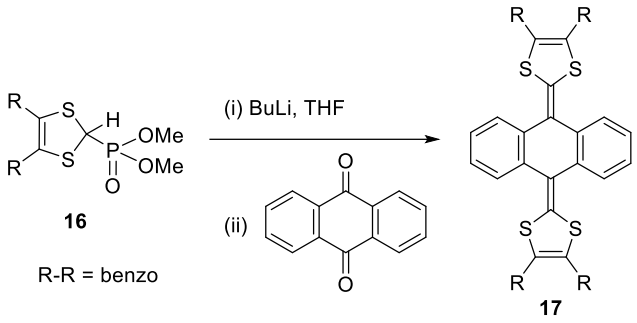

Scheme 1.15: Synthesis of TTFAQ **17** by the HWE reaction.

In the neutral state, TTFAQ has a saddle-like molecular shape which minimizes the steric interactions between the sulfur atoms in the dithiole rings and the adjacent hydrogen atoms on the central anthraquinoid moiety. Upon oxidation, TTFAQ releases two π-electrons simultaneously to form a stable dication with a dramatic structural change (Scheme 1.16). In the dicationic state, the central unit takes an anthracene structure and becomes planar. The positive charges are mainly located on the two dithiolium groups which rotate to be perpendicular to the central anthracene plane to reduce electrostatic repulsion (see Figure 1.4).[5,28]

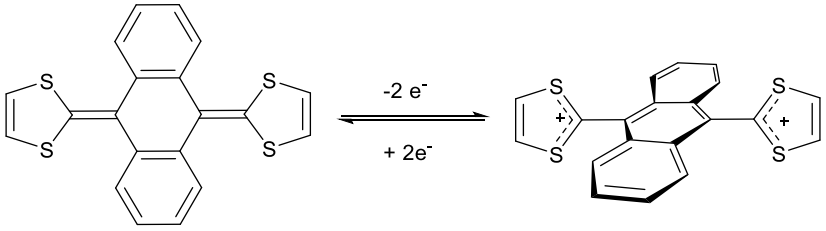

Scheme 1.16: Two-electron oxidation of TTFAQ.

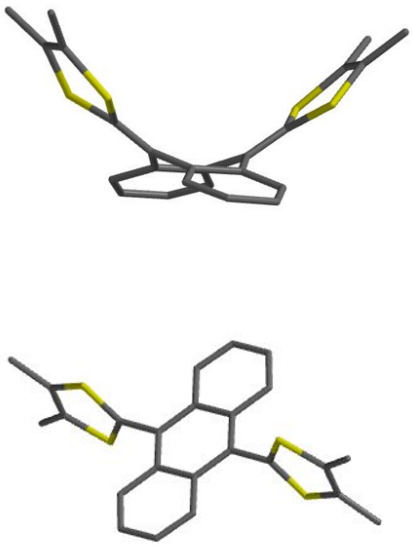

Figure 1.4: Conformations of TTFAQ in neutral (top) and dicationic (CCDC number: 1186299) (bottom) states (CCDC number: 1186300).The drawing is reproduced from the crystallographic data stored at the Cambridge Crystallographic Data Center (CCDC).

Because of their strong electron-donating ability and redox activity, TTFAQ derivatives can be used as electron donors for organic solar cells,[29,30] ion sensors,[31] molecular receptors.[32,33] In 2006, Martín *et al*. reported the first TTFAQ-based receptor **18** for fullerene in aromatic solvents (Scheme 1.17). Receptor **18** was synthesized from available exTTF methyl alcohol and commercially available isophthaloyl dichloride. The combination of two exTTF units and an isophthalate diester gives **18** a concave molecular shape that facilitates non-covalent interactions with C_{60}.[34]

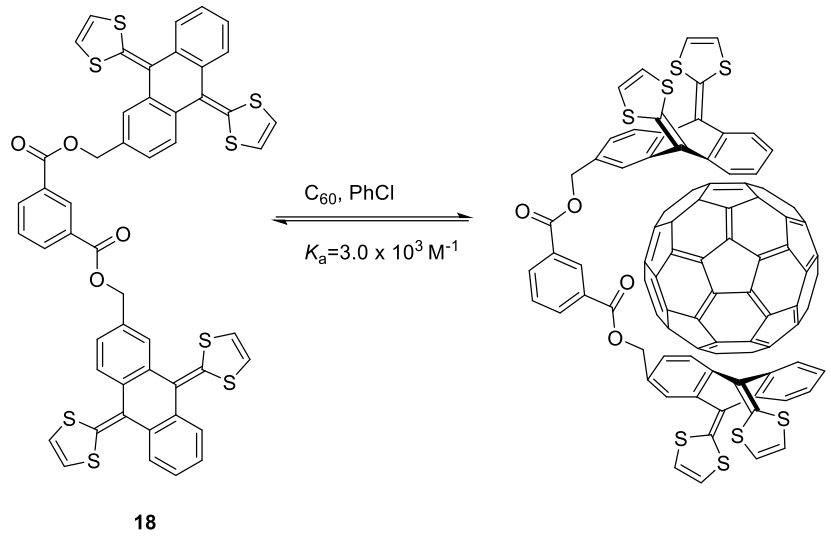

Scheme 1.17: Complexation of TTFAQ receptor **18** with C_{60} in PhCl.

The synthesis of chemical sensors containing exTTFs as the redox-active components is usually more tedious and difficult than the synthesis of systems carrying simple TTF groups. The synthetic challenges account for the family of exTTF-based chemical sensors still being relatively small. In 2010 Zhao *et al*. designed and synthesized a biscrown-annulated TTFAQ **19** as an electrochemical sensor for metal ions. The compound was found to show a high sensitivity for the large alkaline earth metal cation Ba^{2+}. Photoinduced electron transfer (PET) from the TTFAQ donor to the anthracene unit of the uncomplexed TTFAQ **19** quenched the fluorescence (turn off). After complexation with a metal cation, the electron-donating ability of the TTFAQ moiety is attenuated due to the cation-π interaction. This in turn suppresses the PET process and therefore increases the fluorescence of the anthracene group (turn on) (Scheme 1.18).[35]

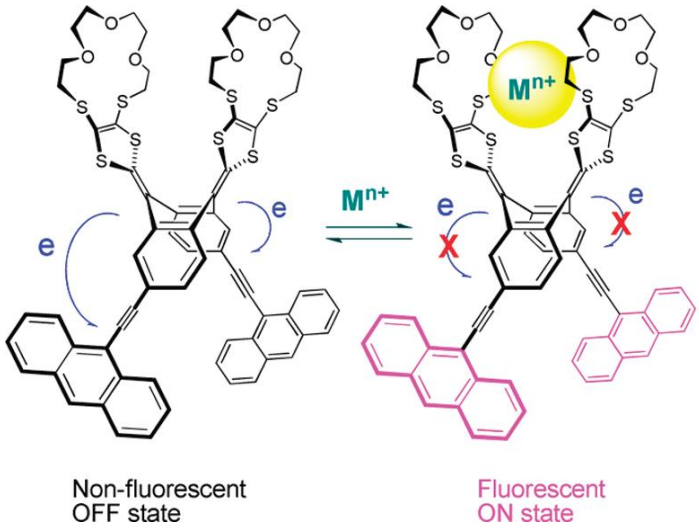

Scheme 1.18: TTFAQ **19** as a fluorescence turn-on sensor for metal ions. Reprinted with permission from {Shao, M.; Dongare, P.; Dawe, L.; Thompson, D.; Zhao, Y**.** *Org. Lett.* **2010,** *12*, 3050–3053}. Copyright {2010} American Chemical Society.

Recently, Misaki *et al.*[36] developed a new class of multiply fused π-electron donors containing extended TTF with an anthraquinoid spacer (**20** and **21**, Figure 1.5). The anthraquinoid units are known to adopt a saddle-like conformation. Because both compounds **20** and **21** possess multiple anthraquinoid moieties, they can have two and three conformational isomers; for example, transoid and cisoid isomers for **20**, and transoid−transoid, transoid−cisoid, and cisoid−cisoid combinations for **21**. Density functional theory (DFT) with the B3LYP/6–31G level of theory calculations for **21** showed that the transoid−transoid isomer is slightly more stable than the transoid−cisoid isomer by 0.25 kcal mol^{-1}. However, X-ray structural analysis (Figure 1.6) shows that the molecule adopts a transoid−cisoid conformation, which is related to the lattice energy and the intermolecular interactions of the transoid−cisoid conformation. On the other hand, variable temperature (VT) NMR analysis indicated that various isomers of **20** or **21** co-existed in solution at room temperature.

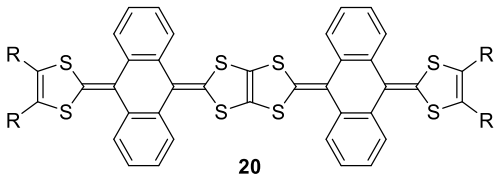

20

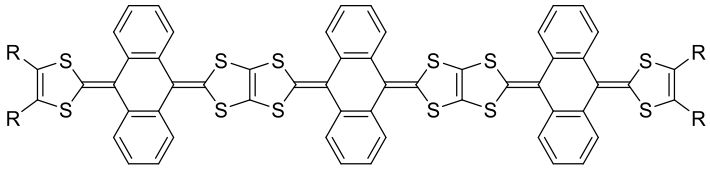

21

Figure 1.5 Structures of multiply fused TTFAQ derivatives **20** and **21**.[36]

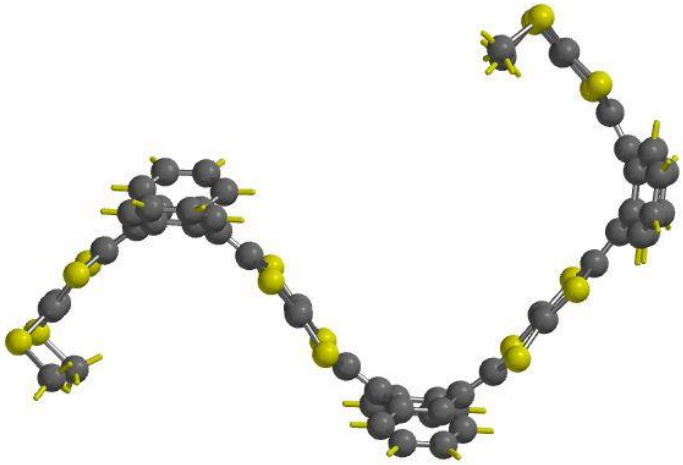

Figure 1.6: Crystal structure of **21**, R = CH_3. The drawing is re-produced from the data stored at the Cambridge Crystallographic Data Center (CCDC), CCDC number: 1510578.[36]

1.2 Polyacenes and Polycyclic Aromatic Hydrocarbons (PAHs)

1.2.1 Introduction to Acenes

Acenes (Figure 1.5) are class of polycyclic aromatic hydrocarbons (PAHs) made up of planar sets of linearly fused benzene rings. Acenes have unique optoelectronic properties that make them highly useful in molecular electronic devices such as organic light-emitting diodes (OLEDs)[37,38] and organic field-effect transistors (OFETs).[39,40] In addition, oligoacenes are the building blocks of important carbon materials such as graphite and carbon nanotubes.

The small members of the acene family, benzene to anthracene, are found in nature and can be extracted from coal. However, acenes higher than anthracene can only be obtained by multi-step syntheses. Benzene is a very stable hydrocarbon due to its aromaticity. However, large acenes starting from heptacene are reactive and can easily decompose through photoinduced oxidation[41-43] or through dimerization or oligomerization processes.[44] According to Clar's aromatic sextets rules, acene owns only one aromatic sextet over the whole conjugated system as shown in Figure 1.6. As a result, a rapid decrease in the HOMO–LUMO gap occurs, increasing their chemical reactivity with each additional fused ring.[45]

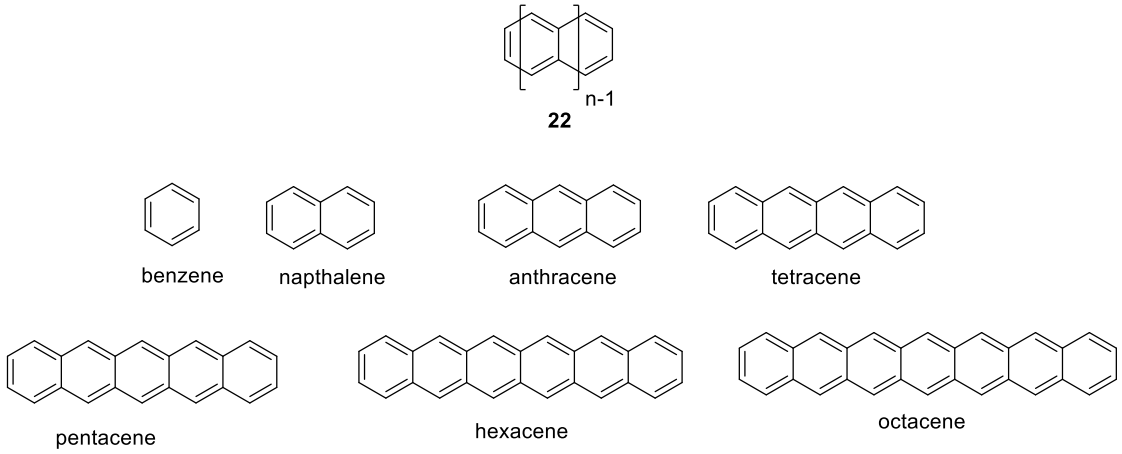

Figure 1.7: Structures of representative acenes.

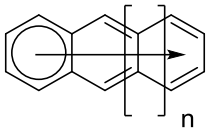

Figure 1.8: Clar's sextet in an acene.

1.2.2 Synthesis of Acenes

Although acenes have promising optoelectronic properties, extended acenes as functional materials are limited, and this is mainly due to their low solubility and relatively low chemical stability. The development of new methods is necessary for the preparation and modification of higher acenes with better processibility and stability. Recently, a wide class of stabilized acene derivatives has been synthesized using different strategies. There is no general approach for the synthesis and functionalization of linearly condensed ring systems. However, the synthesis of polyacene systems can be categorized according to the type of precursors being used (Scheme 1.19).[46]

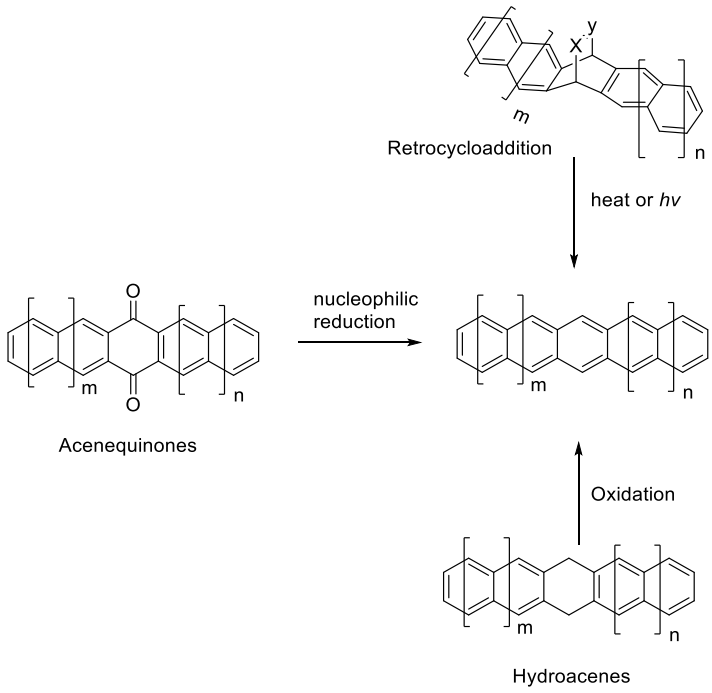

Scheme 1.19: Synthetic approaches for higher acenes.[46]

1.2.3 Pentacene

Pentacene is a deep blue crystalline material that has low solubility in most organic solvents, producing bright pink solutions due to its intense red fluorescence.[47] Pentacene was first synthesized by Clar and John.[48-50] The precursor was *m*-xylophenone which was subjected to a vigorous Friedel−Crafts reaction to yield 4,6-dibenzoyl-1,3-dimethylbenzene **22**, from which dihydropentacene **23** was obtained by copper-promoted thermal annulation. Finally, dehydrogenation of **23** in boiling nitrobenzene in the presence of phenanthraquinone gave the pentacene product (Scheme 1.20A). Nowadays, pentacene is usually synthesized by a simple reduction of pentacenequinone **24**, which can be prepared by a fourfold aldol condensation

between phthalaldehyde and 1,4-cyclohexanedione as shown in Scheme 1.20B.

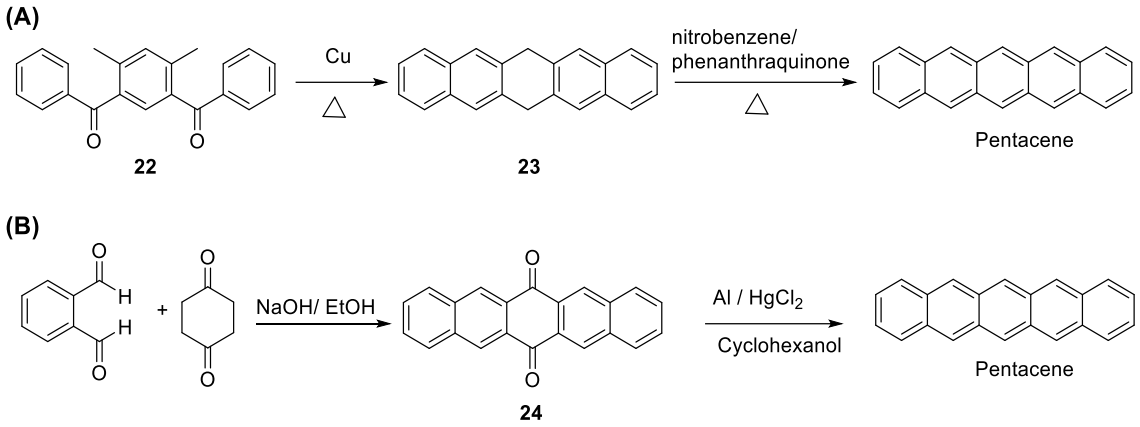

Scheme 1.20: Two synthetic approaches for pentacene.

Furthermore, pentacene can be obtained by stepwise reduction of 6,13-pentacenequinones **24**. The reduction of **24** is carried out using a reducing agent like $NaBH_4$ to provide diol compound **25,** which then can be treated with a Lewis acid ($SnCl_2$) in aqueous acid to yield the target pentacene in a good yield (Scheme 1.21).[51]

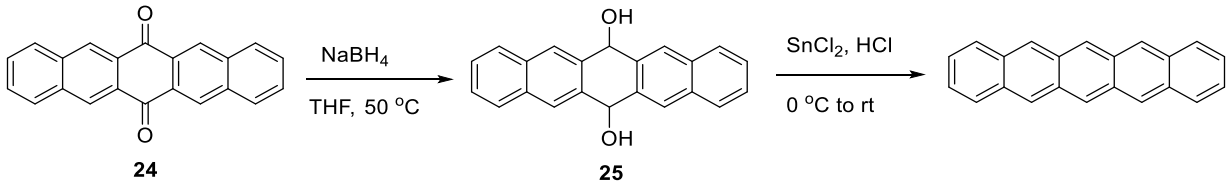

Scheme 1.21: Synthesis of pentacene by reduction of pentacenedione **24**.

In the presence of molecular oxygen, pentacene is known to have a half-life of a few minutes in solution.[52] Pentacene can react with dioxygen to give an endoperoxide. This reactivity

can be explained by the Clar's sextet rules. The breaking of π-conjugation of at the middle ring converts the pentacene into two more stable naphthalene units, each showing a sextet character (Scheme1.22). In the absence of oxygen, pentacene can dimerize upon photo-irradiation to form a colourless "butterfly dimer" **26** (Figure 1.7). For example, dimer **26** was synthesized by irradiating a solution of pentacene at 120 ^{o}C in deoxygenated 1-chloronaphthalene. Dimer **26** has low solubility in organic solvents and as a result was formed as a white precipitate over a period of several days.[53]

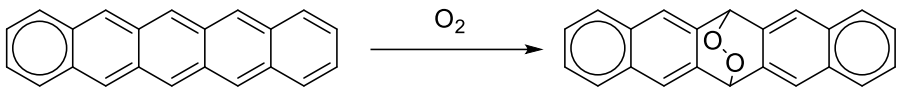

Scheme1.22: Formation of an endoperoxide.

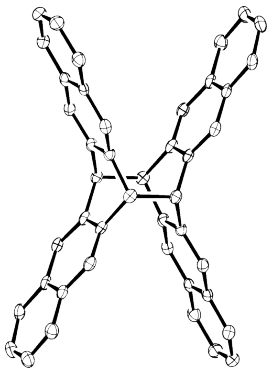

Figure 1.9: Molecular structure of butterfly dimer **26.** Reprinted with permission from {Berg, O.; Chronister, E. L.; Yamashta, G. W.; Scott, G. W.; Sweet, R. M.; Calabrese, J. *J. Phys. Chem. A* **1999**, *103*, 2451- 2459}. Copyright {1999} American Chemical Society.

To overcome the extremely low solubility of pentacene as well as its poor stability, two methods have been developed. The first method is through the formation of Diels-Alder adducts of pentacene precursors. These precursors have a butterfly-like molecular shape, which makes them more soluble in organic solvents than planar pentacene and thus can be easily purified and deposited from solution. Müllen *et al*. first reported this method in 1996.[54] A device containing a high-quality film of pentacene was fabricated in two steps. First, the precursor compound **27** was deposited on a substrate by spin coating of a solution of **27** in dichloromethane. The resulting film was then subjected to heating at 200 °C, providing pentacene through a retro-Diels-Alder reaction as shown in Scheme 1.23.

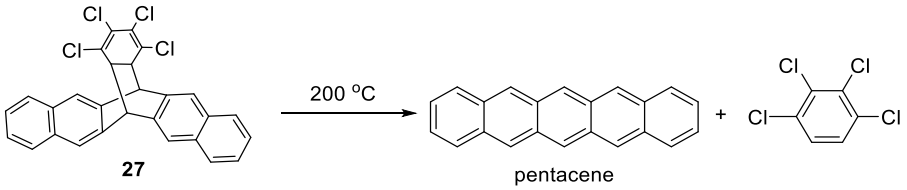

Scheme 1.23: Conversion of the precursor **27** into pentacene.

Later on, a series of different precursors (**28a-c**) containing *N*-sulfinylamide groups was prepared.[55-57] These precursors add a number of advantages to the previous one. The first advantage is the use of a one-step synthetic approach instead of five steps (Scheme 1.19) to make pentacene**.** Second, the removal of the leaving groups is much easier and requires lower temperature, since the elimination involves the cleavages of C–S and C–N bonds which are much easier to break than the strong C–C bonds in the retro-Diels-Alder process of **27** (Scheme 1.24).

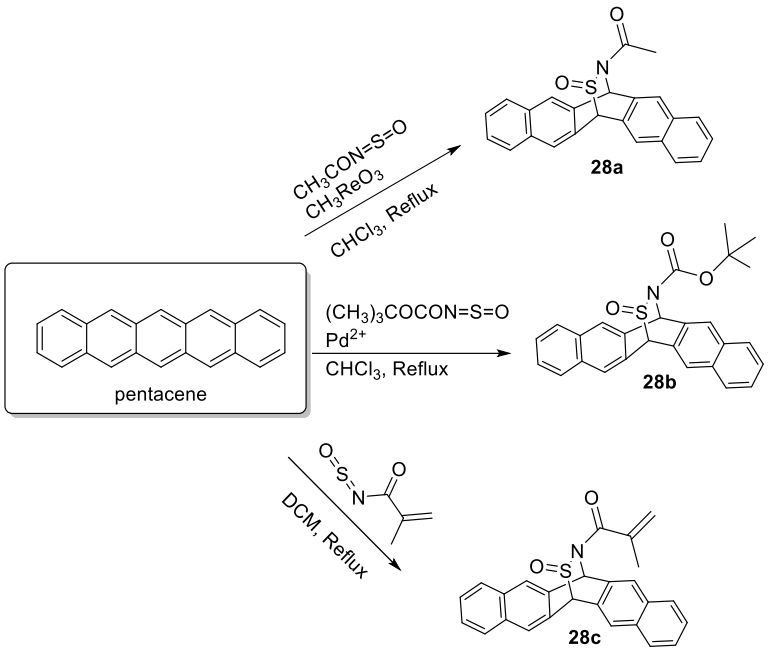

Scheme 1.24: Conversion of pentacene for precursors **28a-c.**

Another method to increase the stability and solubility of pentacene is introducing substituents on the aromatic core. Substituents on pentacene can increase the solubility, which make the purification easier by using routine techniques such as crystallization and chromatography. On the other hand, substituents can also improve the stability of pentacene against oxygen, especially when they are attached to the central ring. Moreover, the presence of substituents can increase and modulate intermolecular π-stacking, leading to enhanced intermolecular orbital overlap between the pentacene moieties and hence improve charge carrier transport. Acenequinones are common precursors used for the preparation of pentacene derivatives by nucleophilic addition of organometallic species followed by reductive aromatization. In 2001, Anthony and co-workers reported the synthesis of 6,13-bis(triisopropylsilylethynyl) pentacene **29** from pentacene-6,13-dione through two steps (Scheme 1.25). The first step is a double addition of an alkynyl Gringard reagent to pentacenedione **24**. After that, a reduction was performed using

$SnCl_2$/HCl to give alkynylated pentacene **29**.[58] In addition to the improved stability and solubility in comparison with the parent pentacene, **29** also shows a unique arrangement of molecules in the solid state which significantly improves the conductivity. Following Anthony's work, a series of 6,13-dialkynyl substituted pentacenes has been synthesized and studied as organic semiconductors.[59-65]

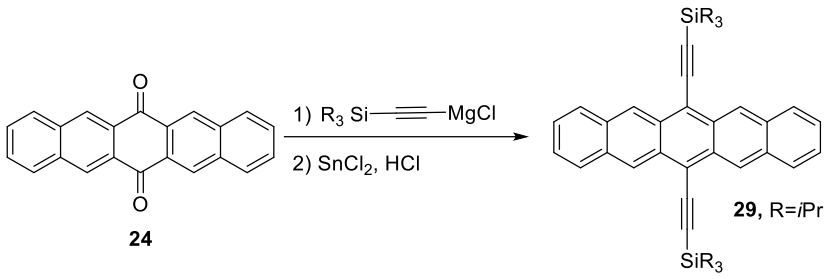

Scheme 1.25: Synthesis of 6,13-bis(triisopropylsilylethynyl) pentacene **29**.

Recently Chi and co-workers designed and synthesized bisindeno-annulated pentacenes **31.** This system has two aryl groups fused onto each side of pentacene along the peri-position. The fusion of two indeno units to the pentacene moiety enhances the electronic properties of these compounds relative to pentacene. Moreover, functionalization along the peri-positions increases the solubility as well as enhancing the stability of **31**, with a half-life time of 11.2 (**31a**) and 32.0 (**31b**) days under light and air conditions. Bis(indeno)-annulated pentacenes **31** were simply synthesized by $FeCl_3$-mediated Scholl reactions on 6,13-diaryl pentacene precursors **30** (Scheme 1.26).[66]

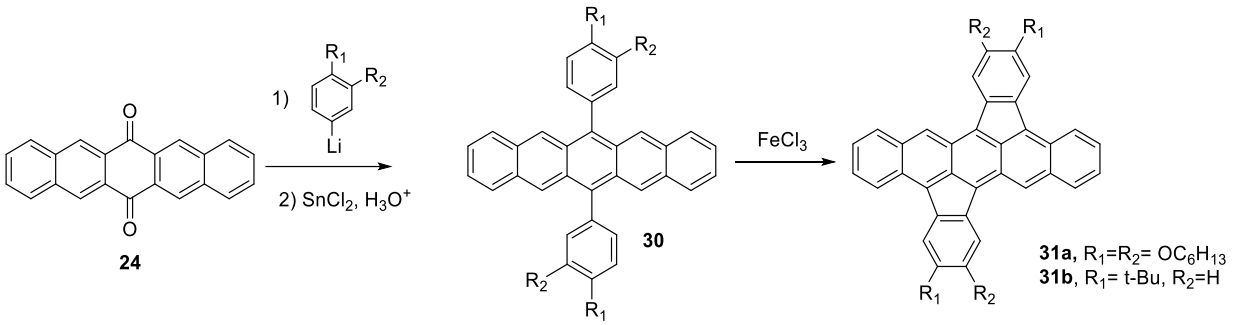

Scheme 1.26: Synthesis of bisindeno-annulated pentacenes **31**.

A similar system was synthesized by Plunkett and co-workers[67] (Scheme 1.27) using the Pd-catalyzed cyclopentyl-annulation of a partially unsaturated pentacene precursor **34** with several diaryl acetylenes. Anthracene-based cyclopentyl-fused polycyclic aromatic hydrocarbons (CP-PAHs) **35** was generated, which went through dehydrogenation aromatization in the presence of 2,3-dichloro-5,6-dicyano-1,4-benzoquinone (DDQ) to give stabilized cyclopentyl-annulated pentacenes **36**. The photostability of these compounds was compared with that of the known TIPS-pentacene derivative and the results showed much better stability. In the meantime, the cyclopentyl-annulated pentacenes were found to have narrow HOMO-LUMO energy gaps and behave as strong electron acceptors.

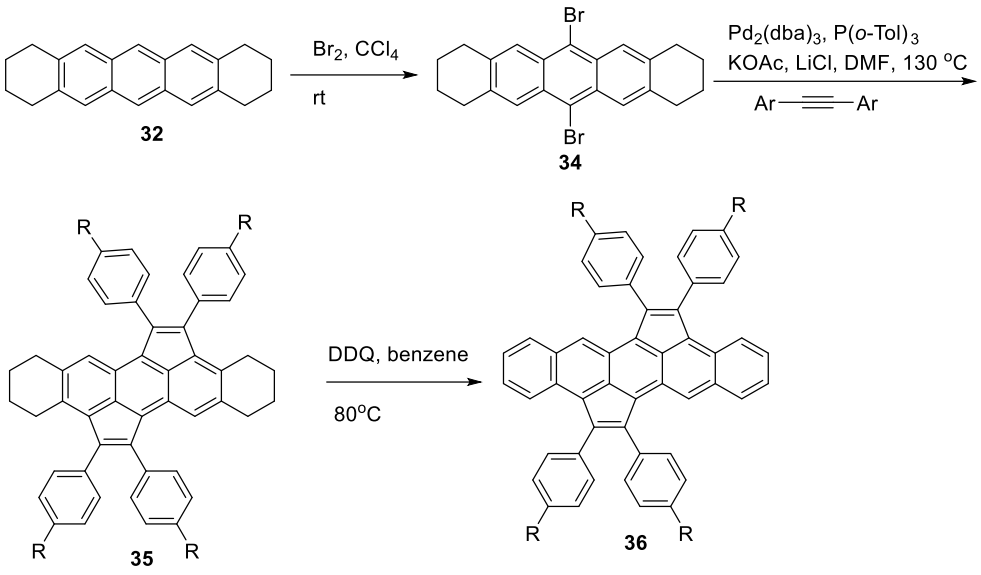

Scheme 1.27: Synthesis of cyclopentyl-annulated pentacenes.

1.2.3 Pentacene-5,7,12,14-tetraone

Pentacene-5,7,12,14-tetraone (**37**) is a flat linear acene derivative consisting of two fused anthraquinone moieties. Mills and Mills, using the Friedel-Craft acylation followed by cyclization in sulfuric acid, synthesized this compound for the first time in 1912. Pentacenetetraone **37** is sparsely soluble in common organic solvents.[68] Baxter and co-workers reported the synthesis of **37** using a much easier method, starting from commercially available and inexpensive starting materials. As shown in Scheme 1.28, compound **37** was obtained from 2-methyl-1,4-naphthoquinone (**38**) in the presence of a secondary amine such as diethylamine (Et_2NH) and using ethanol as solvent. The poorly soluble product was purified by recrystallization.[69]

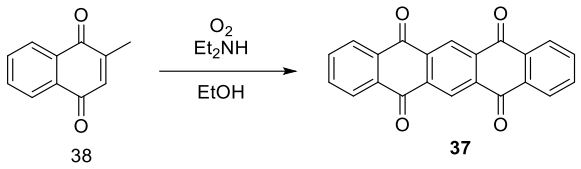

Scheme 1.28: Synthesis of pentacene-5,7,12,14-tetraone (**37**) from 2-methyl-1,4-naphthoquinone (**38**).

Although pentacenetetraone **37** can serves as a unique building block for the creation of large acenes and PAHs, few studies have been carried on this compound so far. Dehaen and co-workers[70] prepared the tetrasubstituted pentacene (Scheme 1.29). They followed the same methodology that was used to prepare the disubstituted pentacene. Pentacenetetraone **37** was added to the solution of aryllithium derivatives in dry THF to form 5,7,12,14-tetraarylpentacene-5′,7′,12′,14′-tetrol **39** as a mixture of diastereomers. Pentacenes **40** were obtained by reductive elimination of these tetrols.

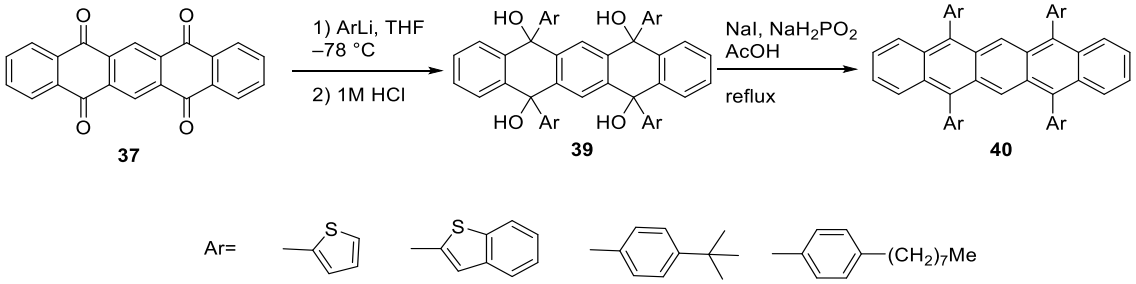

Scheme 1.29: Synthesis of tetrasubstituted pentacene **40**.

In 2009 the research group of Yamashita[71] prepared a class of 7,14-disubsituted pentacene-5,12-diones **42** through nucleophilic substitution reactions of pentacene-5,7,12,14- tetraone (**37**) with three different types of carbanions. About 2.5 equivalents of 2,6-difluorophenyllithium, triisopropylsilylethynyllithium (TIPSLi), or thienyllithium were used to give the 7,14-disubstituted diols **41** as shown in Scheme 1.30. The obtained intermediate was then subjected to a dehydroxylation reaction using tin(II) chloride under acidic conditions to give compounds **42**. When phenyllithium was used (Scheme 1.24), only a tetrasubstituted derivative was obtained. However, the use of 6 equivalents of 2,6-difluorinated phenyllithium leads to the formation of 7,14-disubstituted diol as the major product. For the thiophene derivatives, alkyl groups were introduced to increase steric repulsion.

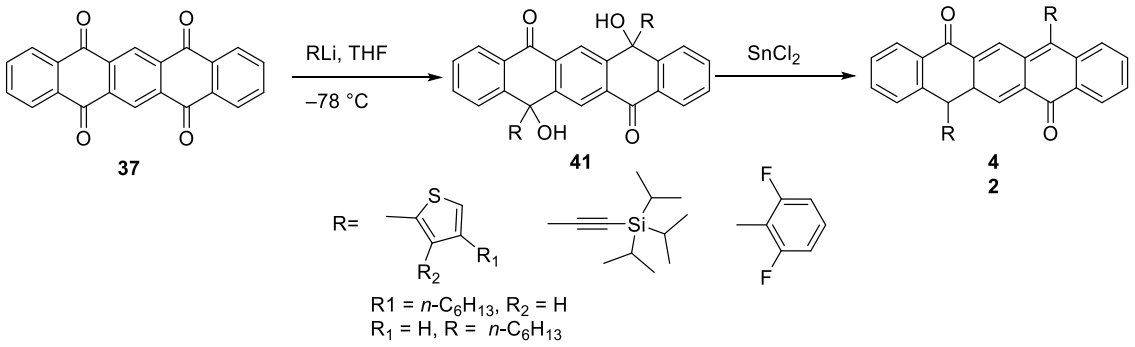

Scheme 1.30: Synthesis of disubstituted pentacene-5,12-diones **42**.

1.3 Graphene and Graphene-like Polycyclic Aromatic Hydrocarbons (PAHs)

Graphene is an allotrope of carbon in the form of a two-dimensional hexagonal lattice of sp^2-hybridized carbons. Graphene has the basic structural element of other allotropes such as graphite, carbon nanotubes, and fullerenes. It was believed that, based on theoretical calculations,

a graphene sheet was thermodynamically unstable in comparison with other fullerene structures.[72] Moreover, several experimental methods were devised to synthesize graphene, but none of these methods produced perfect monolayers of graphene.[73-76] A major breakthrough was made in 2004, when Andre Geim and Konstantin Novoselov[76] used a simple "peeling" method to isolate graphene in high quality with size in hundreds of microns. They used a tape to extract single layers of graphene from graphite flakes. The high quality graphene layers exhibited amazing properties, such as high carrier mobility,[77] high transparency,[78] large specific surface area,[79] high Young's modulus,[80] and excellent thermal conductivity.[81] Since then, functionalization of graphenes as well as exploring their application has grown exponentially. The synthesis of graphene-like molecules using organic synthetic protocols has recently caught increasing interest among many research groups. However, most of the synthesis protocols were not efficient enough due to the low solubility of the products and the occurrence of side reactions.[82-85] In 2008, Mullen's group reported the synthesis of soluble linear two-dimensional graphene nanoribbons **46** with lengths of up to 12 nm. [86] The Suzuki-Miyaura reaction was used as a key step in the synthesis by polymerization of compound **43** with diiodobenzene **44** at 120 °C to produce the polyphenylenes **45** in good yields. The target polymers **46** were then obtained through intramolecular Scholl reaction of **45** using $FeCl_3$ as the oxidative reagent at room temperature (Scheme 1.31). Various microscopic studies, such as SEM and TEM, of these graphene ribbons revealed a high tendency of these compounds to self-assemble into well-ordered layers of graphene.

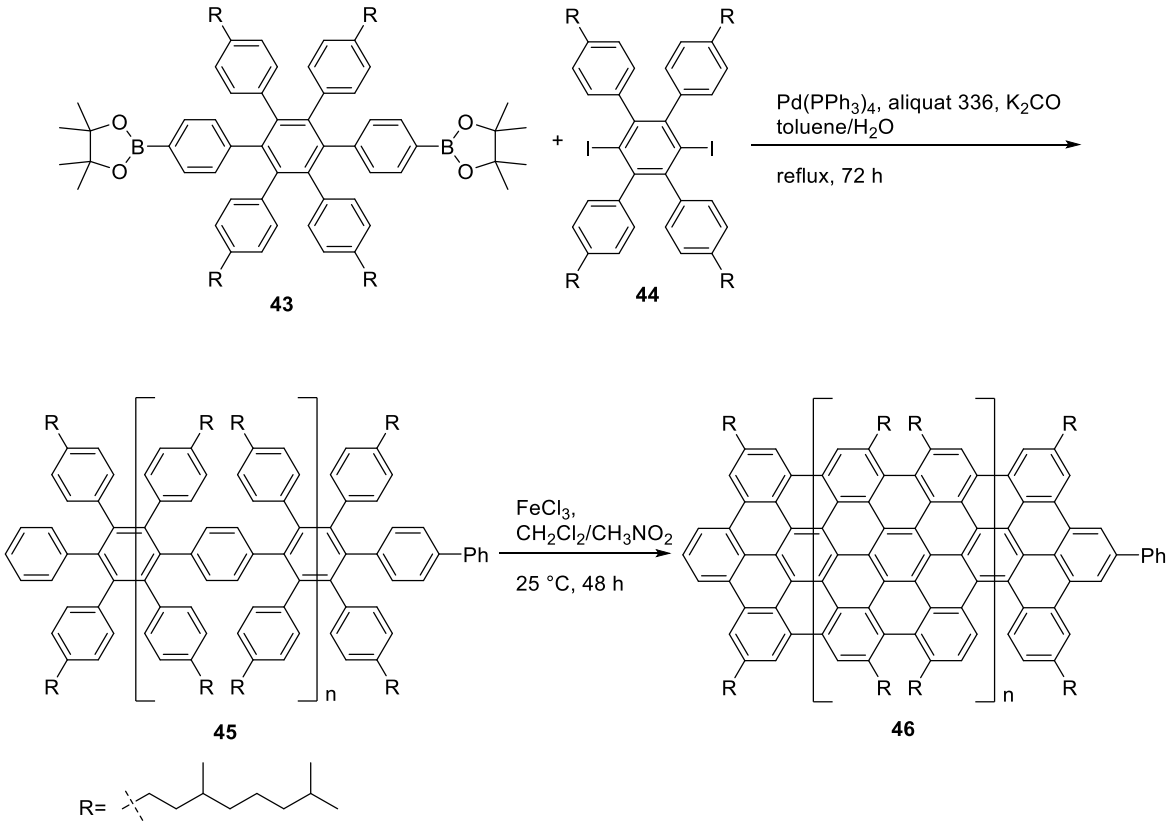

Scheme 1.31: Synthesis of two-dimensional graphene nanoribbons **46**.

Recently, Morin and co-workers[87] reported a new strategy for the preparation of novel nanographenes and graphene nanoribbons fragments **48**. The photochemical cyclodehydrochlorination (CDHC) reaction was used by irradiation of various aryl chlorides **47** in acetone in the presence of a base or in pure benzene (Scheme 1.32). Pure products were obtained in good yields by simple filtration at the end of the reaction. Interestingly, this reaction was found to be compatible for the preparation of nanographenes fused with both electron-rich (thiophene) and electron-poor (pyridine) moieties. Moreover, based on kinetic studies this CDHC reaction under the conditions used was found to be a very fast reaction, some of these reactions completed within minutes.

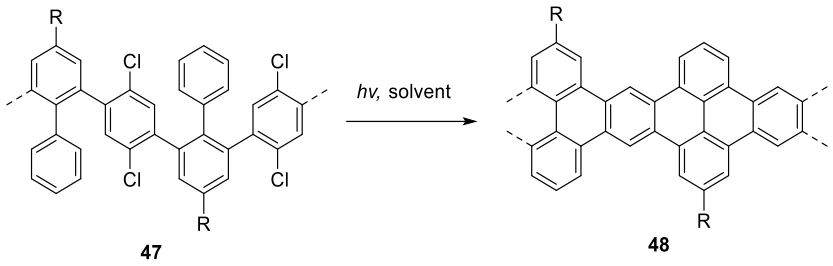

Scheme 1.32: Cyclodehydrochlorination reaction.

The research group of Chalifoux[88] recently devised a new efficient methodology for the synthesis of very narrow (*ca*. 0.5 nm) and highly soluble graphene nanoribbons **50**. These nanoribbons were obtained by using Brønsted acid-promoted alkyne benzannulation of a linear poly(2,6-dialkynyl-*p*-phenylene) (Scheme 1.33). The cyclization process was done in two steps. In the first step polymer **49** was treated with excess TFA at room temperature for 24 h. Significant cyclization was observed by ^{1}H NMR analysis at this stage, but complete cyclization was not achieved. In the second step, triflic acid was added at −40 °C for 1 h to complete the cyclization.

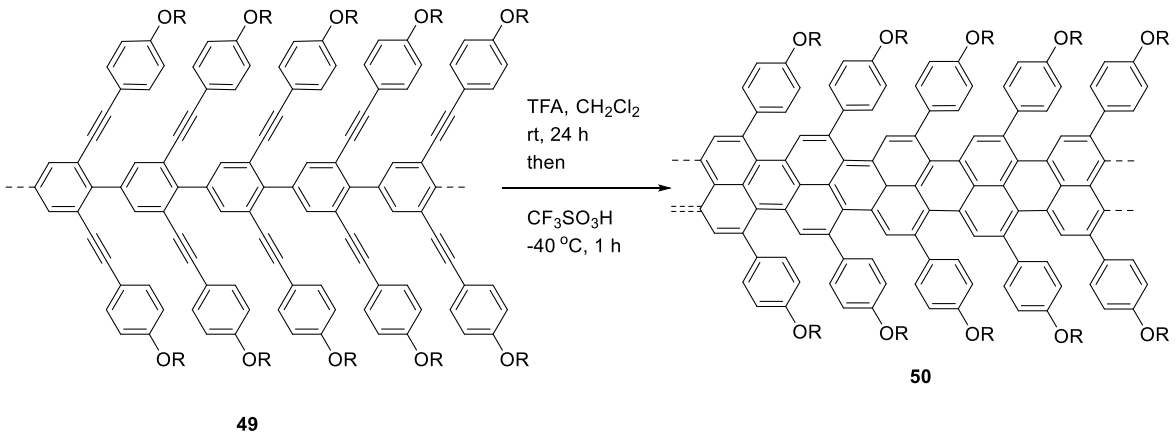

Scheme 1.33: Synthesis of GNRs *via* an alkyne benzannulation strategy.

1.4 Motivations and Structure of This Thesis

The aim of this PhD thesis work was focused on the development of new functional organic materials based on different classes of π-conjugated molecular building blocks, such as TTFV, pyrene, and acenes. As mentioned previously, TTFs and their derivatives have excellent electron-donating properties, which make them unique building blocks for the development of new organic conjugated materials. Redox activity can be used as a key factor to control the structural and electronic properties of molecular devices and nanomaterials. On the other hand, pyrene has remarkable photophysical properties and redox activity and has found extensive applications in organic optoelectronic devices. Co-polymer systems that combine both TTFV and pyrenylene systems as repeat units were not reported in the literature until a collaborative research project conducted between the Zhao and Bodwell groups. This project is described in Chapter 2, in which a new π-conjugated co-polymer that has TTFV and pyrene repeat units was synthesized and characterized. Interestingly, the co-polymer was found to exhibit reversible redox activity similar to TTFV, and its self-aggregation behaviour in solution phase showed responsiveness to external

stimuli such as solvent polarity and pH. Dynamic light scattering (DLS) measurements were used to determine the size range of the polymer aggregates.

The major portion of this thesis work was dedicated to the development of new organic materials that contain fused acenes especially the pentacene moiety. Although pentacene is a benchmark organic semiconductor used in thin-film organic devices, its poor solubility presents a considerable barrier to the use of this material in solution during devices fabrication. Consequently, we synthesized a class of soluble π-extended tetrathiafulvalene analogues, by stepwise olefination reactions on pentacene-5,7,12,14-tetraone, which is capable of reversibly revealing and concealing a central pentacene segment under redox control. The structural, electronic, and redox properties of these materials were investigated by NMR, UV-Vis absorption, electrochemical analyses and density functional theory (DFT) calculations and the details are discussed in Chapter 3 of this thesis.

The attachment of alkyne groups to the pentacene moiety can produce new building blocks for a variety of pentacene-based carbon-rich materials. From this perspective and because of the fascinating properties and promising applications of acenes, a class of pentacene-based π-conjugated systems functionalized with geminal enediyne was synthesized from pentacene-5,7,12,14-tetraone. The geminal enediyne-pentacene system was subjected to selective olefination and cross-coupling reactions to yield more extended polymer networks. Chapters 4 and 5 of this thesis describe the detailed investigations on the synthesis and characterization of these new pentacene-based derivatives.

1.5 References

(1) Wudl, F.; Smith, G. M.; Hufnagel, E. J. *J. Chem. Soc. D* **1970**, 1453-1454.

(2) Rovira, C. *Chem. Rev.* **2004**, *104*, 5289-5318.

(3) Yamada, J.; Sugimoto, T.; Eds., *TTF Chemistry. Fundamentals and Applications of Tetrathiafulvalene*, Springer Verlag, Berlin, 2004.

(4) Frere, P.; Skabara, P. *Chem. Soc. Rev.* **2005**, *34*, 69-98.

(5) Bendikov, M.; Wudl, F.; Perepichka, D. F. *Chem. Rev.* **2004**, *104*, 4891-4946.

(6) Pou-Amérigo, R.; Ortí, E.; Merchán, M.; Rubio, M.; Viruela, P. M. *J. Phys. Chem. A* **2002**, *106*, 631-640.

(7) Bryce, M. R. *J. Mater. Chem*. **2000**, *10*, 589-598.

(8) Nielsen, M. B.; Lomholt, C. Becher. J. *Chem. Soc. Rev.* **2000**, *29*, 153-164.

(9) Bryce, M. R. *Adv. Mater.* **1999**, *11*, 11- 23.

(10) Jorgensen, T.; Hansen, T. K.; Becher. J. *Chem. Soc. Rev*. **1994**, *23*, 41-51.

(11) Day, P.; Kurmoo, M. *J. Mater. Chem*. **1997**, *7*, 1291-1295.

(12) Fabre, J. *Chem. Rev*. **2004**, *104*, 5133-5150.

(13) Nielsen, M. B.; Sauer, S. P. *Chem. Phys. Lett*. **2008**, *453*, 136-139.

(14) Carlier, R.; Hapiot, P.; Lorcy, D.; Robert, A.; Tallec, A. *Electrochim. Acta* **2001**, *46*, 3269-3277.

(15) Bellec, N.; Boubekeur, K.; Carlier, R.; Hapiot, P.; Lorcy, D.; Tallec, A. *J. Phys. Chem. A* **2000**, *104*, 9750-9759.

(16) Bryce, M. R.; Coffin, M. A.; Clegg, W. *J. Org. Chem*. **1992**, *57*,1696–1699.

(17) Zhao, Y. M.; Chen, G.; Mulla, K.; Mahmud, I.; Liang, S.; Dongare, P.; Thompson, D. W.; Dawe, L. N.; Bouzan, *S. Pure Appl. Chem*. **2012**, *84*, 1005-1025.

(18) Schou, S. S.; Parker, C. R.; Lincke, K.; Jennum, K.; Vibenholt, J.; Kadziola, A.; Nielsen, M. B. *Synlett* **2013**, *24*, 231-235.

(19) Christensen, C. A.; Batsanov, A. S.; Bryce, M. R. *J. Org*. *Chem*. **2007**, *72*, 1301-1308.

(20) Steimecke, G.; Sieler, H.-J.; Kirmse, R.; Hoyer, E. *Phosphorus and Sulfur and the Related Elements* **1979**, *7*, 49-55.

(21) Parg, R. P.; Kilburn, J. D.; Ryan, T. G. *Synthesis* **1994**, *1994*, 195-198.

(22) Liang, S.; Zhao, Y.; Adronov, A. *J. Am. Chem. Soc*. **2013**, *136*, 970–977.

(23) Khadem, M.; Zhao, Y. *J. Org. Chem*. **2015**, *80*, 7419−7429.

(24) Mulla, K.; Shaik, H.; Thompson, D. W.; Zhao, Y. *Org. Lett*. **2013**, *15*, 4532-4535.

(25) Chen, G.; Zhao, Y. *Org. Lett*. **2014**, *16*, 668-671.

(26) Wang, Y.; Zhao, Y. *Beilstein J. Org. Chem.* **2015**, *11*, 957–965.

(27) Akiba, K.; Ishikawa, K.; Inamoto, N. *Bull .Chem. Soc*. *Jpn*. **1978**, *51*, 2674-2683.

(28) Bryce, M. R.; Moore, A. J.; Hasan, M.; Ashwell, G. J.; Frraser, A. T.; Clegg, W.; Hursthouse, M. B.; Karaulov, A. I. *Angew. Chem., Int. Ed. Engl.* **1990**, *29*, 1450-1452.

(29) Martin, N; Sanchez, L; Herranz, M; Illescas, B; Guldi, D. *Acc. Chem. Res.* **2007**, *40*, 1015-1024.

(30) Wenger, S.; Bouit, P.-A.; Chen, Q.; Teuscher, J.; Censo, D. D.; Humphry-Baker, R.; Moser, J.-E.; Delgado, J. L.; Martín, N.; Zakeeruddin, S. M.; Grätzel, M. *J. Am. Chem. Soc*. **2010**, *132*, 5164-5169.

(31) Hardouin-Lerouge, M.; Chesneau, B.; Allain, M.; Hudhomme, P. *J. Org. Chem*. **2012**, *77*, 2441-2445.

(32) Isla, H.; Gallego, M; Perez, E.; Viruela, R; Orti, E; Martin, Na, N. *J. Am. Chem. Soc*. **2010**, *132*, 1772-1773.

(33) Bivaud, S.; Goeb, S.; Croue, V.; Dron, P. I.; Allain, M.; Salle, M. *J. Am. Chem. Soc.* **2013**, *135*, 10018-10021.

(34) Perez, E.; Sanchez, L; Fernandez, G; Martin, N. *J. Am. Chem. Soc*. **2006**, *128*, 7172–7173.

(35) Shao, M.; Dongare, P.; Dawe, L.; Thompson, D.; Zhao, Y**.** *Org. Lett.* **2010,** *12*, 3050–3053.

(36) Ogi, D.; Fujita, Y.; Mori, S.; Shirahata, T.; Misaki, Y. *Org. Lett.* **2016**, *18*, 5868−5871.

(37) Odom, S.; Parkin, S.; Anthony, J. *Org. Lett.* **2003**, *5*, 4245–4248.

(38) Wolak, M.; Jang, B.; Palilis, L.; Kafafi, Z. *J. Phys. Chem. B* **2004**, *108*, 5492–5499.

(39) Wang, C.; Dong, H.; Hu, W.; Liu, Y.; Zhu, D. *Chem. Rev.* **2012**, *112*, 2208–2267.

(40) Allard, S.; Forster, M., Souharce, B.; Thiem, H.; Scherf, U. *Angew. Chem. Int. Ed.* **2008**, *47*, 4070–4098.

(41) Chien, S.; Cheng, M.; Lau, K.; Li, W. *J. Phys. Chem. A* **2005**, *109*, 7509–7518.

(42) Reddy, A.; Bendikov, M. *Chem. Commun.* **2006**, 1179– 1181.

(43) Fudickar, W.; Linker, T. *J. Am. Chem. Soc.* **2012**, *134*, 15071–15082.

(44) Zade, S. S.; Zamoshchik, N.; Reddy, A. R.; Fridman-Marueli, G.; Sheberla, D.; Bendikov, M. *J. Am. Chem. Soc.* **2011**, *133*, 10803–10816.

(45) Bettinger, H. *Pure Appl. Chem.* **2010**, *82*, 905–915.

(46) Dorel. R.; Echavarren, A. *Eur. J. Org. Chem.* **2017**, 14–24.

(47) Birks, B. *Photophysics of Aromatic Molecules*, Wiley-Interscience, New York, **1970**.

(48) Clar, E.; John, F. *Chem. Ber.* **1929**, *62*, 3021-3029.

(49) Clar, E.; John, F. *Chem. Ber.* **1930**, *63*, 967-2977.

(50) Clar, E. *Chem. Ber.* **1931**, *64*, 2194- 2200.

(51) Pramanik, C.; Miller, G. *Molecules* **2012**, *17*, 4625–4633.

(52) Berg, O.; Chronister, E. L.; Yamashta, G. W.; Scott, G. W.; Sweet, R. M.; Calabrese, J. *J. Phys. Chem. A* **1999**, *103*, 2451- 2459.

(53) Berg, O.;Chronister, E. L.; Yamashta, G. W.; Scott, G. W.; Sweet, R. M.; Calabrese. *J. Phys. Chem. A* **1999**, *103*, 2451- 2459.

(54) Brown, A.; Pomp, A.; de Leeuw, D.; Klaassen, D.; Havinga, E.; Herwig, P Müllen, K. *J. Appl. Phys.* **1996**, *79*, 2136–2138.

(55) Afzali, A.; Dimitrakopoulos, Ch.; Breen, T. *J. Am. Chem. Soc.* **2002,** *124***,** 8812-8813.

(56) Weidkamp, K.; Afzali, A.; Tromp, R.; Hamers, R. *J. Am. Chem. Soc.* **2004,** *124***,** 12740-12741.

(57) Afzali, A.; Dimitrakopoulos, Ch.; Graham, T. *Adv. Mater*. **2003**, *15*, 2066-2069.

(58) Anthony, J.; Brooks, J.; Eaton, D.; Parkin, S. *J. Am. Chem. Soc*. **2001**, *123*, 9482-9483

(59) Anthony, E.; Eaton, D.; Parkin, S. *Org. Lett.* **2002**, *4*, 15–18

(60) Payne, M.; Delcamp, J.; Parkin, S.; Anthony. *J. Org. Lett.* **2004**, *6*, 1609–1612.

(61) Li, Y.; Wu, Y.; Liu, P.; Prostran, Z.; Gardner, S.; Ong, B. S. *Chem. Mater.* **2007**, *19*, 418–423.

(62) Li, S.; Zhou, L.; Nakajima, K.; Kanno, K.-i.; Takahashi, T. *Chem. Asian J.* **2010**, *5*, 1620-1626.

(63) Shu, Y.*;* Lim, Y.-F.; Li, Z.; Purushothaman, B.; Hallani, R.; Kim, J. E.; Parkin, S. R.; Malliaras, G. G.; Anthony, J. E. *Chem. Sci.* **2011**, *2*, 363-368.

(64) Guo, J.; Liu, D.; Zhang, J.; Zhang.; Miao, Q.; Xie, Z. *Chem. Commun.* **2015**, *51*, 12004-12007.

(65) Kim, H.; Choi, H.; Song, E.; Cho, K.; Choi, E. *RSC Adv.* **2015**, *5*, 8070-8076.

(66) Lakshminarayana, A. N.; Chang, J.; Luo, J.; Zheng, B.; Huang, K.-W.; Chi, C. *Chem. Commun.* **2015**, *51*, 3604–3607.

(67) Bheemireddy, S.; Ubaldo, P. C.; Rose P. W.; Finke, A. D.; Zhuang, J.; Wang, L.; Plunkett, K. N. *Angew. Chem. Int. Ed.* **2015**, *54*, 15762 –15766

(68) MILLS, W. H.; MILLS, M. *J. Chem. Soc. Transactions* **1912**, 101, 2194-2208.

(69) Baxter, I.; Cameron, D. W.; Titman, R. B. *J. Chem. Soc. C* **1971**, 1253- 1256.

(70) Vets, N.; Diliën, H.; Toppet, S.; Dehaen.W. *Synlett*. **2006**, *9*, 1359–1362.

(71) Nishida, J.; Fujiwara, Y., Yamashita, Y. *Org. Lett*. **2009**, *11*, 1813-1816.

(72) Krishnan, A.; Dujardin, E; Treacy, M.; Hugdahl, J.; Lynum, S.; Ebbesen, T.W. *Nature* **1997**, *388*, 451-454.

(73) Land, T. A.; Michely, T.; Behm, R. J.; Hemminger J. C.; Comsa, G. *Surf. Sci.* **1992**, *264*, 261-270.

(74) Nagashima, A.; Nuka, K.; Itoh, H.; Ichinokawa, T.; Oshima, C.; Otani, S. *Surf . Sci.* **1993**, *29*, 93-98.

(75) Berger, C.; Song, Z. M.; Li, T. B.; Li, X. B.; Ogbazghi, A. Y.; Feng, R.; Feng, R.; Dai, Z.; Marchenkov, A. N.; Conrad, E. H.; First, F.; de Heer, W. A. *J. Phys. Chem. B* **2004**, *108*, 19912-19916.

(76) Ohta, T.; Bostwick, A.; Seyller, T.; Horn, K.; Rotenberg, E. *Science* **2006**, *313*, 951-954.

(77) Novoselov, K. S.; Geim, A. K.; Morozov, S. V.; Jiang, D.; Zhang, Y.; Dubonos, S. V.; Grigorieva, I. V.; Firsov, A. A. *Science* **2004**, *306*, 666-669.

(78) Nair, R. R.; Blake, P.; Grigorenko, A. N.; Novoselov, K. S.; Booth, T. J.; Stauber, T.; Peres, N. M. R.; Geim, A. K. *Science* **2008**, *320*, 1308-1308.

(79) Stoller, M. D.; Park, S.; Zhu, Y.; An, J.; Ruoff, R. S. *Nano Lett.* **2008**, *8*, 3498-3502.

(80) Lee, C.; Wei, X.; Kysar, J. W.; Hone, J. *Science* **2008**, *321*, 385-388.

(81) Balandin, A. A.; Ghosh, S.; Bao, W.; Calizo, I.; Teweldebrhan, D.; Miao, F.; Lau, C. N. *Nano Lett.* **2008**, *8*, 902-907.

(82) Scott, L. T. *Angew. Chem., Int. Ed.* **2004**, *43*, 4994-5007.

(83) Tahara, K.; Tobe, Y. *Chem. Re*v. **2006**, *106*, 5274-5290.

(84) Wu, J.; Pisula, W.; Müllen, K. *Chem. Re*v. **2007**, *107*, 718-747.

(85) Lambert, C. *Angew. Chem., Int. Ed.* **2005**, *44*, 7337-7339.

(86) Yang, X.; Dou, X.; Rouhanipour, A.; Zhi, L.; Räder, H. J.; Müllen, K. *J. Am. Chem. Soc.* **2008**, *130*, 4216-4217

(87) Daigle, M.; Picard-Lafond, A.; Soligo, E.; Morin, J-F. *Angew. Chem. Int. Ed*. **2016**, *55*, 2042-2047.

(88) Yang, W.; Lucotti, A.; Tommasini, M.; Chalifoux, W. A. *J. Am. Chem. Soc*. **2016**, *138*, 9137-9144.

Chapter 2

A TTFV–pyrene-based Copolymer: Synthesis, Redox Properties, and Aggregation Behaviour

- This chapter is published as a communication article in *RSC Advances*. "Younes, E.; Williams, K-L. M.; Walsh, J. C.; Schneider, C. M.; Bodwell, G. J.; Zhao, Y. *RSC Adv*. **2015**, *5*, 23952- 23956"
- I would like to thank Prof. Bodwell and his students, Kerry-Lynn Williams and Joshua Walsh, for their collaborations on this project.
- E. Younes is the researcher who carried out most of the experimental work, including polymer synthesis and characterization, redox chemistry, and DLS measurements, under the supervision of Prof. Y. Zhao. K-L. Williams and J. Walsh carried out the synthesis of compounds **51**-**53** under supervision of Prof. G. J. Bodwell. Dr. C. M.Schneider (C-CART, Memorial) conducted the diffusion NMR analysis. Prof. Q. Chen (Physics, Memorial) assisted in the microscopic optical profiling analysis.

2.1 Introduction

π-Conjugated polymers bearing redox active units have found widespread applications in organic semiconducting materials and optoelectronic devices.[1-3] Synthetically, incorporation of the redox active components (*e.g*. electron donors or acceptors) can be attained by having them either embedded in the polymer backbone or appended to the side chains.[1,2] Tetrathiafulvalene vinylogues (TTFVs) have received growing attention over the past few years in the design of novel

redox-active molecules and polymers, owing to their excellent electron-donating properties.[4-6] Of particular interest is the class of aryl-substituted TTFVs, which show not only rich electrochemical activity, but also intriguing conformational switching behaviour associated with redox reactions.[4,7-9] The research group of Zhao and others have recently demonstrated that the incorporation of TTFVs in various π-conjugated systems can afford useful functional molecular materials and devices, ranging from redox-switchable ligands,[10-12] stimuli-responsive foldamers[13-16] and shape-persistent macrocycles[17,18] to redox-regulated molecular rotors,[19] synthetic receptors and chemosensors.[20-23]

In the design of aryl-based π-conjugated materials, pyrene is often chosen as a favourable π-building block because of its remarkable photophysical properties as well as its redox activity.[24,25] Furthermore, pyrene tends to interact strongly with other aromatic systems via π-stacking, which can be utilized to generate pre-organized supramolecular assemblies.[26-30] The combination of TTFV and pyrene has been demonstrated to be an appealing design approach to attain novel supramolecular properties. For example, our research group previously developed a class of pyrene–TTFV-based molecular tweezers that exhibit selective binding to C_{70} fullerene in the presence of a large excess of C_{60}.[22] Along the same lines, we further envisioned that copolymers made of TTFV and pyrene moieties should give rise to very interesting redox activity and supramolecular behaviour that might be useful in materials applications.

For the most part, pyrenylene units that have been placed in π-extended structures have had either 1,6-, 1,8- or 2,7-substitution patterns.[31] The 1,8-substitution pattern has been exploited in our group's recent research, which has led to the synthesis of some shape-persistent macrocycles.[32] However, copolymer systems that incorporate both TTFV and pyrenylene systems as repeat units have not yet been reported in the literature.

2.2 Results and Discussion

2.2.1 Synthesis of Copolymer 55

In this work, the synthesis and characterization of the first TTFV–pyrene-based copolymer **55** will be discussed in details**.** Acetylenic TTFV **54** and 1,8-diiodo-4,5-bis(tetradecyloxy)pyrene **53** were identified as two key building blocks for the synthesis of **51**. The 1,8-pyrenylene pattern was chosen to impart a repeating bend (120°) in the polymer backbone, which was expected to provide access to folded/helical structures. $OC_{14}H_{29}$ side chains were chosen to promote solubility of the copolymer **51**. Diyne 5**4** was synthesized according to literature procedures,[17,18] whereas diiodide **53** was synthesized in short order from diketone **51**[32] (Scheme 2.1). One-pot reductive alkylation of **51** afforded 4,5-dialkoxypyrene **52** (85%), which was iodinated under mild conditions to afford diiodide **53** (88%) with complete 1,8-regioselectivity. The copolymerization of **53** and **54** was conducted under Sonogashira coupling conditions ($Pd(PPh_3)_4$/CuI, *i*-Pr_2NH) in DMF/toluene at 65 °C. The resulting crude polymer was purified by precipitation from MeOH, followed by exhaustive rinsing with MeOH, giving **55** as a yellow solid in 87% yield. Copolymer **55** was found to be non-fluorescent in both solution and the solid state, due to the strong quenching effect of the electron-donating TTFV moiety.

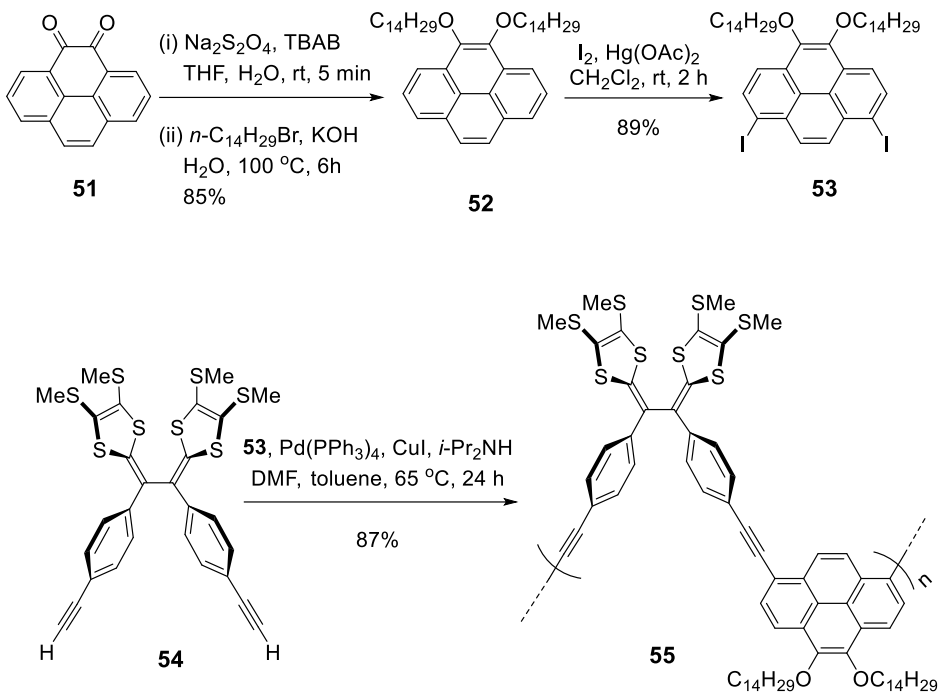

Scheme 2.1: Synthesis of TTFV-pyrene-based copolymer **55** via Sonogashira coupling polymerization. The synthesis of **53** was carried out by Kerry-Lynn M. Williams and Joshua C. Walsh (Bodwell group, Memorial University).

2.2.2 Characterizations of TTFV–pyrene-based Copolymer 55

TTFV–pyrene-based copolymer **55** was characterized by ^{1}H NMR and IR spectroscopy. According to GPC analysis, M_w=6,219 g mol^{-1}, M_n=4,562 g mol^{-1} and PDI=1.32. The GPC data suggest that the average chain length of copolymer **55** is at the stage of the pentamer. The conformational properties of **55** were then studied through molecular mechanics (*MM*) simulations. Using the *MMFF* force field implemented in the Spartan'10 software,[33] conformations at two extremities were optimized (Figure 2.1). The first conformer takes a zig-zag structure (Figure 2.1A), where the TTFV and pyrene moieties do not have any intramolecular π-stacking. The second one is a foldamer (Figure 2.1B and 2.1C), in which the TTFV and pyrene units are tightly

packed together through π-π interactions, such that the folded structure takes a cylinder-like shape. The central cavity of the foldamer is calculated to be too small (*ca*. 0.4-0.5 nm) to encapsulate meaningful organic guest molecules. Calculations show that the foldamer is roughly 31.0 kcal mol^{-1} more stable than the zig-zag conformer (in the gas phase), suggesting the polymer has a strong preference for assuming the folded conformation as a result of self-aggregation. Pulsed gradient spin-echo (PGSE) NMR analysis shows that copolymer **55** has an average diffusion coefficient (*D*) of 1.984×10^{-10} m^2 s^{-1}, which corresponds to a hydrodynamic radius of 2.13 nm according to the Stokes-Einstein equation. Considering that the computational work on **55** used OCH_3 groups and H atoms instead of $OC_{14}H_{29}$ and SCH_3 groups respectively, the diffusion NMR data agrees reasonably well with the calculated molecular dimensions of the folded conformer (see Figure 2.1B and 2.1C) and hence suggests that the folded conformation of **55** is highly favoured in solution.

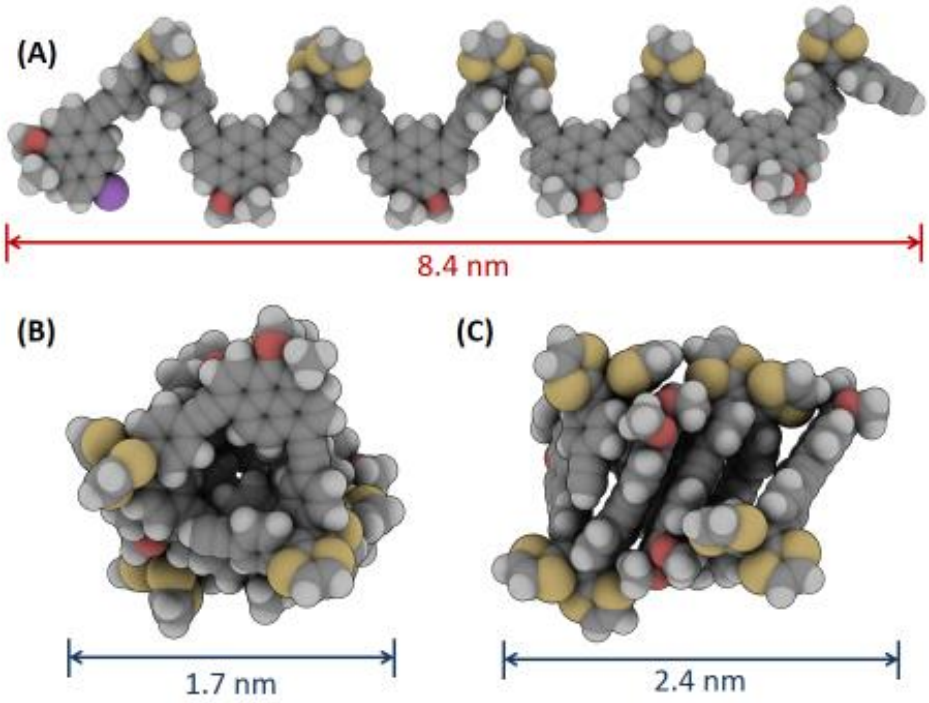

Figure 2.1: (A) Copolymer **55** in a zig-zag conformation. (B) Front view, and (C) side view of **55** in a fully folded conformation. The geometries were optimized using the *MMFF* force field. To save computational cost, the $OC_{14}H_{29}$ and SCH_3 groups in **55** were replaced by OCH_3 groups and H atoms, respectively.

2.2.3 Redox and Electronic Properties

The electrochemical redox properties of TTFV–pyrene copolymer **55** were investigated by cyclic voltammetry (CV). The CV profile measured for a thin film of **55** cast on the surface of a glassy carbon working electrode exhibits a reversible redox wave pair (E_{pa} = +0.71 V, E_{pc} = +0.58 V) with a formal potential ($E^{o'}$) at +0.64 V (Figure 2.2A). This redox pair can be assigned to the simultaneous two-electron transfer at the TTFV unit during the redox processes.[4-12] In comparison to the redox behaviour observed for TTFV precursor **54**, the cathodic and anodic peaks of copolymer **55** are both shifted to the positive direction by +0.10 V. Such a significant anodic shift

is similar to the CV behaviour of a TTFV-based shape-persistent macrocycle we previously studied, in which the TTFV unit was constrained to a pseudo *s-cis* conformation.[17,18] Since the folded conformation of **55** bears more resemblance to the structure of the constrained rigid macrocycle than the unfolded one, this may be taken as an indication that the dominant conformation of copolymer **55** in the solid state is also the self-aggregated foldamer.

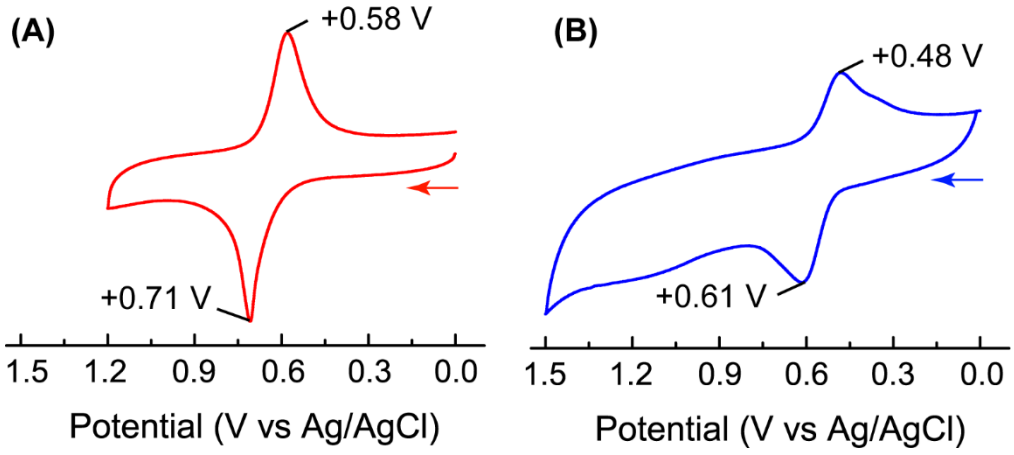

Figure 2.2: Cyclic voltammograms of (A) the thin film of copolymer **55** and (B) acetylenic TTFV **54**. Experimental conditions: solvent: CH_3CN; electrolyte: Bu_4NBF_4 (0.1 M); working electrode: glassy carbon; counter electrode: Pt wire; reference electrode: Ag/AgCl (3 M NaCl); scan rate: 0.1 V s^{-1}.

The electronic absorption properties of copolymer **55** and its two precursors **53** and **54** were examined by UV-Vis spectroscopy (Figure 2.3). In chloroform, copolymer **55** exhibits two absorption bands at 417 and 298 nm. Additionally, a number of shoulder bands are discernible at 383, 361, 333, and 312 nm. The spectrum of TTFV precursor **54** shows two absorption bands at 376 and 261 nm, while the spectrum of pyrene **53** gives characteristic vibronic progression at 379, 360, 344 (sh) nm, along with a high-energy band at 293 nm. Compared with the spectra of **53** and

54, the lowest-energy absorption band of copolymer **55** is substantially red-shifted, presumably due to its extended π-delocalization.

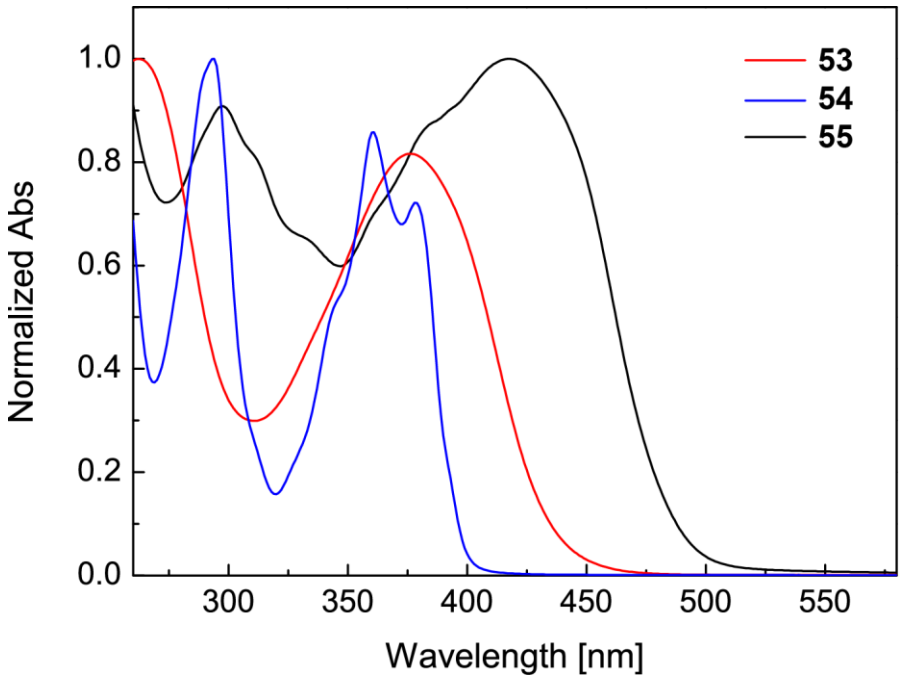

Figure 2.3: UV-Vis absorption spectra of compounds **53-55** measured in $CHCl_3$ at room temperature (1mg/100ml).

2.2.4 Aggregation Behaviour of Copolymer 55

Protic dipolar solvents (*e.g.* water, MeOH) are known to enhance folding and aggregation of arene-based conjugated polymers, leading to significant changes in UV-Vis absorption.[34-36] To investigate the solvent-dependent UV-Vis absorption properties of **55**, MeOH was gradually added to a THF solution of **55** and the process was monitored by UV-Vis analysis. As can be seen in Figure 2.4, the stepwise increase in the proportion of MeOH in the polymer solution causes a two-stage change in the UV-Vis spectra. In the first stage, when the percentage of MeOH is increased from 0% to 30% (v/v), only the absorption band at 286 nm is observed to decrease in intensity, while the other regions of the spectrum do not show any significant variations. In the second stage

(*i.e.* when the percentage of MeOH is increased beyond 30%), the spectrum undergoes more substantial changes: the lowest energy absorption maximum is redshifted and a pronounced low-energy absorption tail emerges.

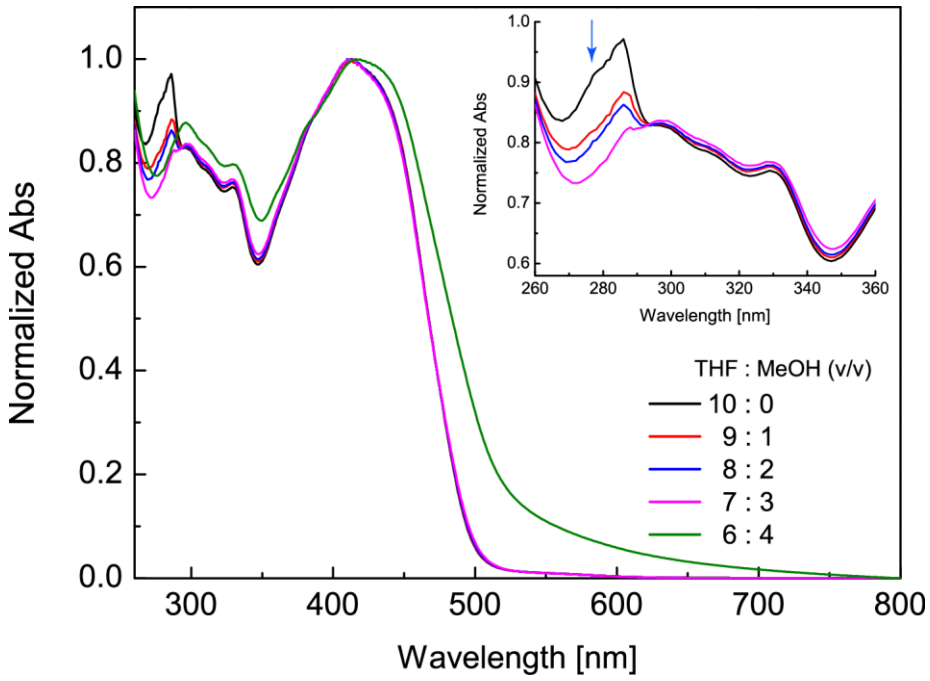

Figure 2.4: UV-Vis spectra of copolymer **55** in THF/MeOH. Inset: expanded spectra (260-360 nm) showing copolymer **55** in THF/MeOH at volumetric ratios from 10:0 to 6:4.

The observed solvent-dependent UV-Vis absorption behaviour suggests that copolymer **55** may undergo dramatic changes in aggregation with increasing solvent polarity. To further understand the microscopic origins for these properties, MeOH (50 µL per portion) was gradually added to a solution of copolymer **55** (3 mg) in THF (1 mL) to induce the formation of polymer aggregates. Dynamic light scattering (DLS) measurements were performed to determine the size range of the polymer aggregates (see Figure 2.5). When the volumetric ratio of THF:MeOH was

gradually increased from 10:0 to 10:3, narrowly distributed particles with an average diameter of *ca*. 240 nm were detected in the solution. As the ratio of THF:MeOH was further increased to 10:6, the average diameter of the particles grew steadily to *ca*. 620 nm. Once the ratio reached 10:7, much larger particles (*ca*. 6.5 μm in diameter) started to form and the size distribution was found to be very broad. In the meantime, the solution became visibly turbid, which is indicative of precipitation.

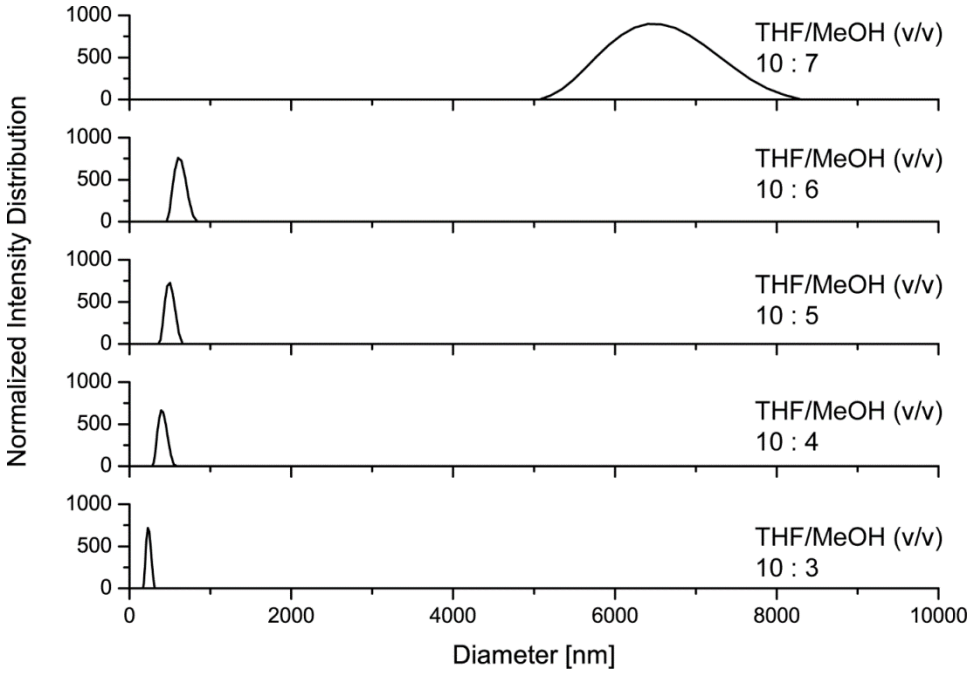

Figure 2.5: DLS analysis of the diameters of polymer aggregates formed in mixture solvent of THF/MeOH at various volumetric ratios.

The kinetics of the MeOH-induced aggregation of **55** in THF appear to be complex and show significant dependence on factors such as time, local concentration, and pH value. Figure

2.6 depicts the time-dependent size variation for the nanoparticles formed in 10:3 THF/MeOH. Within the first 45 min, the nanoparticles did not show any significant changes in size. After standing at room temperature for 75 min, the nanoparticles were found to decrease considerably in number, while more numerous and broadly distributed micron-sized particles began to form. Evidently, the narrowly distributed nanoparticles are metastable and tend to aggregate into much larger particles as a function of time.

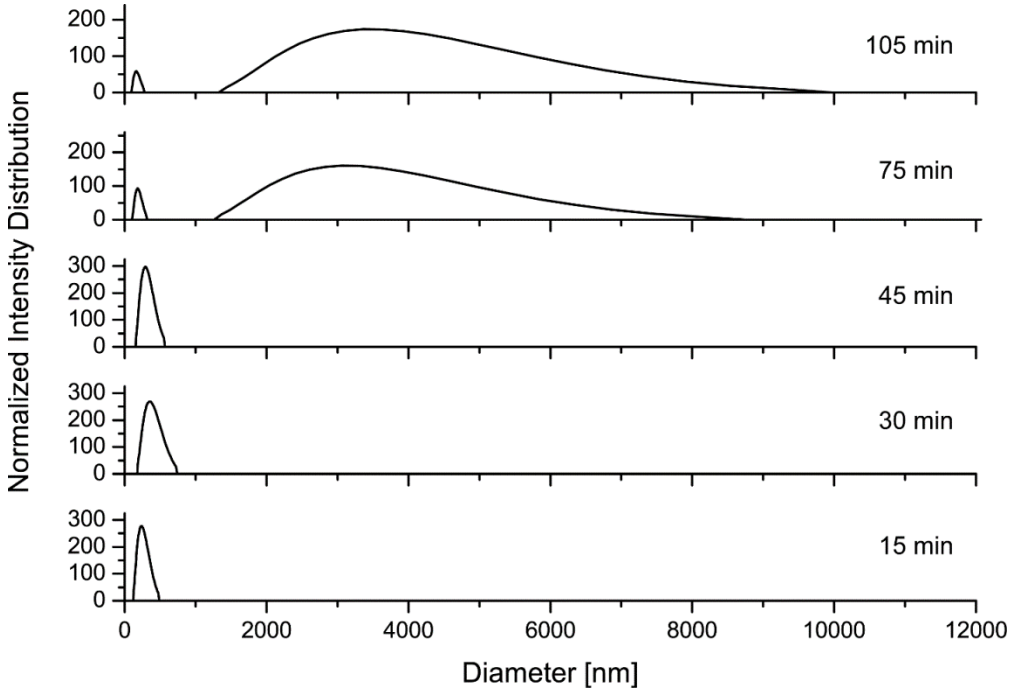

Figure 2.6. DLS analysis monitoring the diameter distribution of the aggregates of polymer **55** (3 mg) in THF/MeOH (10:3, v/v) at different periods of time at room temperature.

The way of adding MeOH to a THF solution of **55** was found to strongly affect the nature of the aggregation. When MeOH was added in one portion, instead of slow addition in small portions, to a THF solution of copolymer **55** to afford a 10:4 THF/MeOH ratio (v/v), a very

broad size distribution was observed (see Figure 2.7). A plausible explanation is that the one-shot addition of MeOH resulted in instantaneously high local concentrations of MeOH in the solution, which in turn promoted the aggregation.

As the conformation of the TTFV moiety is known to be sensitive to pH,[14-16] the possibility of altering particle sizes via protonation of **55** with trifluoroacetic acid (TFA) was then tested. In this experiment, a tiny amount (*ca*. 1 μL) of TFA was added to the THF/MeOH solution of **55** generated by a one-portion MeOH addition. DLS analysis of the acidified mixture showed that the diameter distribution of the protonated aggregates was reversed to a much narrower profile as shown in Figure 2.7. It can also be noted that there was a small portion of particles with an average diameter of *ca*. 18 nm detected in the polymer solution (see the inset in Figure 2.7). These particles are likely due to micelles of copolymer **55**. After addition of TFA, the average diameter of these micelles was observed to increase to *ca*. 40 nm. Protonation of TTFV by TFA has been known to considerably change the conformation of TTFV from a pseudo *s-cis* to a *s-trans* orientation.[14-16] Following this rationale, the entire framework of TTFV-pyrene copolymer **55** upon protonation is expected to change from the folded to a zig-zag like structure. Such a dramatic conformational change may account for the significantly increased micellar diameter after treatment with TFA.

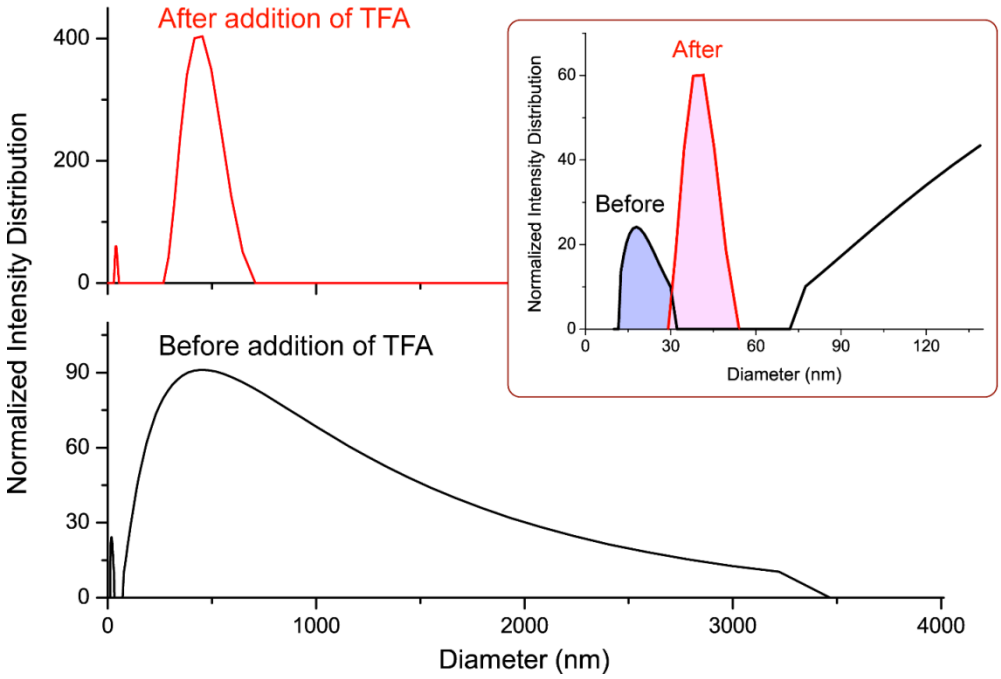

Figure 2.7: DLS analysis showing the diameter distribution of polymer aggregates in 10:4 THF/MeOH before and after addition of TFA. Inset: expansion of the size distributions in the region of 0 to 130 nm.

The responsiveness of the aggregates of copolymer **55** to TFA treatment at a surface was examined by optical surface profiling. As shown in Figure 2.8A, a solid film of **55** dropcast on the surface of a glass slide exhibits "worm-like" structures on the scale of tens of microns in height and hundreds of microns in length. These features indicate strong inter-polymer aggregation in the neutral solid state. After exposure to TFA vapour for *ca*. 20 min, the surface pattern was found to change substantially into a morphology featuring a more dispersed and particle-like pattern, with considerably reduced discrete dimensions. The surface profiling results confirm that the aggregation of copolymer **55** in the solid state is also responsive to pH, and such a property can be utilized as a "bottom-up" control over the solid-state assembly and ordering at the microscopic level.

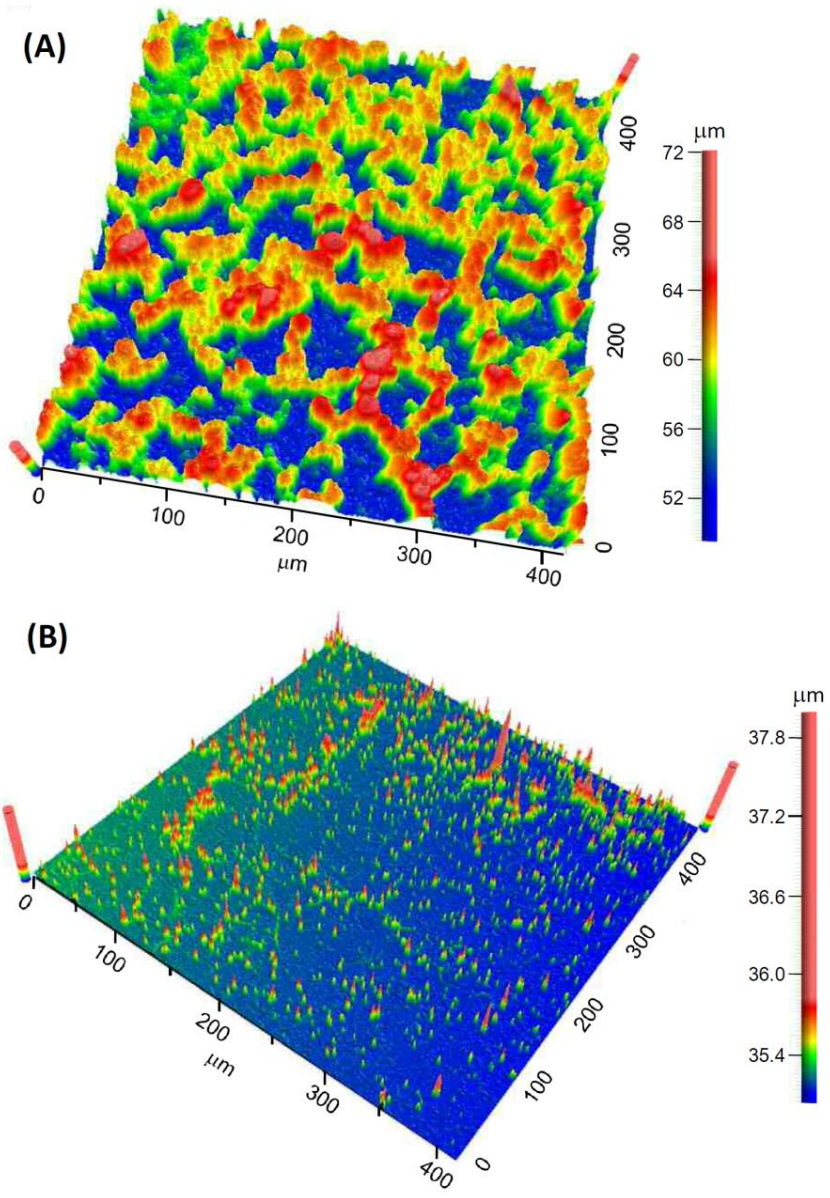

Figure 2.8 Surface topography for the thin film of copolymer **55** deposited on a glass substrate (A) before and (B) after exposure to TFA vapour for 20 min.

2.3 Conclusions

In conclusion, a new type of redox-active TTFV–pyrene-based copolymer **55** was synthesized and investigated. The aggregation of the polymer evolves in two distinct stages ("nano" and "micron") and shows dependence on solvent polarity, time, and pH. Even in the solid state, the polymer aggregates exhibit significant responsiveness to acidic vapours. We anticipate that this type of copolymer can be further developed to "intelligent" materials with controllable microscopic structures and programmable responsiveness to external stimuli (*e.g.* pH, solvent, and redox conditions).

2.4 Experimental

2.4.1 General

Chemicals and reagents were purchased from commercial suppliers and used without further purification. All reactions were performed in standard dry glassware under an inert atmosphere of N_2 unless otherwise noted. Evaporation and concentration was done at H_2O-aspirator pressure. Flash column chromatography was carried out with silica gel 60 (230-400 mesh) from VWR International. ^{1}H and ^{13}C NMR spectra were measured on a Bruker AVANCE III 300 MHz spectrometer. Chemical shifts (δ) are reported in ppm downfield from the signal of the internal reference $SiMe_4$ or relative to the signals of residual solvents ($CHCl_3$: δ H = 7.24 ppm, δ C = 77.2 ppm). Coupling constants (*J*) are given in Hz. UV-Vis-NIR absorption spectra were recorded on a Cary 6000i spectrophotometer. Infrared spectra (IR) were recorded on a Bruker Tensor 27 spectrometer equipped with a ZnSe ATR module. Polymer molecular weight and polydispersity index (PDI) were estimated from gel permeation chromatography (GPC) using a

Waters 2695 Separations Module equipped with a Waters 2996 photodiode array detector, a Waters 2414 refractive-index detector, and two Jordi Labs Jordi Gel DVB columns. Polystyrene standards were used for calibration, and THF was used as the eluent at a flow rate of 1.0 mL/min. Cyclic voltammetric (CV) analyses were carried out in a standard three-electrode setup controlled by a BASi Epsilon workstation. Delsa Nano S particle analyzer (Beckman Coulter, Inc.) were used for dynamic light scattering (DLS) measurements. Polymer solution was filtered through a 0.20 μm Millex-FG filter. The calculations of the particle size distributions were performed with the Delsa Nano software 2.30 (Beckman Coulter, Inc). Surface topography was obtained using a NewView 8000 3D optical surface profiler (Zygo Corp.). Pyrene precursors 51-53[32] and TTFV 54[37,38] were prepared according to literature procedures with suitable modifications.

2.4.2 Synthetic Procedures

4,5-Bis(tetradecyloxy)pyrene (52)

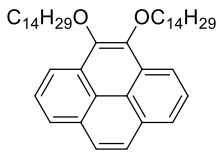

52

To a solution of pyrene-4,5-dione (**51**) (2.02 g, 9.98 mmol) in THF (100 mL) and H_2O (100 mL) were added TBAB (0.3 equiv.) and $Na_2S_2O_4$ (4.55 g, 26.1 mmol). The resulting clear orange solution was stirred at room temperature for 5 min. To the solution was added a solution of KOH (2.03 g, 3.62 mmol) in H_2O (100 mL). The resulting solution turned a deep red in colour, and the

flask was immediately capped. To this solution was added the 1-bromododecane (9.98 g, 40.0 mmol). The flask was equipped with a capped condenser and was stirred at 100 °C for 6 h. The reaction mixture was cooled to room temperature and the layers were separated. The aqueous layer was extracted with ethyl acetate (3 × 15 mL) and the THF layer was washed with H_2O (15 mL) before being combined with the other organic extracts. The combined organic extracts were washed with H_2O (3 × 15 mL) to afford a clear yellow solution, which was then dried over anhydrous $MgSO_4$. The solvent was removed under reduced pressure and the residue was subjected to column chromatography (hexanes and then 10% CH_2Cl_2/hexanes) to afford 4,5-bis(dodecyloxy)pyrene (**52**) (2.08 g, 8.43 mmol, 85%) as a pale yellow solid. Mp: 53–54 °C; ^{1}H NMR (300 MHz, $CDCl_3$): δ 8.49 (dd, *J* = 1.1, 7.8 Hz, 2H), 8.13 (dd, *J* = 1.2, 7.6 Hz, 2H), 8.04 (s, 2H), 8.02 (t, *J* = 7.7 Hz, 2H), 4.33 (t, *J* = 6.7 Hz, 4H), 1.93–2.02 (m, 4H), 1.56–1.66 (m, 4H), 1.27–1.54 (m, 32H), 0.86–0.90 (m, 6H); ^{13}C NMR (75 MHz, $CDCl_3$): δ 144.1, 131.1, 128.9, 127.3, 126.0, 124.3, 122.9, 119.4, 73.8, 32.0, 30.7, 29.8, 29.7, 29.6, 29.4, 26.4, 22.7, 14.2. MS (APCI-(+), CH_2Cl_2): *m/z* (%) 627.6 ($[M+H]^+$); HRMS (ESI-(+), CH_2Cl_2): calcd for $C_{44}H_{66}O_2$ 626.5063, found 626.5045 (M^+).

1,8-Diiodo-4,5-bis(tetradecyloxy)pyrene (3)

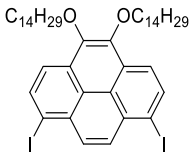

53

To a stirred solution of 4,5-bis(tetradecyloxy)pyrene (**52**) (1.50 g, 2.39 mmol) in CH_2Cl_2 (30 mL) was added mercuric acetate (1.68 g, 5.27 mmol). The reaction mixture was left to stir for 5 min. Iodine (1.34 g, 5.27 mmol) was then added and the resulting mixture was left to stir for 2.5 h at room temperature. The reaction mixture was filtered through a plug of Celite and extracted with CH_2Cl_2 (3 × 20 mL). The combined organic extractions were then washed with a saturated solution of sodium bisulfite (50 mL), 5% $NaHCO_3$ solution (50 mL), water (2 × 50 mL) and brine (50 mL). The resulting clear yellow solution was then dried over $MgSO_4$ and excess solvent was removed under reduced pressure. The residue was adsorbed onto silica gel and subjected to column chromatography (10% CH_2Cl_2/hexanes) to afford 1,8-diiodo-4,5-bis(tetradecyloxy)pyrene (**53**) (1.87 g, 2.13 mmol, 89%) as a white solid. Mp: 89.0-90.0 °C; ^{1}H NMR (300 MHz, $CDCl_3$): δ 8.54 (d, *J* = 8.4 Hz, 2H), 8.37 (s, 2H), 8.22 (d, *J* = 8.4 Hz, 2H), 4.31 (t, *J* = 6.7 Hz, 4H), 1.95 (quint, *J* = 7.1 Hz, 4H), 1.59–1.61 (m, 6H), 1.26–1.45 (m, 38H), 0.88 (t, *J* = 6.2 Hz, 6H); ^{13}C NMR (75 MHz, $CDCl_3$): δ 181.3, 143.9, 137.5, 132.9, 132.4, 129,4, 123.1, 121.3, 96.2, 73.9, 34.1, 32.0, 30.5, 29.7, 29.7, 29.7, 29.6, 29.5, 29.4, 28.2, 26.3, 22.7, 14.2; MS (APCI, positive): *m/z* 879.8 ($[M+H]^+$); HRMS (ESI, positive): calcd for $C_{44}H_{64}O_2I_2$, 878.7867, found 878.7868 (M^+)

TTFV-pyrene copolymer 55

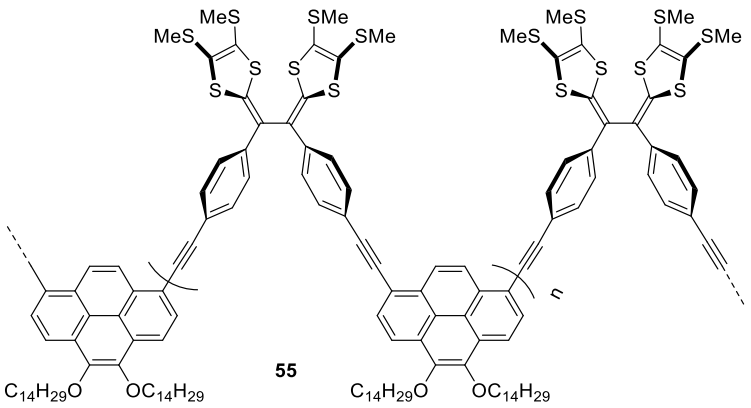

55

TTFV **54** (36 mg, 0.060 mmol) and 1,8-diiodopyrene **53** (52 mg, 0.060 mmol) were mixed with *i*-Pr_2NH (1 mL) in a mixed solvent of DMF (1.5 mL) and toluene (2.5 mL). The mixture was stirred with a magnetic bar at room temperature and to the mixture was added catalytic amounts of $Pd(PPh_3)_4$ (7.3 mg, 0.0060 mmol) and CuI (3.6 mg, 0.0020 mmol). The mixture was heated at 65 °C under N_2 for 24 h under stirring. The reaction mixture was then cooled to room temperature and poured into MeOH (200 mL) to give a brown colored precipitate, which was collected by vacuum filtration and washed with MeOH several times to afford copolymer **55** (65 mg, 87%) as a brown solid. IR (neat): 2916, 2846, 1592, 1463, 1373, 1297, 1214, 1086, 1007, 966, 873, 817, 718 cm^{-1}. ^1H NMR (300 MHz, $CDCl_3$): δ 8.72-8.18 (m, 6H), 7.72-7.33 (m, 8H), 4.36-4.27 (m, 4H), 2.47-2.38 (m, 12H), 2.01-1.89 (m, 4H), 1.56-1.36 (m, 44H), 0.91-0.83 (m, 6H); a meaningful ^{13}C NMR spectrum could not be obtained. GPC: M_n = 4,562 g mol^{-1}, M_w = 6,219 g mol^{-1}, PDI = 1.32.

2.5 NMR Spectra of New Compounds

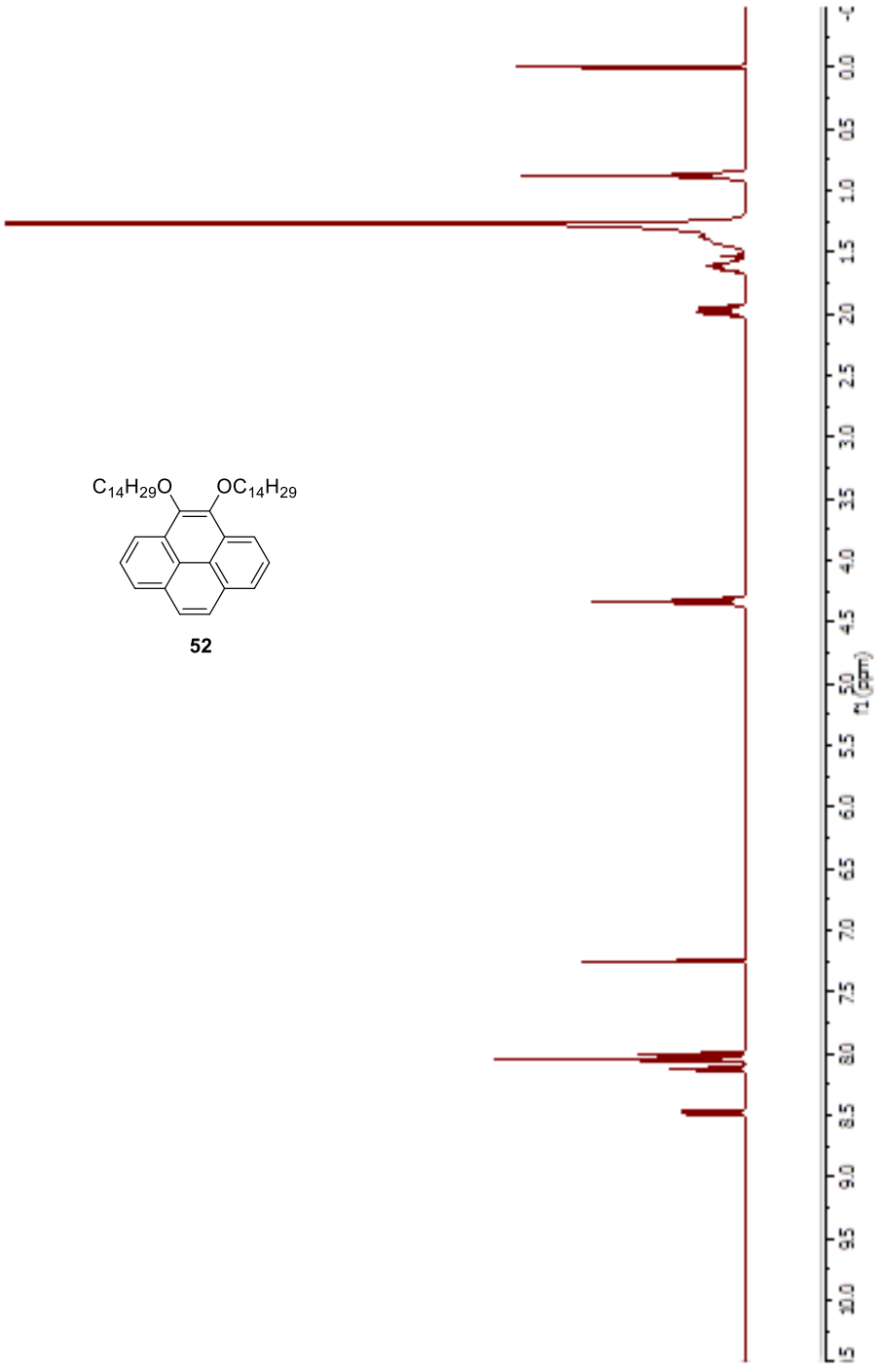

Fig. S-2.1 ^{1}H NMR (300 MHz, $CDCl_3$) spectrum of compound **52**.

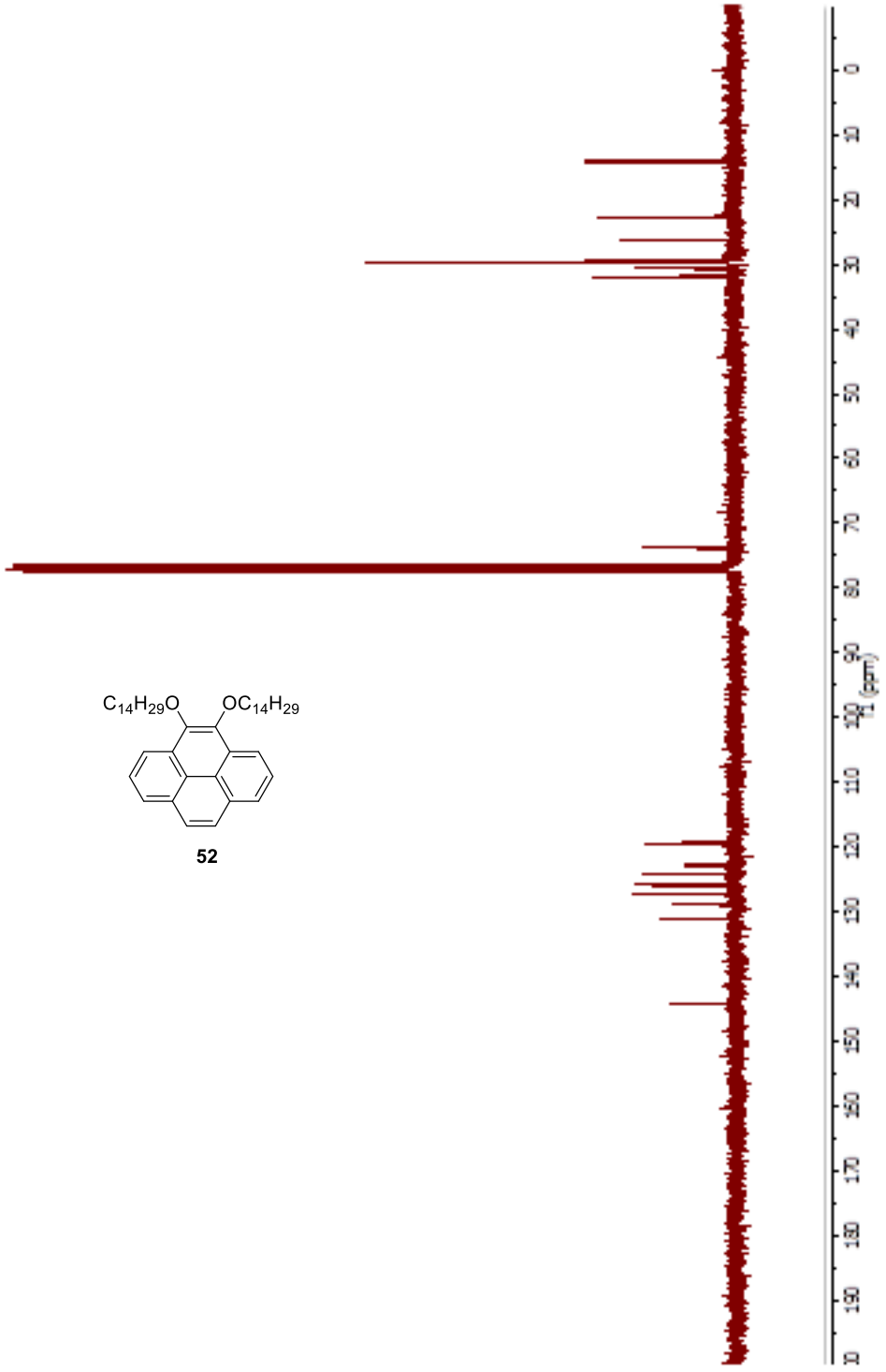

Fig. S-2.2 ^{13}C NMR (75 MHz, $CDCl_3$) spectrum of compound **52**.

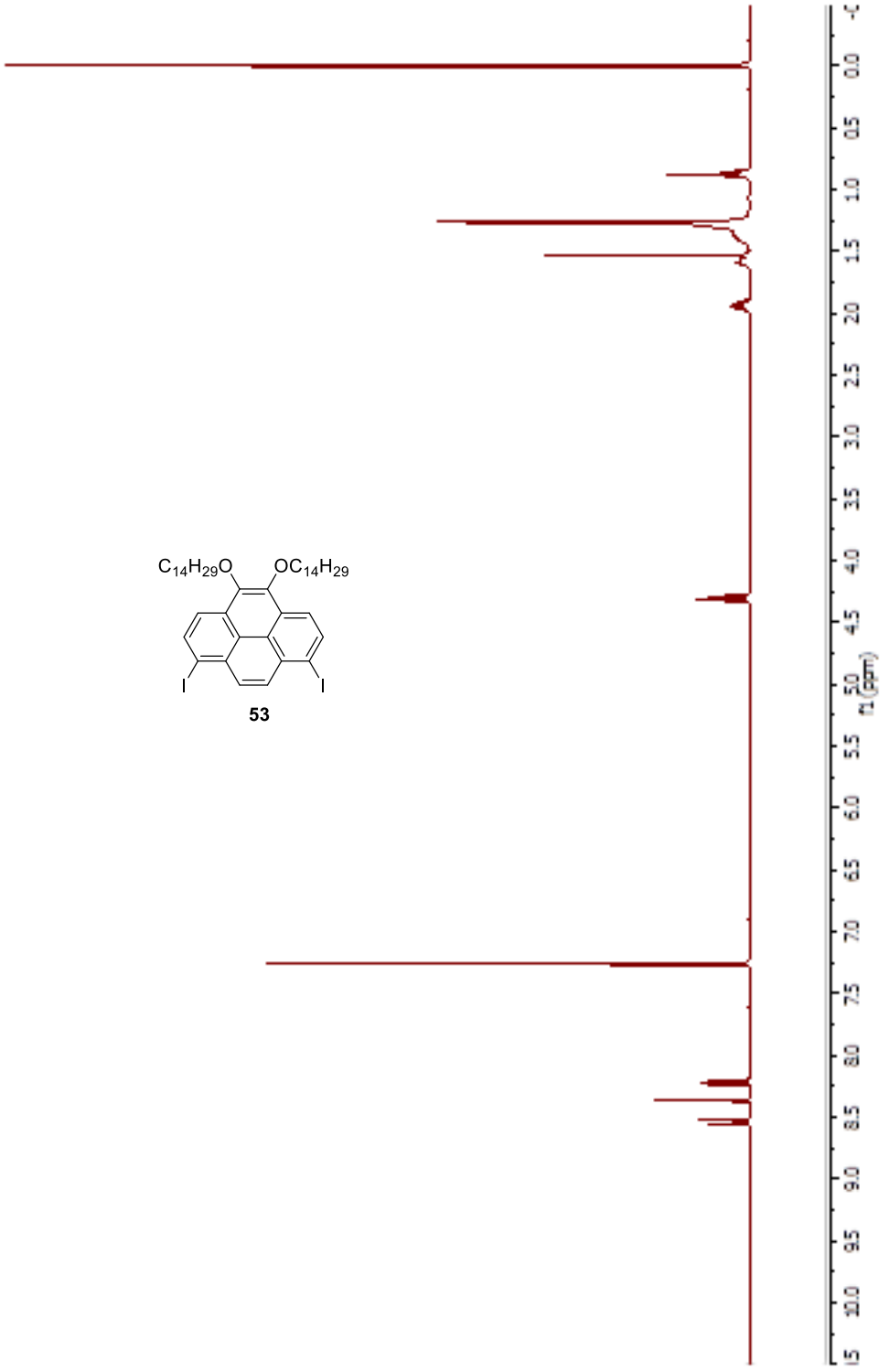

Fig. S-2.3 ^{1}H NMR (300 MHz, $CDCl_3$) spectrum of compound **53**.

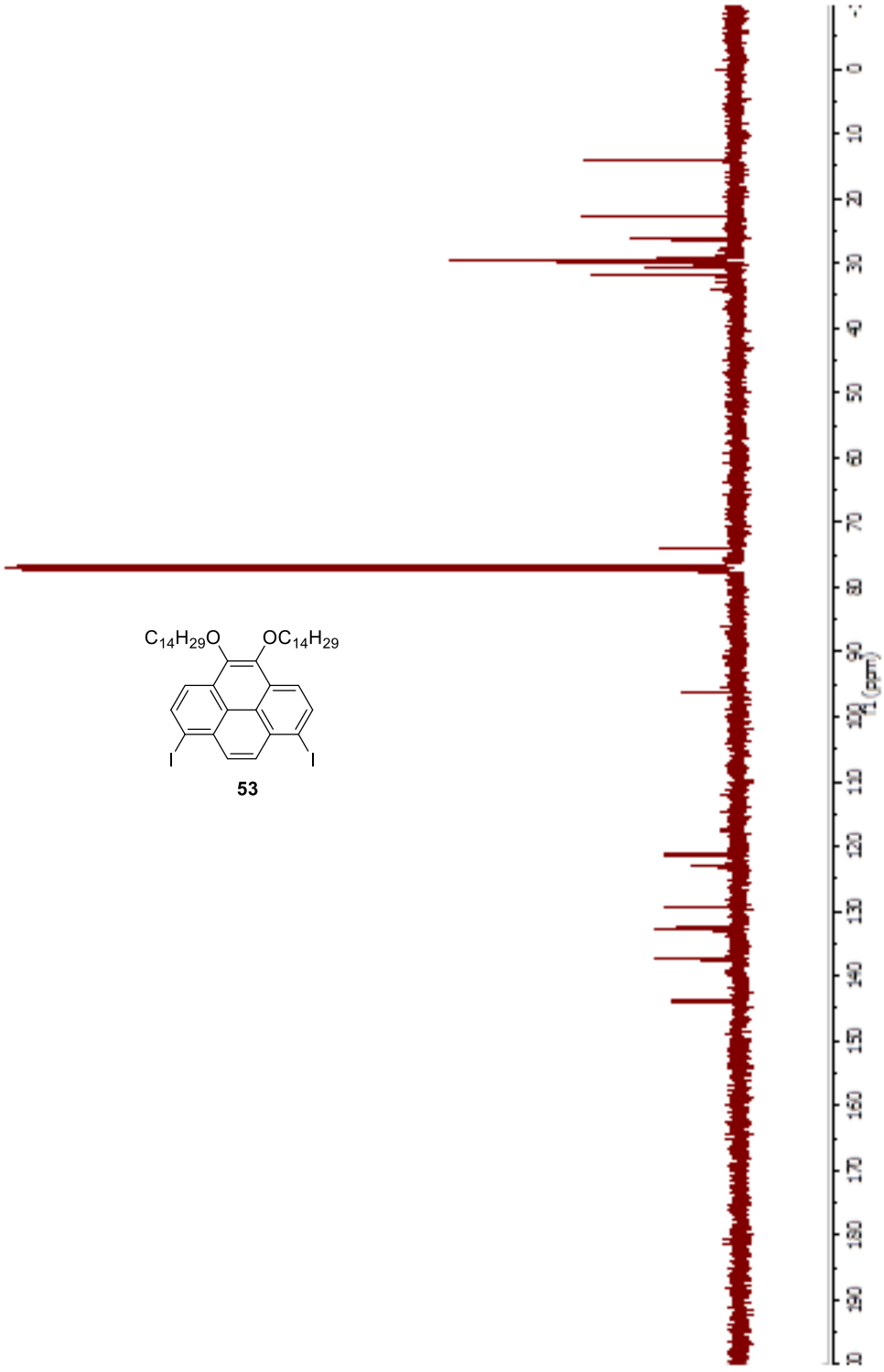

Fig. S-2.4 ^{13}C NMR (75 MHz, $CDCl_3$) spectrum of compound **53**.

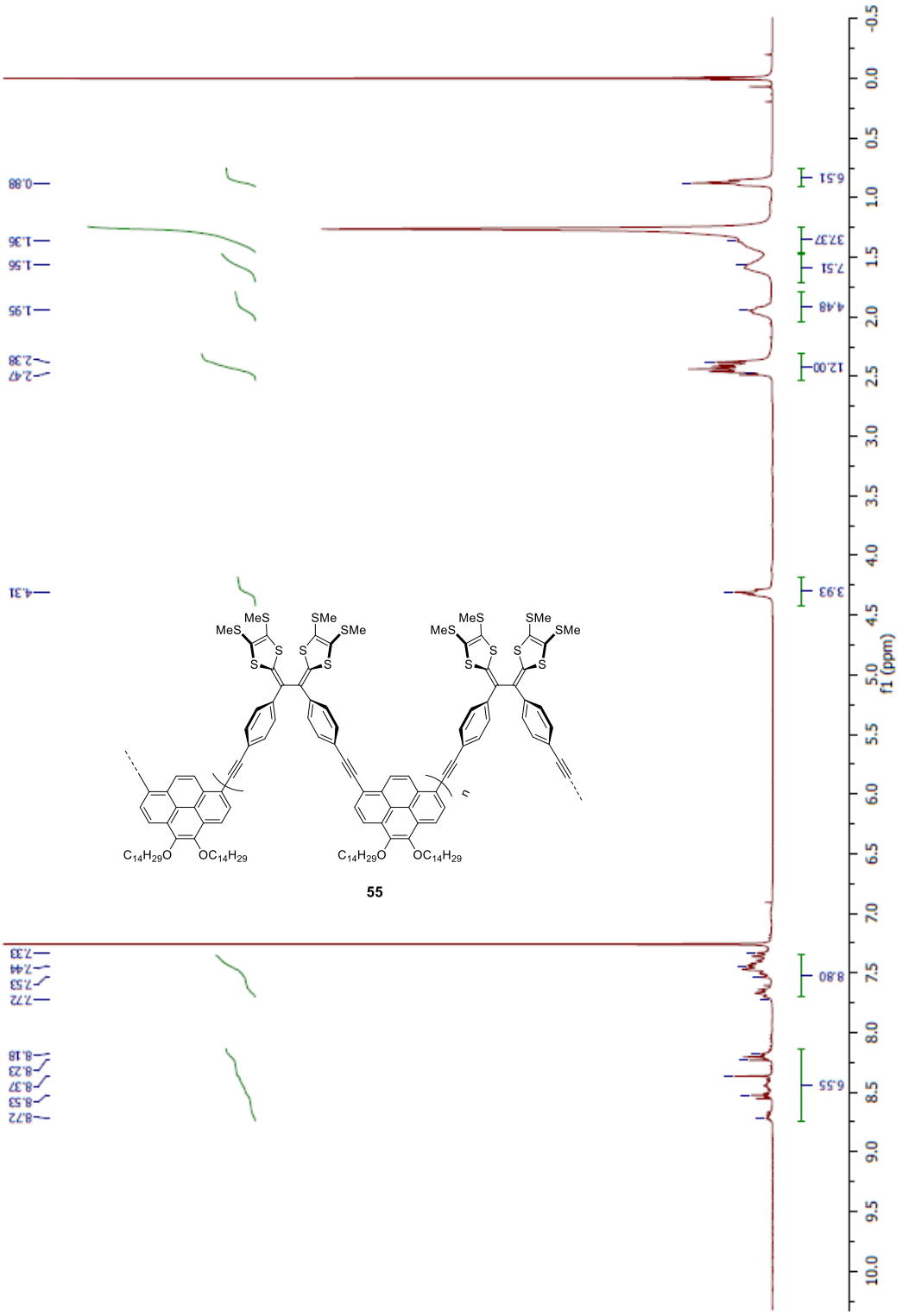

Fig. S-2.5 ^{1}H NMR (300 MHz, $CDCl_3$) spectrum of compound **55**.

2.6 GPC Analytical Result

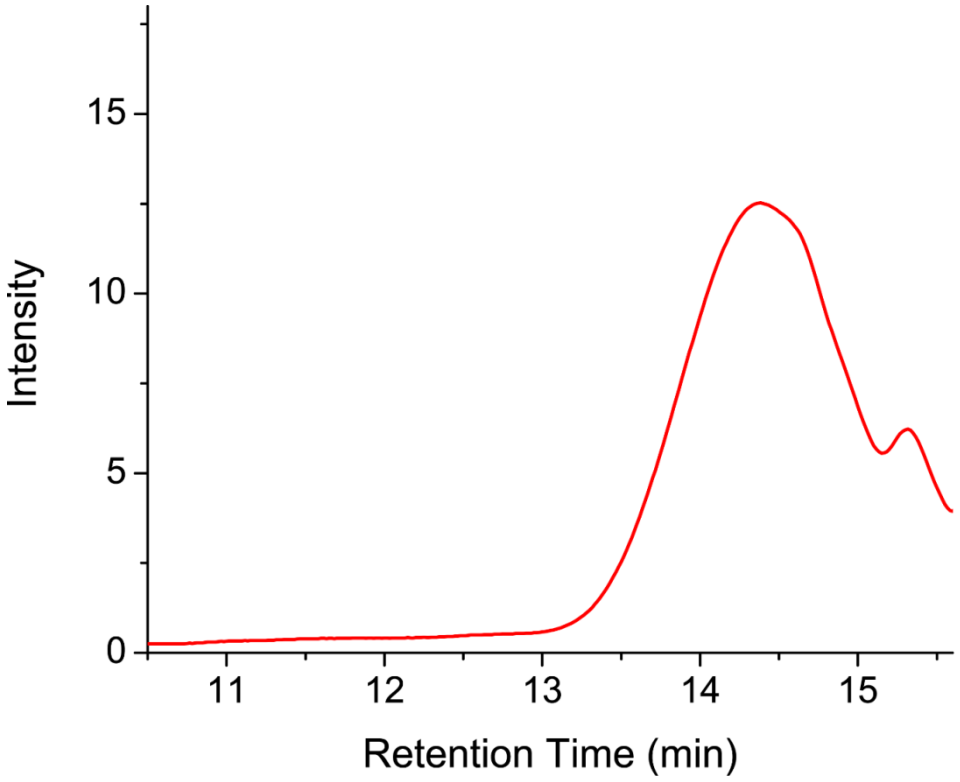

Fig. S-2.6 GPC profile of TTFV-pyrene copolymer **55**.

2.7 Diffusion NMR Data Analysis

Pulsed gradient spin echo (PGSE) NMR experiments were performed on copolymer **55** in $CDCl_3$, and the data extracted from these experiments enable the determination of a diffusion coefficient, from which a hydrodynamic radius can be calculated using the Stokes-Einstein equation:

$$D = \frac{k_B T}{6\pi\eta r_H}$$

where D is the diffusion coefficient, k_B is the Boltzmann constant ($1.3806448 \times 10^{-23}$ J K^{-1}), T is temperature (298 K), η is viscosity of chloroform (0.517 mPa S), and r_H is the hydrodynamic radius. This equation is for molecules which are spherical in shape. Using the average diffusion coefficient, 1.984×10^{-10} m^2/s, obtained from the PGSE diffusion NMR experiments, the hydrodynamic radius r_H was calculated to be 2.13 nm.

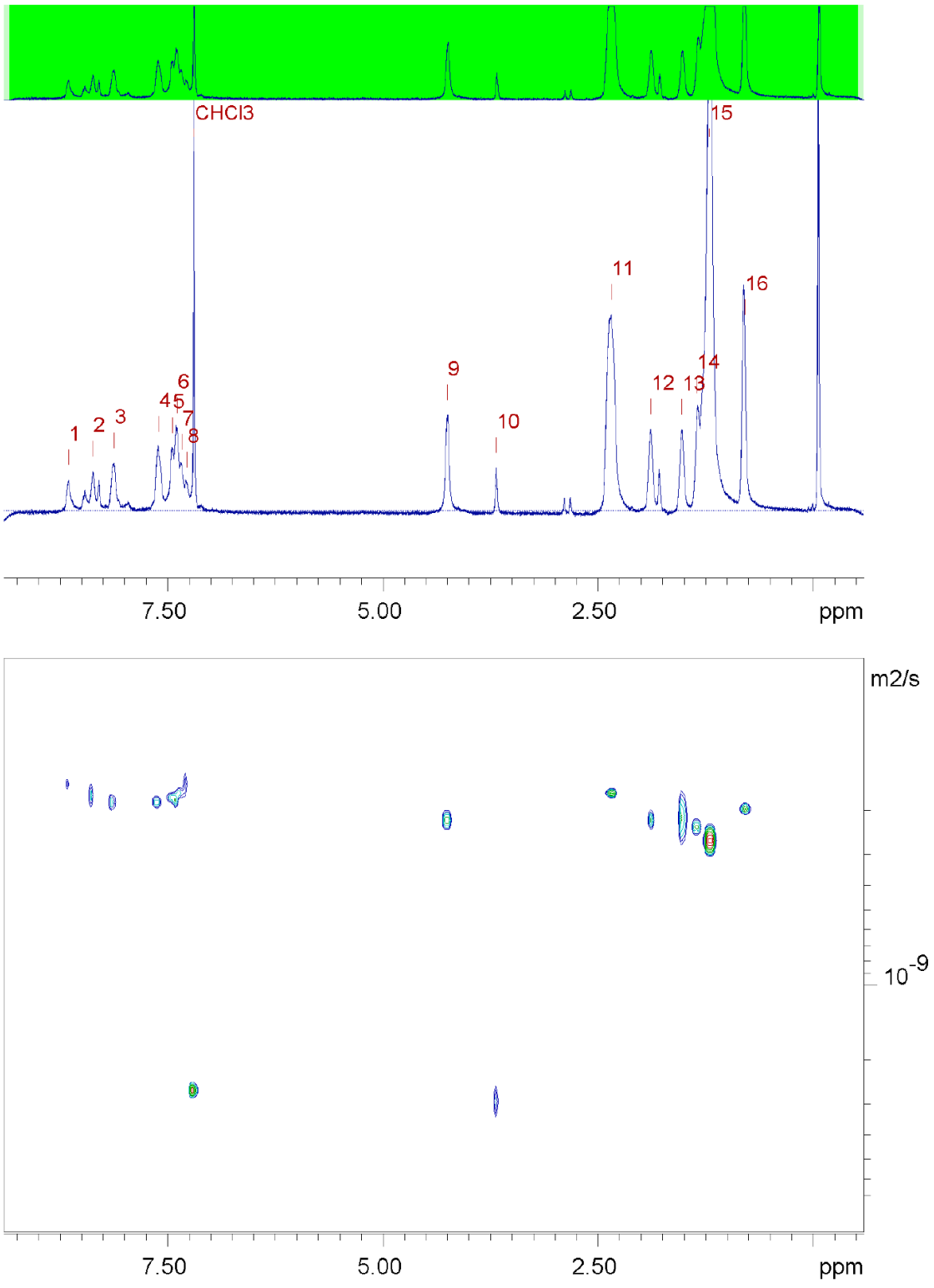

Fig. S-2.7 PGSE NMR (500 MHz, $CDCl_3$, 298 K) spectra of TTFV-pyrene copolymer **55**. The mean diffusion coefficient is 1.984×10^{-10} m^2/s.

2.8 UV-Vis Absorption Properties of 53-55

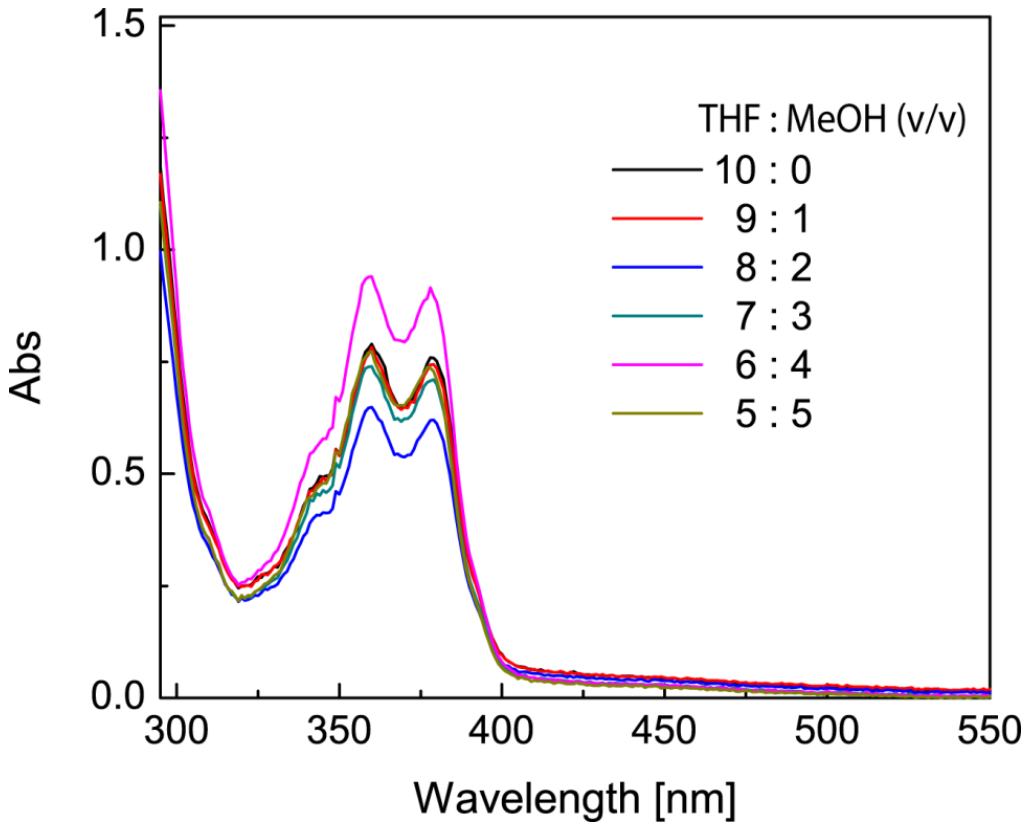

Fig. S-2.8 UV-Vis spectra of pyrene precursor **53** in THF/MeOH (1mg/100ml).

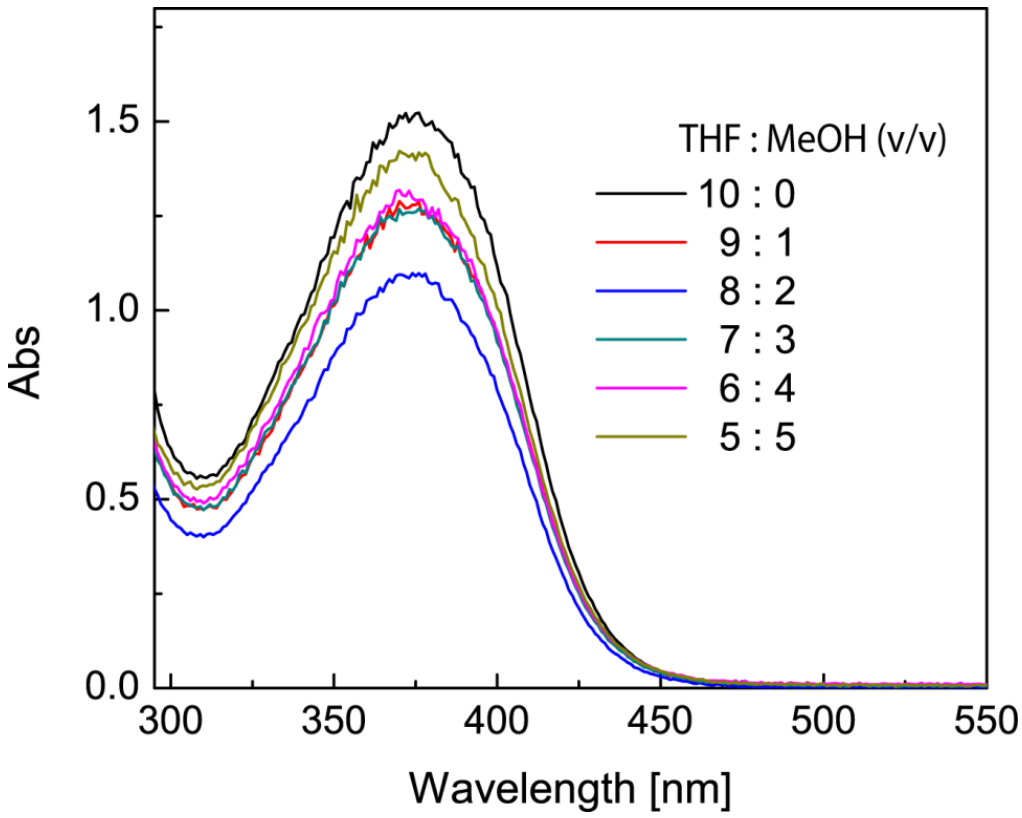

Fig. S-2.9 UV-Vis spectra of TTFV precursor **54** in THF/MeOH (1mg/100ml).

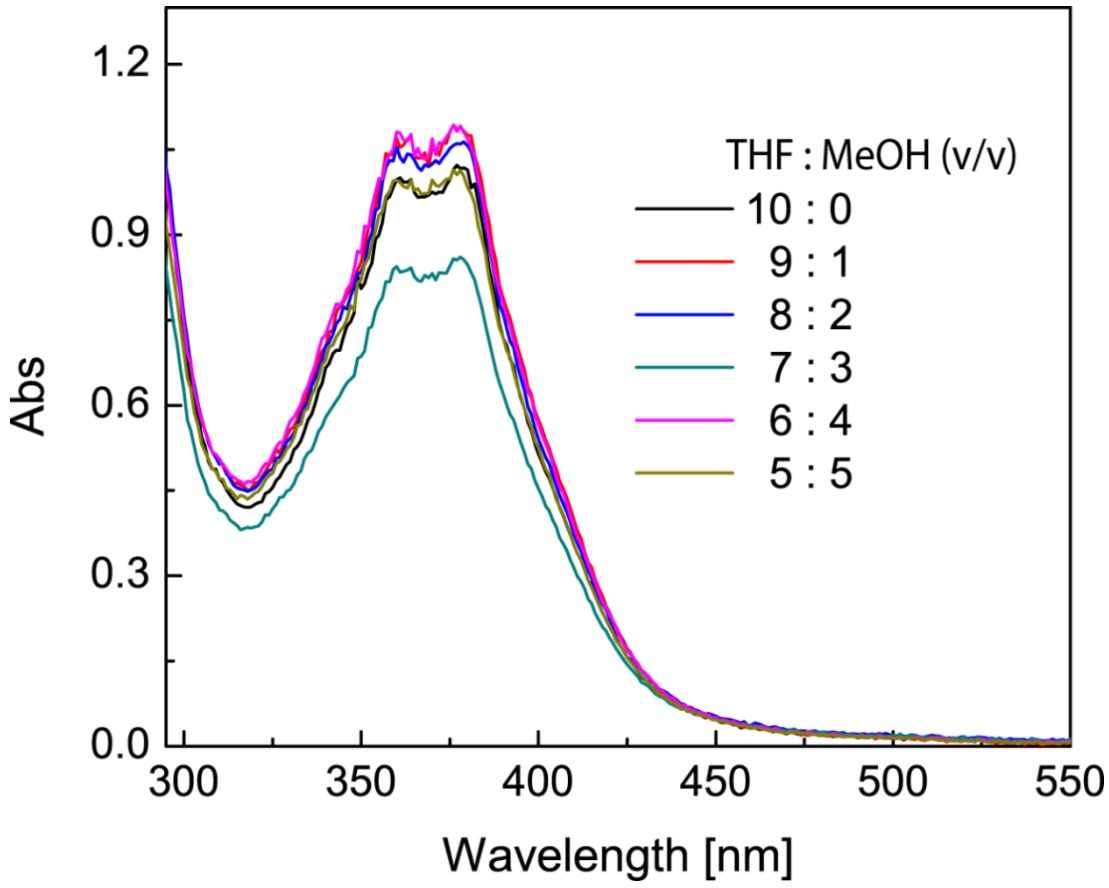

Fig. S-2.10 UV-Vis spectra of an equimolar mixture of **53** and **54** in THF/MeOH (1mg/100ml).

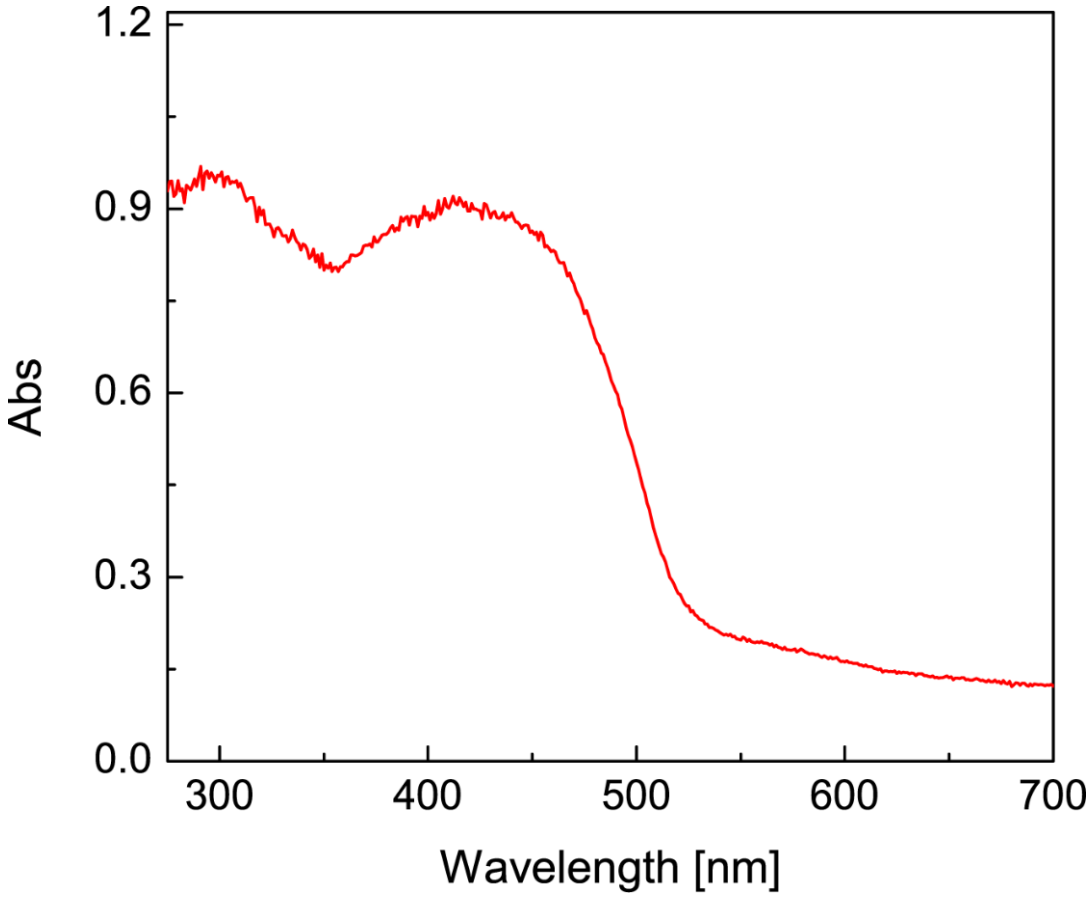

Fig. S-2.11 UV-Vis spectrum of the solid thin film of copolymer **55**.

2.9 References

(1) Inzelt, G. *Conducting Polymers: A New Era in Electrochemistry*, Springer-Verlag, Berlin Heidelberg, 2008.

(2) Skotheim, T. A.; Elsenbaumer, R. L.; Reynolds, J. R. *Handbook of Conducting Polymers*, 2nd ed., M. Dekker, New York, 1998.

(3) Heinze, J.; Frontana-Uribe, B. A.; Ludwigs, S. *Chem. Rev*. **2010**, *110*, 4724- 4771.

(4) Zhao, Y.; Chen, G.; Mulla, K.; Mahmud, I.; Liang, S.; Dongare, P.; Thompson, D. W.; Dawe, L. N.; Bouzan, S. *Pure Appl. Chem.* **2012**, *84*, 1005- 1025.

(5)Bendikov, M.; Wudl, F.; Perepichka, D. F. *Chem. Rev.* **2004**, *104*, 4891- 4946.

(6) Roncali, J. *J. Mater. Chem.* **1997**, *7*, 2307- 2321.

(7) Carlier, R.; Hapiot, P.; Lorcy, D.; Robert, A.; Tallec, A. *Electrochim. Acta* **2001**, *46*, 3269- 3277.

(8) Bellec, N.; Boubekeur, K.; Carlier, R.; Hapiot, P.; Lorcy, D.; Tallec, A. *J. Phys. Chem. A* **2000**, *104*, 9750- *9759*.

(9) Hapiot, P.; Lorcy, D.; Tallec, A.; Carlier, R.; Robert, A. *J. Phys. Chem.***1996**, *100*, 14823- 14827.

(10) Lorcy, D.; Guerro, M.; Bergamini, J.-F.; Hapiot, P. *J. Phys. Chem. B* **2013**, *117*, 5188- 5194.

(11) Gontier, E.; Bellec, N.; Brignou, P.; Gohier, A.; Guerro, M.; Roisnel, T.; Lorcy, D. *Org. Lett.* **2010**, *12*, 2386- 2389.

(12) Guerro, M.; Carlier, R.; Boubekeur, K.; Lorcy, D.; Hapiot, P. *J. Am. Chem. Soc*. **2003**, *125*, 3159- 3167.

(13) Mulla, K.; Liang, S.; Shaik, H.; Younes, E. A.; Adronov, A.; Zhao, Y. *Chem. Commun*. **2015**, *51*, 149- 152.

(14) Liang, S.; Zhao, Y.; Adronov, A. *J. Am. Chem. Soc*. **2013**, *136*, 970-977.

(15) Liang, S.; Chen, G.; Zhao, Y. *J. Mater. Chem. C* **2013**, *1*, 5477- 5490.

(16) Liang, S.; Chen, G.; Peddle, J.; Zhao, Y. *Chem. Commun*. **2012**, *48*, 3100- 3102.

(17) Chen, G.; Mahmud, I.; Dawe, L. N.; Daniels, L. M.; Zhao, Y. *J. Org. Chem.* **2011**, *76*, 2701- 2715.

(18) Chen, G.; Mahmud, I.; Dawe, L. N.; Zhao, Y. *Org. Lett.*, **2010**, *12*, 704- 707.

(19) Chen, G.; Zhao, Y. *Org. Lett*. **2014**, *16*, 668- 671 .

(20) Mulla, K.; Zhao, Y. *Tetrahedron Lett*. **2014**, *55*, 382-386 .

(21) Mulla, K.; Shaik, H.; Thompson, D. W.; Zhao, Y. *Org. Lett.* **2013**, ***15***, 4532- 4535; (22) Mulla, K.; Dongare, P.; Thompson, D. W.; Zhao, Y. *Org. Biomol. Chem*. **2012**, *10*, 2542-2544.

(23) Massue, J.; Bellec, N.; Guerro, M.; Bergamini, J.-F.; Hapiot, P.; Lorcy, D. *J. Org. Chem*. **2007**, *72*, 4655- 4662.

(24) Figueira-Duarte, T. M.; Müllen, K. *Chem. Rev*. **2011**, *111*, 7260- 7314.

(25) Winnik, F. M. *Chem. Rev*. **1993**, *93*, 587- 614.

(26) Wu, N.-W.; Zhang, J.; Ciren, D.; Han, Q.; Chen, L.-J.; Xu, L.; Yang, H.-B. *Organometallics* **2013**, *32*, 2536- 2545.

(27) Takemoto, K.; Karasawa, M.; Kimura, M. *ACS Appl. Mater. Interf.* **2012**, ***4***, 6289- 6294;

(28) Tran, P. D.; Le Goff, A.; Heidkamp, J.; Jousselme, B.; Guillet, N.; Palacin, S.; Dau, H.; Fontecave, M.; Artero, V. *Angew. Chem. Int. Ed*. **2011**, *50*, 1371- 1374.

(29) Liu, Y.; Yu, Z.-L.; Zhang, Y.-M.; Guo, D.-S.; Liu, Y.-P.; *J. Am. Chem. Soc*. **2008**, *130*, 10431- 10439.

(30) Ehli, C.; Rahman, G. M. A.; Jux, N.; Balbinot, D.; Guldi,D. M.; Paolucci, F.; Marcaccio, M.; Paolucci, D.; Melle-Franco, M.; Zerbetto, F.; Campidelli, S.; Prato, M. *J. Am. Chem. Soc*. **2006**, *128*, 11222- 11231.

(31) Casas-Solvas, J. M.; Howgego, J. D.; Davis, A. P.; *Org. Biomol. Chem*. **2014**, *12*, 212-232.

(32) Venkataramana, G.; Dongare, P.; Dawe, L. N.; Thompson, D. W.; Zhao, Y.; Bodwell, G. J. *Org. Lett.* **2011**, *13*, 2240- 2243.

(33)Spartan'10, Wavefunction Inc., Irvine, CA, USA.

(34) Stone, M. T.; Heemstra, J. M.; Moore, J. S. *Acc. Chem. Res*. **2005**, *39*, 11-20.

(35) Ray, C. R.; Moore, J. S. *Adv. Polym. Sci*. **2005**, *177*, 91- 149.

(36) Nelson, J. C.; Saven, J. G.; Moore, J. S.; Wolynes, P. G. *Science* **1997**, *277*, 1793- 1796.

(37) Chen, G.; Mahmud, I.; Dawe, L. N.; Daniels, L. M.; Zhao, Y. *J. Org. Chem.* **2011**, *76*, 2701-2715.

(38) Chen, G.; Mahmud, I.; Dawe, L. N.; Zhao, Y. *Org. Lett.* **2010**, *12*, 704-707.

Chapter 3

Highly π-extended Tetrathiafulvalene Analogues Derived from Pentacene-5,7,12,14-tetraone

- This chapter is published as a communication article in *RSC Advances*. "Younes, E.; Zhao, Y. *RSC Adv.*, **2015**, *5*, 88821–88825".
- E. Younes is the researcher who carried out most of the experimental work, including synthesis and characterization of exTTF **60** and **57b,** redox chemistry, and DFT calculations, under the supervision of Prof. Y. Zhao.

3.1 Introduction

Small-molecule semiconductors have been actively pursued in recent years, owing to their promising application in advanced molecular optoelectronic devices.[1–3] Of many organic semiconductors developed so far, fused acenes constitute a very appealing class of p-type semiconducting organic molecules; especially, pentacene-based molecules have been developed into a benchmark material for organic field effect transistors (OFETs) in light of their very high hole mobilities.[4–7] Electron deficient acenes, on the other hand, also attract considerable attention as n-type semiconductors.[4,8] Attachment of electron-withdrawing groups, such as halogen,[9,10] cyano,[11,12] or imide groups[12–15] onto the backbone of pentacene lowers the HOMO and LUMO energies, favouring electron transport in device application. It also renders the pentacene unit to be more resistant to oxygen-caused decomposition. Linking redox-active functional groups to

various molecular/macromolecular structures is a popular design approach for generating novel functional materials with wide-ranging applications, since in this way the properties of materials can be readily modulated or tuned by straightforward redox controls.[16,17] In theory, the electronic nature of a redox-active unit can be switched between electron-donating and electron-withdrawing in different oxidation states. It is hence reasonable to assume that functionalization of pentacene with redox-active substituents would give rise to redox-switchable structural and electronic characteristics. Tetrathiafulvalene (TTF) and related p-extended analogues (i.e., exTTFs) are excellent organic electron donors, many of which can undergo facile reversible redox processes induced by electrochemical and/or chemical means.[7,18–20] A well-known representative of exTTFs is the anthraquinone-derived system 1 (Scheme 3.1), generally referred to as TTFAQ.[7,19,21–23] In the neutral state, TTFAQ **56** adopts a non-planar saddle-like conformation.[24–27] Under moderate oxidative conditions, TTFAQ can release two π-electrons simultaneously to form a stable dication.[28–30] As depicted in Scheme 3.1, the two -electron oxidation transforms the central anthraquinoidal unit of TTFAQ **56** into a planar anthracene structure, while the two dithiolium rings rotate to an orientation perpendicular to the central anthracene so as to minimize disfavoured charge repulsion.[7,21] In a sense, TTFAQ can be deemed as concealing an anthracene moiety that can be fully revealed after oxidizing its two dithiole groups. The dication of TTFAQ, as a matter of fact, is an electron-deficient anthracene, given the electron-withdrawing nature of the dithiolium rings attached. Along this line, an unprecedented fused TTFAQ dimer **57a** (Scheme 3.1) recently caught our attention. Conceptually, compound **57a** not only represents an intriguing type of exTTFs with increased electron donating ability compared with TTFAQ, but also exhibits an electron-deficient pentacene structure in its tetracationic state. As this type of exTTF has not yet

been known in the current literature, it is of great fundamental importance to conduct pertinent synthetic and characterization studies.

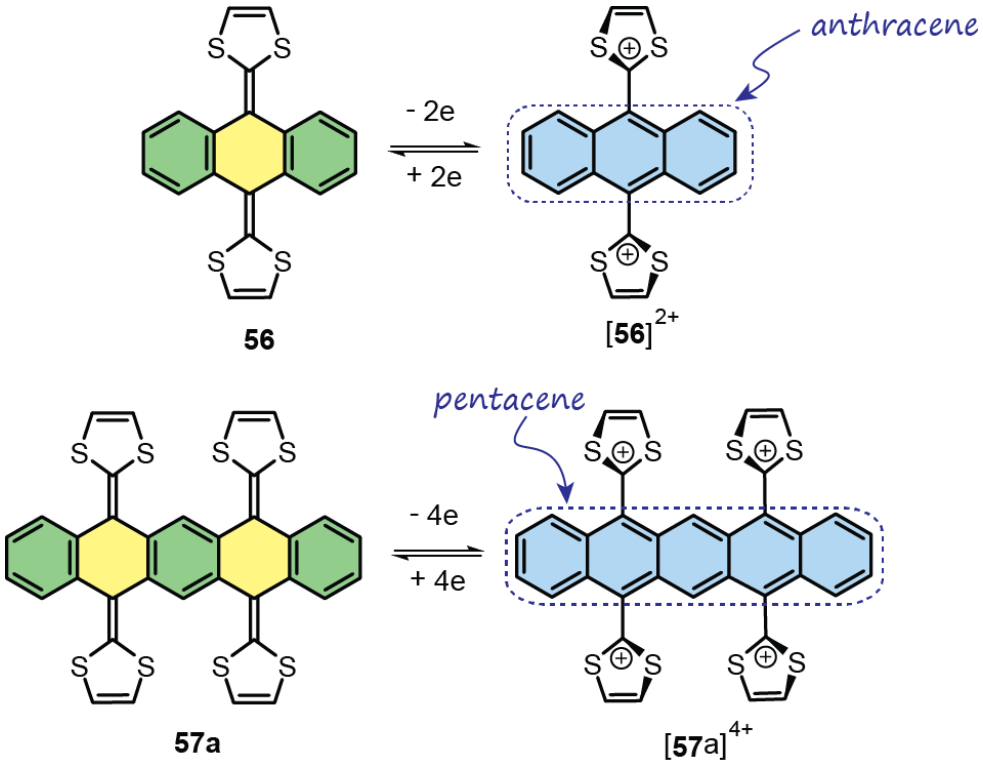

Scheme 3.1: Unmasking anthracene and pentacene moieties via oxidation reactions on the dithiole units in TTFAQ **56** and exTTF **57a**.

3.2 Results and Discussion

3.2.1 Synthesis of exTTF System

In this work, pentacene-5,7,12,14-tetraone (**58**)[31] was chosen as the starting material for synthesis. Initially, a fourfold $P(OMe)_3$-promoted olefination reaction[32] with thione **59** at elevated temperature (Scheme 3.2) was expected to directly lead to the target exTTF. However, this reaction only yielded trisubstituted compound **60** as the major product in 41% yield. Worth noting is that

there were no significant amounts of mono- and di-substituted products formed in this reaction. The inertness of **60** toward olefination with thione **59** can be ascribed to the strong electron-donating effects of the three-dithiole groups, which significantly reduce the electrophilicity of the last keto group. To accomplish the synthesis, a more reactive Horner-Wittig olefination approach was adopted, where a phosphonate ylide generated in situ by deprotonation of **61** (ref. 28 and 30) with *n*-BuLi was reacted with compound **60** to furnish the target exTTF **57b** in 65% yield.

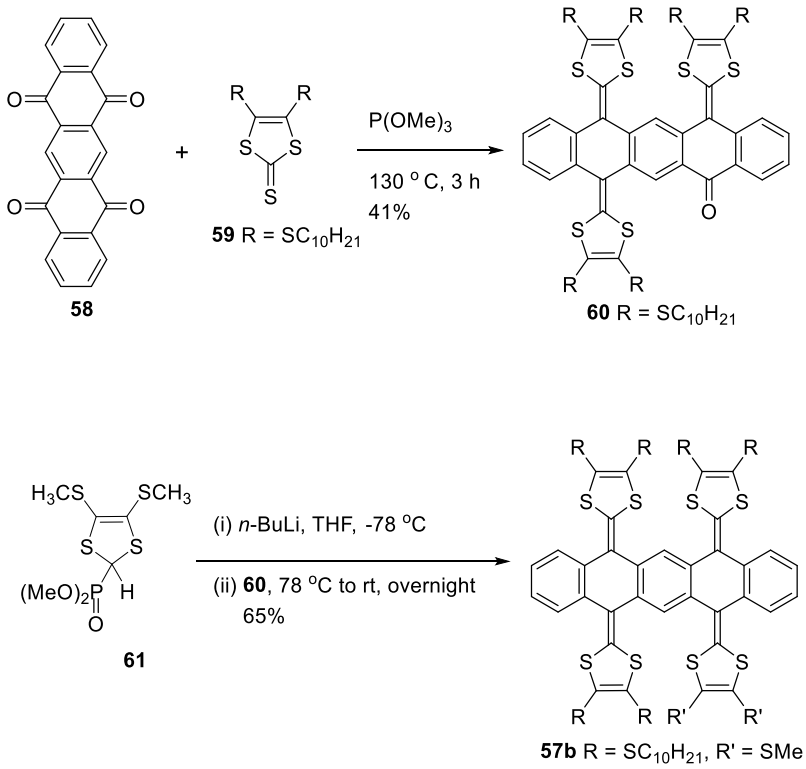

Scheme 3.2: Synthesis of exTTF **57b** via olefination reactions.

3.2.2 Redox and Electronic Properties

The electronic absorption properties of exTTFs **57b** and **60** were investigated by UV-Vis spectroscopy (Fig. 3.1). Compound **57b** is a stable yellow coloured semisolid, and in chloroform its UV-Vis absorption spectrum exhibits four well-resolved relatively sharp peaks at 478, 401, 356, and 250 nm. In addition, two shoulder bands are discernible at 449 and 294 nm. The finely structured spectral profile is indicative of a rigid π-backbone for compound **57b**. Compound **60** is a dark-red semisolid, which shows absorption bands at 512, 418, 310 (shoulder) and 255 nm in its UV-Vis absorption spectrum. The lowest-energy absorption band of **60** is considerably redshifted compared with that of exTTF **57a**, which can be attributed to the electron push-and-pull effects[33] between the electron-donating dithiole groups and the electron-withdrawing ketone group in the molecular structure of **60**. This result indicates that **60** has a more narrowed HOMO–LUMO gap than **57a** does.

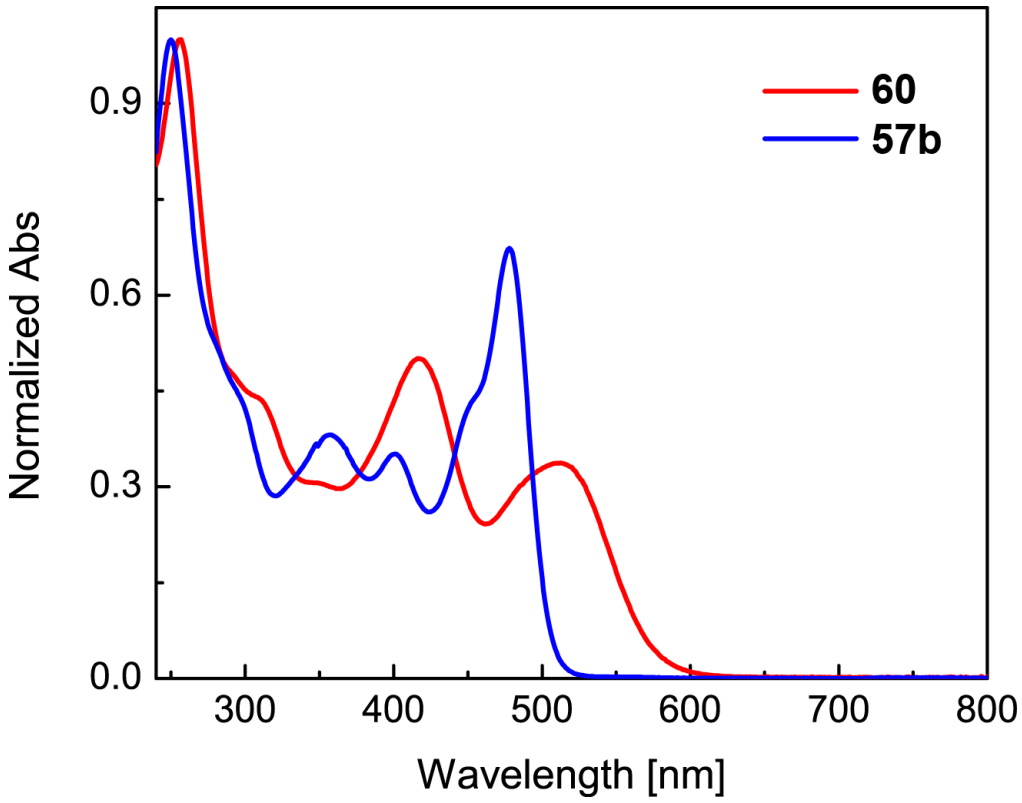

Fig. 3.1: Normalized UV-Vis spectra of compounds **57b** and **60** measured in $CHCl_3$ at room temperature (1mg/100 ml).

The redox activity of compounds **57b** and **60** were probed by cyclic voltammetric (CV) and differential pulse voltammetric (DPV) analyses (see Fig. 3.2). The CV profile of exTTF **57b** clearly shows two reversible redox wave pairs which are consistent with the two oxidation peaks observed at +0.46 and +0.72 V in its DPV. The results indicate that exTTF **57b** undergoes two distinctive steps of oxidation, with each step involving the transfer of two electrons given the nearly equal intensities of the two current peaks. Also worth noting is that the first oxidation potential of exTTF **57b** is significantly lower than that of a typical TTFAQ[7,28–30] by ca. 0.1 V, indicating that **57b** is a better electron donor than TTFAQ **56**. The DPV data of compound **60** shows three major oxidation peaks at +0.59, +0.96, and +1.21 V respectively. Together with the

observation of three quasi-reversible redox wave pairs in the CV profile of **60**, the electrochemical oxidation of **60** can be attributed to three sequential single-electron transfer steps. Interestingly, there is a weak current peak observed at +0.77 V in the DPV of **60**. The origin of this peak is not quite clear at this moment and awaits further investigations to understand.

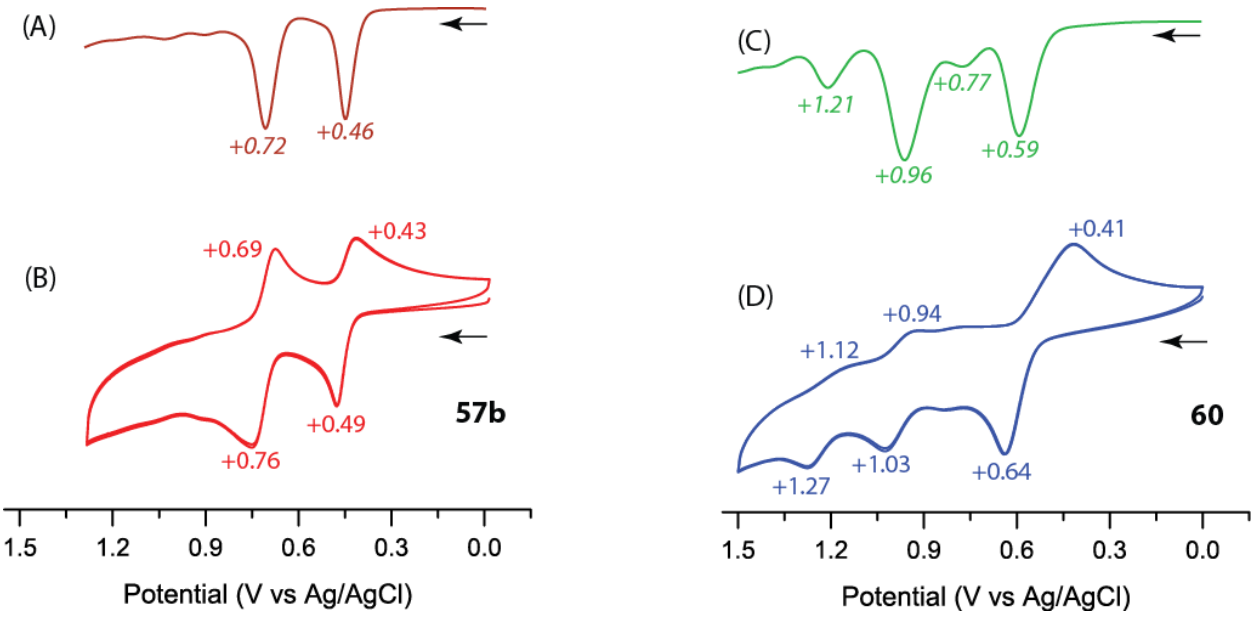

Fig. 3.2: Electrochemical analysis of compounds **57b** and **60** measured in CH_2Cl_2. (A) DPV of **57b**, (B) CV of **57b**, (C) DPV of **60**, and (D) CV of **60**. The arrows indicate the scan direction. Supporting electrolyte: Bu_4NBF_4 (0.1 M), working electrode: glassy carbon, counter electrode: Pt wire, reference electrode: Ag/AgCl (3M NaCl). CV: scan rate =100 mV s^{-1}; DPV: step = 4 mV, pulse amplitude = 50 mV, pulse width =50 ms, pulse period =200 ms.

Apart from electrochemical analysis, the oxidation properties of compounds **57b** and **60** were also studied by oxidative UV-Vis titration experiments in which a mixture of $PhI(OAc)_2$/ CF_3SO_3H (1:4 molar ratio) was utilized as the oxidant.[34] The titration results of exTTF **57b** as

shown in Fig. 3.3 manifest two stages of spectral changes upon chemical oxidation. In the first stage (Fig. 3A), four isosbestic points can be clearly seen and the lowest-energy absorption band of **57b** at 478 nm decreases substantially. A long-wavelength absorption tail ranging from 500 to 800 nm emerges and grows steadily, and this absorption feature can be ascribed to the formation of dithiolium cations during the oxidation of **57b**.[27,28,30] The second stage of spectral changes (Fig. 3.3B) exhibits three isosbestic points, while the overall variations of spectral profiles do not appear to be as dramatic as those in the first stage. Of note is that the long wavelength absorption tail shows a significant degree of redshift. The two-stage spectral changes observed in the oxidative UV-Vis titration of **57b** coincide with the two steps of electron transfer disclosed by electrochemical analysis. It is therefore reasonable to correlate the two stages in Fig. 3.3 with the formation of the dication and tetracation of **57b** in a sequential manner.

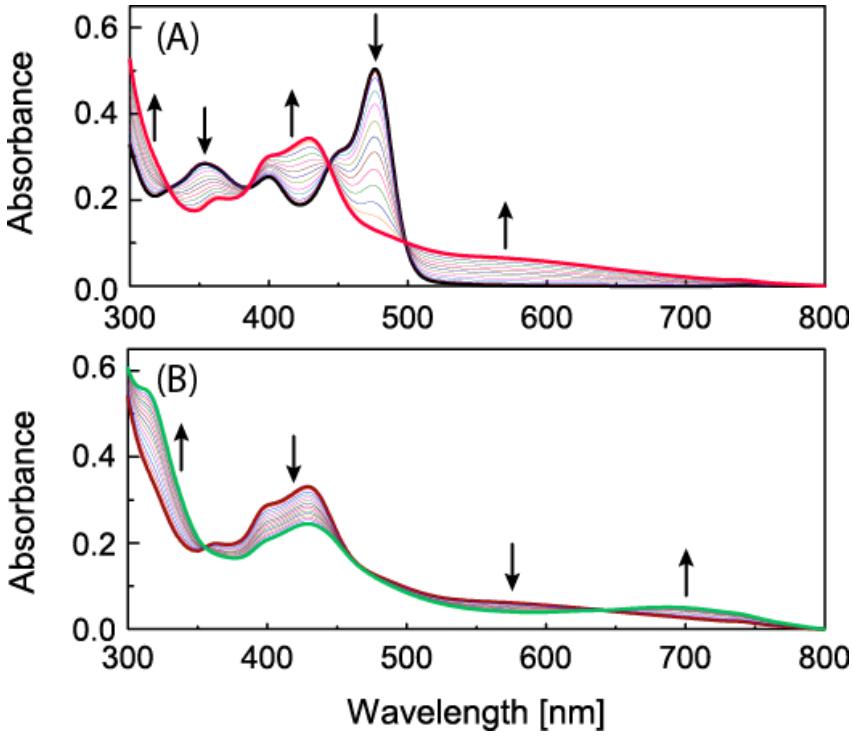

Fig. 3.3: UV-Vis spectra monitoring the titration of compound **57b** with $PhI(OAc)_2/CF_3SO_3H$ in THF at different stages. Addition of PhI(OAc)2: (A) 0 to 6.5 molecular equivalents, and (B) 7 to 14 molecular equivalents. The arrows indicate the trend of increasing oxidation.

The oxidative UV-Vis titration results of compound **60** can be divided into three stages of spectral changes as depicted in Fig. 3.4. In the first stage, the UV-Vis absorption profile of **60** changes considerably with four isosbestic points clearly seen (Fig. 3.4A). Unlike the case of **57b**, the characteristic long wavelength tail of dithiolium cation is rather weak in the oxidative titration of **60**. This phenomenon is likely associated with the electron-withdrawing keto group present in the π-framework of compound **60**. In the second and third stages, the spectral profiles change only to a small extent in comparison with the first stage. In view of the stepwise single-electron transfers observed in electrochemical experiments, the three stages shown in Fig. 3.4 are assigned to the formation of the radical cation, dication, and trication of **60** respectively.

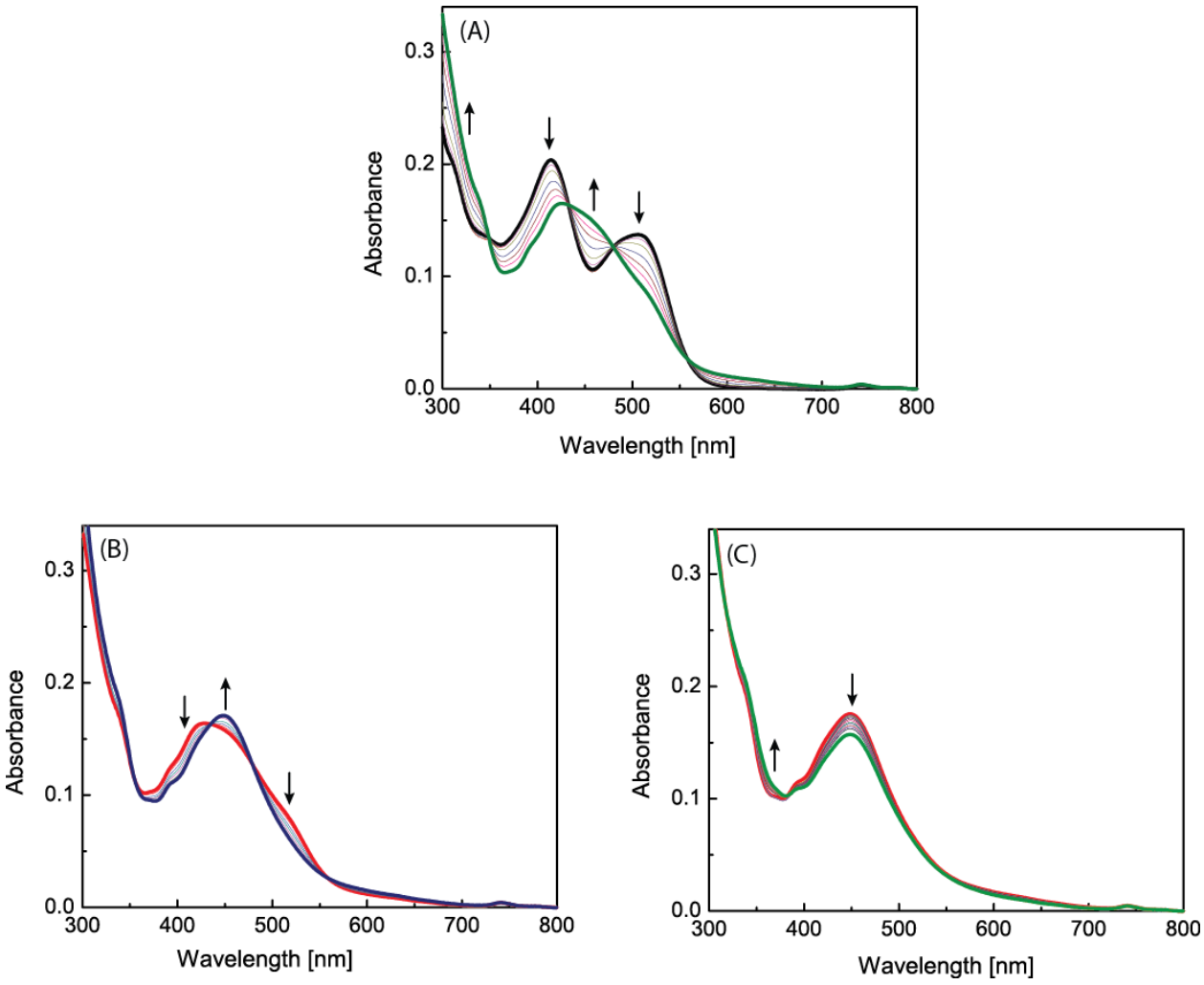

Fig. 3.4: UV-Vis spectra monitoring the titration of compound **60** with $PhI(OAc)_2/CF_3SO_3H$ in in THF at different stages. Addition of $PhI(OAc)_2$: (A) 0 to 10 molecular equivalents, (B) 11 to 18 molecular equivalents, and (C) 19 to 36 molecular equivalents. The arrows indicate the trend of increasing oxidation.

3.2.3 Theoretical Modeling Studies

To further understand the structural properties of exTTF **57b** in neural and oxidized states, its unsubstituted parent structure **57b** was subjected to theoretical modeling studies using density functional theory (DTF) approach i.e. B3LYP/6-31G(d). In the neutral state, two stable conformers (denoted as *cis* and *trans*, see Fig. 3.5A and B) were obtained from the DFT calculations. In each of the structures, the TTFAQ segments take a saddle-like shape similar to those reported in the literature.[24–27] The two conformers differ in the positions of the dithiole rings relative to the central polyaromatic unit. Energetically, the *trans* conformer is more stable than *cis* by 0.56 kcal mol^{-1} in the gas phase. DFT calculations also indicate that the two conformers of **57b** possess very similar frontier molecular orbital properties; however, the *cis* conformer has a slightly smaller

HOMO–LUMO gap (4.45 eV) than *trans* (4.40 eV), as a result of its relatively higher HOMO energy. The optimized geometry of the singlet tetracation of **57b** exhibits a dramatically changed conformation in comparison with the neutral state. As expected, the central π-unit turns into a planar, fully conjugated pentacene structure, to which the four dithiolium rings are in a perpendicular orientation (Fig. 3.5C). The HOMO–LUMO gap of [**57b**]$^{4+}$ is significantly reduced to 1.99 eV (in the gas phase), which accounts for the rise of a long-wavelength absorption tail in the oxidative UV-Vis titration of **57b.**

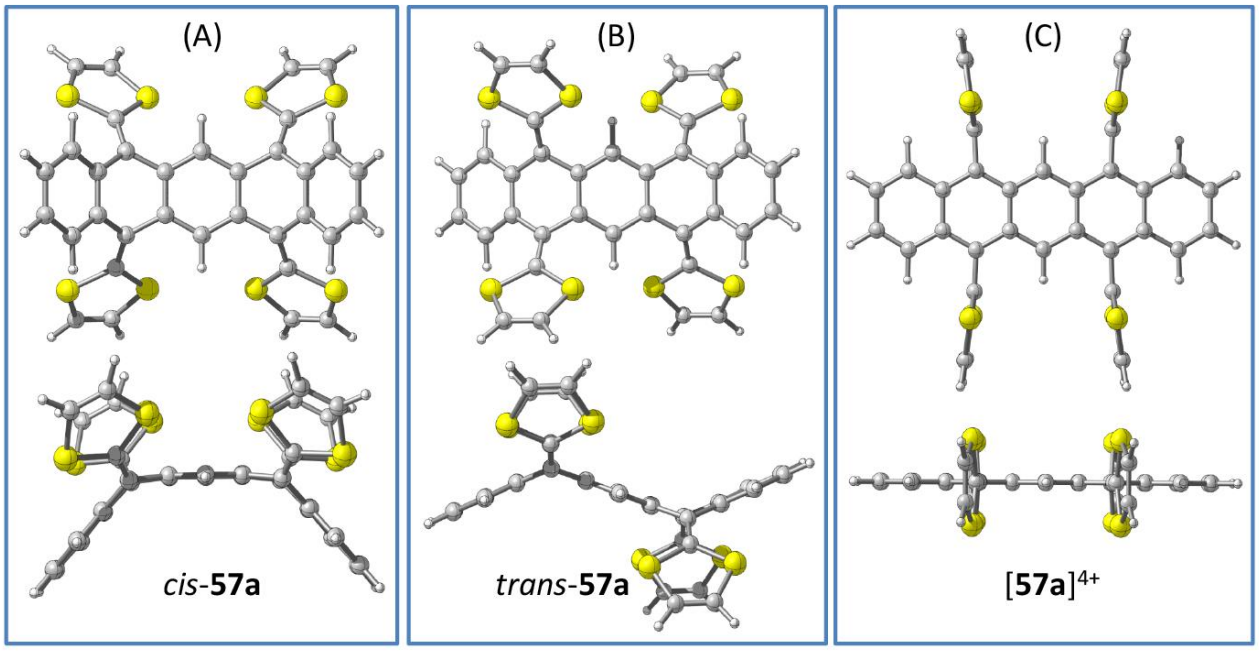

Fig. 3.5: Front (top) and side (bottom) views of (A) and (B) the optimized molecular geometries of exTTF **57a** and (C) its singlet tetracation calculated at the B3LYP/6-31G(d) level of theory.[35]

3.2.4 Variable Temperature (VT) NMR Study

The interchange of the conformers of **57b** does not undergo a very large energy barrier, as manifested by the variable temperature (VT) NMR study. In Fig. 3.6, the two SCH_3 groups of **57b** clearly give a set of two singlets (2.42 and 2.43 ppm) at room temperature (298 K), suggesting that the conformers of **57b** are in rapid equilibria at kinetic rates much faster than the time scale of NMR. As the temperature decreases from 298 K to 218 K, the two SCH_3 singlets gradually merge into one broad peak. In the meantime, the range of the CH_2 proton peaks become significantly widened. This phenomenon may be related to enhanced intermolecular aggregation at lowered temperature. When the temperature is further lowered to 198 K, the broad SCH_3 peak splits into several different peaks, signifying considerably slowed down interconversion between different conformers at this temperature.

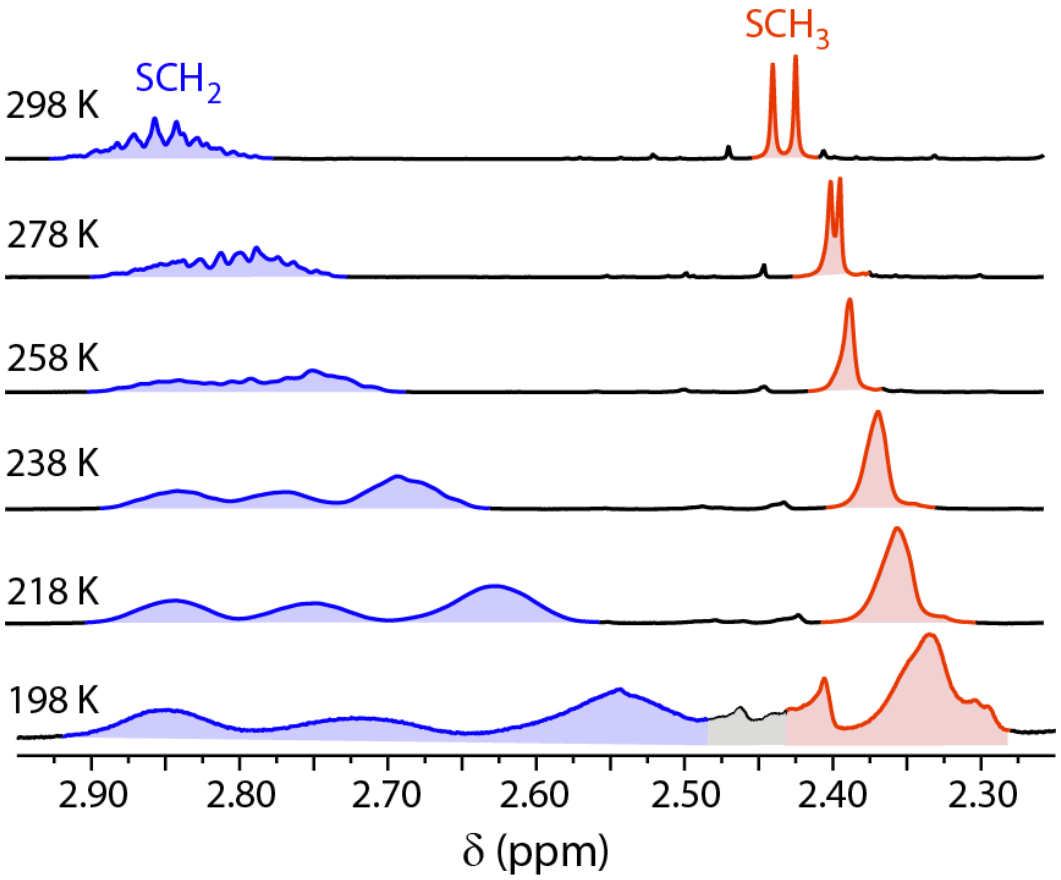

Fig. 3.6: Partial variable temperature (VT) ^{1}H NMR spectra (CD_2Cl_2, 500 MHz) of exTTF **57b** showing the regions of SCH_2 and SCH_3 protons.

3.3 Conclusions

In summary, stepwise olefination reactions on pentacen-5,7,12,14-tetraone have successfully led to a new class of highly π-extended TTF analogues **57b** and **60**. The redox chemistry of these compounds features multi-stage electron transfers accompanied by dramatic conformational changes. Of great fundamental interest is that the central moiety of exTTF **57b** can be transformed into a full pentacene structure after exhaustive oxidation. It is anticipated that this

type of exTTFs can be developed into useful redox-switchable building blocks for advanced molecular materials and devices.

3.4 Experimental

3.4.1 General

Chemicals and reagents were purchased from commercial suppliers and used directly without purification. All reactions were conducted in standard, dry glassware and under an inert atmosphere of nitrogen unless otherwise noted. Evaporation and concentration were carried out with a water-aspirator. Flash column chromatography was performed with silica gel 60 (240-400 mesh). Thin-layer chromatography (TLC) was carried out with silica gel F254 covered on plastic sheets and visualized by UV light. ^{1}H and ^{13}C NMR spectra were measured on a Bruker Avance III 300 MHz multinuclear spectrometer. Chemical shifts (δ) are reported in ppm downfield relative to the signal of the internal reference $SiMe_4$. Coupling constants (J) are given in Hz. Infrared spectra (IR) were recorded on a Bruker Alfa spectrometer. HRMS analyses were performed on an Agilent 6230 TOF LC/MS instrument using an APPI ionizer. UV-Vis absorption spectra were measured on a Cary 6000i spectrophotometer. Cyclic voltammetric (CV) and differential pulse voltammetric (DPV) were carried out in a standard three-electrode setup controlled by a BASi epsilon workstation. Pentacene-5,7,12,14-tetraone (**58)**[36], thione (**59)**[37], and S-methyl phosphonate (**61)**[38] were prepared according to literature procedures with suitable modifications.

3.4.2 Synthetic procedures

Compound 60

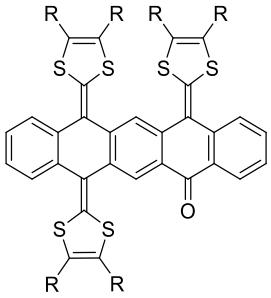

60 R = $SC_{10}H_{21}$

Pentacene–5,7,12,14–tetraone **58** (0.051 g, 0.15 mmol) and thione **59** (0.43 g, 0.90 mmol) were mixed in $P(OCH_3)_3$ (40 mL), and the mixture was heated to 130 ^oC for 3 h. The unreacted $P(OCH_3)_3$ was then removed under reduced pressure. The resulting crude product was subjected silica flash column chromatography (CH_2Cl_2/hexanes, 1:1) to yield pure compound **5** (0.10 g, 0.061 mmol, 41%) as a dark red semisolid. IR (neat): 2953, 2921, 2851, 1655, 1596, 1522, 1489, 1462, 1259, 758 cm^{-1}; ^1H NMR (300 MHz, $CDCl_3$) δ 8.29 (d, *J* = 9.0 Hz, 1H), 8.08 (s, 1H), 7.84 (d, *J* = 7.6 Hz, 1H), 7.69-7.60 (m, 3H), 7.48-7.44 (m, 1H), 7.37-7.33 (m, 3H), 2.86-2.78 (m, 12H), 1.66-1.59 (m, 12H), 1.40-1.22 (m, 84H), 0.89-0.83 (m, 18H). ^{13}C NMR (75 MHz, $CDCl_3$) δ 182.6, 140.5, 139.0, 137.9, 136.5, 134.6, 134.4, 134.2, 133.3, 132.6, 131.5, 130.9, 128.2, 128.2, 127.8, 127.6, 127.0, 126.7, 126.6, 126.5, 126.2, 125.6, 125.5, 125.2, 123.8, 122.1, 122.1, 121.7, 118.6, 37.0, 36.9, 36.8, 36.5, 36.4, 31.9, 29.7, 29.6, 29.5, 29.5, 29.4, 29.3, 29.2, 29.1, 28.6, 28.5, 22.7, 14.2. HRMS (APCI, positive) *m/z* calcd for $C_{96}H_{137}OS_{12}$ ($[M + H]^+$) 1629.7318, found 1629.7266.

Compound 57b

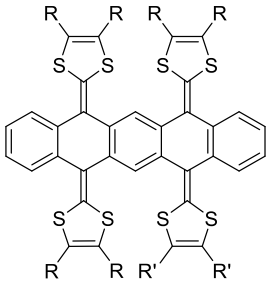

57b R = $C_{10}H_{21}$, R' = CH_3

To a solution of *S*-methyl phosphonate **61** (0.025 g, 0.086 mmol) in dry THF (15 mL) at -78 ^{o}C was added *n*-BuLi (0.034 mL, 2.5M, 0.086 mmol). After stirring for 15 min, a solution of compound **60** (0.070 g, 0.043 mmol) in dry THF (5 mL) was added to the reaction mixture through a syringe. The resulting mixture was allowed to warm to rt and kept stirring overnight. Then the solvent was removed under reduced pressure, and the residue was diluted with CH_2Cl_2. The solution was collected and washed with brine and H_2O sequentially, and the organic phase was dried over $MgSO_4$ and then concentrated under vacuum, affording the crude product of **57b** which was purified by silica flash column chromatography (CH_2Cl_2/hexanes, 1:4) to yield compound **57b** (0.051 g, 0.028 mmol, 65%) as a yellow semisolid. IR (neat): 2953, 2921, 2851, 1732, 1539, 1455, 1260, 1092, 1021, 851, 772, 653 cm^{-1}; ^{1}H NMR (300 MHz, $CDCl_3$) δ 7.69-7.57(m, 5H), 7.42-7.33 (m, 5H), 2.90-2.78 (m, 12H), 2.46 (s, 3H), 2.42 (s, 3H), 1.68-158 (m, 12H), 1.41-1.25 (m, 84H), 0.89- 0.85 (m, 18H). ^{13}C NMR (75 MHz, $CDCl_3$) δ 134.5, 134.5, 134.4, 132.8, 132.5, 131.2, 130.9, 130.8, 130.1, 127.1, 126.8, 126.7, 126.3, 126.3, 126.1, 125.4, 125.3, 124.7, 124.0, 122.8, 122.7, 121.5, 121.4, 36.7, 36.3, 31.9, 29.9, 29.8, 29.7, 29.6, 29.5, 29.3, 29.3, 29.2, 28.7, 28.6, 28.60, 22.7, 19.5, 19.3, 14.1. HRMS (APCI, positive) *m/z* calcd for $C_{96}H_{143}S_{16}$ ($[M + H]^{+}$) 1807.6721, found 1807.6629.

3.4.3 Oxidative UV-Vis Titration Experiments

3.4.3.1 Titration of 60

A solution of **60** in THF (7.38×10^{-6} M) was prepared and then titrated with a mixture solution of $PhI(OAc)_2$/ CF_3SO_3H, (1: 4 molar ratio, $[PhI(OAc)_2] = 2.60 \times 10^{-2}$ M) using a microsyringe. In each titration step, *ca*. 1 molar equivalent of oxidant was added. The mixture solution was allowed to stand for *ca.* 5 min before a UV-Vis absorption spectrum of the solution was recorded.

3.4.3.2 Titration of 57b

A solution of **57b** in THF (8.29×10^{-6} M) was prepared, and then titrated with a mixture solution of $PhI(OAc)_2$/ CF_3SO_3H, (1: 4 molar ratio, $[PhI(Oac)_2] = 2.57 \times 10^{-2}$ M) using a microsyringe. In each step of titrations, *ca*. 0.5 molar equivalent of oxidant was added. The mixture solution was allowed to stand for *ca.* 5 min before a UV-Vis absorption spectrum of the solution was recorded.

3.5 NMR Spectra of New Compounds

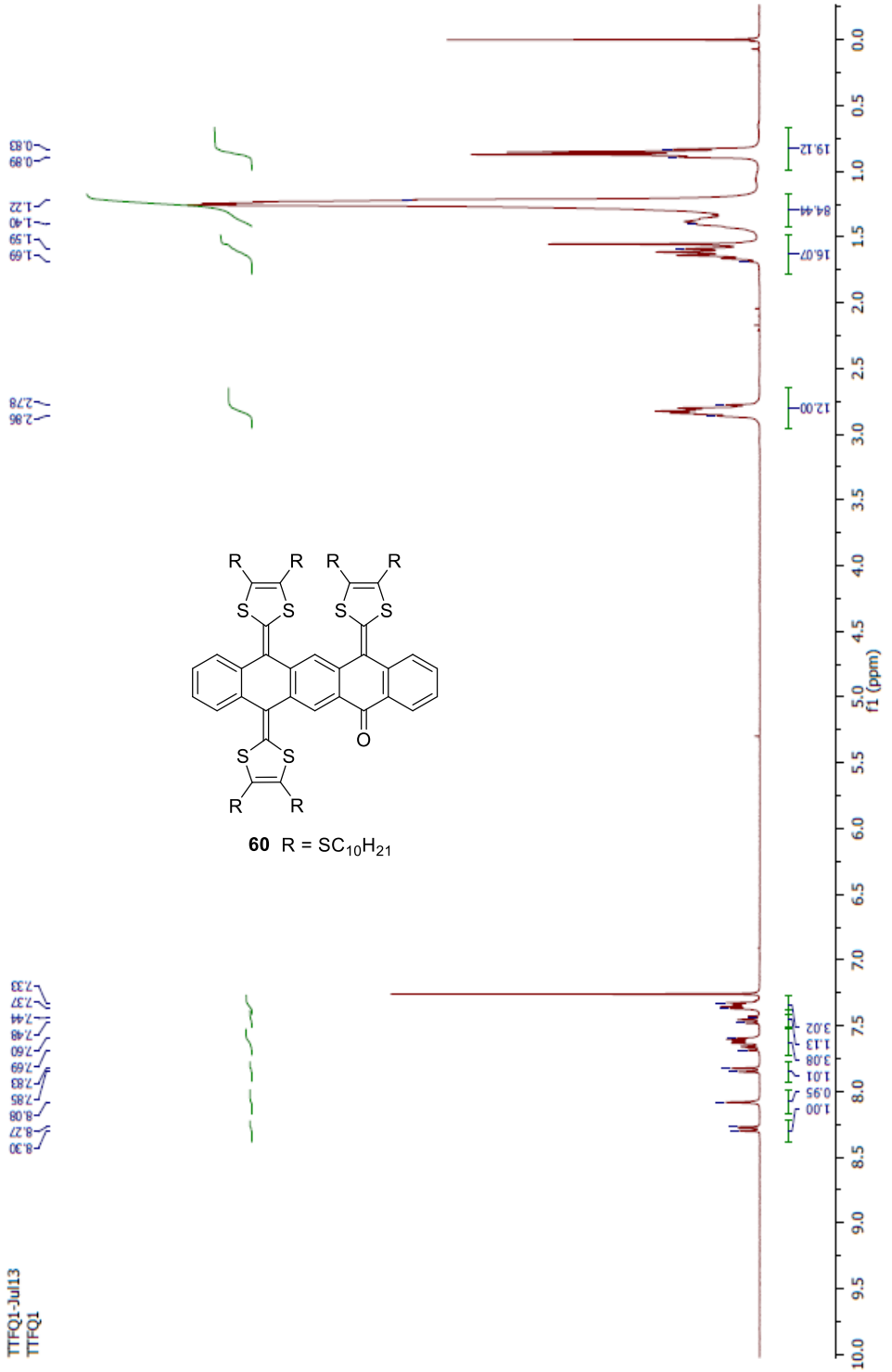

Fig. S-3.1: ^{1}H NMR (300 MHz, $CDCl_3$) spectrum of compound **60**.

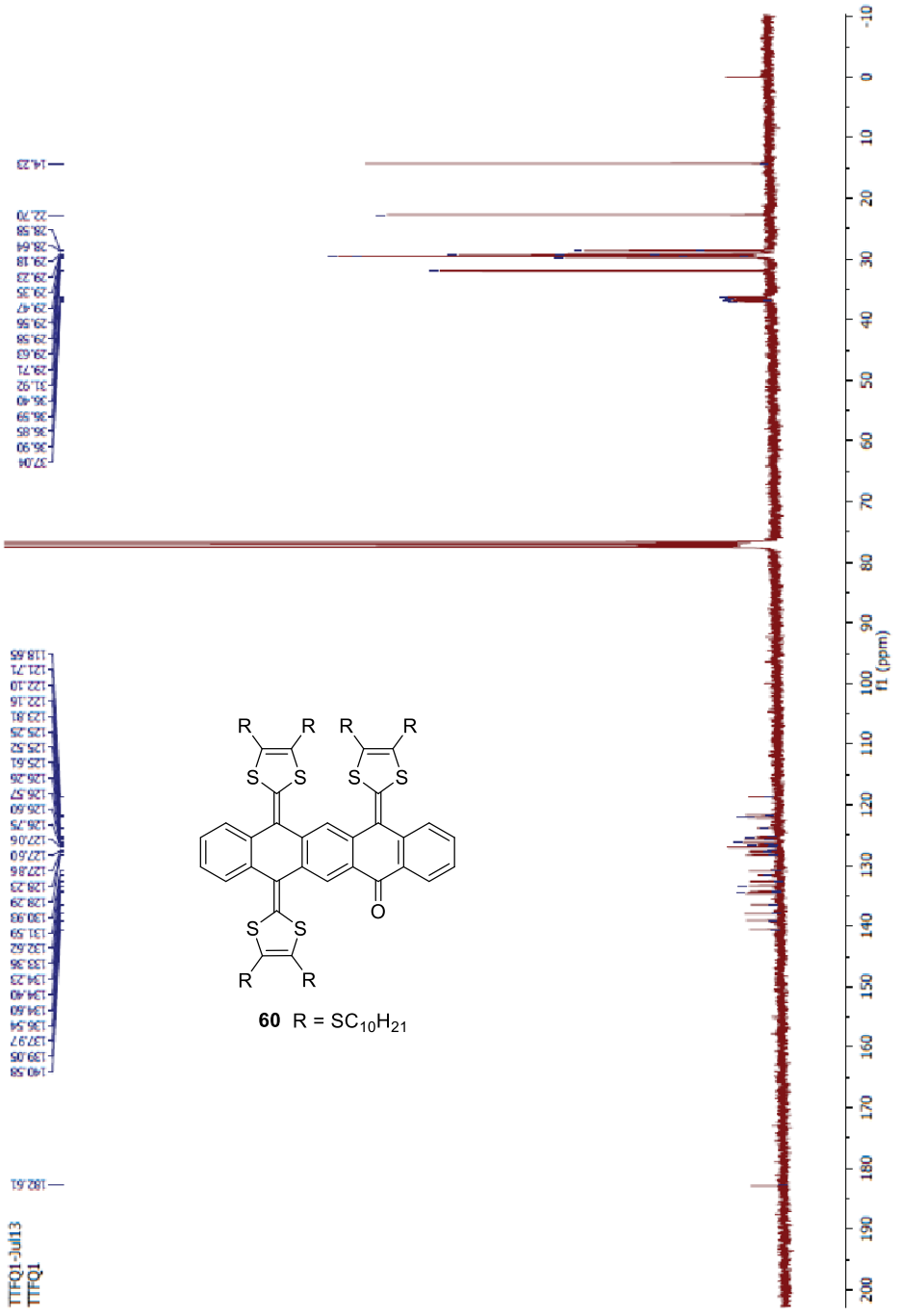

Fig. S-3.2: ^{13}C NMR (75 MHz, $CDCl_3$) spectrum of compound **60**.

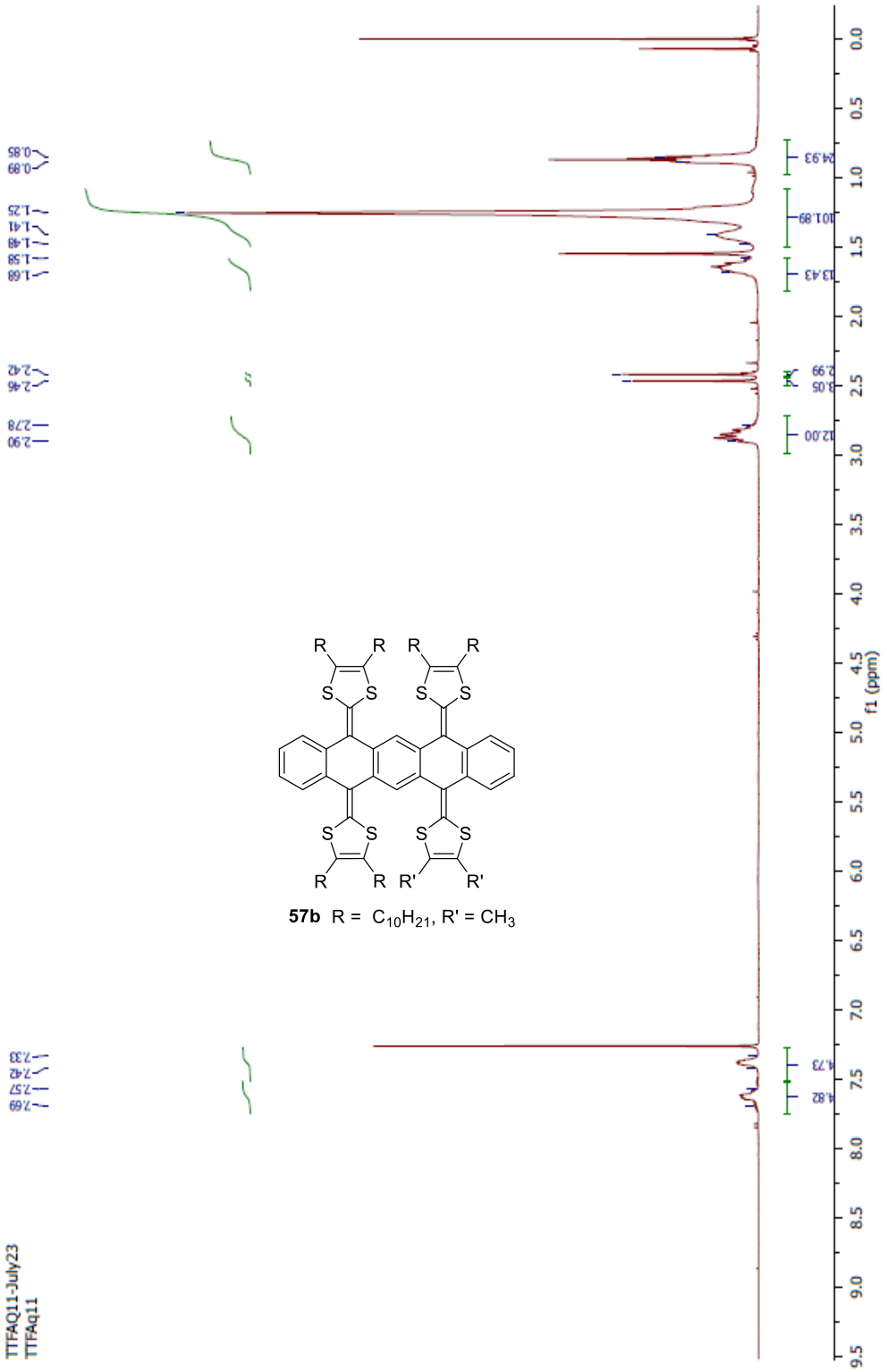

Fig. S-3.3: ^{1}H NMR (300 MHz, $CDCl_3$) spectrum of compound **57b**.

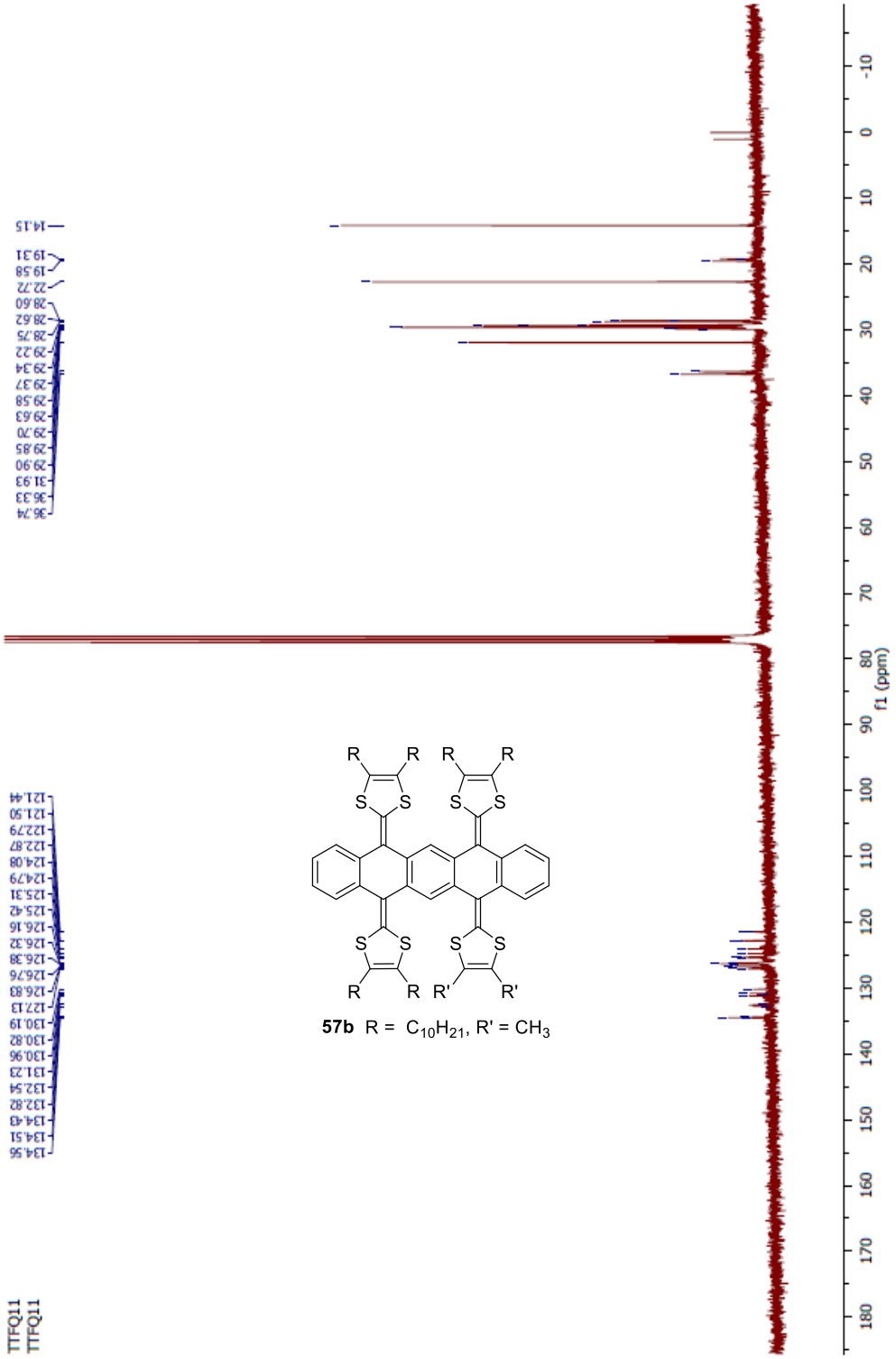

Fig. S-3.4: ^{13}C NMR (75 MHz, $CDCl_3$) spectrum of compound **57b**.

3.6 DFT Calculations on Compound 57a

The structural and frontier molecular orbital (FMO) properties of compound **57a** in different oxidation states were investigated by density functional theory (DFT) calculations using the Gaussain 09 software package.[39] The molecular geometries were optimized at the B3LYP/6-31G(d) level and visualized with CYLview, while the FMO plots were visualized with Gaussview 5.[40]

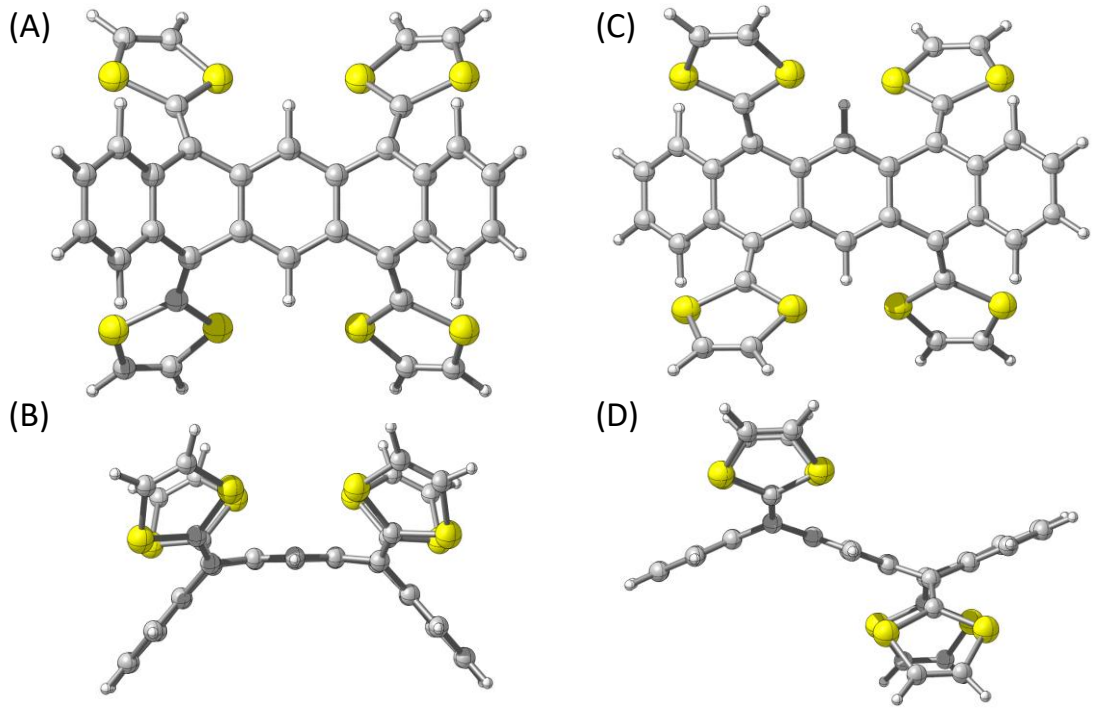

Fig. S-3.5: Optimized geometries of compound **57a** in the neutral state computed using B3LYP/6-31G(d) . (A) and (B): *cis* conformer E (*cis*) = -4491.86093507 hartrees, dipole moment = 3.1984 Debye), (C) and (D) *trans* conformer E(*trans*) = -4491.86251228 hartrees, dipole moment = 0 Debye).

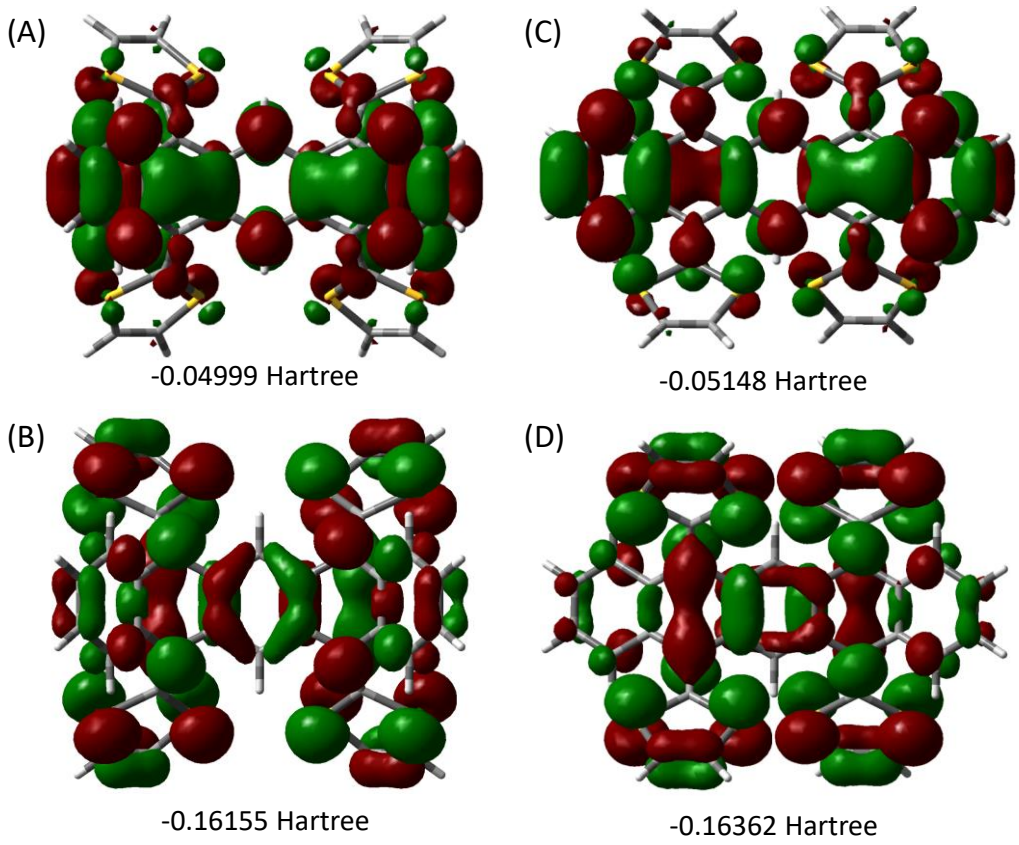

Fig. S-3.6: Plots and energies of FMOs for compound **57a** in the neutral state. (A) LUMO of *cis* conformer, (B) HOMO of *cis* conformer, (C) LUMO of *trans* conformer, and (D) HOMO of *trans* conformer.

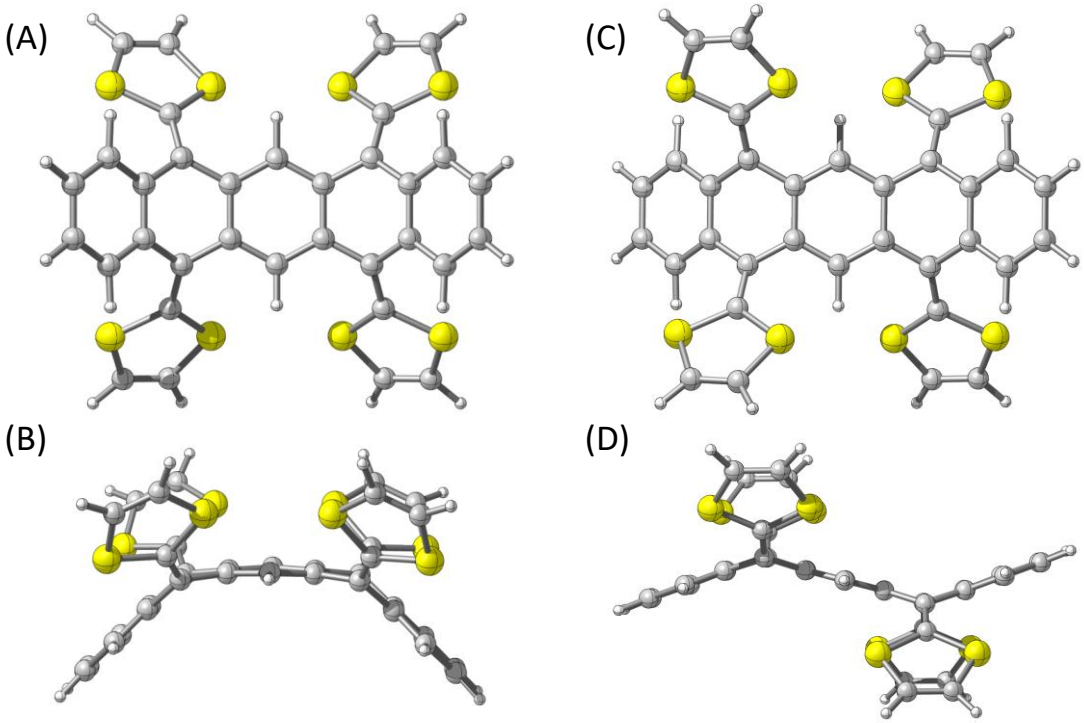

Fig. S-3.7: Optimized geometries of compound **57a** in the singlet dicationic state computed using UB3LYP/6-31G(d). (A) and (B): *cis* conformer *E*(*cis*) = -4491.36838584 hartees, dipole moment = 4.8715 Debye), (C) and (D) *trans* conformer *E* (*trans*) = -4491.36742237 hartees, dipole moment = 0 Debye).

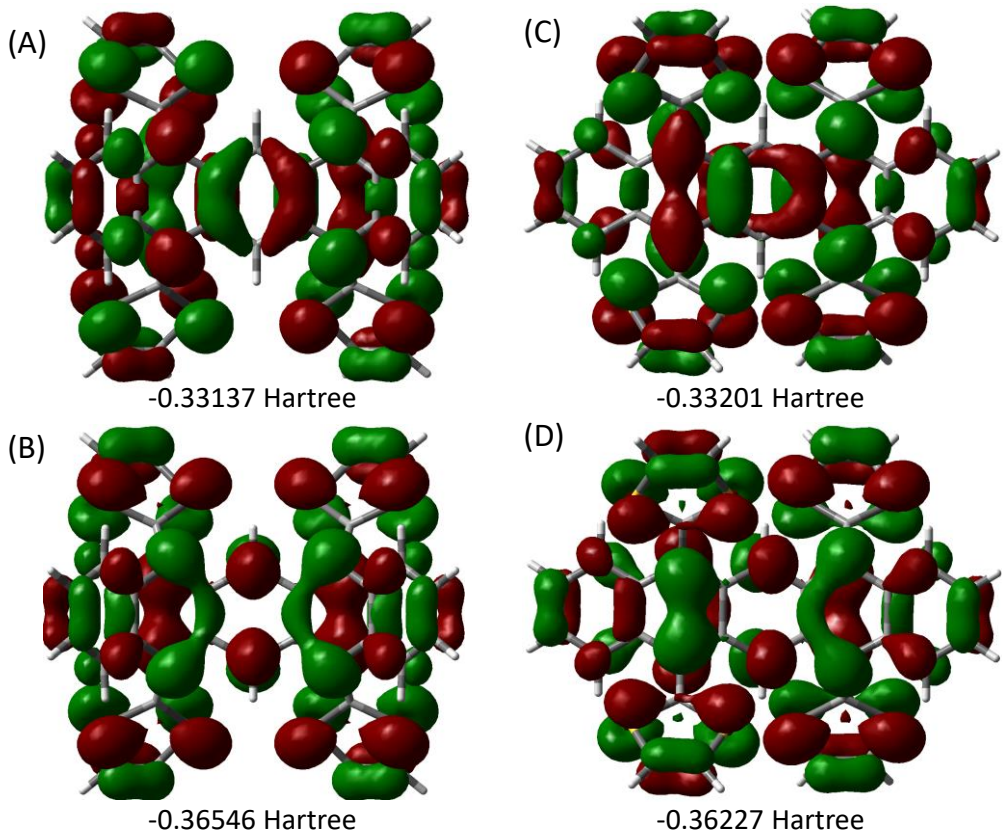

Fig. S-3.8: Plots and energies of FMOs for compound **57a** in the singlet dicationic state. (A) LUMO of *cis* conformer, (B) HOMO of *cis* conformer, (C) LUMO of *trans* conformer, and (D) HOMO of *trans* conformer.

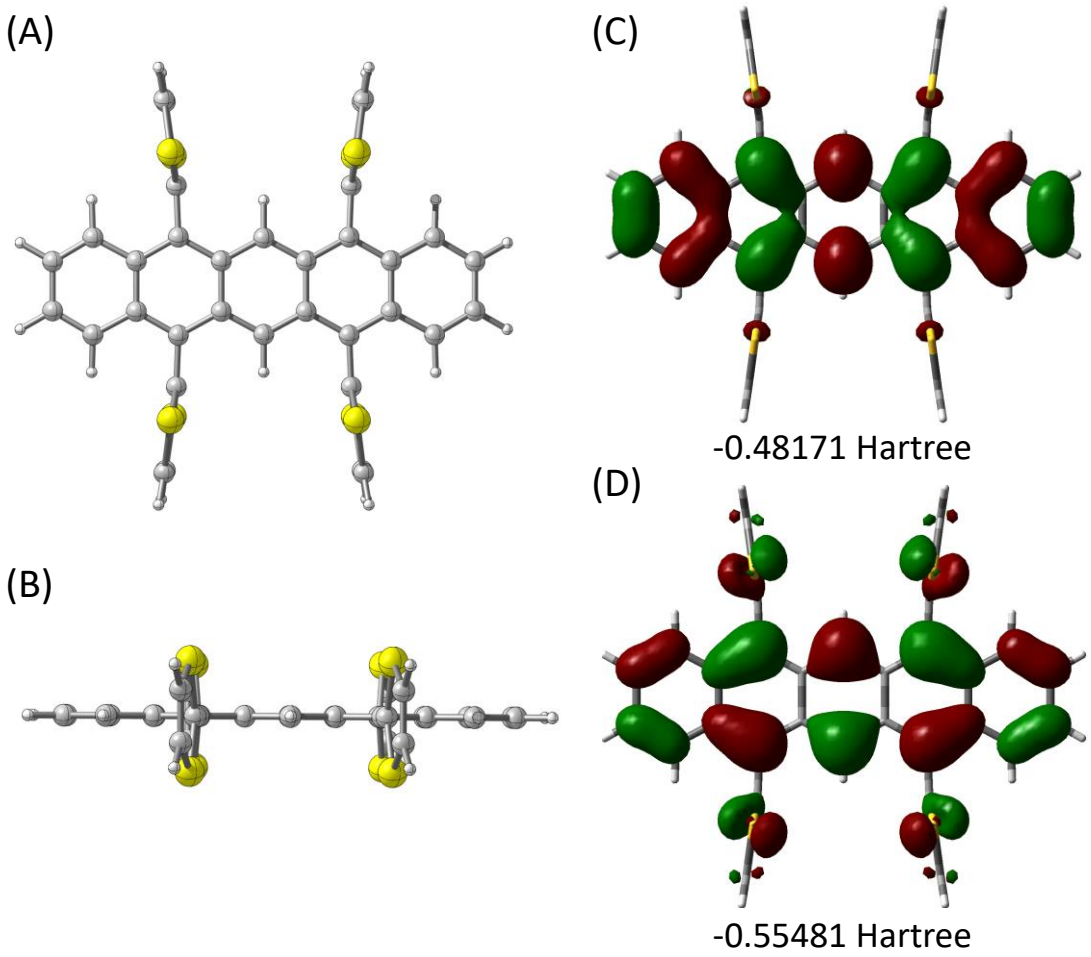

Fig. S-3.9: Optimized geometries of compound **57a** in the singlet tetracationic state computed using B3LYP/6-31G(d). *E*= -4490.50168326 hartees, dipole moment = 0.0024 Debye). (A) Front view, (B) side view. Plots and energies of FMOs for compound **57a** in the singlet tetracationic state. (C) LUMO and (D) HOMO.

3.7 VT-NMR Results for Compound 57b

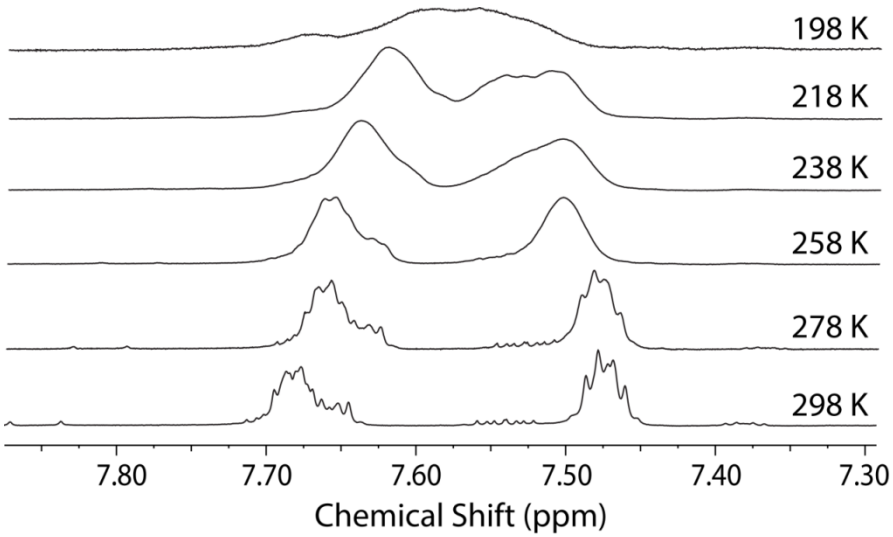

Fig. S-3.10: Partial VT ^{1}H NMR (CD_2Cl_2, 500 MHz) spectra of **57a** showing the aromatic region.

3.8 References

(1) Lin, Y.; Li, Y.; Zhan, X.; Qu, Y.; Xie, Z.; Yan, D.; Geng, Y.; Wang, F.; Brédas, J.-L.; McGehee, M. D.; Sellinger, A.; Drees, M.; Jiang, L.; Shu, C.; Wang, C. *Chem. Soc. Rev.* **2012**, *41* (11), 4245–4272.

(2) Mishra, A.; Bäuerle, P. *Angew. Chemie Int. Ed.* **2012**, *51* (9), 2020-2067.

(3) Murphy, A. R.; Fréchet, J. M. J. *Chem. Rev.* **2007**, *107*, 1066–1096.

(4) Ye, Q.; Chi, C. *Chem. Mater.* **2014**, *26*, 4046–4056.

(5) Anthony, J. E. *Angew. Chem. Int. Ed.* **2008**, *47*, 452–483.

(6) Anthony, J. E. *Chem. Rev.* **2006**, *106*, 5028–5048.

(7) Bendikov, M.; Wudl F.; Perepichka, D. F. *Chem. Rev.* **2004**, *104*, 4891–4945.

(8) Qu, H.; Chi, C. *Curr. Org. Chem.* **2010**, *14*, 2070–2108.

(9) Shu, Y.; Lim, Y.-F.; Li, Z.; Purushothaman, B.; Hallani, R.; Kim, J. E.; Parkin, S. R.; Malliaras, G. G.; Anthony, J. E. *Chem. Sci.* **2011**, *2*, 363–368.

(10) Qu, H.; Chi, C. *Org. Lett.* **2010**, *12*, 3360–3363.

(11) Katsuta, S.; Miyagi, D.; Yamada, H.; Okujima, T.; Mori, S.; Nakayama, K.-i.; Uno, H. *Org. lett.* **2011**, *13*, 1454–1457.

(12) Lin, Y.-C.; Lin, C.-H.; Chen, C.-Y.; Sun, S.-S.; Pal, B. *Org. Biomol. Chem.* **2011**, *9*, 4507–4517.

(13) Qu, H.; Cui, W.; Li, J.; Shao, J.; Chi, C. *Org. lett.* **2011**, *13*, 924–927.

(14) Ye, Q.; Chang, J.; Huang, K.-W.; Chi, C. *Org. lett.* **2011**, *13*, 5960–5963.

(15) Yin, J.; Zhang, K.; Jiao, C.; Li, J.; Chi, C.; Wu, J.; *Tetrahedron Lett.* **2010**, 51, 6313–6315.

(16) Inzelt, G. *Conducting Polymers: A New Era in Electrochemistry*, Sprin, Berlin, 2nd edn, **2012**.

(17) Müller, J. J.; Bunz, U. H. F. *Functional Organic Materials: Syntheses, Strategies and Applications*, ed. Wiley-VCH, Weinheim, Germany, 2006.

(18) Canevet, D.; Salle, M.; Zhang, G.; Zhang, D.; Zhu, D. *Chem. Commun.* **2009**, 245–2269.

(19) Segura, J. L.; Martín, N. Angew. Chem. Int. Ed. **2001**, *40*, 1372–1409.

(20) Yamada, J.-i.; Sugimoto, T. TTF Chemistry: *Fundamentals and Applications of Tetrathiafulvalene, ed. Springer, Berlin*, 2004.

(21) Brunetti, F. G.; López, J. L.; Atienza, C.; Martín, N. *J. Mater. Chem*. **2012**, *22*, 4188–4205.

(22) Pérez, E. M.; Martín, N. *Chem. Soc. Rev.* **2008**, *37*, 1512–1519.

(23) Bryce, M. R.; Moore, A. J. *Synth. Met.* **1988**, *25*, 203–205.

(24) García, R.; Herranz, M. A.; Torres, M. R.; Bouit, P.-A.; Delgado, J. L.; Calbo, J.; Viruela, P. M.; Ortí, E.; Martín, N.; *J. Org. Chem.* **2012**, *77*, 10707–10717.

(25) Shao, M.; Dongare, P.; Dawe, L. N.; Thompson, D. W.; Zhao, Y. *Org. Lett.* **2010**, *12*, 3050–3053.

(26) Christensen, C. A.; Batsanov, A. S.; Bryce, M. R. *J. Am. Chem. Soc.* **2006**, *128*, 10484–10490

(27) Christensen, C. A.; Bryce, M. R.; Batsanov, A. S.; Becher, J. *Org. Biomol. Chem.* **2003**, *1*, 511–522.

(28) Shao, M.; Chen, G.; Zhao, Y. *Synlett* **2008**, 371–376.

(29) Gruhn, N. E.; Macías-Ruvalcaba, N. A.; Evans, D. H. *Langmuir* **2006**, *22*, 10683–10688.

(30) Chen, G.; Zhao, Y. *Tetrahedron Lett.* **2006**, *47*, 5069–5073.

(31) Vets, N.; Diliën, H.; Toppet, S.; Dehaen, W. *Synlett* **2006**, 1359–1362.

(32) Christensen, C. A.; Batsanov, A. S.; Bryce, M. R. *J. Org. Chem.* **2007**, *27*, 1301–1308.

(33) Meier, H. *Angew. Chem., Int. Ed.* **2005**, *44*, 2482–2506.

(34) Shao, M.; Zhao, Y. *Tetrahedron Lett.* **2010**, *51*, 2892–2895.

(35) Becke, A. D. *J. Chem. Phys.* **1993**, *98*, 5648–5652.

(36) Vets, N.; Diliën, H.; Toppet, S.; Dehaen, W. *Synlett* **2006**, 1359-1362.

(37) (a) Steimecke, G.; Sieler, H. J.; Kirmse, R.; Hoyer, E. *Phosphor. Sulf.* **1979**, *7*, 49-55; (b) Bryce, M. R.; Moore, A. J. *Synthesis* **1991**, 26-28.

(38) Moore, A. J.; Bryce, M. R. *Tetrahedron Lett.* **1992**, *33*, 1373-1376

(39) Gaussian 09, Revision **E.01**, Frisch, M. J.; Trucks, G. W.; Schlegel, H. B.; Scuseria, G. E.; Robb, M. A.; Cheeseman, J. R.; Scalmani, G.; Barone, V.; Mennucci, B.; Petersson, G. A.; Nakatsuji, H.; Caricato, M.; Li, X.; Hratchian, H. P.; Izmaylov, A. F.; Bloino, J.; Zheng, G.; Sonnenberg, J. L.; Hada, M.; Ehara, M.; Toyota, K.; Fukuda, R.; Hasegawa, J.; Ishida, M.; Nakajima, T.; Honda, Y.; Kitao, O.; Nakai, H.; Vreven, T.; Montgomery, J. A., Jr.; Peralta, J. E.; Ogliaro, F.; Bearpark, M.; Heyd, J. J.; Brothers, E.; Kudin, K. N.; Staroverov, V. N.; Kobayashi, R.; Normand, J.; Raghavachari, K.; Rendell, A.; Burant, J. C.; Iyengar, S. S.; Tomasi, J.; Cossi, M.; Rega, N.; Millam, J. M.; Klene, M.; Knox, J. E.; Cross, J. B.; Bakken, V.; Adamo, C.; Jaramillo, J.; Gomperts, R.; Stratmann, R. E.; Yazyev, O.; Austin, A. J.; Cammi, R.; Pomelli, C.; Ochterski, J. W.; Martin, R. L.; Morokuma, K.; Zakrzewski, V. G.; Voth, G. A.; Salvador, P.; Dannenberg, J. J.; Dapprich, S.; Daniels, A. D.; Farkas, Ö.; Foresman, J. B.; Ortiz, J. V.; Cioslowski, J.; Fox, D. J. Gaussian, Inc., Wallingford CT, **2009**.

(40) GaussView, Version 5, Dennington, R.; Keith, T.; Millam, J.; Semichem Inc., Shawnee Mission KS, **2009**

Chapter 4

Functionalization of Pentacene-5,7,12,14-tetraone with Geminal Enediyne and 1,3-dithiole Groups

- This chapter is published as a full research article in *Organic Chemistry Frontiers.* "Younes, E.; Zhao, Y. *Org. Chem. Front*. **2017**, *4*, 804–810."
- Younes, E. is the principal researcher who carried out most of the experimental work, including synthesis and characterization of the new compounds, redox chemistry, and DFT calculations, under the supervision of Prof. Y. Zhao.

4.1 Introduction

Acenes and acenequinones are π-conjugated building blocks widely employed in the field of molecular electronic and photonic materials, owing to their unique structural, redox, and semiconducting properties.[1-10] Synthetically, the presence of keto groups in acenequinones allows the acene backbones to be functionalized with diverse electronic and redox-active moieties through numerous reactions. Fig. 4.1 depicts two functionalization routes which have drawn considerable interest in our recent research. First, quinone can undergo Wittig-type olefination to form π-extended tetrathiafulvalene analogues (exTTFs),[11-13] which have wide applications in chemical sensing,[14,15] supramolecular guest-host chemistry,[16-22] photovoltaics,[23-26] and so forth. Second, the keto groups can be

subjected to the Corey-Fuchs reaction to give geminal dihalovinyl intermediates, from which various π-conjugated scaffolds can be installed *via* cross-coupling reactions.[27-30]

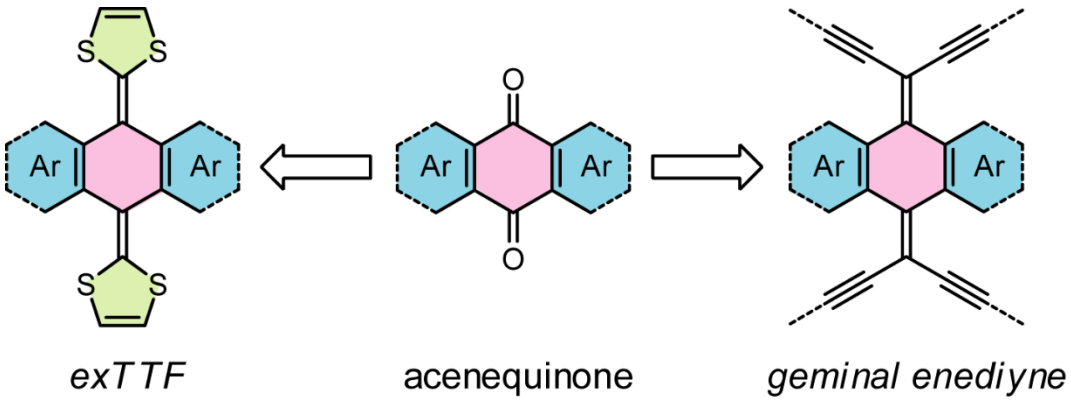

Fig. 4.1: Derivatization of acenequinones with geminal enediyne and 1,3-dithiole groups.

So far, in the literature, many reported acene-based exTTFs and geminal enediyne derivatives are derivatized from acene- diones (e.g., anthraquinones and pentacenediones).[11-13,22,31-35] Acene-polyones however are less utilized precursors because they do not have the easy synthetic access as the diones. Conceptually, derivatization of acene-polyones not only allows more functional groups to be incorporated to attain enhanced and/or unprecedented properties, but also leads to a multitude of structural variations as a consequence of the rich regioselectivity and conformational isomerism involved. Motivated by this consideration, we have recently synthesized a new class of π-extended TTF derivatives (**A**, Fig. 4.2) using pentacene-5,7,12,14-tetraone (**58**) as the precursor.[36] To further develop new π-molecular systems from pentacenetetraone, we subsequently adopted an approach of combining geminal enediyne and 1,3-dithiole groups[37-39] (see motifs **B** and **C**, Fig. 4.2). The enediyne was anticipated to function as an

electron-deficient group to modulate the π-electron characteristics and to serve as structural elements for the formation of more extended polymer networks. The following sections described our detailed investigations on the synthesis and characterization of these new pentacene-based derivatives.

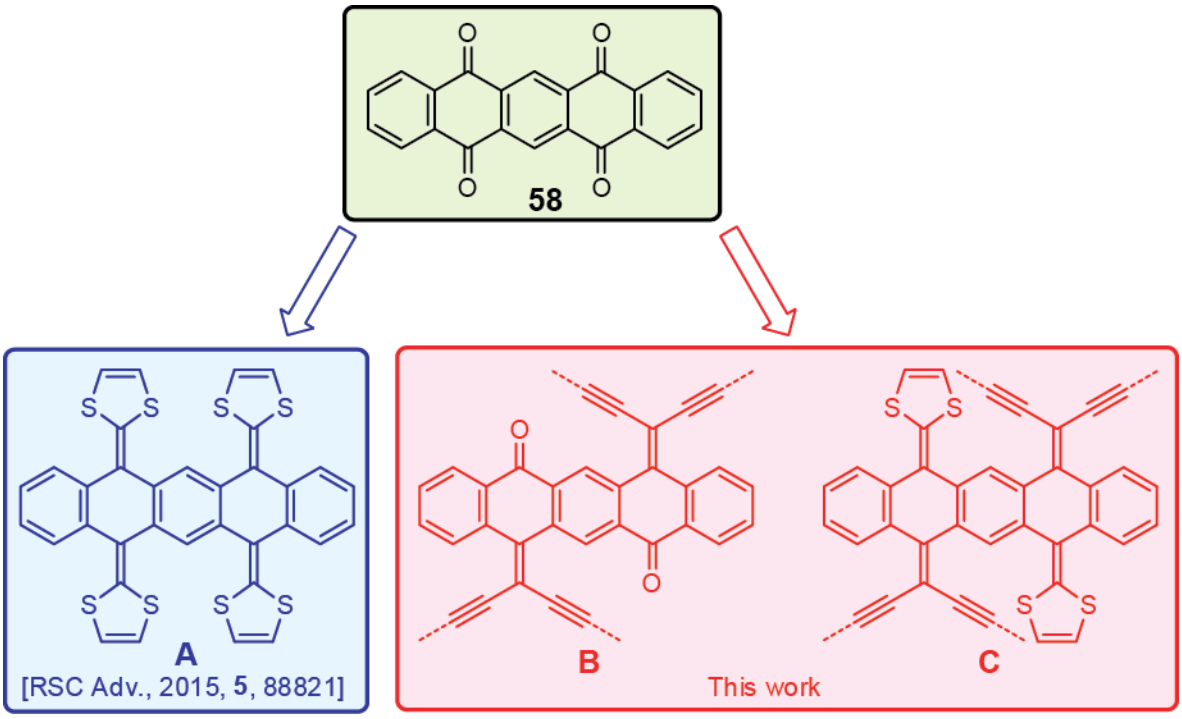

Fig. 4.2: Derivatizations of pentacene-5,7,12,14-tetraone into π-extended redox-active systems.

4.2 Results and Discussion

4.2.1 Synthesis of Enediyne and Dithiole-functionalized Pentacene Derivatives 63 and 64

In the synthesis (see Scheme 4.1), pentacene-5,7,12,14-tetraone (**58**) was first subjected to the Corey-Fuchs reaction[27-30] with excess CBr_4 and PPh_3 for 24 hours, affording tetrabromide **62** as a colourless solid in a yield of 60%. It is worth noting that only two of

the four keto groups in **58** at the 5- and 12-positions underwent olefination, while the other two remained intact. Such regioselectivity is similar to the nucleophilic substitution of pentacene-5,7,12,14-tetraone with aryl- or ethynyllithiums reported by Yamashita *et al*.[24] The C_2 symmetric structure of **62** was clearly evidenced by its ^{1}H NMR data, where five distinctive signals are seen in the aromatic region and the two chemically equivalent protons on the 6- and 13-positions resonate as a singlet at 8.80 ppm. Tetrabromide **62** then underwent the Sonogashira-Hagihara coupling reaction with excess trimethylsilylacetylene (TMSA), yielding compound **63** as a yellow solid in 87% yield. Finally compound **63** was reacted with 1,3-dithiol-2-thione **59** in $P(OEt)_3$ at 110 °C to afford compound **64** as a deep-red solid in 52% yield.[40]

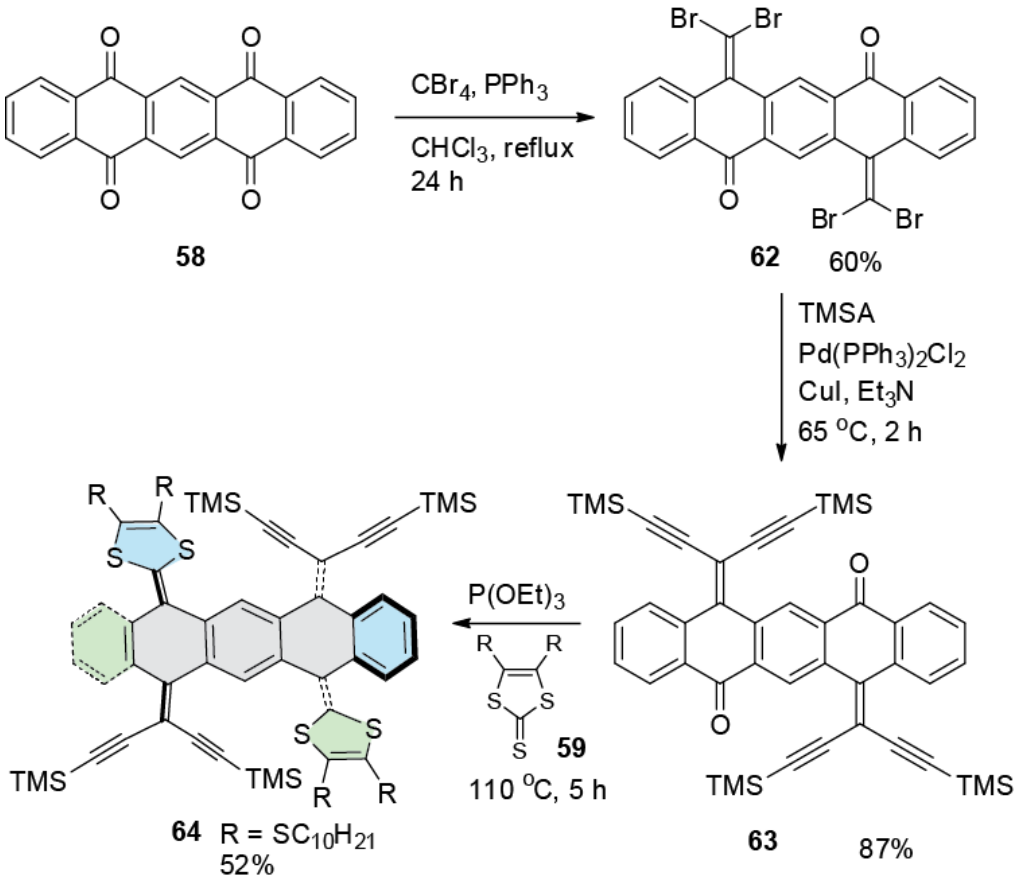

Scheme 4.1: Synthesis of enediyne and 1,3-dithiole-functionalized pentacene derivatives **63** and **64.**

4.2.2 Structural and Electronic Properties of Compounds 63 and 64

The molecular structures of compounds **62**, **63** and **64** were characterized by NMR, IR and MS analyses. The ground-state geometries of **63** and **64** were modelled by density functional theory (DFT) calculations at the B3LYP/6-31G(d) level of theory and the optimized structures are shown in Fig. 4.3 and Fig. 4.4. For compound **63**, two stable conformers were found, namely *trans* and *cis* (Fig. 4.3A,B) in terms of the orientations of the two enediyne moieties relative to the central pentacene unit. The central pentacene

structure of the *trans* conformer shows a zig-zag shape, while the *cis* conformer adopts a curved shape. Energetically, the *cis* conformer is slightly more stable than *trans* by 0.614 kcal/mol, the *trans* has much greater dipole moment (0.817 Debye) than that the *cis* has (0.0005 Debye). The observation of five distinctive aromatic signals in the ^{1}H NMR spectrum of **63** at room temperature suggests that the *cis* and *trans* conformers are interchange rapidly in the solution phase with a very low energy barrier.

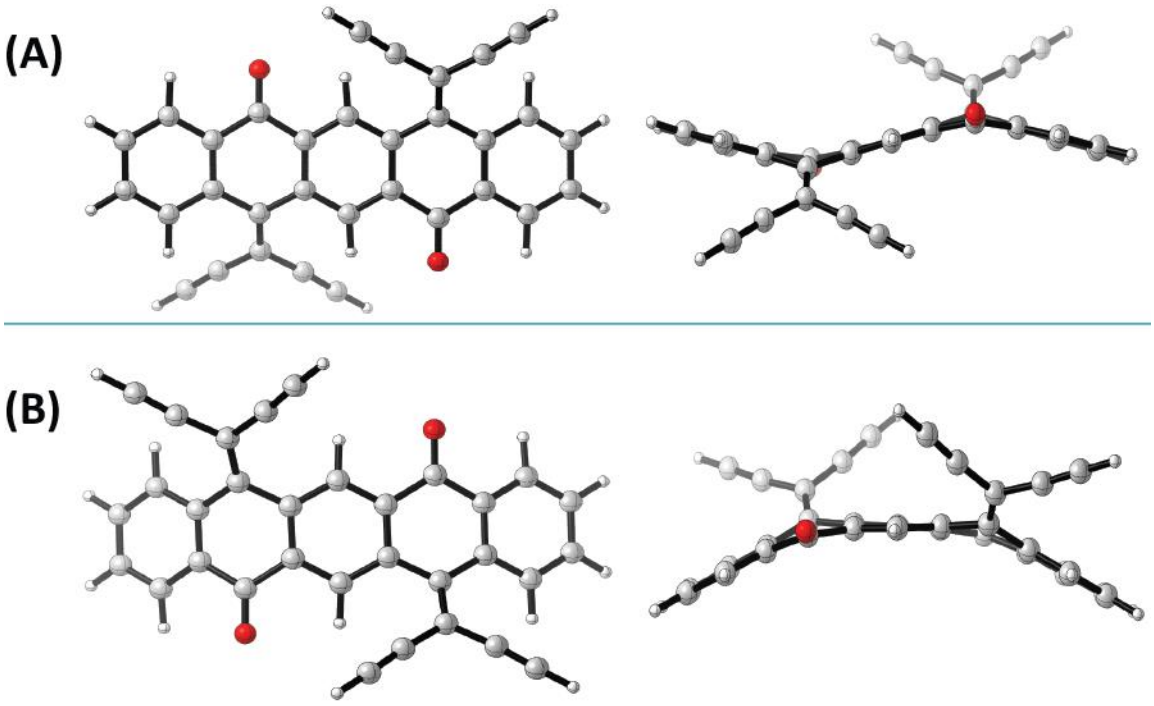

Fig. 4.3: Optimized structures of compounds (A) **63** (*trans* conformer), and (B) **63** (*cis* conformer). Calculations were done at the B3LYP/6-31G(d) level of theory. TMS groups replaced with H atoms to reduce computational expenses.

The DTF calculations showed that compound **64** has two stable conformers, *cis* and *trans*, as well (Fig. 4.4). However, the *trans* conformer is more stable than *cis* by 2.04 kcal/mol, which is consistent with the preference for minimal dipole moment; that is, the dipole moment of *trans* (0.0024 Debye) is much smaller than that of *cis* (0.746 Debye). The relatively large energy difference between the two conformers of **64** suggests that *trans* is the major conformation for compound **64** in the solution phase at room temperature.

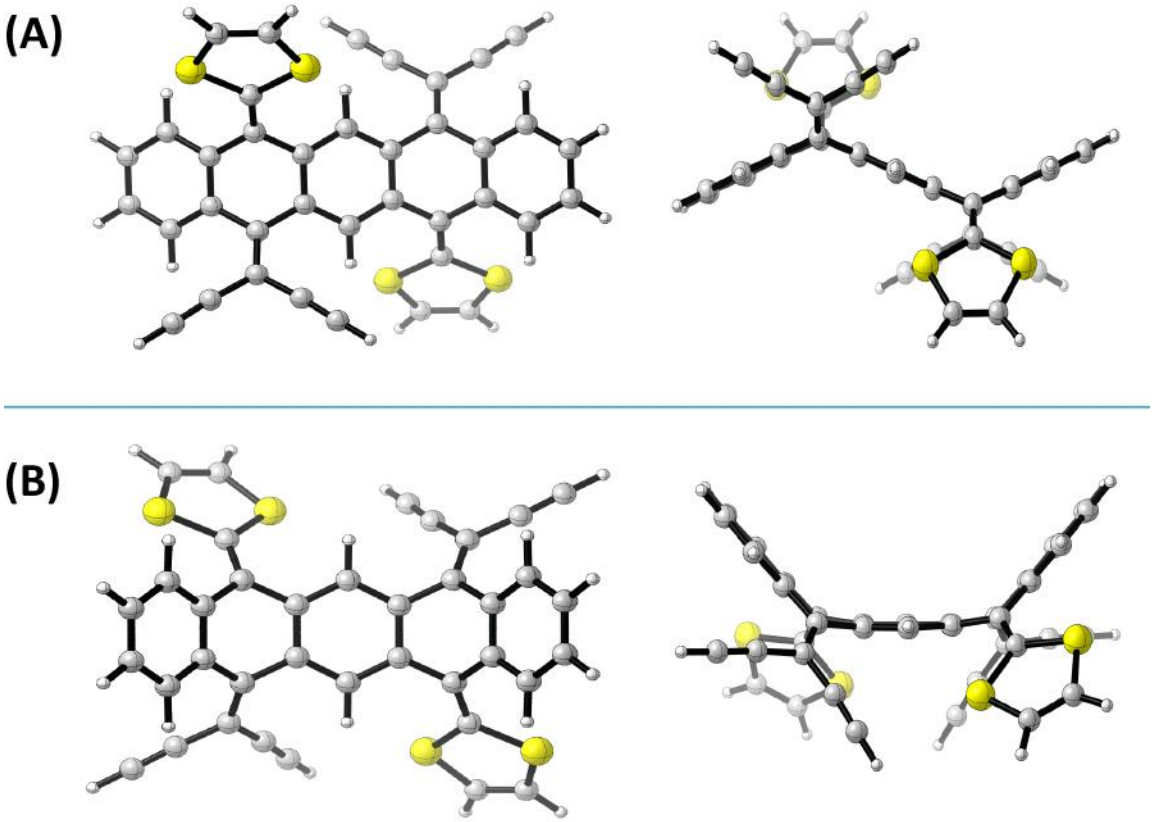

Fig. 4.4: Optimized structures of compounds (A) **64** (*trans* conformer), and (B) **64** (*cis* conformer). Calculations done at the B3LYP/6-31G(d) level of theory. TMS and $SC_{10}H_{21}$ groups were replaced with H atoms to reduce computational expenses.

4.2.3 The electronic properties of 63 and 64

The electronic properties of **63** and **64** were investigated by UV-Vis absorption analysis (Fig. 4.5). In $CHCl_3$ compound **63** gives rise to two $\pi \rightarrow \pi^*$ absorption bands at 436 nm and 358 nm. The low-energy band is mainly due to the HOMO→LUMO transition according to time-dependent (TD) DFT calculations (Table 4.1). Compound **64** in $CHCl_3$ gives three absorption bands at 516 nm, 407 nm, and 337 nm, respectively. Compared with compound **63**, the HOMO→LUMO transition of **64** (516 nm) is greatly redshifted, as a result of the "push-and-pull" effect arising from the electron-donating dithioles and the electron-withdrawing geminal enediyne groups. The solid thin film of compound **64** gives three absorption bands at 516 nm, 419 nm, and 338 nm, which are similar to those measured in the solution phase. However, it is notable that the HOMO→LUMO band (516 nm) of the solid film is significantly enhanced in intensity than that in the solution-phase spectrum. Moreover, close comparison of the normalized low-energy bands in the solution-phase and solid-film spectra (inset of Fig. 4.5) clearly shows a notable redshift of cut-off energy in the solid state. These results can be rationalized by that the molecules of **64** are in a more organized state in the solid film than in solution. TD-DFT calculations show that the $S_o \rightarrow S_1$ transition of *cis* **64** is at 541 nm, which is redshifted relative to that of *trans* **64** (Table 4.1). It is likely that *cis* **64** has a molecular shape more suitable for solid-state packing than *trans* **64**, and hence becomes more favoured in the solid state.

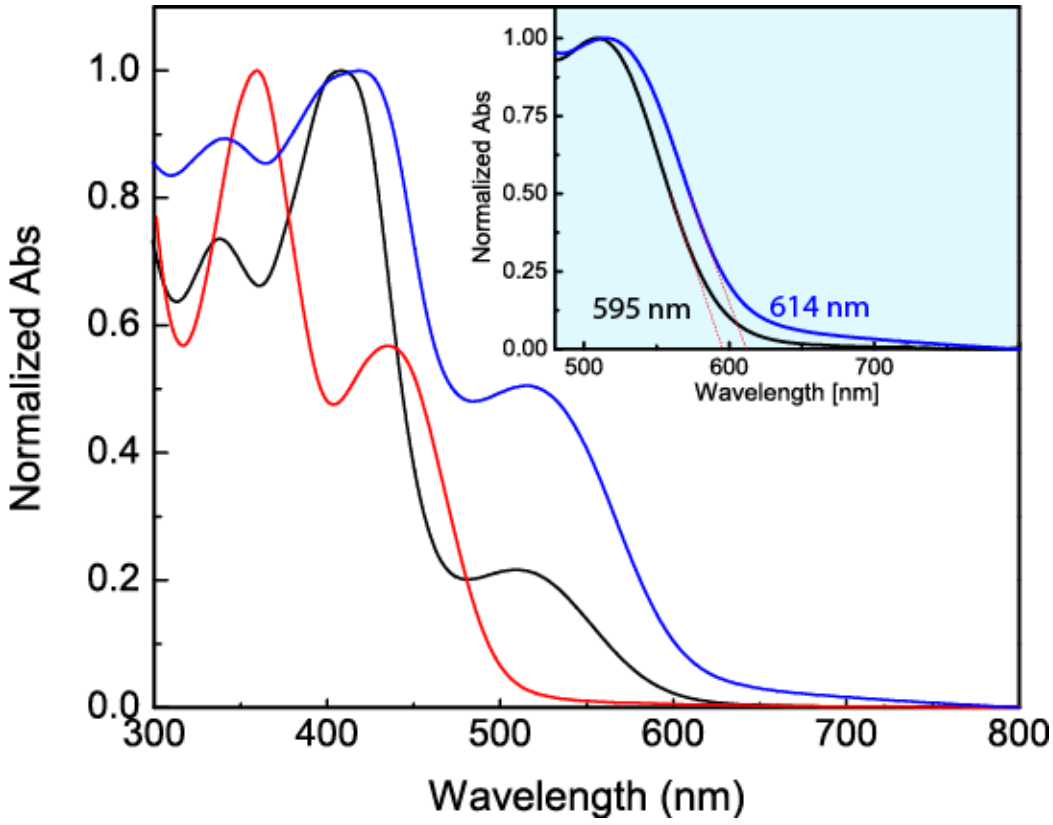

Fig. 4.5: Normalized UV-Vis absorption spectra of compounds **63** and **64** measured in $CHCl_3$ and as a solid film (**63**) at room temperature. Inset: Comparison of the normalized low-energy absorption bands in the solution-phase and solid-state UV-Vis spectra. (Red: **63** in $CHCl_3$, black: **64** in $CHCl_3$, blue: **64** as solid film).

Table 4.1: TD-DFT calculated electronic transitions, oscillator strength (*f*), and MO composition for compounds **63** and **64** (*trans* and *cis* conformers)

Entry	$\lambda_{max(exp)}$	$\lambda_{max(calcd)}$	*f*	MO composition
	436	457	0.345	H→L(93.4%), H→L+2(2.8%)
		407	0.004	

		368	0.071	H-7→L(5.9%), H-6→L(5.3%), H-3→L+1(9.4%), H-2→L(68.7%), H-2→L+2(3.2%)
63 *trans*		363	0.052	H-7→L(10.1%), H-4→L(13.7%), H-2→L(3.0%), H-1→L+1(10.6%), H→L+2(58.0%)
	358	350	0.150	H-4→L(73.7%), H→L+3(16.7%)
		339	0.217	H-7→L(22.8%), H-6→L(33.5%), H-5→L+1(2.4%), H-4→L(2.8%), H-2→L(14.3%), H-1→L+1(5.2%), H→L+2(14.1%)
	436	459	0.287	H-7→L(3.1%), H-6→L(27.2%), H-1→L+1(56.8%), H→L+2(6.0%)
		376	0.103	H→L(93.9%), H→L+2(2.5%)
		369	0.066	H-6→L(3.4%), H-1→L(11.6%), H-1→L+2(5.2%), H→L+1(76.5%)
63 *cis*		364	0.034	H-7→L(4.7%), H-5→L(3.7%), H-4→L(23.7%), H-1→L+1(9.7%), H→L+2(54.8%)
	358	350	0.130	H-5→L(2.7%), H-4→L(67.2%), H→L+2(20.4%)
		341	0.158	H-6→L+1(2.4%), H-5→L(64.8%), H-2→L(11.8%), H-1→L+1(2.3%), H→L+2(12.9%)
	516	519	0.153	H-7→L(15.0%), H-5→L(5.3%), H-4→L(3.0%), H-1→L+1(63.5%), H→L+2(6.4%)
				H→L(95.8%), H-2→L(2.5%)

64	407	402	0.093	H-2→L(53.6%), H-1→L+1(40.1%), H→L+2(3.6%)
trans		380	0.473	H-2→L(39.3%), H-1→L+1(56.0%)
		368	0.342	H-2→L(2.8%), H→L+2(88.9%), H→L+4(2.9%)
	337	349	0.038	H-1→L+3(16.1%), H-1→L+5(11.2%), H→L+2(4.1%), H→L+4(62.4%)
	516	541	0.157	H→L(96.3%)
64	407	406	0.003	H-2→L(16.8%), H-1→L+1(68.9%), H→L+2(12.4%)
cis		387	0.340	H-1→L+1(12.5%), H→L+2(83.4%)
		378	0.449	H-2→L(79.1%), H-1→L+1(16.5%)
		361	0.004	H-3→L(16.8%), H-2→L+1(20.6%), H-1→L+2(58.2%)
	337	337	0.013	H-4→L(2.4%), H-1→L+5(16.4%), H→L+4(74.0%)
		336	0.002	H-2→L+1(8.5%), H-1→L+2(6.6%), H-1→L+4(10.6%), H→L+3(51.9%), H→L+5(17.7%)

4.2.4 Frontier Molecular Orbitals (FMOs)

The frontier molecular orbitals (FMOs) of the most stable conformers of **63** and **64** are depicted in Fig. 4.6. As can be seen, the HOMO of **63** is mainly populated on the enediyne moieties and the central phenyl ring of the pentacene unit. The LUMO of **63** is evenly distributed along the entire molecular framework. The patterns of the FMOs of compound **64** clearly reveal a donor-acceptor

(D-A) characteristic, where the HOMO is distributed along the electron-rich dithioles and central phenyl group, while the LUMO is primarily on the electron-deficient enediyne and central phenyl segments. Compound **64** has a much higher HOMO energy than that of **63**, indicating a stronger electron-donating ability due to the presence of dithiole groups. The LUMO energy of **63** is higher than that of **64**. As such, compound **64** possesses a narrower HOMO-LUMO gap, which is congruous with the results of UV-Vis analysis

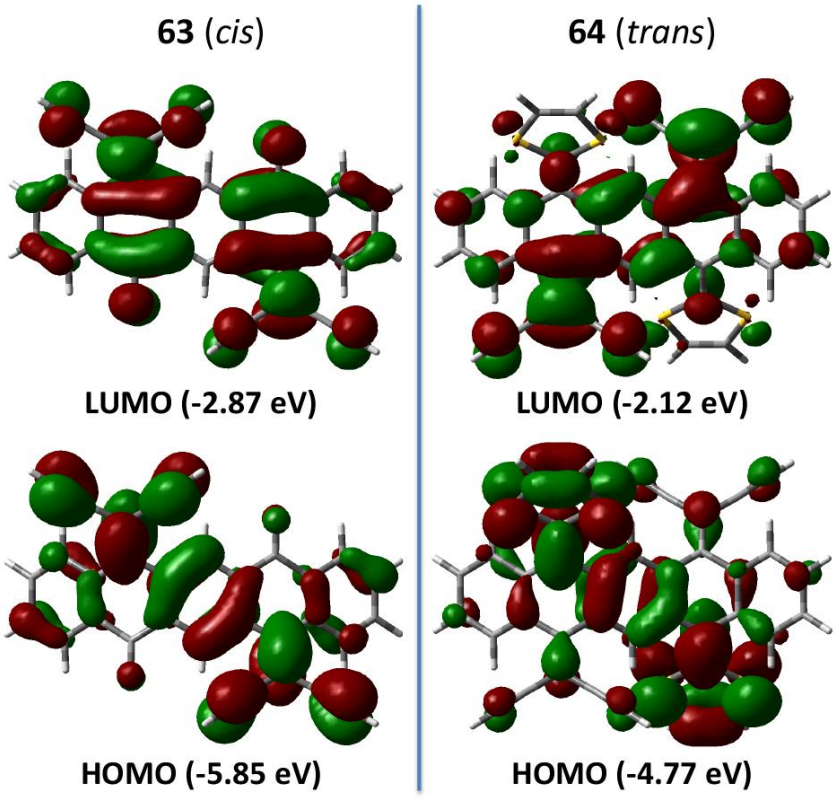

Fig. 4.6: Plots and eigenvalues of frontier molecular orbitals (FMOs) for compounds **63** (*cis* conformer) and **64** (*trans* conformer).

4.2.5 Redox Properties of Compounds 63 and 64

The redox activity of compounds **63** and **64** were investigated by cyclic voltammetric (CV) and differential pulse voltammetric (DPV) analyses. Fig. 4.7A shows the CV profiles of compound **63** measured in solution. There are two quasi-reversible redox wave pairs appear at E_{pc1} = -0.76 V, E_{pa1} = -0.65 V, E_{pc2} = -1.06 V, E_{pa2} = -0.88 V, respectively. The first redox couple can be assigned to the reduction/oxidation of the keto groups,[36, 41] while the second is associated with the geminal enediyne moieties[32, 33] which are poorer electron-acceptors than the keto groups. The CV profiles of **64** in solution show amphoteric behaviour (Fig. 4.7B). In the positive potential window, a quasi-reversible wave pair is seen at E_{pa} = +0.86 V and E_{pc} = +0.48 V, which are due to the redox reactions on the electron-donating dithiole units. In the negative potential window, a quasi-reversible couple is observed at E_{pc} = -1.03 V and E_{pa} = -0.96 V. These peaks are consistent with the second redox couple in the cyclic voltammogram of **63**, hence confirming that they are due to the electron transfers occurring on the electron-withdrawing enediyne moieties.

The solid thin film of **64** was prepared on the surface of a glassy carbon working electrode by the dropcasting method. The thin film was subjected to CV and DPV analyses (Fig. 4.7 C,D). In contrast to the solution-phase CV data, the first cycle of the CV scan on the thin film of **64** shows a dramatically different profile than the ensuing scan cycles. As can be seen in Fig. 4.7C, the first forward scan clearly shows a major anodic peak at +0.72 V and a number of minor anodic peaks in the range of +0.86 V to +1.29 V. These features are very different from the CV profiles of **64** measured in the solution phase. During the first reverse scan a cathodic peak emerges at +0.57 V, which is higher than that in the solution phase CV. Starting from the second cycle of CV scans, the voltammograms show less distinctive redox features and bear more resemblance to those

measured in the solution phase. Similar results can also be seen in the DPV data (Fig. 4.7D), where the first DPV scan shows a very different profile than the following scans. The electrochemical analysis on the solid thin film of **64** concurs with the UV-Vis results; that is, compound **64** has an ordered microscopic structure in the solid state, likely due to strong intermolecular π-stacking. During the multi-cycle CV and DPV scans, the intermolecular interactions within the solid thin film were substantially altered by the redox reactions, which in turn re-oriented the molecules into a less ordered state similar to the solution phase. This outcome indicates that the solid-state ordering of **64** can be modulated by external electrochemical inputs, which might be useful for stimuli-responsive materials or devices.

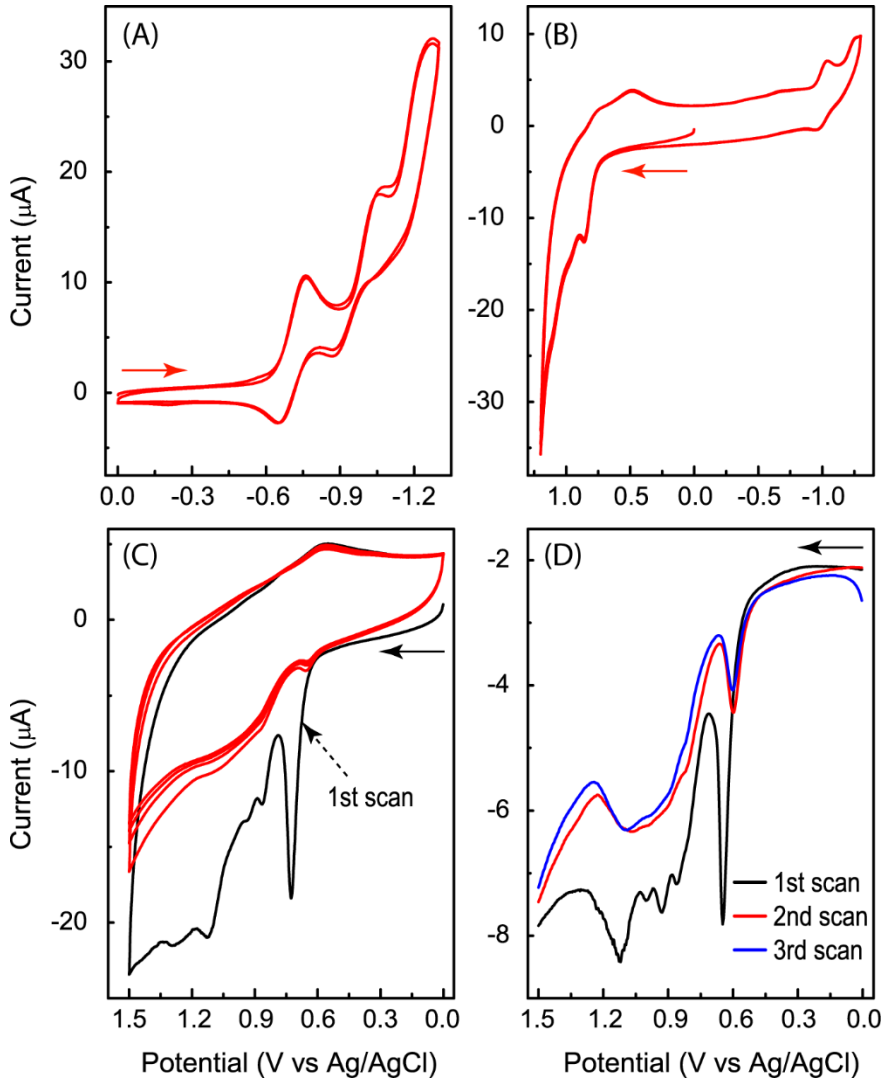

Fig. 4.7: (A) Multi-cycle CV scans of compound **63** dissolved in CH_2Cl_2. (B) Multi-cycle CV scans of compound **64** dissolved in CH_2Cl_2. (C) Multi-cycle CV scans of the solid thin film of **64** measured in CH_3CN. (D) DPV profiles of the solid thin film of **64** measured in CH_3CN. Experimental conditions: electrolyte: Bu_4NPF_6 (0.1 M); working electrode: glassy carbon; reference electrode: Ag/AgCl; counter electrode: Pt wire; CV scan rate: 100 mV/s; DPV pulse width: 50 ms, pulse period: 200 ms, pulse amplitude: 50 mV, step: 4 mV.

4.3 Generation of Carbon-rich Polymeric Materials with 62 and 63

Compounds **62** and **63** were subjected to Pd-catalyzed cross-coupling reaction in order to form polymer products. Two synthetic routes were executed as shown in Scheme 4.2. In the first route, tetrabromide **62** was cross-coupled with phenylacetylene **65** under Sonogashira-Hagihara coupling conditions. In a similar way, compound **63** after desilylation was cross-coupled with diiodoarene **66** (route 2, Scheme 4.2) under Pd/Cu catalysis. Experimentally, the resulting products **P1** and **P2** were obtained as shiny dark-coloured solids, which are insoluble in most organic solvents. The low solubility prevents clear identification of the exact molecular structures of **P1** and **P2**; however, the data from IR, UV-Vis, and CV analyses suggest that these polymers contain extended π-frameworks containing C≡C, C=O, and arene units. In theory, **P1** and **P2** should have similar molecular backbones. This is supported by their IR spectral data, which bear great resemblance to one another. It is also interesting to note that the microscopic morphology of **P1** exhibits microporous features with pore sizes on the dimension of a few hundred nanometers as revealed by SEM imaging (see Fig. S-4.1D). Apart from the Pd-catalyzed polymerization reactions, a Ru-catalyzed reaction of compound **63** was also performed (Scheme 4.2). The enediyne moieties are known to undergo cyclization under Ru-catalysis to afford benzannulated products.[42] Experimentally, the reaction ended up with the formation of a black solid product (**P3**) with extremely low solubility in common organic solvents. IR analysis shows the absence of an alkynyl vibrational band, indicating the complete consumption of the enediyne groups during the Ru-catalyzed reaction (Fig. S-4.2B). The UV-Vis absorption spectrum of **P3** features a significant absorption tail in the Vis-NIR region, extending to as far as 1100 nm. This property suggests that **P3** has highly π-extended molecular structure, mostly likely a polymeric product rather than a small molecule. Power XRD and SEM analyses reveal a certain degree of ordering of **P3** at the

microscopic level (see Fig. S-4.2D and Fig. S-4.3). Overall, the three reactions described in Scheme 4.2 demonstrate the potential of compounds **62** and **63** to be used as molecular building blocks in generating carbon-rich polymeric materials. Further studies are warranted in order to fully understand the mechanisms of these reactions as well as the exact molecular structures of the products.

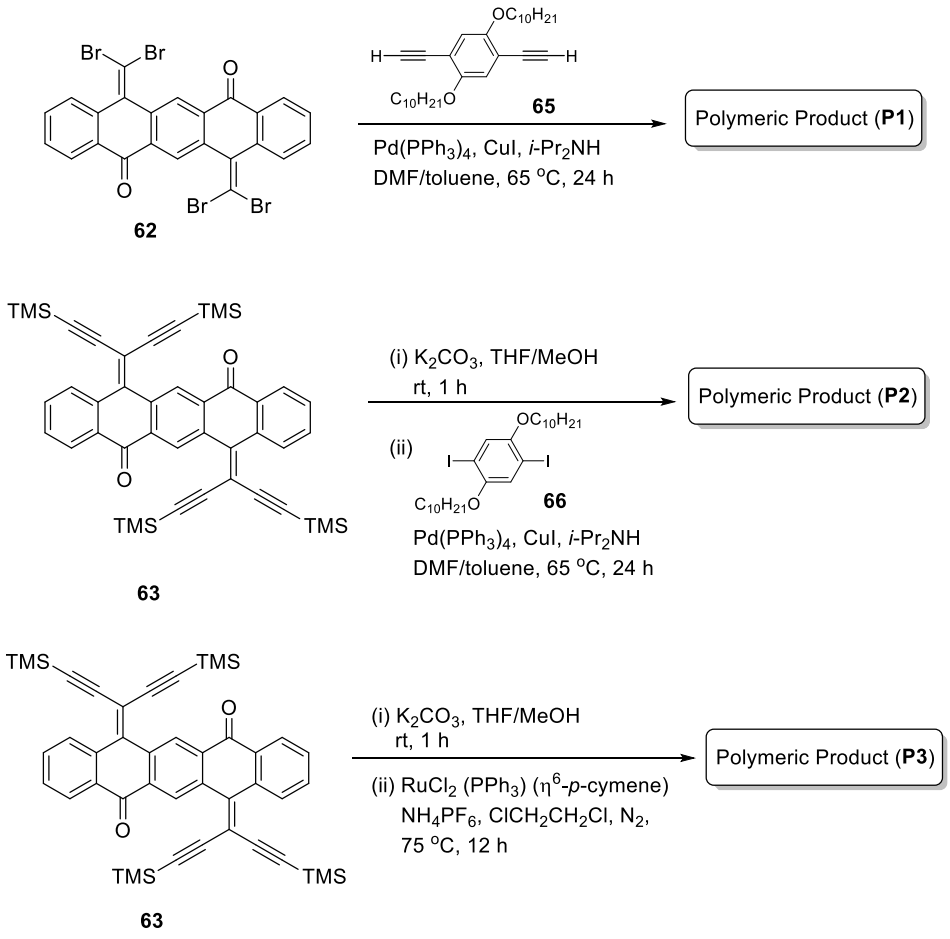

Scheme 4.2: Preparation of carbon-rich polymeric materials P1-P3 via transition metal-catalyzed reactions.

4.4 Conclusions

In summary, the functionalization of pentacene-5,7,12,14-tetraone with electron-withdrawing geminal enediyne and electron-donating 1,3-dithiole groups provided new π-conjugated D/A systems with intriguing electronic and redox properties. The geminal enediyne moieties can provide synthetic access to π-extended carbon-rich materials through transition metal-catalyzed reactions. The pentacenedione derivatives reported in this work are expected to offer access to a new family of redox-active π-building blocks and have application in the preparation of novel π-conjugated carbon nanomaterials.

4.5 Experimental Section

4.5.1 General

Chemicals were purchased from commercial suppliers and used directly without purification. All reactions were conducted in standard, dry glassware and under an inert atmosphere of nitrogen (N_2) unless otherwise noted. Evaporation and concentration were carried out with a rotary evaporator. Flash column chromatography was performed with 240-400 mesh silica gel, and thin-layer chromatography (TLC) was carried out with silica gel F254 covered on plastic sheets and visualized by UV light. ^{1}H and ^{13}C NMR spectra were measured on a Bruker Avance III 300 MHz multinuclear spectrometer. Chemical shifts (δ) are reported in ppm downfield relative to the signals of the internal reference $SiMe_4$ or residual solvents ($CHCl_3$: δ_H = 7.24 ppm, δ_C = 77.2 ppm; CH_2Cl_2: δ_H = 5.32 ppm, δ_C = 54.0 ppm). Coupling constants (*J*) are given in Hz. Infrared spectra (IR) were recorded on a Bruker Alfa spectrometer. High resolution APCI-TOF MS analysis was carried out on

a GCT premier Micromass Technologies instrument. UV-Vis absorption spectra were measured on a Cary 6000i spectrophotometer. Cyclic voltammetric (CV) and differential pulse voltammetric (DPV) analyses were carried out in a standard three-electrode setup controlled by a BASi Epsilon potentiostat. Powder X-ray diffraction (XRD) analysis was done on a Rigaku Ultima IV diffractometer equipped with a copper X-ray source with a wavelength of 1.54 nm. Scanning electron microscopic (SEM) imaging was performed on an FEI MLA 650 FEG microscope. Compounds **58**,[43] **59**,[44, 45] **65**,[46] **66**,[46] and $RuCl_2(PPh_3)(\eta^6$-*p*-cymene)[47] were prepared according to literature procedures. Molecular modelling studies were carried out using the Gaussian 09 software.[48] Visualization of the calculated molecular structures and orbitals were performed by the CYLview[49] and GaussView 5[50] software packages.

4.5.2 Synthetic Procedures

7,14-Bis(dibromomethylene)pentacene-5,12(7*H*,14*H*)-dione (62)

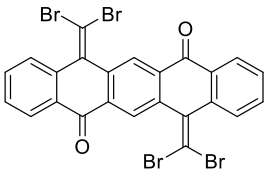

Pentacene–5,7,12,14–tetraone (**58**) (0.30 g, 0.89 mmol) and PPh_3 (2.3 g, 8.9mmol) were mixed in $CHCl_3$ (100 mL) under an atmosphere of N_2. The mixture was stirred for 10 min at room temperature, CBr_4 (1.5 g, 4.5 mmol) was then added. The resulting mixture was refluxed overnight. The white precipitate was filtered off, and then the filtrate was washed with brine, water, and dried over $MgSO_4$. The organic layer was collected and concentrated under vacuum. The residue was

subjected to silica flash column chromatography (CH_2Cl_2/hexanes, 1:1) to yield compound **62** (0.35 g, 0.45mmol. 60%) as white solid. IR (neat) ν_{max}: 3064, 1671, 1582, 1330, 951, 682 cm^{-1}; ^1H NMR (300 MHz, $CDCl_3$): δ 8.80 (s, 2H), 8.32 (dd, J = 5.8, 3.3 Hz, 2H), 7.89 (dd, *J* = 5.8, 3.3 Hz, 2H), 7.82 (dd, *J* = 5.8, 3.3 Hz, 2H), 7.35 (dd, *J* = 5.8, 3.3 Hz, 2H). ^{13}C NMR (75 MHz, $CDCl_3$): δ 182.3, 141.2, 138.4, 135.0, 134.4, 133.5, 131.5, 127.9, 127.7, 127.4, 126.9, 93.3. HRMS (APCI, positive mode): *m/z* calcd for $[C_{24}H_{11}Br_4O_2]^+$ ($M + H^+$): 650.7452; found: 650.7436.

7,14-Bis(1,5-bis(trimethylsilyl)penta-1,4-diyn-3-ylidene)pentacene-5,12(7*H*,14*H*)-dione (63)

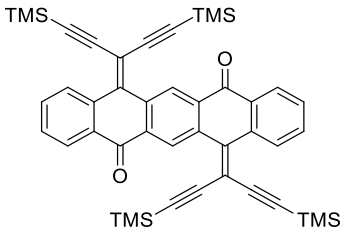

Compound **62** (0.25 g, 0.38 mmol) was dissolved in dry Et_3N (15 mL). To this solution were added $Pd(PPh_3)_2Cl_2$ (27 mg, 0.038 mmol) and CuI (2.3 mg, 0.019mmol). The mixture was heated to 65 °C. TMSA (0.37 g, 3.8 mmol) was then added dropwise via a syringe over 5 min. The resulting mixture was heated for another 2 h. Et_3N was then removed under vacuum, and the residue was subjected to silica flash column chromatography (CH_2Cl_2/hexanes, 1:9) to yield compound **63** (0.24 g, 0.33 mmol. 87%) as yellow solid. IR (neat) ν_{max}: 2957, 2898, 2143, 2119, 1680, 1590, 1208, 910, 646 cm^{-1}; ^1H NMR (300 MHz, $CDCl_3$): δ 9.27 (s, 2H), 8.35 (td, *J* = 5.7, 3.3 Hz, 4H), 7.83 (dd, *J* = 5.8, 3.3 Hz, 2H), 7.36 (dd, *J* = 5.9, 3.3 Hz, 2H), 0.28 (s, 18H), 0.26 (s, 18H). ^{13}C NMR (75 MHz, $CDCl_3$): δ 182.6, 146.1, 139.6, 134.3, 134.19, 133.7, 131.7, 127.9, 127.9, 127.5, 127.1, 103.5, 103.4, 103.1,

102.6, 102.1, 0.0. HRMS (APCI, positive mode): *m/z* calcd for $[C_{44}H_{47}O_2Si_4]^+$ (M + H^+): 719.2653; found: 719.2634.

Compound 64

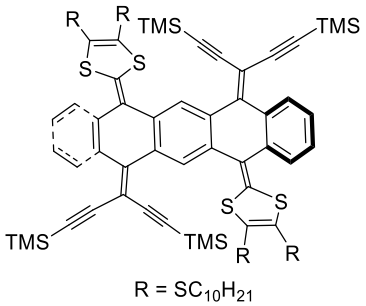

Compound **63** (0.15 g, 0.21 mmol) and 1,3-dithiole-2-thione **59** (0.22 g, 0.46 mmol) were mixed in $P(OEt)_3$ (10 mL), and the mixture was heated to 110 °C for 5 h. The unreacted $P(OEt)_3$ was then removed under reduced pressure. The residue was subjected to silica flash column chromatography (CH_2Cl_2/hexanes, 1:9) to yield pure compound **64** (0.17 g, 0.11 mmol, 52%) as a dark red semisolid. IR (neat) ν_{max}: 2954, 2923, 2852, 2141, 1531, 1490, 1418, 1248, 932 cm^{-1}; ^1H NMR (300 MHz, CD_2Cl_2): δ 8.83 (s, 2H), 8.44 (dd, *J* = 5.9, 3.3 Hz, 2H), 7.60 (dd, *J* = 5.8, 3.3 Hz, 2H), 7.42 (dd, *J* = 5.9, 3.3 Hz, 2H), 7.37 (dd, *J* = 5.8, 3.3 Hz, 2H), 2.92–2.73 (m, 8H), 1.83–1.59 (m, 8H), 1.39–1.22 (m, 56H), 0.91 (t, *J* = 6.6 Hz, 12H), 0.30 (s, 18H), 0.26 (s, 18H). ^{13}C NMR (75 MHz, CD_2Cl_2): δ 147.4, 135.8, 134.6, 133.6, 132.4, 128.6, 128.2, 127.8, 127.3, 127.2, 126.3, 124.2, 122.8, 104.1, 103.5, 102.8, 101.8, 101.2, 37.3, 37.1, 32.6, 30.5, 30.44, 30.38, 30.35, 30.32, 30.31, 30.14, 30.13, 30.03, 29.95, 29.92, 29.30, 29.25, 23.8, 14.6, 0.0, -0.1. HRMS (APCI, positive mode) *m/z* calcd for $[C_{90}H_{131}S_8Si_4]^+$ (M + H^+): 1580.7127; found: 1580.7113.

Synthesis of P1

Compound **62** (100 mg, 0.153 mmol) and **65** (134 mg, 0.306 mmol) were mixed with *i*-Pr2NH (1 mL) in a mixed solvent of DMF (1.5 mL) and toluene (2.5 mL). The mixture was stirred at room temperature for 5 min, and to this mixture was added $Pd(PPh_3)_4$ (35 mg, 0.031 mmol) and CuI (3.0 mg, 0.016 mmol). The mixture was heated at 65 °C under N_2 for 24 h. The reaction mixture was then cooled to room temperature and the resulting precipitate was collected by vacuum filtration and washed with MeOH several times to afford **P1** (150 mg, 0.125 mmol, 82 %) as a shiny black solid.

Synthesis of P2

Compound **63** (100 mg, 0.139 mmol) and K_2CO_3 (85.1 mg, 0.616 mmol) were stirred in THF/MeOH (1:1, 10 mL) under N_2 for 1 h. The solvent was removed under vacuum. The residue was dissolved in CH_2Cl_2, washed with water, dried over $MgSO_4$, and concentrated under vacuum, giving desilylated **63**. The desilylated intermediate was added to a solution of diiodobenzene **66** (179 mg, 0.278 mmol) and *i*-Pr_2NH (1.0 mL) in DMF (1.5 mL) and toluene (2.5 mL). The mixture was stirred at room temperature for 5 min and to the mixture were added $Pd(PPh_3)_4$ (32 mg, 0.028 mmol) and CuI (2.7 mg, 0.0014 mmol). The mixture was heated at 65 °C under N_2 for 24 h. The reaction mixture was then cooled to room temperature and the resulting precipitate was collected by vacuum filtration and washed with MeOH several times to afford **P2** (110 mg, 0.0903 mmol, 65%) as a shiny black solid.

Synthesis of P3

Compound **63** (150 mg, 0.209 mmol) and K_2CO_3 (127 mg, 0.917 mmol) were stirred in THF/MeOH (1:1, 10 mL) under N_2 for 1 h. The solvent was removed under vacuum. The residue was dissolved in CH_2Cl_2, washed with water, dried over MgSO4, concentrated under vacuum, giving desilylated **63**. The desilylated intermediate was diluted in 1,2-dichloroethane (5 mL). This solution was drawn into a syringe to be used in the next step.

$RuCl_2(PPh_3)(\eta 6\text{-}p\text{-cymene})$ (24 mg, 0.042 mmol) and NH_4PF_6 (14 mg, 0.084 mmol) were dissolved in 1,2-dichloroethane (15 mL). The mixture was heated to 75 °C under N_2, and to this reaction mixture the solution of desilylated **63** was slowly added *via* a syringe over a period of 6 h. After addition, the reaction mixture was heated for another 12 h. The reaction mixture was then cooled to room temperature. The resulting precipitate was collected by vacuum filtration and washed with MeOH and CH_2Cl_2 to afford a black solid product (85 mg, 0.20 mmol, 94%).

4.6 Characterizations of P1-P3

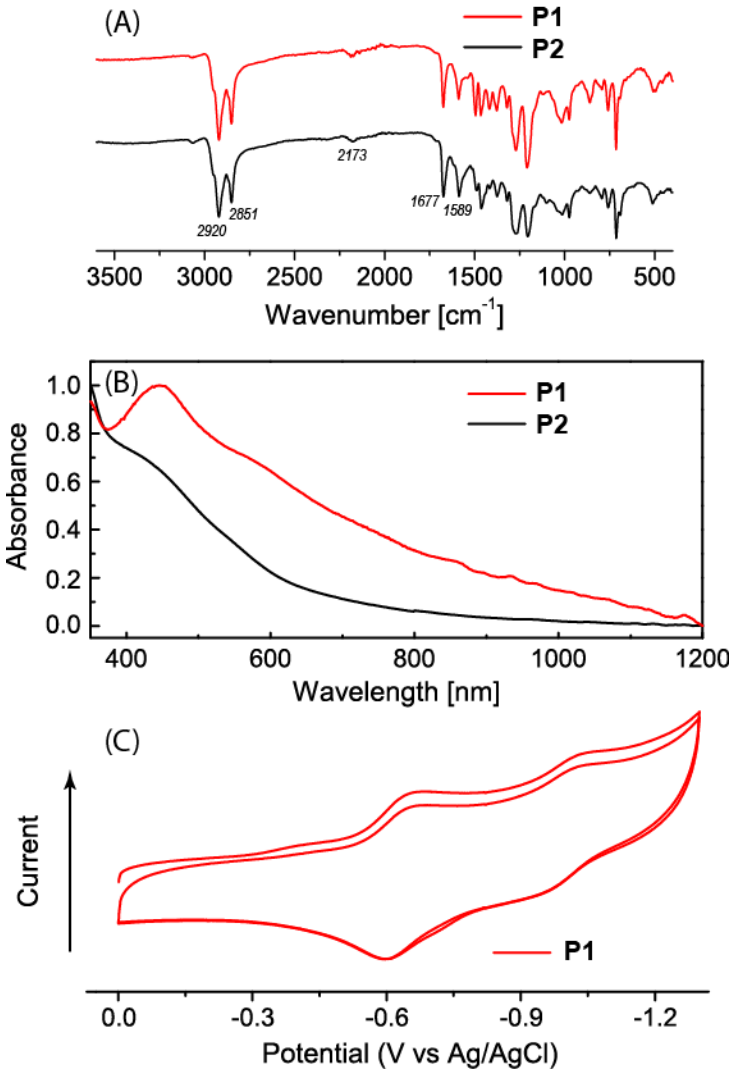

Fig. S-4.1: (A) IR spectra of **P1** and **P2**. (B) UV-Vis absorption spectra of **P1** measured in DMF. (C) CV scans of **P1**. Experimental conditions: solvent: DMF; electrolyte: Bu_4NPF_6 (0.1 M); working electrode: glassy carbon; reference electrode: Ag/AgCl; counter electrode: Pt wire; scan rate: 100 mV/s.

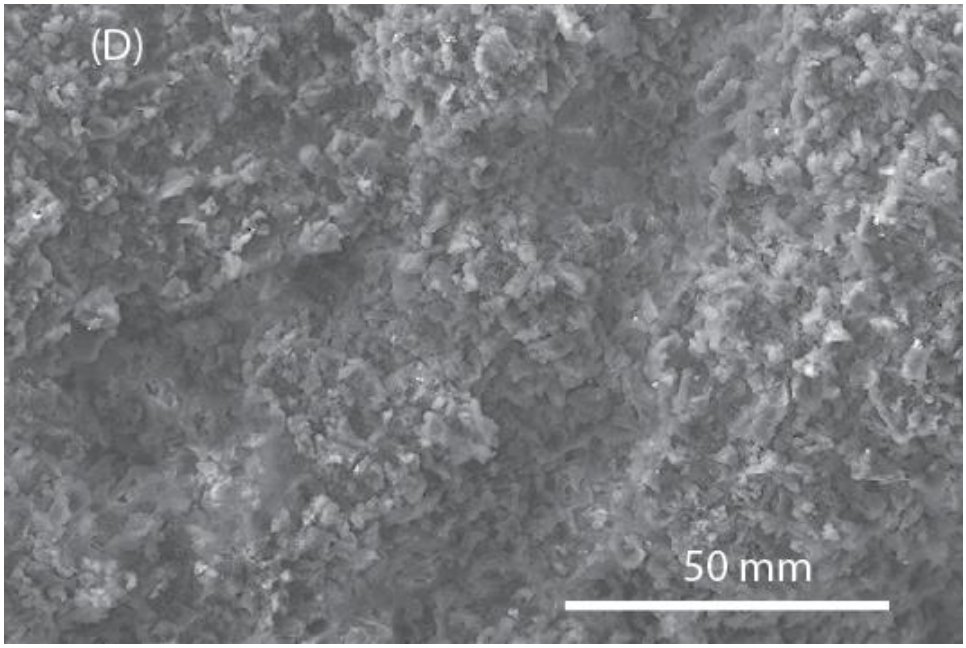

Fig. S-4.1D: SEM image of **P1**.

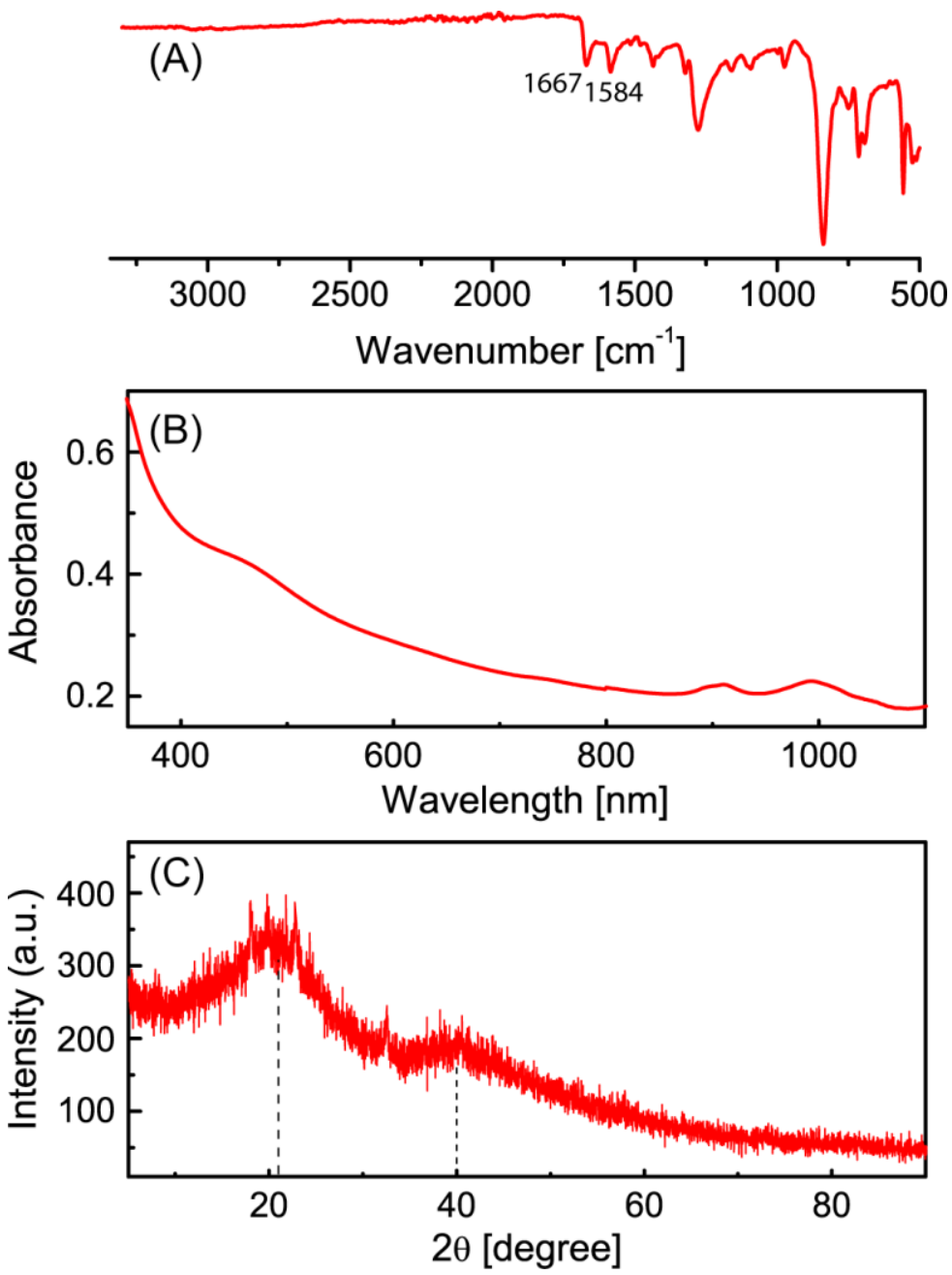

Fig. S-4.2 (A) IR spectrum of **P3** resulting from Ru-catalyzed cyclization reactions. (B) UV-Vis-NIR spectrum of **P3** suspended in DMF. (C) Powder XRD patterns of **P3**.

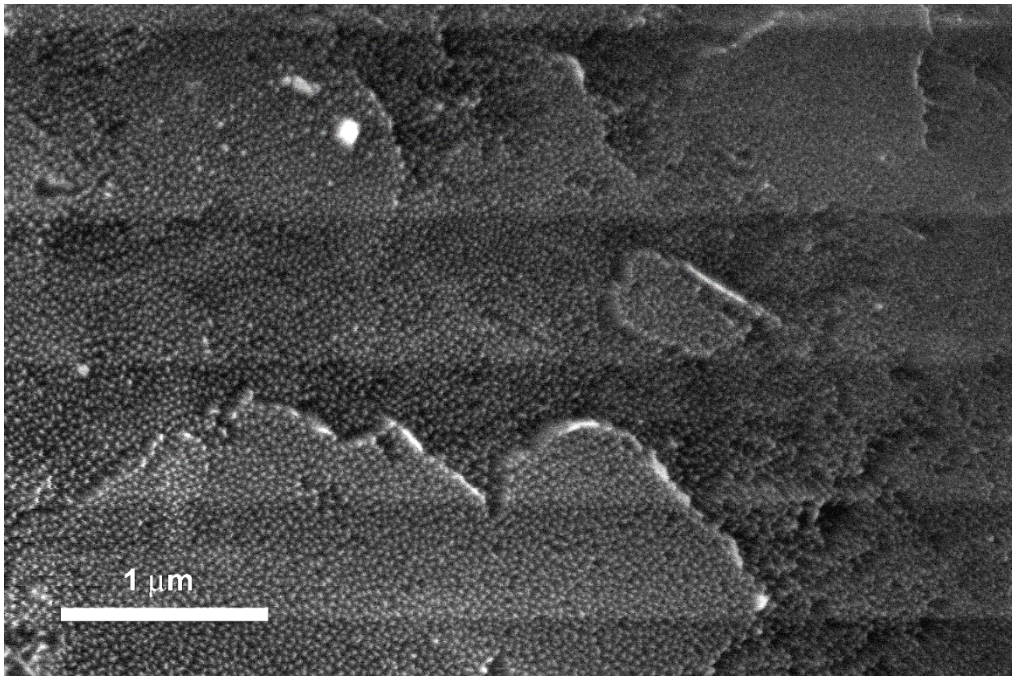

Fig. S-4.3 SEM image of **P3** prepared from Ru-catalyzed reactions of desilylated **63**.

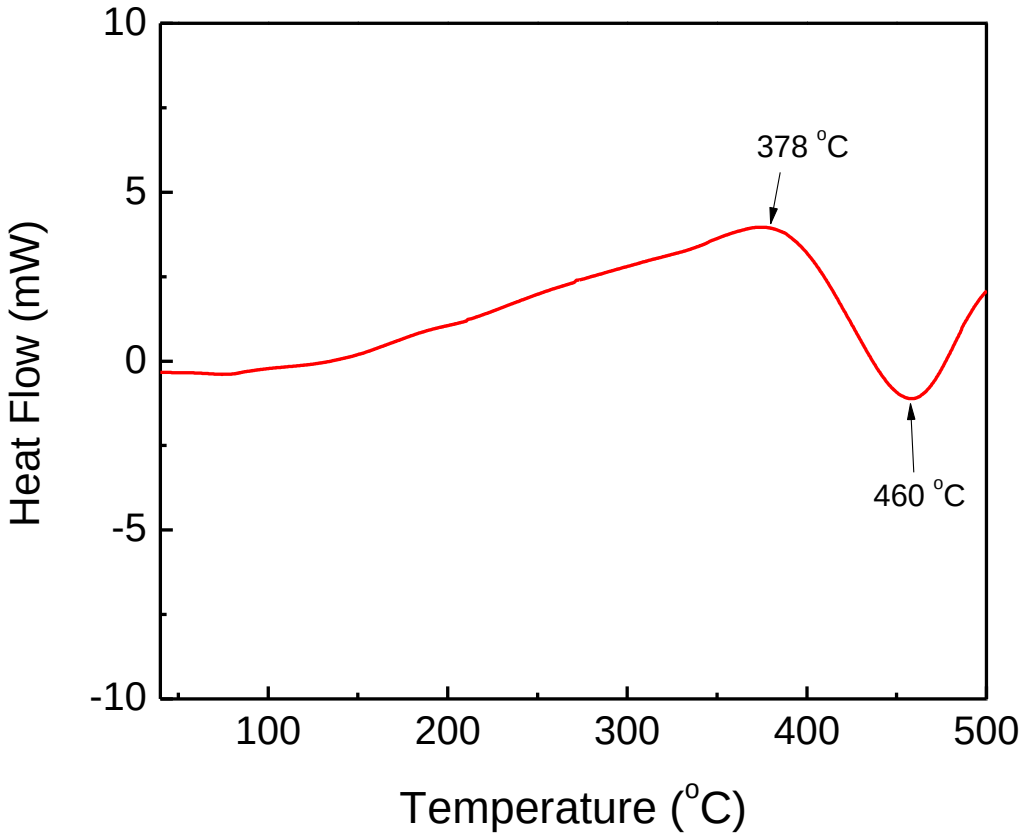

Fig. S-4.4 DSC trace of **P1** (scan rate: 10 °C/min, under nitrogen).

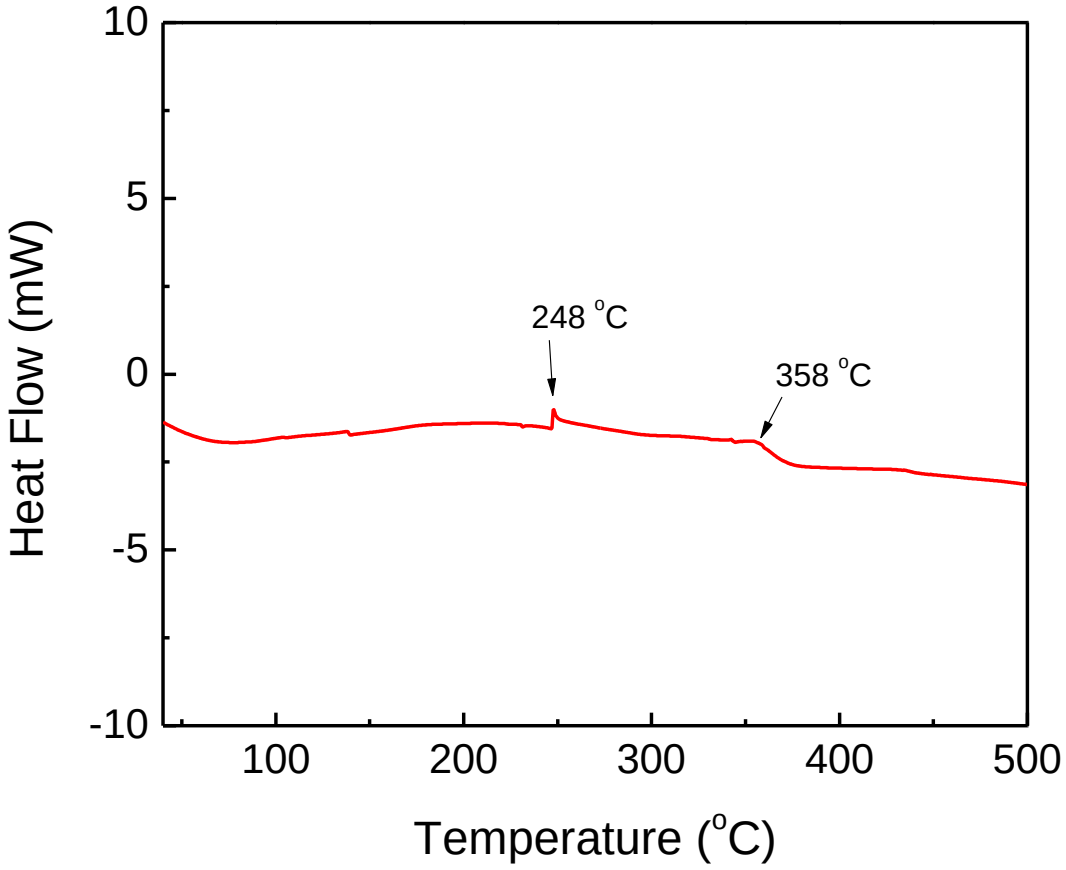

Fig. S-4.5 DSC trace of **P3** (scan rate: 10 °C/min, under nitrogen).

4.7 NMR Spectra for New Compounds

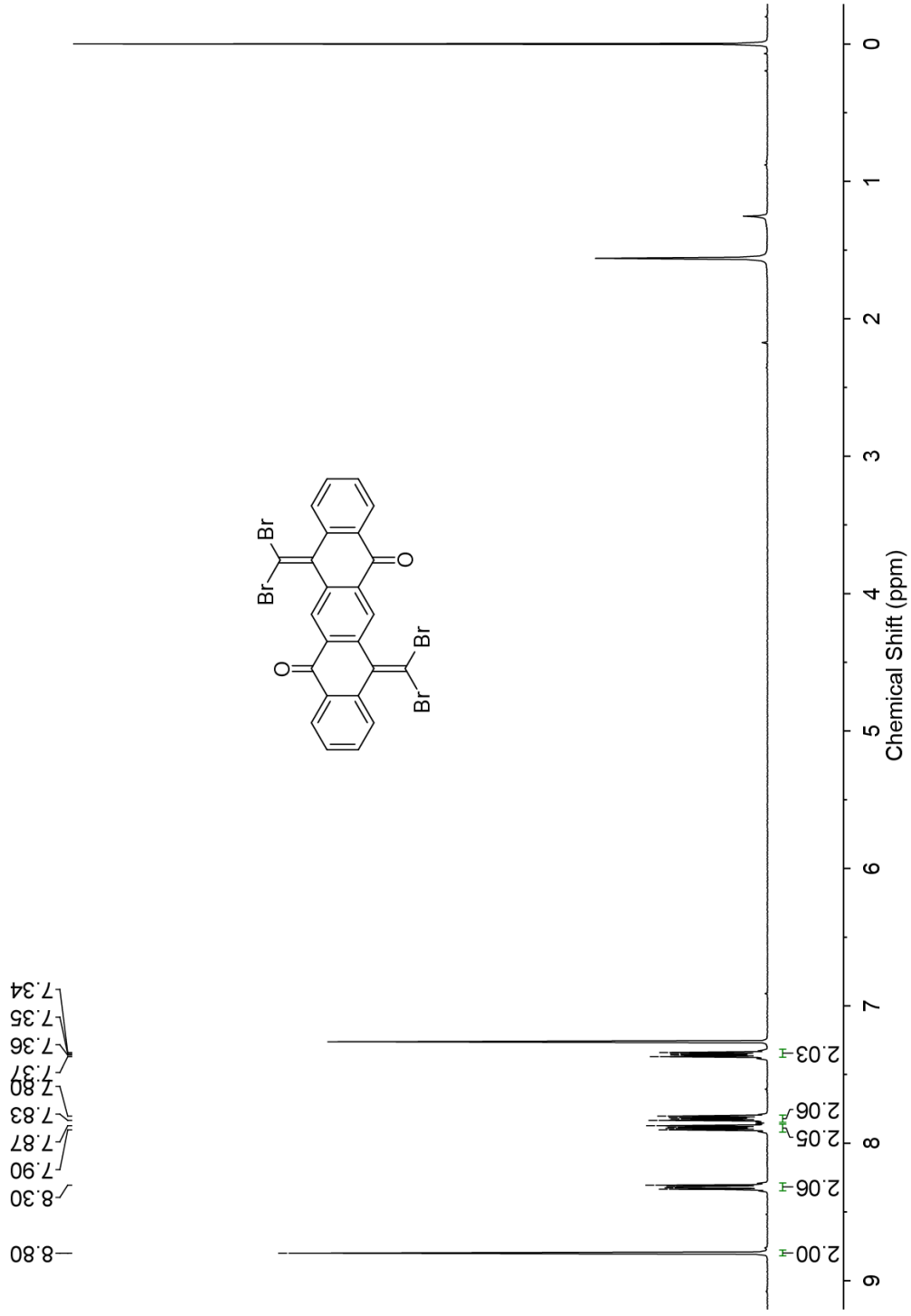

Fig. S-4.6 ^{1}H NMR (300 MHz, $CDCl_3$) of compound **62**.

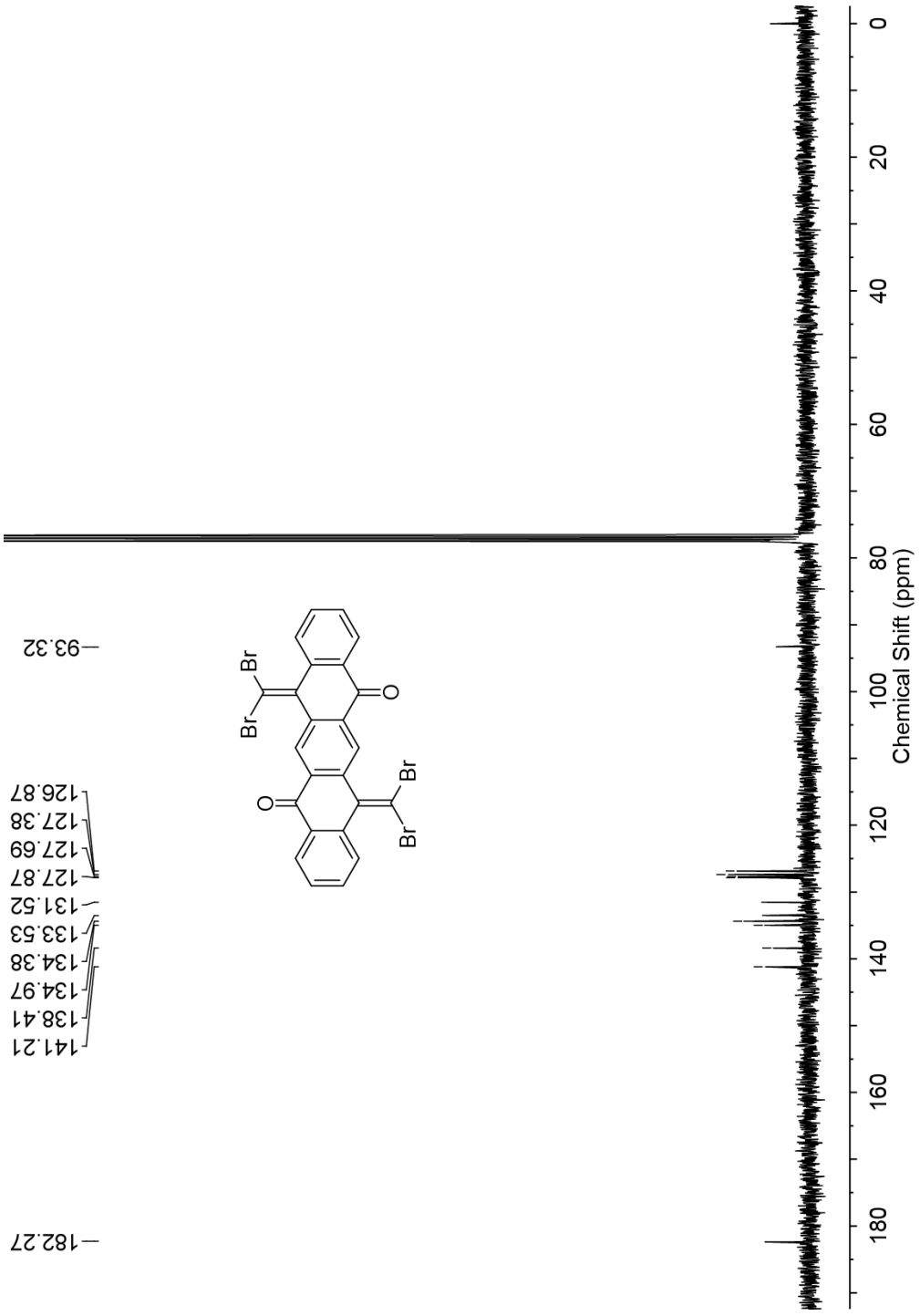

Fig. S-4.7 ^{13}C NMR (75 MHz, $CDCl_3$) of compound **62**.

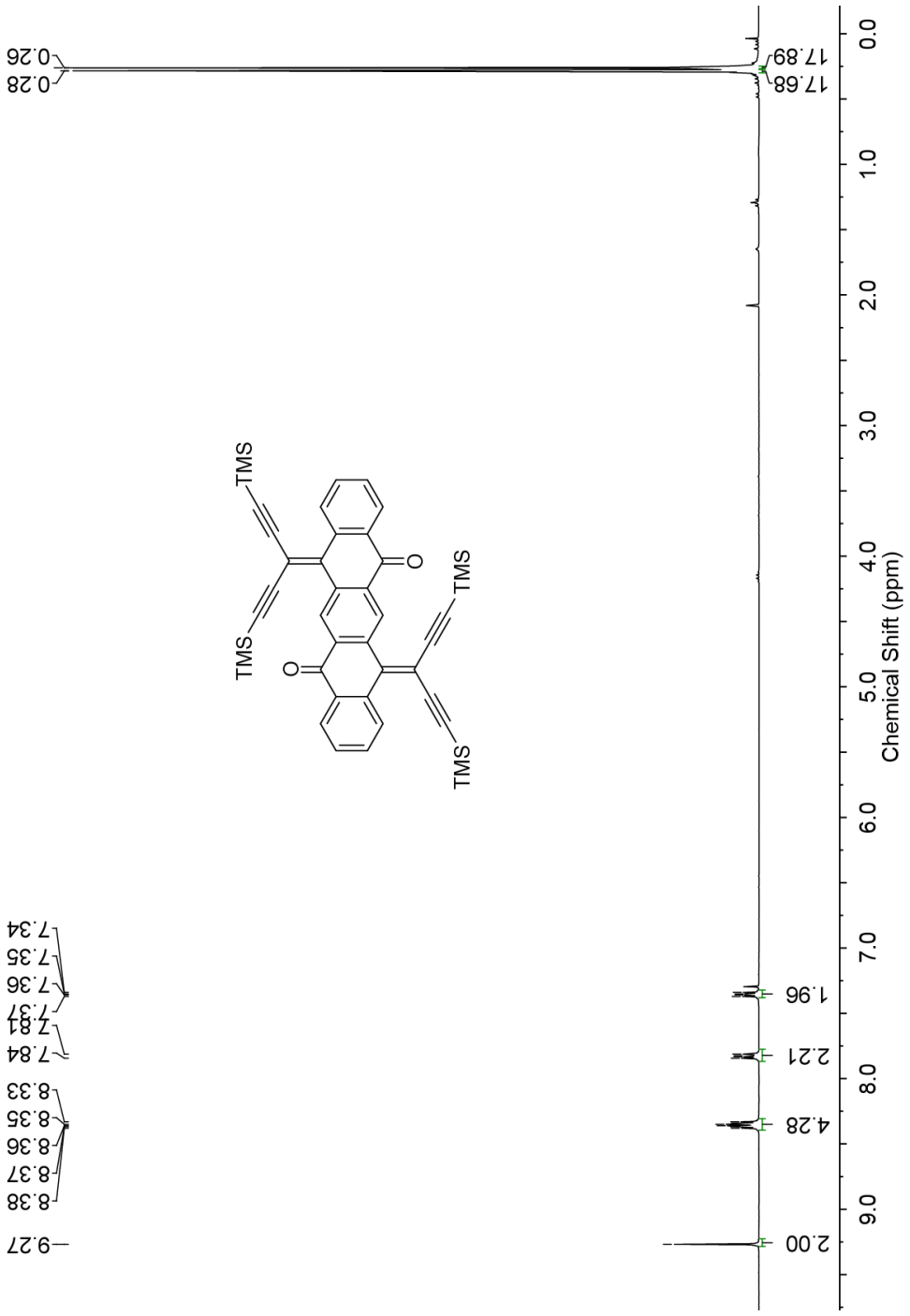

Fig. S-4.8 ^{1}H NMR (300 MHz, $CDCl_3$) of compound **63**.

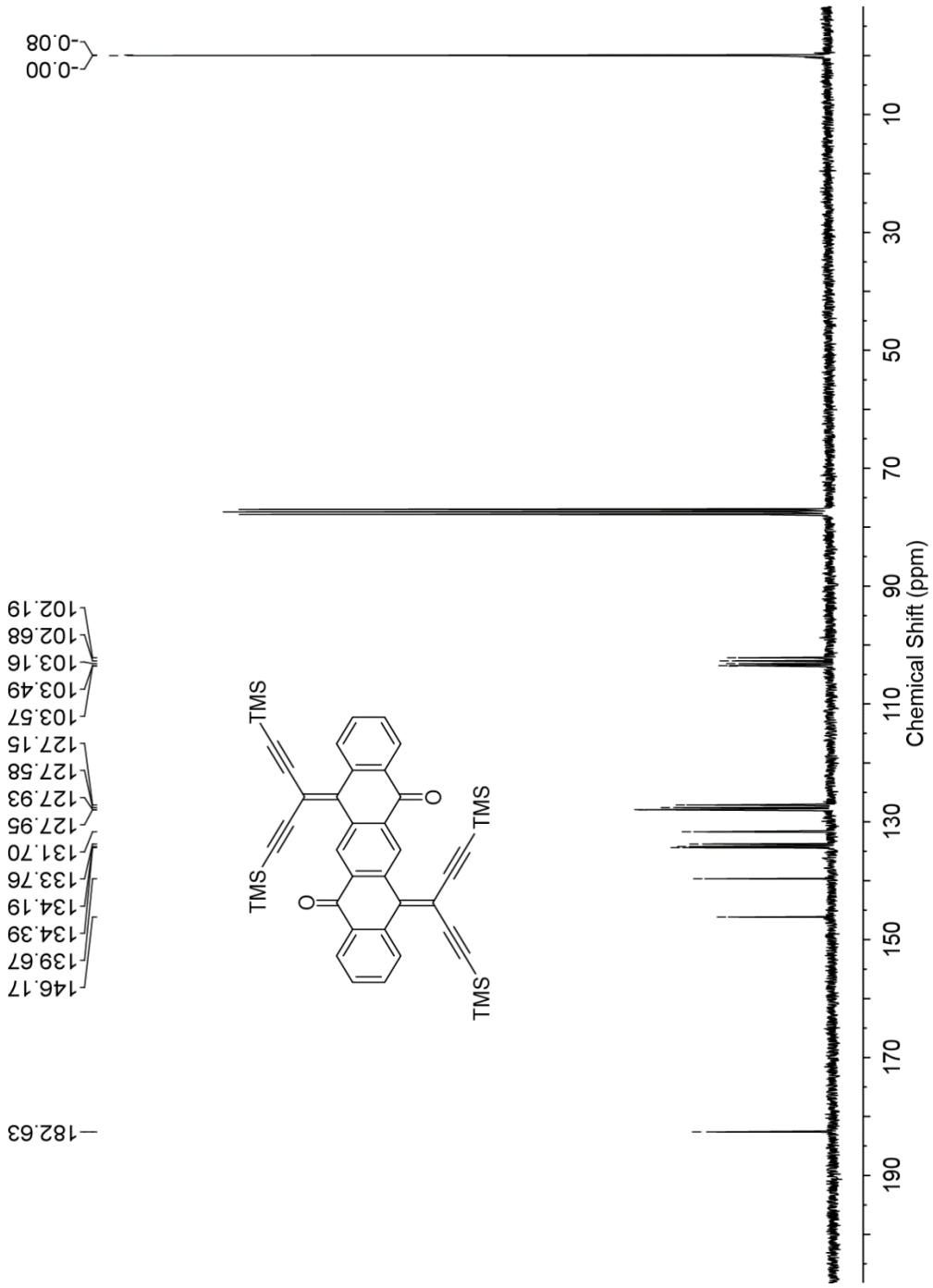

Fig. S-4.9 ^{13}C NMR (75 MHz, $CDCl_3$) of compound **63**.

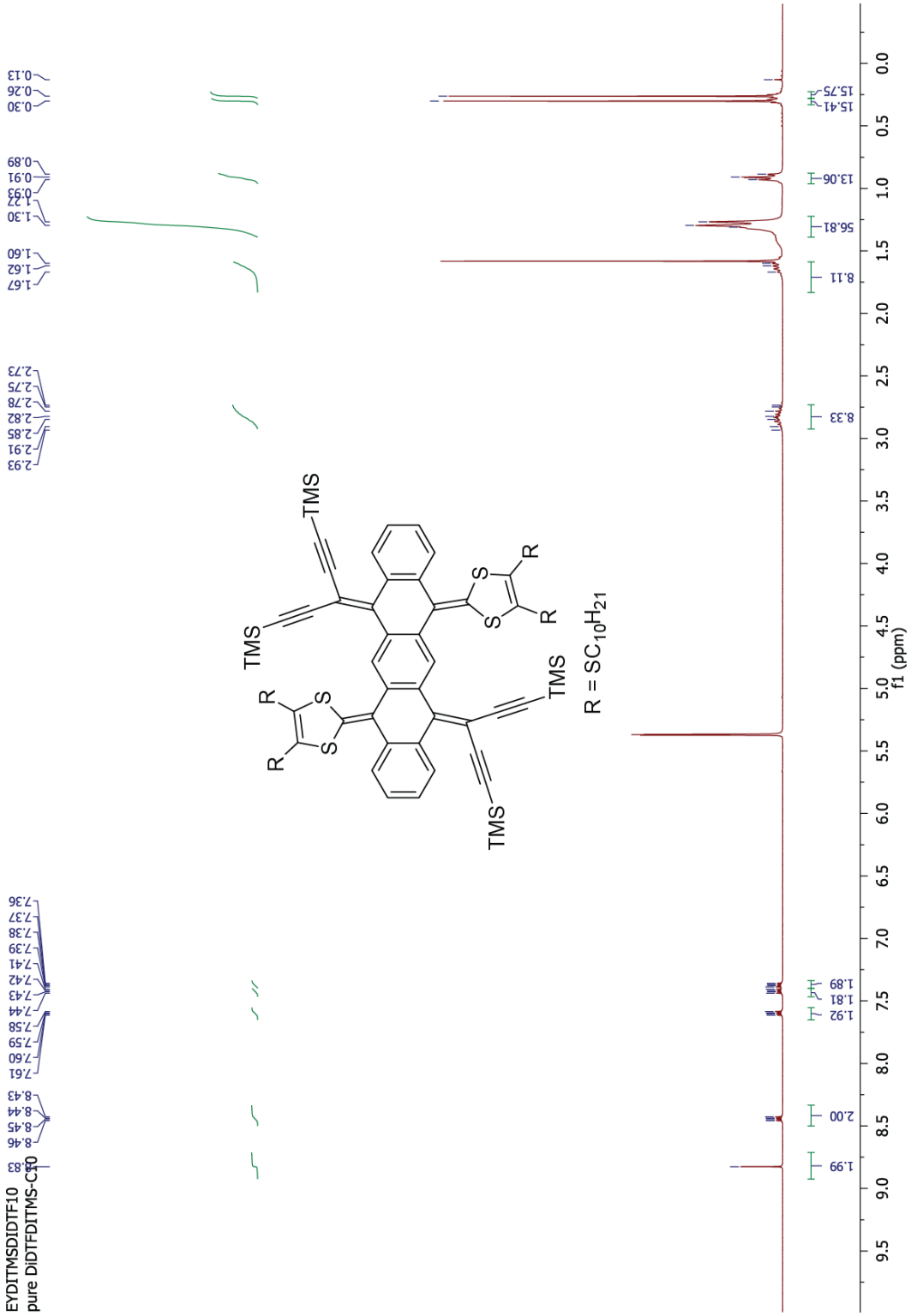

Fig. S-4.10 ^{1}H NMR (300 MHz, CD_2Cl_2) of compound **64**.

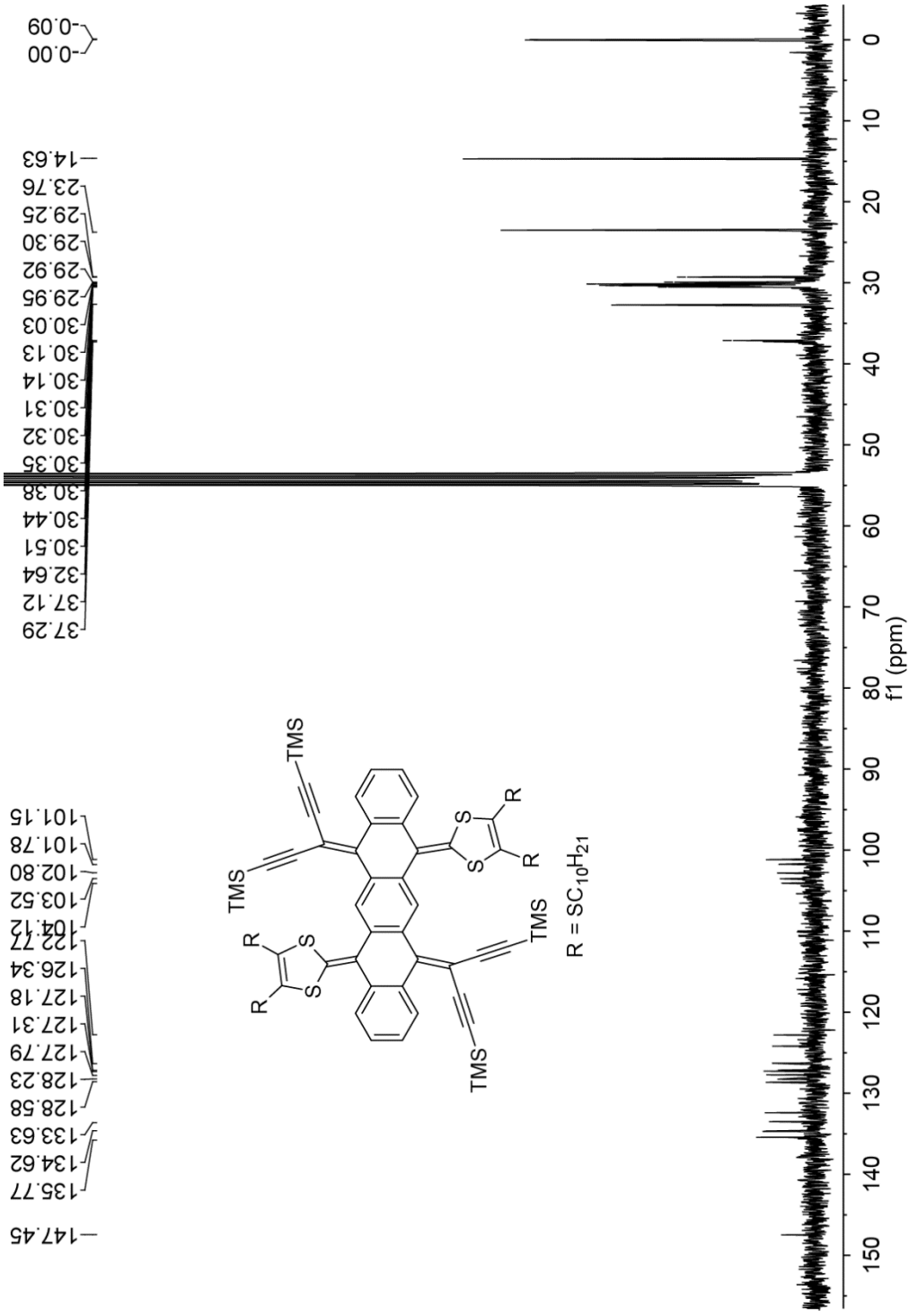

Fig. S-4.11 ^{13}C NMR (75 MHz, CD_2Cl_2) of compound **64**.

4.8 DFT Calculation Results

Cartesian coordinates and optimized **63** (*cis* conformer): *E*(RB3LYP) = -1378.00275315 hartees.; Dipole Moment = 0.8167 Debye; Basis Set = 6-31G(d)

C	-2.53675900	1.41345600	0.10820600
C	-3.67625000	0.71601600	-0.52813000
C	-5.85285600	-0.71056400	-1.63342200
C	-3.65914600	-0.69736100	-0.60742200
C	-4.78426900	1.39171900	-1.06857700
C	-5.85285600	0.68773400	-1.61728000
C	-4.75255700	-1.39615100	-1.13364100
H	-4.80190200	2.47338800	-1.07824700
H	-6.68969200	1.23682400	-2.04046200
H	-4.69972800	-2.47987200	-1.15301600
H	-6.69485800	-1.25486200	-2.05153100
C	-1.23248100	0.72357600	0.02462500
C	1.23248100	-0.72357600	0.02462500
C	-0.00230600	1.39069800	-0.01297500
C	-1.20436500	-0.69086200	-0.04039500
C	0.00230600	-1.39069800	-0.01297500

C	1.20436500	0.69086200	-0.04039500
H	0.05341800	2.46991600	-0.05448500
H	-0.05341800	-2.46991600	-0.05448500
C	-2.69920900	2.56538600	0.85625100
C	-2.46169300	-1.47307500	-0.19629300
C	2.46169300	1.47307500	-0.19629300
C	2.53675900	-1.41345600	0.10820600
C	3.65914600	0.69736100	-0.60742200
C	5.85285600	-0.68773400	-1.61728000
C	4.75255700	1.39615100	-1.13364100
C	3.67625000	-0.71601600	-0.52813000
C	4.78426900	-1.39171900	-1.06857700
C	5.85285600	0.71056400	-1.63342200
H	4.69972800	2.47987200	-1.15301600
H	4.80190200	-2.47338800	-1.07824700
H	6.69485800	1.25486200	-2.05153100
H	6.68969200	-1.23682400	-2.04046200
C	2.69920900	-2.56538600	0.85625100

O	2.48147000	2.69535500	-0.08318300
O	-2.48147000	-2.69535500	-0.08318300
C	-1.64160500	3.20924700	1.57282300
C	-3.95851100	3.20152700	1.09901600
H	-5.86371700	4.32686900	1.63648600
C	-4.96238400	3.81143500	1.39273500
H	-0.06702700	4.33625700	2.77000200
C	-0.82519300	3.82162400	2.22393200
C	1.64160500	-3.20924700	1.57282300
C	3.95851100	-3.20152700	1.09901600
H	5.86371700	-4.32686900	1.63648600
C	4.96238400	-3.81143500	1.39273500
H	0.06702700	-4.33625700	2.77000200
C	0.82519300	-3.82162400	2.22393200

Cartesian coordinates and optimized **63** (*trans* conformer): *E*(RB3LYP) = -1378.00177508 hartees.; Dipole Moment = 0.0005 Debye; Basis Set = 6-31G(d)

C	-3.19444500	-2.11221700	-0.16312500
C	-2.79119200	-0.81230800	0.08320700

C	-3.76179700	0.29759200	0.21460900
C	-3.41783000	1.57257700	-0.29490900
C	-2.05131300	1.84829100	-0.80608700
C	-1.00795800	0.85738400	-0.42120200
C	0.32731700	1.25165700	-0.51000200
C	1.36581600	0.42013000	-0.07423100
C	1.00795600	-0.85738100	0.42118900
C	2.05131000	-1.84828900	0.80607100
O	1.77488200	-2.87874800	1.41287000
C	3.41782900	-1.57257300	0.29489900
C	3.76179500	-0.29758700	-0.21461900
C	2.79118900	0.81231300	-0.08321800
C	3.19444600	2.11221900	0.16311400
C	4.55938300	2.51886800	0.30980500
C	5.66771200	2.97666700	0.47711000
H	6.65623000	3.35015500	0.62140700
C	2.30032100	3.20119500	0.41222500
C	1.64152200	4.18842000	0.65106100

H	1.02165200	5.03523900	0.84188600
C	5.01939500	-0.14984700	-0.82497300
C	5.91719500	-1.21283300	-0.87734600
C	5.59146500	-2.45014400	-0.31287400
C	4.34012100	-2.62577000	0.26491900
H	4.03647700	-3.57818000	0.68728700
H	6.30109900	-3.27199700	-0.34510400
H	6.87698800	-1.07417700	-1.36769100
H	5.28950900	0.79470500	-1.27830600
C	-0.32731900	-1.25165400	0.50999000
C	-1.36581800	-0.42012600	0.07422000
H	-0.52429700	-2.22626000	0.93421500
H	0.52429400	2.22626200	-0.93422900
O	-1.77488300	2.87875200	-1.41288000
C	-4.34012100	2.62577600	-0.26492500
C	-5.59146100	2.45015400	0.31287500
C	-5.91719100	1.21284400	0.87734900
C	-5.01939300	0.14985600	0.82497300

H	-5.28950500	-0.79469500	1.27831000
H	-6.87698100	1.07419000	1.36770200
H	-6.30109400	3.27200800	0.34511000
H	-4.03647600	3.57818600	-0.68729400
C	-2.30031400	-3.20118900	-0.41222900
C	-1.64151500	-4.18842700	-0.65101100
H	-1.02180500	-5.03547600	-0.84133900
C	-4.55938000	-2.51887200	-0.30981800
C	-5.66770200	-2.97668900	-0.47711900
H	-6.65620700	-3.35020500	-0.62143600

Cartesian coordinates and optimized **64** (*cis* conformer): *E*(RB3LYP) = -3051.28175927 hartees.; Dipole Moment = 0.7461 Debye; Basis Set = 6-31G(d)

C	2.51787400	1.39822100	0.23656100
C	3.42173200	0.74482300	1.20594900
C	5.02761500	-0.60096400	3.07200900
C	3.42173200	-0.67398100	1.24473200
C	4.22462700	1.45908200	2.10637400
C	5.02764100	0.79359700	3.02956600

C	4.22580100	-1.32502200	2.19153600
H	4.20437700	2.54213900	2.09247700
H	5.63639500	1.36421100	3.72538600
H	4.19131800	-2.40662200	2.27297100
H	5.63221200	-1.12765200	3.80536000
C	1.22039900	0.70387400	0.09437800
C	-1.22039900	-0.70387400	0.09437800
C	0.00028700	1.39140700	0.08463500
C	1.22532600	-0.71515200	0.11738100
C	-0.00028700	-1.39140700	0.08463500
C	-1.22532600	0.71515200	0.11738100
H	0.01699700	2.47352000	0.14994900
H	-0.01699700	-2.47352000	0.14994900
C	2.87104500	2.50365300	-0.50322500
C	2.53025600	-1.39126400	0.30473300
C	-2.53025600	1.39126400	0.30473300
C	-2.51787400	-1.39822100	0.23656100
C	-3.42173200	0.67398100	1.24473200

C	-5.02764100	-0.79359700	3.02956600
C	-4.22580100	1.32502200	2.19153600
C	-3.42173200	-0.74482300	1.20594900
C	-4.22462700	-1.45908200	2.10637400
C	-5.02761500	0.60096400	3.07200900
H	-4.19131800	2.40662200	2.27297100
H	-4.20437700	-2.54213900	2.09247700
H	-5.63221200	1.12765200	3.80536000
H	-5.63639500	-1.36421100	3.72538600
C	-2.87104500	-2.50365300	-0.50322500
C	2.05308100	3.04843500	-1.54309700
C	4.14197500	3.15519100	-0.39467700
H	6.12360300	4.27528400	-0.35516400
C	5.18948500	3.76197400	-0.38114400
H	0.94039100	3.98273100	-3.29489600
C	1.46718600	3.56034700	-2.47058900
C	-2.05308100	-3.04843500	-1.54309700
C	-4.14197500	-3.15519100	-0.39467700

H	-6.12360300	-4.27528400	-0.35516400
C	-5.18948500	-3.76197400	-0.38114400
H	-0.94039100	-3.98273100	-3.29489600
C	-1.46718600	-3.56034700	-2.47058900
C	2.91360100	-2.51168100	-0.37383800
C	-2.91360100	2.51168100	-0.37383800
S	1.89652200	-3.32252700	-1.59737200
S	4.52997100	-3.26823900	-0.22535200
C	4.33294400	-4.38409300	-1.56892000
H	5.18153500	-5.00958100	-1.82095700
C	3.14703800	-4.40872200	-2.18535600
H	2.88920000	-5.05873900	-3.01358900
S	-1.89652200	3.32252700	-1.59737200
S	-4.52997100	3.26823900	-0.22535200
C	-3.14703800	4.40872200	-2.18535600
H	-2.88920000	5.05873900	-3.01358900
C	-4.33294400	4.38409300	-1.56892000
H	-5.18153500	5.00958100	-1.82095700

Cartesian coordinates and optimized **64** (*trans* conformer): *E*(RB3LYP) = -3051.28501525 hartees.; Dipole Moment = 0.0024 Debye; Basis Set = 6-31G(d)

C	-5.19609600	3.34144400	1.35045000
S	-5.20234300	1.96745800	0.25380300
C	-3.43321500	1.69373200	0.28550500
C	-2.82584000	0.58104000	-0.22457700
C	-1.37721600	0.31489500	-0.10198700
C	-0.96776300	-1.00963300	0.20143300
C	0.39881600	-1.29453000	0.29758400
C	1.37721400	-0.31486100	0.10198500
C	2.82583600	-0.58101000	0.22457100
C	3.56857800	0.53216500	0.85484600
C	4.61723500	0.33735500	1.76544800
C	5.26610700	1.41922300	2.35720000
C	4.86362700	2.72106400	2.05790200
C	3.81518300	2.93484500	1.16651100
C	3.16129400	1.85824100	0.54985500
C	2.01604000	2.03686400	-0.36832000
C	0.96776200	1.00966600	-0.20143800

C	-0.39881700	1.29456300	-0.29758800
H	-0.70030500	2.29912100	-0.56252100
C	1.96350800	3.02868700	-1.32455100
C	0.89982200	3.16093900	-2.27388900
C	0.05785700	3.34127200	-3.12505400
H	-0.69775200	3.47482900	-3.86531000
C	3.01456900	3.97740000	-1.53900000
C	3.85273600	4.80903400	-1.80710400
H	4.61035100	5.52605400	-2.02758300
H	3.48608300	3.94554700	0.95782600
H	5.35099500	3.56917600	2.53067500
H	6.06738800	1.24200500	3.06944500
H	4.89838900	-0.67097500	2.05169000
C	3.43319800	-1.69372000	-0.28548600
S	2.56915300	-2.98237600	-1.17738300
C	4.01049100	-3.79797100	-1.76590300
C	5.19604800	-3.34156500	-1.35027500
S	5.20231900	-1.96748300	-0.25374800

H	6.15769000	-3.76107500	-1.62242800
H	3.86360800	-4.64484700	-2.42627000
H	0.70030600	-2.29908800	0.56251300
C	-2.01603800	-2.03683600	0.36830300
C	-3.16128500	-1.85821200	-0.54988000
C	-3.56857200	-0.53213600	-0.85486700
C	-4.61721900	-0.33732600	-1.76547800
C	-5.26608300	-1.41919300	-2.35724100
C	-4.86360400	-2.72103500	-2.05794300
C	-3.81516700	-2.93481600	-1.16654400
H	-3.48606800	-3.94551800	-0.95785700
H	-5.35096700	-3.56914700	-2.53072200
H	-6.06735800	-1.24197500	-3.06949300
H	-4.89837400	0.67100400	-2.05172100
C	-1.96351500	-3.02865900	1.32453500
C	-3.01459200	-3.97735100	1.53899300
C	-3.85271800	-4.80907000	1.80696200
H	-4.60991900	-5.52691100	2.02619300

C	-0.89986000	-3.16088800	2.27391000
C	-0.05782800	-3.34121300	3.12501100
H	0.69869600	-3.47468800	3.86434700
S	-2.56919400	2.98236000	1.17746600
C	-4.01054600	3.79785500	1.76609100
H	-3.86367500	4.64468100	2.42652500
H	-6.15774600	3.76089900	1.62265900

4.9 References

(1) Holger, F. B. *Pure Appl. Chem.* **2010**, *82*, 905-915.

(2) Davy, N. C.; Man, G.; Kerner, R. A.; Fusella, M. A.; Purdum, G. E.; Sezen, M.; Rand, A. Kahn, B. P.; Loo, Y.-L. *Chem. Mater.* **2016**, *28*, 673-681.

(3) Kumar, S.; Ho, M.-T.; Tao, Y.-T. *Org. Lett.* **2016**, *18*, 200-203.

(4) Kuo, C.-H.; Huang, D.-C.; Peng, W.-T.; Goto, K.; Chao, I.; Tao, Y.-T. *J. Mater. Chem. C* **2014**, *2*, 3928-3935.

(5) Pola, S.; Kuo, C.-H.; Peng, W.-T.; Islam, M. M.; Chao, I.; Tao, Y.-T. *Chem. Mater.* **2012**, *24*, 2566-2571.

(6) Chen, L.; Puniredd, S. R.; Tan, Y.-Z.; Baumgarten, M.; Zschieschang, U.; Enkelmann, V.; Pisula, W.; Feng, X.; Klauk, H.; Müllen, K. *J. Am. Chem. Soc.* **2012**, *134*, 17869-17872.

(7) Zhang, W.; Zhong, X.; Zhao, Y. *J. Phys. Chem. A* **2012**, *116*, 11075-11082.

(8) Plunkett, K. N.; Godula, K.; Nuckolls, C.; Tremblay, N.; Whalley, A. C.; Xiao, S. *Org. Lett.* **2009**, *11*, 2225-2228.

(9) Giguère, J.-B.; Verolet, Q.; Morin, J.-F. *Chem. Eur. J.* **2013**, *19*, 372-381.

(10) Chen, Z.; Swager, T. M. *Org. Lett.* **2007**, *9*, 997-1000.

(11) Loo, Y.-L.; Hiszpanski, A. M.; Kim, B.; Wei, S.; Chiu, C.-Y.; Steigerwald, M. L.; Nuckolls, C. *Org. Lett.* **2010**, *12*, 4840-4843.

(12) Ball, M.; Zhong, Y.; Wu, Y.; Schenck, C.; Ng, F.; Steigerwald, M.; Xiao, S.; Nuckolls, C. *Acc. Chem. Res.* **2015**, *48*, 267-276.

(13) Brunetti, F. G.; Lopez, J. L.; Atienza, C.; Martin, N. *J. Mater. Chem.* **2012**, *22*, 4188-4205.

(14) Jørgensen, K. B. *Molecules* **2010**, *15*, 4334-4358.

(15) Mallory, F. B.; Wood, C. S.; Gordon, J. T. *J. Am. Chem. Soc.* **1964**, *86*, 3094-3102.

(16) Molloy, M. S.; Snyder, J. A.; DeFrancisco, J. R.; Bragg, A. E. *J. Phys. Chem. A* **2016**, *120*, 3998-4007.

(17) Mallory, F. B.; Wood, C. S.; Gordon, J. T.; Lindquist, L. C.; Savitz, M. L. *J. Am. Chem. Soc.* **1962**, *84*, 4361-4362.

(18) Liu, L.; Yang, B.; Katz, T. J.; Poindexter, M. K. *J. Org. Chem.* **1991**, *56*, 3769-3775.

(19) Wood, C. S.; Mallory, F. B. *J. Org. Chem.* **1964**, *29*, 3373-3377.

(20) Grzybowski, M.; Skonieczny, K.; Butenschön, H.; Gryko, D. T. *Angew. Chem. Int. Ed.* **2013**, *52*, 9900-9930.

(21) Rieger, R.; Müllen, K. *J. Phys. Org. Chem.* **2010**, *23*, 315-325.

(22) Zhou, Z.; Qin, Y.; Xu, W.; Zhu, D. *Chem. Commun.* **2014**, *50*, 4082-4084.

(23) He, Z.; Shan, L.; Mei, J.; Wang, H.; Lam, J. W. Y.; Sung, H. H. Y.; Williams, I. D.; Gu, X.; Miao, Q.; Tang, B. Z. *Chem. Sci.* **2015**, *6*, 3538-3543.

(24) Nishida, J.-i.; Fujiwara, Y.; Yamashita, Y. *Org. Lett.* **2009**, *11*, 1813-1816.

(25) Herranz, M. Á.; Martín, N.; Campidelli, S.; Prato, M.; Brehm, G.; Guldi, D. M. *Angew. Chem. Int. Ed.* **2006**, *45*, 4478-4482.

(26) Bouit, P.-A.; Villegas, C.; Delgado, J. L.; Viruela, P. M.; Pou-Amérigo, R.; Ortí, E.; Martín, N. *Org. Lett.* **2011**, *13*, 604-607.

(27) Neidlein, R.; Winter, M. *Synthesis* **1998**, *1998*, 1362-1366.

(28) Chelucci, G. *Chem. Rev.* **2012**, *112*, 1344-1462.

(29) Donovan, P. M.; Scott, L. T. *J. Am. Chem. Soc.* **2004**, *126*, 3108-3112.

(30) Chen, Z.-Q.; Chen, T.; Liu, J.-X.; Zhang, G.-F.; Li, C.; Gong, W.-L.; Xiong, Z.-J.; Xie, N.-H.; Tang, B. Z.; Zhu, M.-Q. *Macromolecules* **2015**, *48*, 7823-7835.

(31) Bandyopadhyay, A.; Varghese, B.; Hopf, H.; Sankararaman, S. *Chem. Eur. J.* **2007**, *13*, 3813-3821.

(32) Ito, S.; Inabe, H.; Morita, N.; Tajiri, A. *Eur. J. Org. Chem.* **2004**, *2004*, 1774-1780.

(33) Ito, S.; Iida, T.; Kawakami, J.; Okujima, T.; Morita, N. *Eur. J. Org. Chem.* **2009**, 5355-5364.

(34) Ryhding, T.; Petersen, M. Å.; Kilså, K.; Nielsen, M. B. *Synlett* **2007**, 0913-0916.

(35) Shoji, T.; Ito, S.; Toyota, K.; Morita, N. *Tetrahedron Lett.* **2009**, *50*, 2825-2827.

(36) Younes, E. A.; Zhao, Y. *RSC Adv.* **2015**, *5*, 88821-88825.

(37) Bouit, P.-A.; Marszalek, M.; Humphry-Baker, R.; Viruela, R.; Ortí, E.; Zakeeruddin, S. M.; Grätzel, M.; Delgado, J. L.; Martín, N. *Chem. Eur. J.* **2012**, *18*, 11621-11629.

(38) Chen, G.; Wang, L.; Thompson, D. W.; Zhao, Y. *Org. Lett.* **2008**, *10*, 657-660.

(39) Bouit, P.-A.; Infantes, L.; Calbo, J.; Viruela, R.; Ortí, E.; Delgado, J. L.; Martín, N. *Org. Lett.* **2013**, *15*, 4166-4169.

(40) Christensen, C. A.; Batsanov, A. S.; Bryce, M. R. *J. Org. Chem.* **2007**, *72*, 1301-1308.

(41) Shao, M.; Zhao, Y. *Tetrahedron Lett.* **2010**, *51*, 2892-2895.

(42) Aguilar, E.; Sanz, R.; Fernández-Rodríguez, M. A.; García-García, P. *Chem. Rev.* **2016**, *116*, 8256-8311.

(43) Baxter, I.; Cameron, D. W.; Titman, R. B. *J. Chem. Soc. C: Organic* **1971**, 1253-1256.

(44) Moore, A. J.; Bryce, M. R. *Tetrahedron Lett.* **1992**, *33*, 1373-1376.

(45) Chen, G.; Zhao, Y. *Tetrahedron Lett.* **2006**, *47*, 5069-5073.

(46) Zhao, Y.; Shirai, Y.; Slepkov, A. D.; Cheng, L.; Alemany, L. B.; Sasaki, T.; Hegmann, F. A.; Tour, J. M. *Chem. Eur. J.* **2005**, *11*, 3643-3658.

(47) Bennett, M. A.; Smith, A. K. *J. Chem. Soc., Dalton Trans.* **1974**, 233-241.

(48) Gaussian 09, Revision **E.01**, Frisch, M. J.; Trucks, G. W.; Schlegel, H. B.; Scuseria, G. E.; Robb, M. A.; Cheeseman, J. R.; Scalmani, G.; Barone, V.; Mennucci, B.; Petersson, G. A.; Nakatsuji, H.; Caricato, M.; Li, X.; Hratchian, H. P.; Izmaylov, A. F.; Bloino, J.; Zheng, G.; Sonnenberg, J. L.; Hada, M.; Ehara, M.; Toyota, K.; Fukuda, R.; Hasegawa, J.; Ishida, M.; Nakajima, T.; Honda, Y.; Kitao, O.; Nakai, H.; Vreven, T.; Montgomery, J. A., Jr.; Peralta, J. E.; Ogliaro, F.; Bearpark, M.; Heyd, J. J.; Brothers, E.; Kudin, K. N.; Staroverov, V. N.; Kobayashi, R.; Normand, J.; Raghavachari, K.; Rendell, A.; Burant, J. C.; Iyengar, S. S.; Tomasi, J.; Cossi, M.; Rega, N.; Millam, J. M.; Klene, M.; Knox, J. E.; Cross, J. B.; Bakken, V.; Adamo, C.; Jaramillo, J.; Gomperts, R.; Stratmann, R. E.; Yazyev, O.; Austin, A. J.; Cammi, R.; Pomelli, C.; Ochterski, J. W.; Martin, R. L.; Morokuma, K.; Zakrzewski, V. G.; Voth, G. A.; Salvador, P.; Dannenberg, J. J.; Dapprich, S.; Daniels, A. D.; Farkas, Ö.; Foresman, J. B.; Ortiz, J. V.; Cioslowski, J.; Fox, D. J. Gaussian, Inc., Wallingford CT, **2009**.

(49) CYLview, 1.0b; Legault, C. Y. Université de Sherbrooke, **2009** (http://www.cylview.org).

(50) GaussView, Version 5, Dennington, R.; Keith, T.; Millam, J.; Semichem Inc. Shawnee Mission KS, **2009**.

Chapter 5

Attempted Synthesis of Dinaphthopentacene

5.1 Introduction

Since the discovery of graphene, several methods have been developed for synthesizing nanographene molecules as they have great potential in optoelectronics, nanoelectronics, and spintronics.[1-5] Polycyclic aromatic hydrocarbons (PAHs) that are composed of all-sp^2 carbons can be regarded as the smallest possible graphene segments.[6,7] Throughout the 20th century, Scholl[8-10] and Clar[11-13] contributed intensively to the development and synthesis of PAHs. Recently extended PAHs, particularly graphene-like molecules with different sizes, symmetries and properties have been synthesized and investigated. Among most of the synthetic methods to prepare PAHs, the Scholl reaction is the most common used and it can be performed with a variety of oxidants and Lewis acids,[14] $FeCl_3$,[15], and 2,3-dichloro-5,6-dicyano-1,4-benzoquinone (DDQ)/Brønsted or Lewis acid.[16] However, these synthetic methods have some limitations, such as incomplete cyclization[17] and unexpected structural rearrangements, which are commonly seen outcomes of many Scholl reactions.[18-20] For this reason, further development of new methods for the synthesis of nanographenes is necessary.

Liu *et al*. reported a synthetic approach toward PAHs **69** (Scheme 5.1) using platinum-catalyzed electrophilic cycloaromatization of *ortho*-alkynylated biaryls. As shown in Scheme 5.1, a diyne-linked PAH **67** was subjected to an intramolecular double cyclization under the catalysis of $PtCl_2$ (10 mol%) in hot toluene to give compound **68**. Compound **68** then underwent a Scholl reaction in the presence of DDQ /CH_3SO_3H yielding target compound **69**.[21]

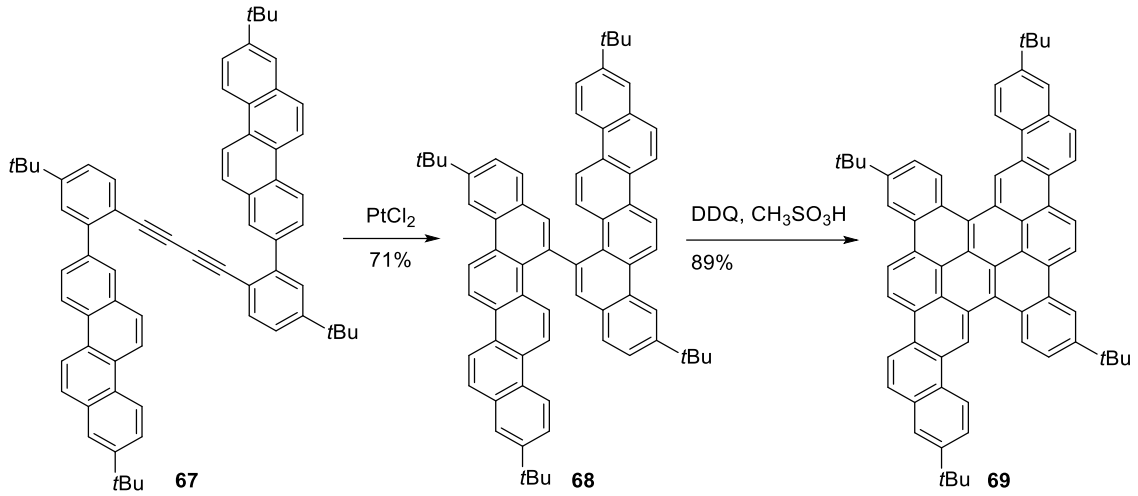

Scheme 5.1: Synthesis of nanographene **69**.

The research group of Scott[22] reported a new synthetic method for PAHs **71** (Scheme 5.2) that contain a naphthalene ring moiety embedded in larger polycyclic systems based on transition metal-catalyzed ring closures reactions. As shown in Scheme 5.2, Ru complex ($(Ph_3P)Ru(cymene)Cl_2$) was used in a catalytic amount to produce new benzene rings from the two 1-aryl-1-buten-3-yne moieties. Mechanistically, the terminal alkynes of **71** are first activated by coordination to the Ru center to generate carbene-Ru complex which then rapidly undergoes intramolecular cyclization to form PAHs in excellent yields.

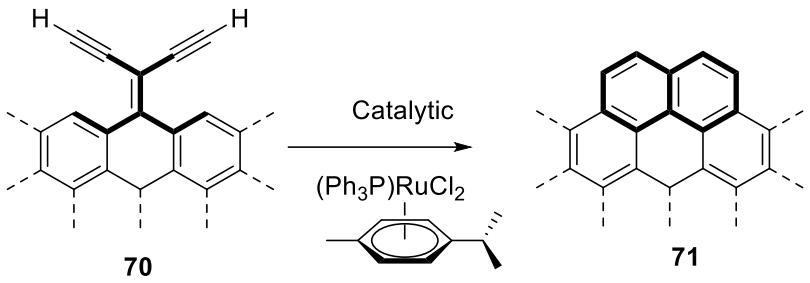

Scheme 5.2: Ru-catalyzed benzannulation reaction of compound **70**.

Based on the known Ru-catalyzed alkyne benzannulation reactions, it was envisioned that enediyne-substituted pentacenetetraone **63** (Scheme 5.3) could be used as a synthetic precursor to certain nanographene structures. The following section describes an attempted synthesis of a bisnaphthopentacene **74**, in which alkyne benzannulation was anticipated to take place as a key step for directly assembling the extended fused aromatic rings in a one-pot manner.

5.2 Results and Discussion

5.2.1 Attempted Synthesis of Nanographene 74

The attempted synthesis of nanographene **74** is outlined in Scheme 5.3. The synthesis began with reduction of the two keto groups of compound **63** with excess sodium borohydride, [23] affording **72** as a yellow solid in an excellent yield (91%). The diol **72** was supposed to be formed as a pair of diastereomers, in which the diol groups take *cis* and *trans* relationships. Since the next step was reductive elimination of the diol groups, it was unnecessary to have the two diastereomers of **72** separated. Instead, they were together subjected to the next step. Upon the treatment by $SnCl_2$ and acetic acid, compound **72** underwent dehydroxylation reaction to give compound **73** in 32% yield.

With compound **73** in hand, a benzannulation step was expected to furnish the target nanogarphene **74**. The structure of **73** features two benzene sextets, while the structure of nanographene **74** contains two pyrene segments fused in one PAH system and gives four benzene sextets. The increased aromaticity in the product was expected to serve as a strong driving force for the benzannulation reaction. Various catalytic conditions for the benzannulation could fulfill the task of benzannulation. According to literature reported methods, a series of catalytic systems, including $PtCl_2$, Ru complex $(Ph_3P)Ru(cymene)Cl_2$, and Brønsted acids was considered to be useful. Because of limited time, the benzannulation of **73** has not yet been experimentally explored. Nevertheless, the use of a strong Brønsted acid such as TFA was considered to be a reasonable choice for the first synthetic attempt given the several advantages of using TFA: (1) the TFA-promoted reaction usually occurred at room temperature with little formation of side products; (2) the excess TFA can be removed by simple methods such as neutralization with a base, aqueous washing, or just vacuum evaporation. Experimental efforts to accomplish the last step of benzannulation reaction are currently underway. It is also noticed that the final product is a fully planar PAH without any solubility-assisting groups. Very likely, the final product would suffer from poor solubility in organic solvents. To overcome this problem, installation of solubility increasing side chains needs to be planned during the synthesis of intermediates.

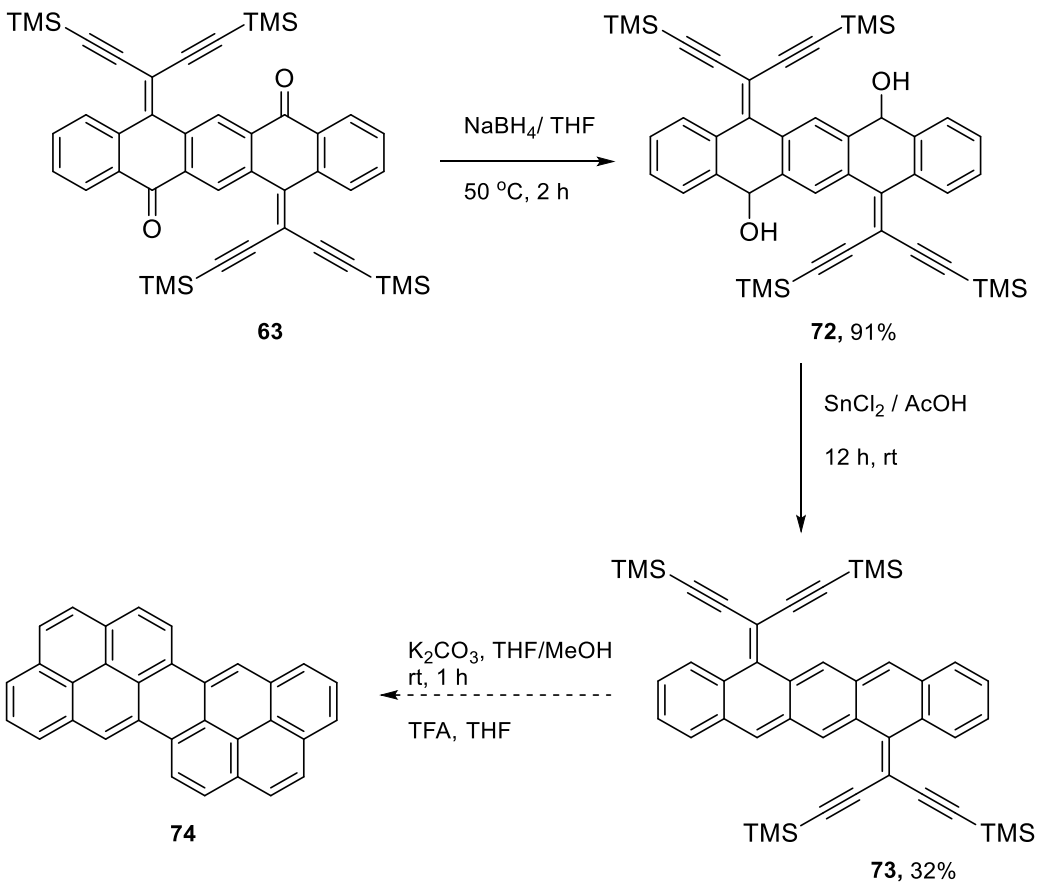

Scheme 5.3: Synthesis of the target nanographene **74**.

5.2.2 Structural and Electronic Properties

The molecular structures of compounds **72** and **73** were characterized by NMR, IR, and mass spectrometry. The reduction of compound **63** was confirmed by ^{13}C NMR analysis where the carbonyl peak at 182 ppm was observed to completely disappear. It was also evidenced by the IR data, which showed the absence of the ketone vibrational band. The ^{1}H NMR spectrum of precursor **73** showed six distinctive signals in the aromatic region. Two signals resonate as singlets at δ 8.88 (2H), and 8.36 (2H), and these two signals can be assigned to protons on the (6, 13) and (7, 14) positions.

Besides synthetic efforts, theoretical modeling studies were also conducted. The ground-state geometries of **73** and the target nanographene **74** were optimized by DFT calculations at the B3LYP/6-31G(d) level of theory. The optimized structures are shown in Fig. 5.1. For compound **73** two stable conformers were found. The first conformer, namely *trans*, takes a zig-zag shape where the two enediyne moieties are oriented in the opposite direction (Fig. 5.1A), while the second conformer, namely *cis*, adopts a curved shape and its two enediyne moieties take the same direction Fig. (5.1B). Energetically, the *cis* conformer is more stable than *trans* by 1.184 kcal/mol. The optimized structure of the target nanographene **74** is shown in Fig. 5.1C and it was found to be completely planar with a zero dipole moment.

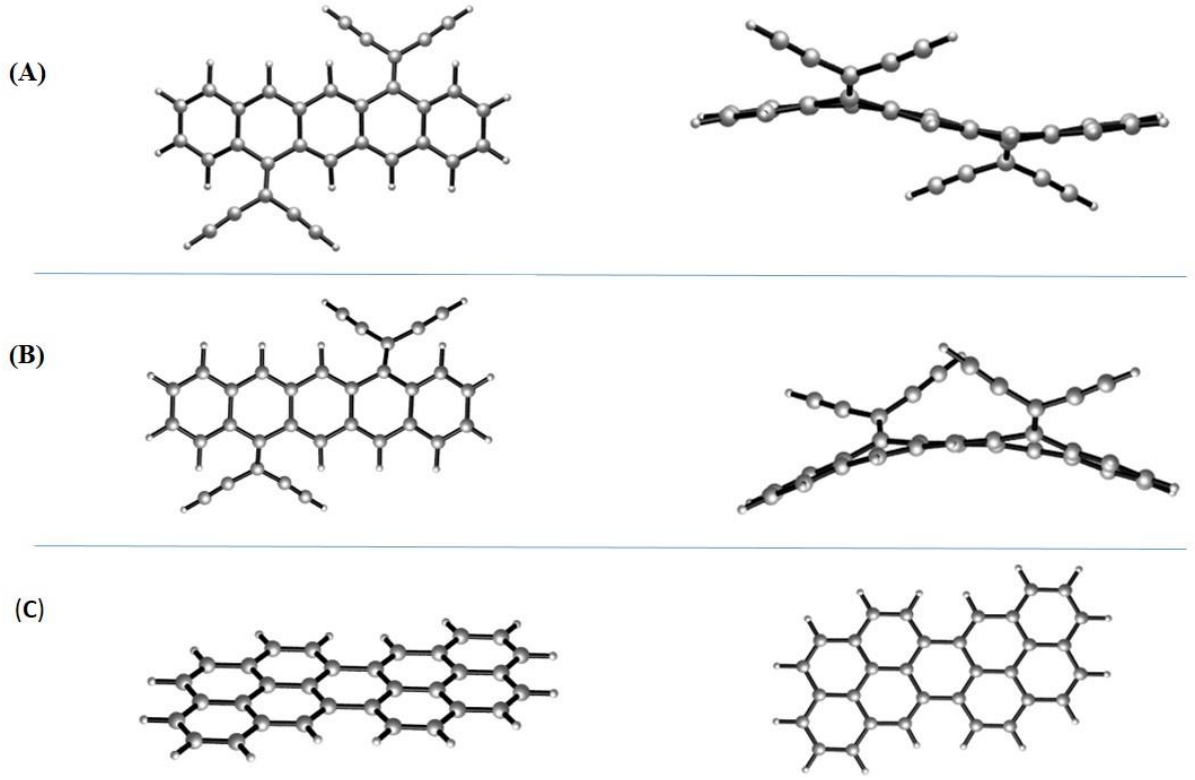

Fig. 5.1: Optimized structures of compounds (A) **73** (*trans* conformer), (B) **73** (*cis* conformer), (C) nanographene **74**. Calculations done at the B3LYP/6-31G(d) level of theory. TMS and $SC_{10}H_{21}$ groups were replaced with H atoms to reduce computational expenses.

The electronic properties of compounds **72** and **73** were investigated by UV-Vis absorption analysis (Fig. 5.2). Compound **72** is a yellow solid and its UV-Vis absorption was measured from a dilute chloroform solution. The spectrum exhibits two absorption bands at 398 and 336 nm. UV-Vis analysis of compound **73** was done both in chloroform solution and as a solid thin film. In chloroform, **73** shows two absorption bands 381 and 317 nm, along with a tail covering the range from 443 to 489 nm. The long-wavelength tail is tentatively assigned to the HOMO→LUMO transition. The solid thin film of **73** also gives two absorption bands at 377 and 316 nm and an

absorption tail from 443 to 489 nm. Compared with the solution-phase UV-Vis data, the maximum absorption band in the solid-state spectrum is blue-shifted by 4 nm and the low-energy band is notably enhanced in intensity.

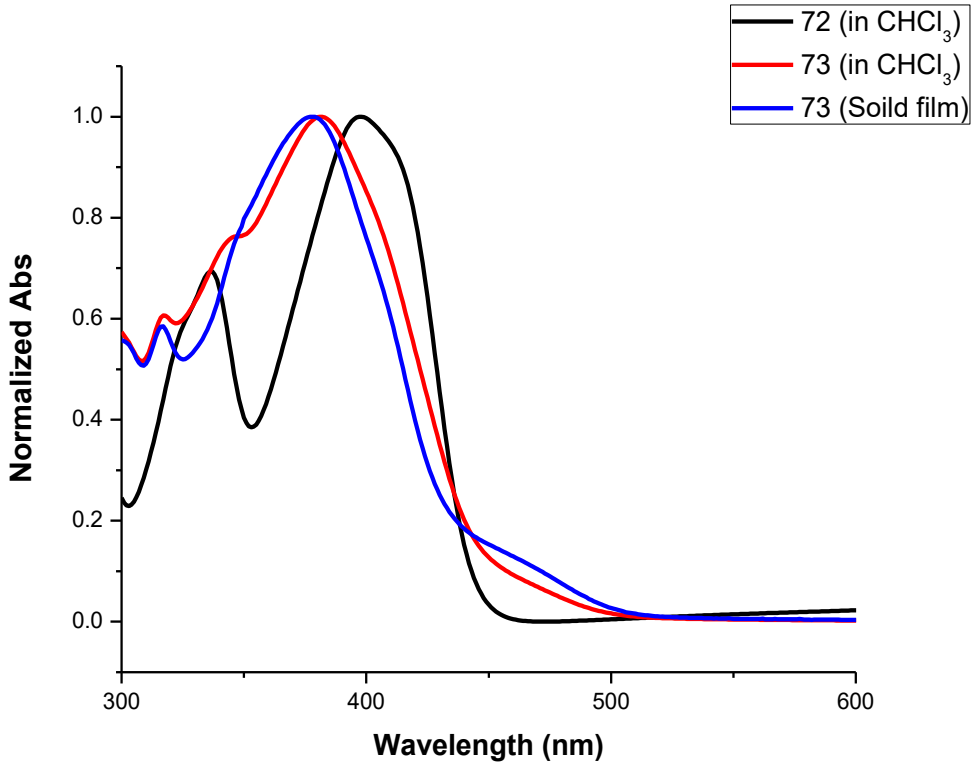

Fig. 5.2: Normalized UV-Vis absorption spectra of compounds **72** and **73** measured in $CHCl_3$ (1mg/100ml) and as a solid film (**73**) .

5.3 Conclusions

In summary, the synthetic goal of the work in this chapter has only been partially fulfilled, with the key intermediate, compound **73**, successfully synthesized by sequential reduction and dehydroxylation reactions. Compound **73** now is poised for cyclization or benzannulation to give

extended pentacene-containing PAHs. Continued efforts to further develop this chemistry will open a new avenue for the synthesis of nanographene-like materials. Although it is foreseeable that the proposed nanographene **74** is not an easy synthetic target, well-documented transition metal-catalyzed cyclization methodologies would be of great value for eventually solving this synthetic challenge. If efficient cyclization methods are found, new PAH systems will be created and they are expected to show unique electronic and photophysical properties, which may further lead to appealing application in organic electronic and optoelectronic devices.

5.4 Experimental

5.4.1 General

Chemicals were purchased from commercial suppliers and used directly without purification. All reactions were conducted in standard, dry glassware and under an inert atmosphere of nitrogen (N_2) unless otherwise noted. Evaporation and concentration were carried out with a rotary evaporator. Flash column chromatography was performed with 240-400 mesh silica gel, and thin-layer chromatography (TLC) was carried out with silica gel F254 covered on plastic sheets and visualized by UV light. ^{1}H and ^{13}C NMR spectra were measured on a Bruker Avance III 300 MHz multinuclear spectrometer. Chemical shifts (δ) are reported in ppm downfield relative to the signals of the internal reference $SiMe_4$ or residual solvents ($CHCl_3$: δ_H = 7.24 ppm, δ_C = 77.2 ppm; CH_2Cl_2: δ_H = 5.32 ppm, δ_C = 54.0 ppm). Coupling constants (*J*) are given in Hz. Infrared spectra (IR) were recorded on a Bruker Alfa spectrometer. High resolution APCI-TOF MS analysis was done on a GCT premier Micromass Technologies instrument. UV-Vis absorption spectra were measured on a Cary 6000i spectrophotometer.

5.4.2 Synthetic Procedures

Synthesis of 72

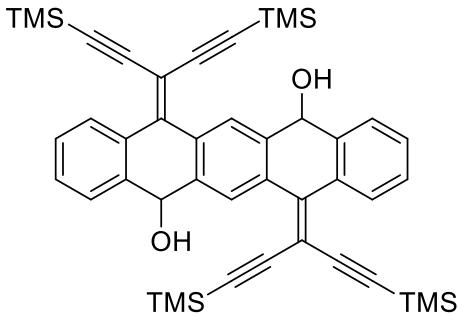

72

Compound **63** (200 mg, 0.278 mmol) was dissolved in THF (10 mL). The mixture was placed under a N_2 atmosphere and cooled to 0 ^oC with an ice-water bath. $NaBH_4$ (215 mg, 5.56 mmol) was then slowly added over 5 min, followed by addition of water (7 mL). The reaction mixture was heated to 50 °C for two hours. THF was removed under reduced pressure. Another portion of water (20 mL) was added. The resulting solids was filtered and washed with cooled water. After drying, compound **72** (190 mg, 0.263 mmol, 94%) was collected as a yellow solid. ^1H NMR (300 MHz, $CDCl_3$) δ 8.50 (s, 2H), 8.28 (dd, *J* = 5.9, 3.3 Hz, 2H), 7.62 – 7.44 (m, 2H), 7.36 (dd, *J* = 8.5, 3.1 Hz, 2H), 5.49 (d, *J* = 15.4 Hz, 2H), 0.23 (s, 36H). ^{13}C NMR (75 MHz, $CDCl_3$) δ 139.6, 134.3, 127.86, 127.6, 103.7, 101.1, 101.0, 71.3, 68.5, 68.0, 0.17, 0.00. HRMS (APCI, positive mode) *m/z* calcd for $C_{44}H_{49}OSi_4$ $[M - OH]^+$ 705.2860; found: 705.2827.

Synthesis of 73

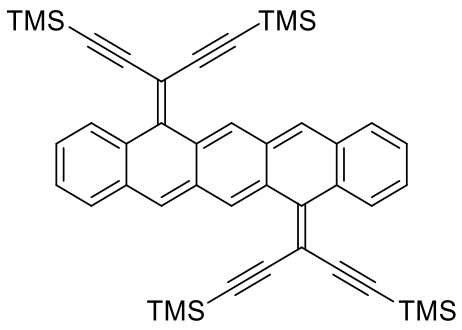

73

A solution of **72** (80 mg, 0.0111 mmol) in THF (10 mL) was cooled to 0 ^{o}C. A solution of tin(II) chloride dihydrate (499 mg, 2.21 mmol) in aqueous 50% acetic acid (5 mL) was then added dropwise. The resulting mixture was stirred at rt for 24 h. THF was removed under vacuum, and then water (15 mL) was added. The aqueous layer was extracted with CH_2Cl_2. The organic layer was then dried over $MgSO_4$, and excess solvent was removed under reduced pressure. The residue was subjected to column chromatography (CH_2Cl_2/hexane, 1:9) to yield compound **73** (25 mg, 0.0363 mmol, 32%) as a yellow solid. ^{1}H NMR (300 MHz, $CDCl_3$) δ 8.88 (s, 2H), 8.36 (s, 2H), 8.29 (dd, *J* = 5.9, 3.3 Hz, 2H), 7.99 (dd, *J* = 6.5, 3.3 Hz, 2H), 7.47 (dd, *J* = 6.5, 3.2 Hz, 2H), 7.29 (dd, *J* = 6.8, 2.5 Hz, 2H), 0.24 (s, 18H), 0.22 (s, 18H). ^{13}C NMR (75 MHz, $CDCl_3$) δ 148.2, 134.50, 132.5, 131.1, 130.0, 128.4, 127.7, 127.4, 127.4, 126.8, 125.8, 103.8, 103.6, 100.5, 100.1, 100.0, 0.0. HRMS (APCI, positive mode) *m/z* calcd for $[C_{44}H_{49}Si_4]^+$ $(M + H)^+$: 689.2911; found: 689.3429.

5.5 NMR Spectra for New Compounds

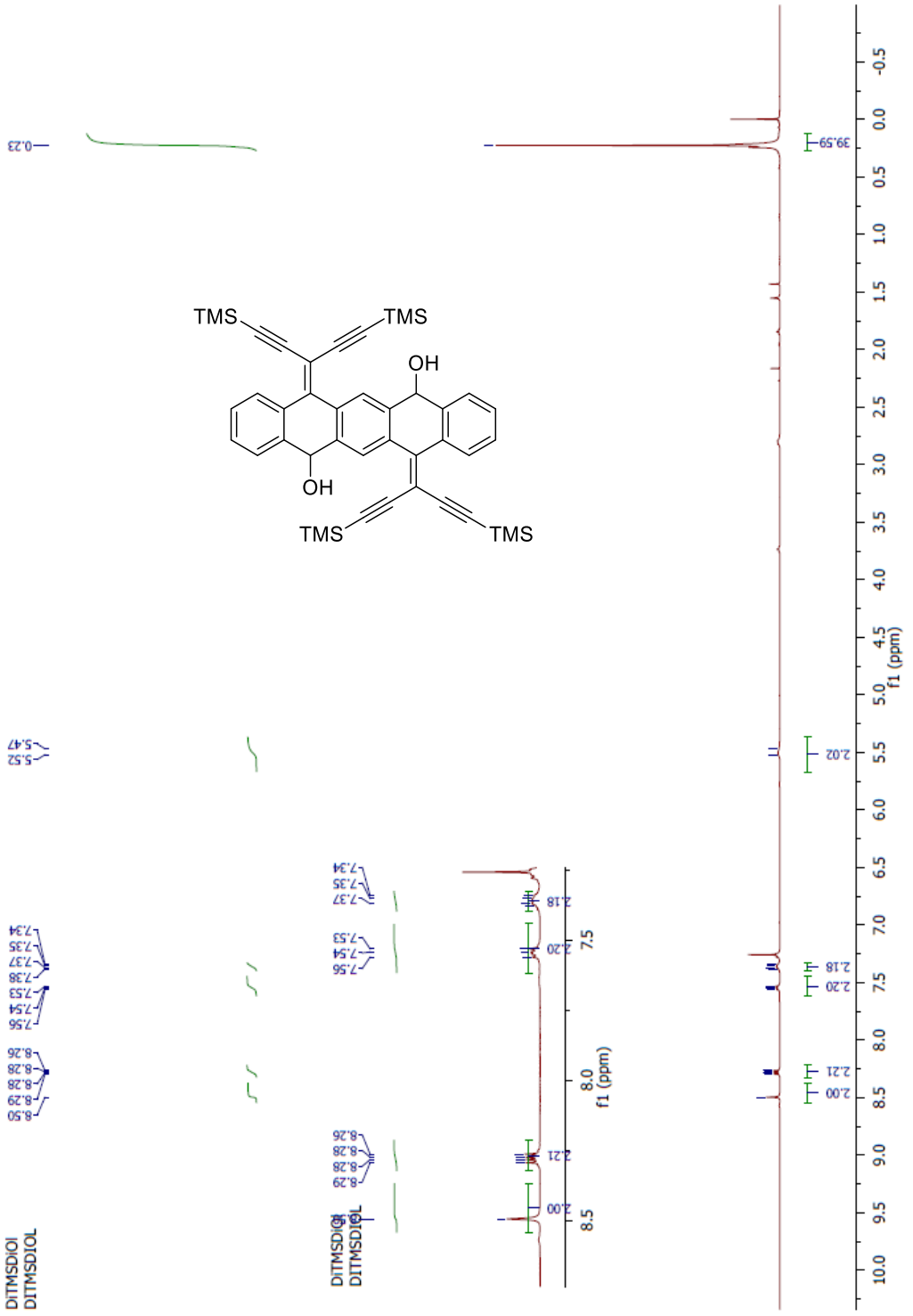

Fig. S-5.1 ^{1}H NMR (300 MHz, $CDCl_3$) of compound **72.**

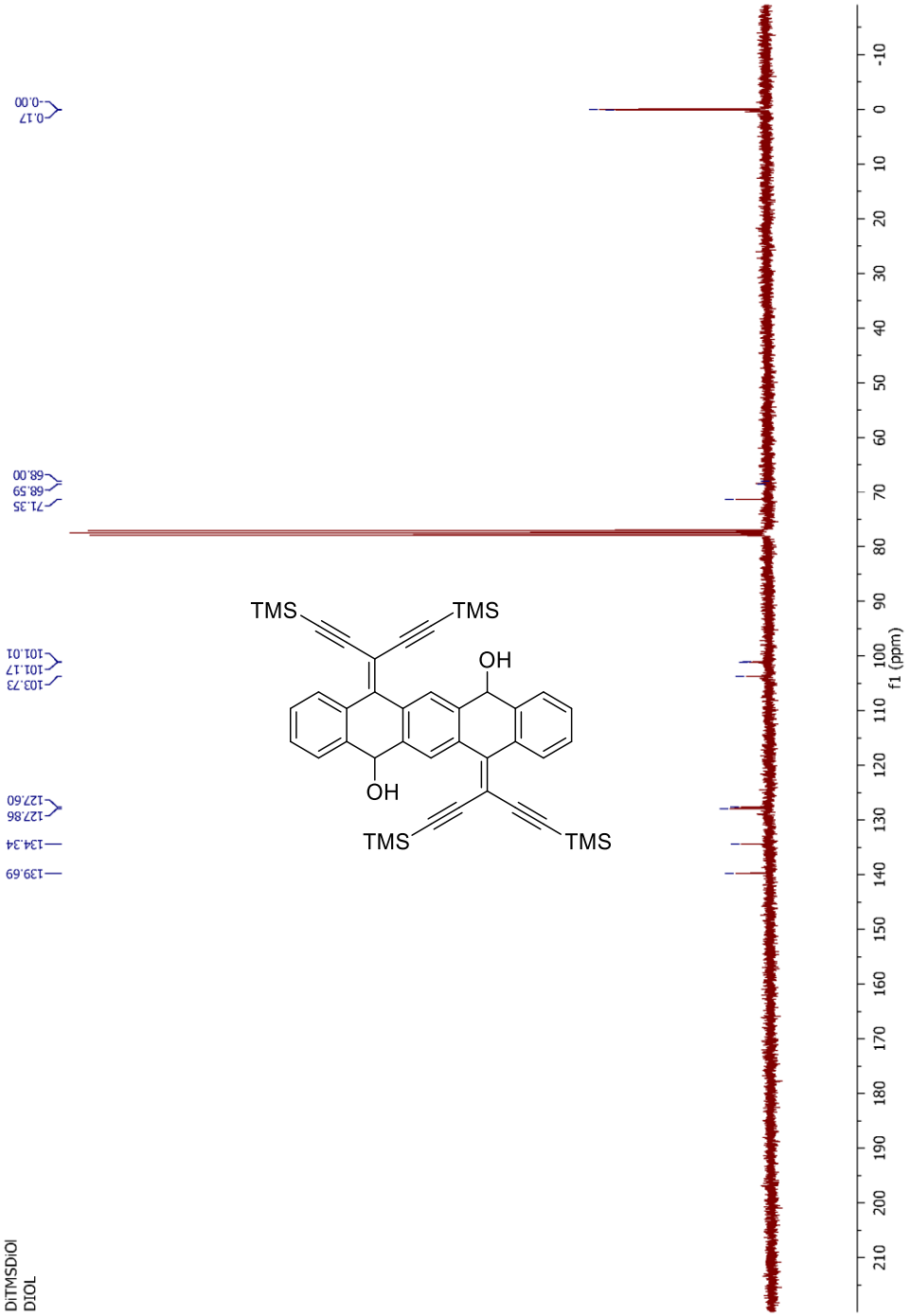

Fig. S-5.2 ^{13}C NMR (75 MHz, $CDCl_3$) of compound **72**.

.

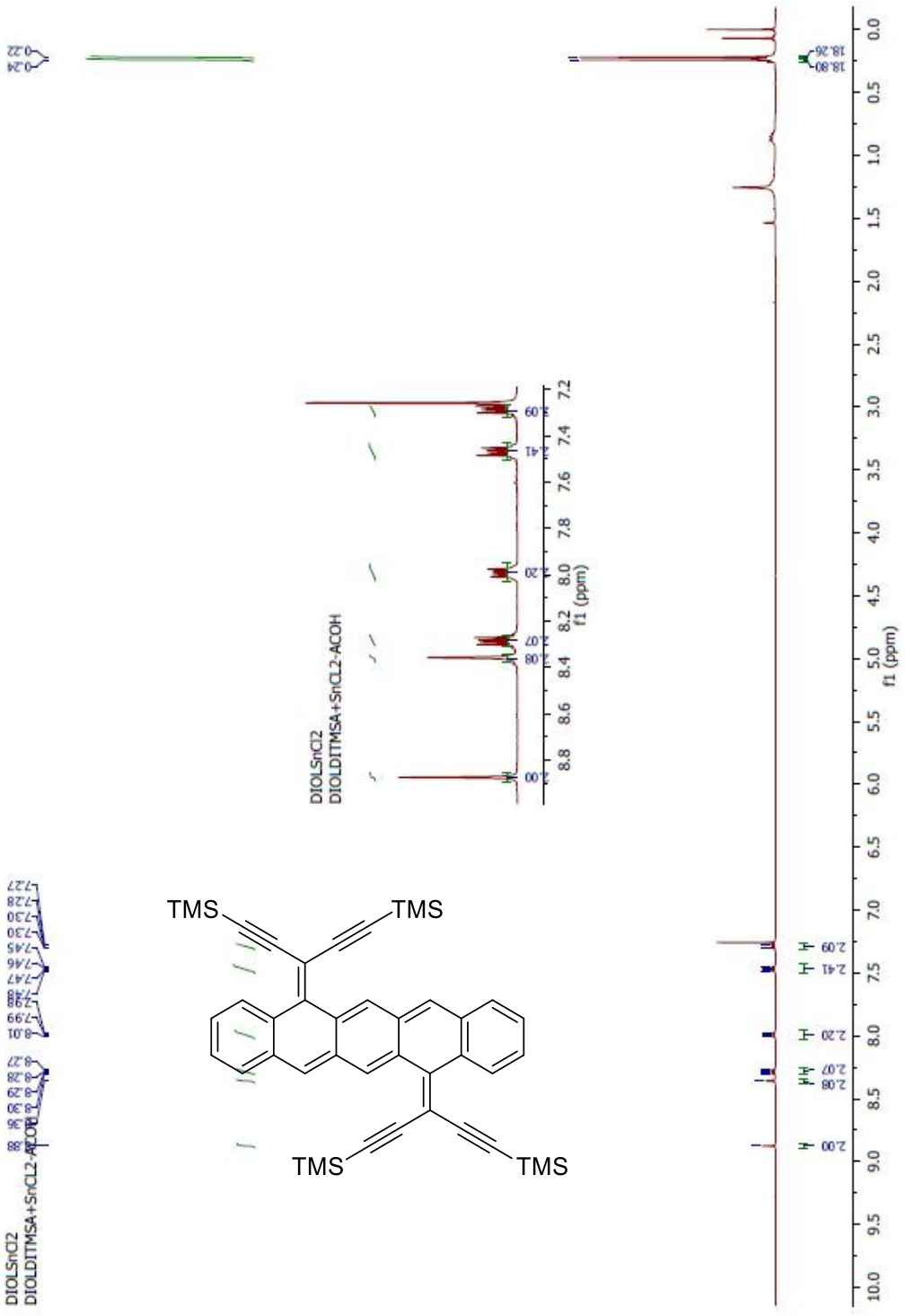

Fig. S-5.3[1]H NMR (300 MHz, $CDCl_3$) of compound **73**.

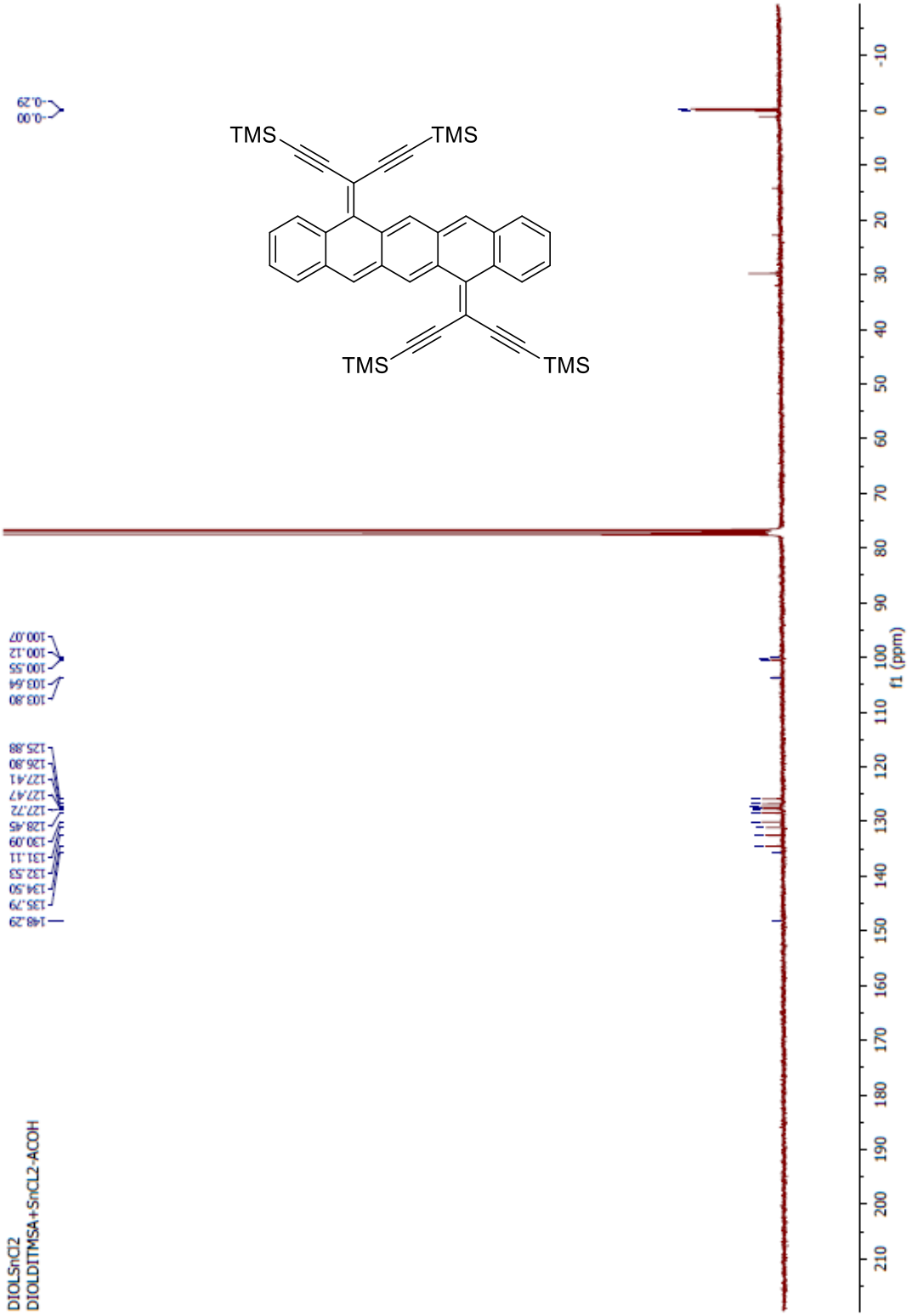

Fig. S-5.4 ^{13}C NMR (75 MHz, $CDCl_3$) of compound **73**.

5.6 DFT Calculation Results

Cartesian coordinates and optimized **73** (*cis* conformer): *E*(RB3LYP) = -1228.73234733 hartees.; Dipole Moment = 0.9806 Debye; Basis Set = 6-31G(d)

C	1.917440	1.992855	-0.427524
C	3.288497	1.666030	-0.689876
C	3.751631	0.326022	-0.516488
C	2.834791	-0.659542	0.087031
C	3.283798	-1.718191	0.869515
C	2.420854	-2.616197	1.572317
C	1.791986	-3.420940	2.224733
H	1.211993	-4.110392	2.794924
C	4.655956	-1.983352	1.171832
C	5.775617	-2.294532	1.515219
H	6.771977	-2.538398	1.806090
C	1.394731	-0.376062	-0.063048
C	0.979931	1.019014	-0.188435
C	-0.419902	1.335859	-0.117389
C	-1.394812	0.376009	-0.063051
C	-0.980017	-1.019064	-0.188452

C	-1.917537	-1.992897	-0.427530
C	-3.288600	-1.666065	-0.689844
C	-3.751729	-0.326054	-0.516445
C	-2.834860	0.659505	0.087048
C	-3.283752	1.718203	0.869528
C	-4.655854	1.983467	1.172008
C	-5.775433	2.294798	1.515526
H	-6.771686	2.539164	1.806345
C	-2.420652	2.616188	1.572167
C	-1.791526	3.420862	2.224421
H	-1.211510	4.110443	2.794432
C	-5.056775	-0.018016	-0.938779
C	-5.902859	-0.997762	-1.449616
C	-5.469772	-2.325697	-1.548188
C	-4.173930	-2.649753	-1.177164
H	-3.811583	-3.669466	-1.283025
H	-6.135917	-3.093050	-1.932905
H	-6.902792	-0.724388	-1.774699

H	-5.408735	1.003041	-0.883138
H	-1.603510	-3.029295	-0.527654
C	0.419817	-1.335910	-0.117423
H	0.687223	-2.385060	-0.144146
H	-0.687314	2.385012	-0.144054
C	5.056687	0.017992	-0.938793
C	5.902763	0.997738	-1.449640
C	5.469661	2.325668	-1.548236
C	4.173818	2.649719	-1.177209
H	3.811467	3.669431	-1.283068
H	6.135802	3.093022	-1.932956
H	6.902705	0.724373	-1.774705
H	5.408663	-1.003061	-0.883106
H	1.603407	3.029252	-0.527634

Cartesian coordinates and optimized **73** (*trans* conformer): *E*(RB3LYP) = -1228.73045985 hartees.; Dipole Moment = 0.0001 Debye; Basis Set = 6-31G(d)

C	1.931448	1.861424	0.753955
C	3.305501	1.698884	0.379660
C	3.759387	0.453661	-0.151738

C	2.836276	-0.697584	-0.122521
C	3.289707	-2.002404	0.045160
C	2.438835	-3.137286	0.227593
C	1.826307	-4.166450	0.413936
H	1.263293	-5.055312	0.586299
C	4.664016	-2.374584	0.179962
C	5.784939	-2.810475	0.328121
H	6.782695	-3.161638	0.462147
C	1.396678	-0.369771	-0.120550
C	0.987118	0.914081	0.443697
C	-0.413589	1.202493	0.584654
C	-1.396704	0.369755	0.120577
C	-0.987145	-0.914097	-0.443667
C	-1.931478	-1.861438	-0.753921
C	-3.305529	-1.698891	-0.379627
C	-3.759416	-0.453665	0.151766
C	-2.836299	0.697577	0.122544
C	-3.289693	2.002409	-0.045166

C	-4.663981	2.374637	-0.180033
C	-5.784854	2.810626	-0.328274
H	-6.782582	3.161831	-0.462396
C	-2.438779	3.137252	-0.227644
C	-1.826208	4.166389	-0.413984
H	-1.263211	5.055258	-0.586361
C	-5.062828	-0.394206	0.674058
C	-5.917116	-1.491562	0.616163
C	-5.494210	-2.687115	0.022735
C	-4.199250	-2.786732	-0.462180
H	-3.843631	-3.721073	-0.889772
H	-6.167019	-3.538181	-0.037124
H	-6.915467	-1.414752	1.037664
H	-5.407075	0.514808	1.148092
H	-1.619435	-2.812902	-1.178134
C	0.413562	-1.202509	-0.584627
H	0.671805	-2.143047	-1.053738
H	-0.671834	2.143034	1.053760

C	5.062801	0.394195	-0.674025
C	5.917091	1.491549	-0.616127
C	5.494184	2.687102	-0.022700
C	4.199224	2.786723	0.462215
H	3.843607	3.721063	0.889810
H	6.166995	3.538167	0.037162
H	6.915444	1.414737	-1.037623
H	5.407047	-0.514825	-1.148050
H	1.619403	2.812885	1.178173

Cartesian coordinates and optimized **74**: *E*(RB3LYP) = -1229.16888015 hartees.;

Dipole Moment = 0.0000 Debye; Basis Set = 6-31G(d)

C	1.931448	1.861424	0.753955
C	3.305501	1.698884	0.379660
C	3.759387	0.453661	-0.151738
C	2.836276	-0.697584	-0.122521
C	3.289707	-2.002404	0.045160
C	2.438835	-3.137286	0.227593
C	1.826307	-4.166450	0.413936

H	1.263293	-5.055312	0.586299
C	4.664016	-2.374584	0.179962
C	5.784939	-2.810475	0.328121
H	6.782695	-3.161638	0.462147
C	1.396678	-0.369771	-0.120550
C	0.987118	0.914081	0.443697
C	-0.413589	1.202493	0.584654
C	-1.396704	0.369755	0.120577
C	-0.987145	-0.914097	-0.443667
C	-1.931478	-1.861438	-0.753921
C	-3.305529	-1.698891	-0.379627
C	-3.759416	-0.453665	0.151766
C	-2.836299	0.697577	0.122544
C	-3.289693	2.002409	-0.045166
C	-4.663981	2.374637	-0.180033
C	-5.784854	2.810626	-0.328274
H	-6.782582	3.161831	-0.462396
C	-2.438779	3.137252	-0.227644

C	-1.826208	4.166389	-0.413984
H	-1.263211	5.055258	-0.586361
C	-5.062828	-0.394206	0.674058
C	-5.917116	-1.491562	0.616163
C	-5.494210	-2.687115	0.022735
C	-4.199250	-2.786732	-0.462180
H	-3.843631	-3.721073	-0.889772
H	-6.167019	-3.538181	-0.037124
H	-6.915467	-1.414752	1.037664
H	-5.407075	0.514808	1.148092
H	-1.619435	-2.812902	-1.178134
C	0.413562	-1.202509	-0.584627
H	0.671805	-2.143047	-1.053738
H	-0.671834	2.143034	1.053760
C	5.062801	0.394195	-0.674025
C	5.917091	1.491549	-0.616127
C	5.494184	2.687102	-0.022700
C	4.199224	2.786723	0.462215

H	3.843607	3.721063	0.889810
H	6.166995	3.538167	0.037162
H	6.915444	1.414737	-1.037623
H	5.407047	-0.514825	-1.148050
H	1.619403	2.812885	1.178173

5.7 References

(1) Yan, X.; Li, L.-S. *J. Mater. Chem*. **2011**, *21*, 3295-3300.

(2) Baldridge, K. K.; Siegel, J. S.; *Angew. Chem., Int. Ed.* **2013**, *52*, 5436-5438.

(3) Ball, M.; Zhong, Y.; Wu, Y.; Schenck, C.; Ng, F.; Steigerwald, M.; Xiao, S.; Nuckolls, C.; *Acc. Chem. Res.* **2015**, 48, 267-276.

(4) Pisula, W.; Feng, X. L.; *Müllen*, K. *Chem. Mater*. **2011**, *23*, 554-567.

(5) Morita, Y.; Suzuki, S.; Sato, K.; Takui, T.; *Nat. Chem*. **2011**, *3*, 197-204.

(6) *Müllen*, K. *ACS Nano* **2014**, *8*, 6531-6541.

(7) Narita, A.; Wang, X.-Y.; Fengb, X.; *Müllen*, K., K. *Chem. Soc. Rev.* **2015**, *44*, 661- 6643.

(8) Scholl, R.; Seer, C. *Liebigs Ann. Chem*. **1912**, *394*, 111-177.

(9) Scholl, R.; Seer, C. *Chem. Ber*.1922, **55**, 330-341.

(10) Scholl, R.; Seer, C.; *Weitzenböck*, R. *Chem. Ber*. **1910**, *43*, 2202- 2209.

(11) Clar, E.; Stephen, J. F. *Tetrahedron* **1965**, *21*, 467-470.

(12) Clar, E.; Schmidt, W. *Tetrahedron* **1979**, *35*, 2673-2680.

(13) Clar, E.; Stewart, D. G. *J. Am. Chem. Soc*. **1953**, *75*, 2667-2672.

(14) Grzybowski, M.; Skonieczny, K.; Butenschön, H.; Gryko, D. T. *Angew. Chem., Int. Ed.* **2013**, *52*, 9900-9930.

(15) Sarhan, A. A.; Bolm, C. *Chem. Soc. Rev*. **2009**, *38*, 2730-2744.

(16) Zhai, L.; Shukla, R.; Rathore, R. *Org. Lett.* **2009**, *11*, 3474-3477.

(17) Morgenroth, F.; Kubel, C.; *Muller*, M.; Wiesler, U. M.; Berresheim, A. J.; Wagner, M.; *Müllen*, K. *Carbon* **1998**, *36*, 833-837.

(18) Ormsby, J. L.; Black, T. D.; Hilton.; Bharat.; King, B. T.; *Tetrahedron*, **2008**, *64*, 11370-11378 .

(19) Dotz, F.; Brand, J. D.; Ito, S.; Gherghel, L.; *Müllen*, K. *J. Am. Chem*. Soc. **2000**, *122*, 7707-7717.

(20) Dou, X.; Yang, X.; Bodwell, G. J.; Wagner, M.; Enkelmann, V.; *Müllen*, K. *Org. Lett*. **2007**, *9*, 2485-2488.

(21) Chen, T.-A.; Liu, R.-S. *Chem. – Eur. J.* **2011**, *17*, 8023- 8027-*8027*.

(22) Donovan, P. M.; Scott, L. T. *J. Am. Chem*. Soc. **2004**, *126*, 3108-3112.

(23) Pramanik, C.; Miller, G. P. *Molecules* **2012**, *17*, 4625-4633

(24) Nishida, J.-i.; Fujiwara, Y.; Yamashita, Y. *Org. Lett.* **2009**, *11*, 1813-1816.

Chapter 6

Conclusions and Future Work

This thesis has accomplished the development of efficient synthetic methods for novel organic materials based on TTFVs, exTTFs, and annulated acenes. The major design concept employed throughout this thesis work is to take advantage of the excellent electron-donating and redox properties of TTFs and their derivatives. Integration of these molecular building blocks into various π-conjugated frameworks has successfully produced new organic π-conjugated materials. In the first project, a new TTFV–pyrene-based copolymer was synthesized and characterized. The electrochemical properties of the polymer were found to be consistent with its TTFV precursor. The aggregation behaviour of the polymer in the solution phase showed responsiveness to various external stimuli, in particular solvent polarity and pH. Moreover, the solid state ordering of the polymer was greatly modified by exposure to acidic vapour, pointing to potential application in the field of stimuli-responsive nanodevices.

In the second project, pentacen-5,7,12,14-tetraone was investigated as a building block to produce novel acenes-based nanomaterials. Although the rich electronic and structural properties of pentacenetetraone can be easily expected due to its highly π-extended nature, the use of this molecule as precursor for conjugated materials had not been extensively reported in the literature prior to this thesis work. The development of pentacene-based π-extended TTFs and enediyne analogues not only allows the knowledge of π-conjugated materials to be expanded, but also offers new synthetic access to carbon-rich nanomaterials, particularly nanographene-like materials which have received growing interest in recent years. In a long-term perspective, continued studies on

this topic may lead to applications in advanced nano-electronic and optoelectronic materials and devices.

At this juncture, two new research directions are proposed for future work. The first one is the construction of new 3D framework-like polymeric materials with rich microporosity and tuneable functionality. Scheme 6-1 illustrates a strategy to prepare a 3D cross-linked polymer, the intrinsic micropores of which are expected to creates a chiral microscopic environment useful for chiral separation and stereoselective synthesis. The key step of this research is to find an efficient way to perform stereoselective reduction of compound **63**. It is also envisioned that various ligand groups can be flexibly and modularly attached to the 3D polymer network to give porous materials with different functions useful in advanced binding and synthetic applications.

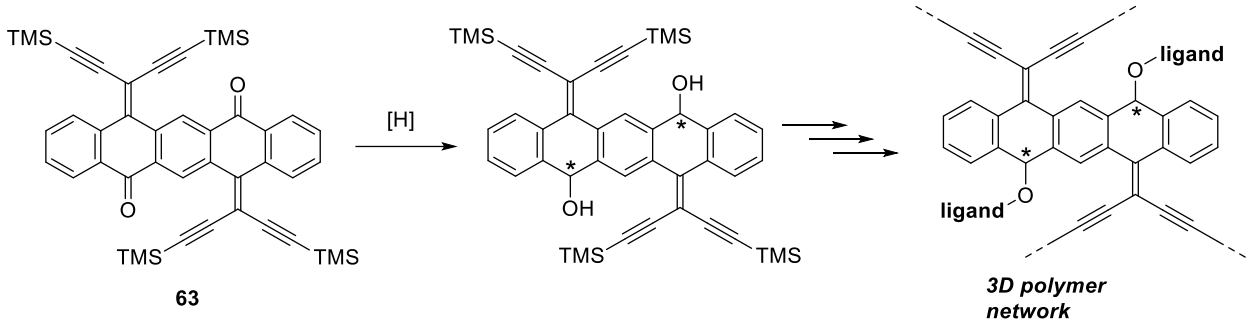

Scheme 6.1: Proposed synthesis of microporous cross-linked polymers with optically active repeat units.

The second research theme is to prepare nanographene polymers using compound **73** as the precursor. As shown in Scheme 6-2, when compound **73** is subjected to desilylation and then alkynyl homocoupling, carbon-rich cross-linked polymers are expected to form. These polymers can then undergo transition metal-catalyzed benzannulation to form nanographene polymers. The major challenges here are: (1) to make the intermediates keep reasonable solubility, (2) to establish an efficient benzannulation method, and (3) to clearly characterize the molecular structures of the

resulting polymers. Another interesting issue worth pondering at this moment is the presence of axial chirality if the target polymer can be made. It is anticipated that if control over chirality can be eventually achieved, the resulting polymer will be of enormous interest to the synthetic and materials community. This research goal, albeit very challenging, certainly deserves to be pursued in future work.

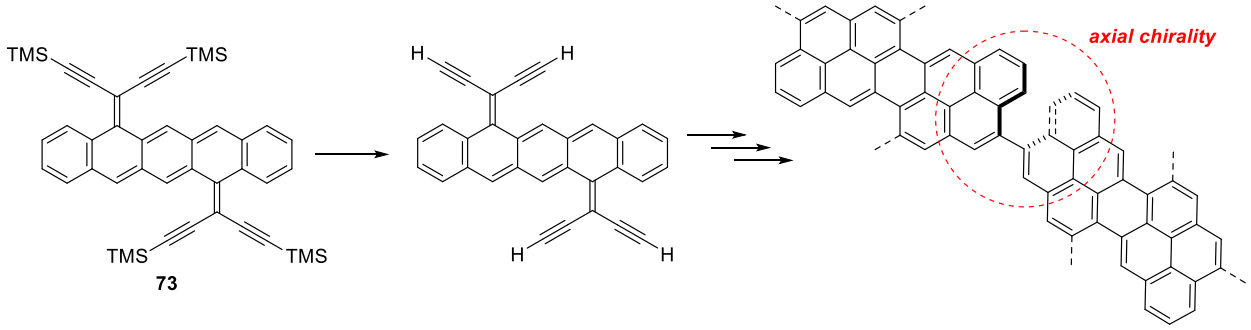

Scheme 6.2: proposed synthesis of nanographene polymers with axial chirality.